

University of Windsor

Scholarship at UWindor

Electronic Theses and Dissertations

Theses, Dissertations, and Major Papers

1982

ELASTIC AND ULTIMATE BEHAVIOUR OF WAFFLE SLAB STRUCTURES.

IBRAHIM SAYED AHMED. EL-SEBAKHY
University of Windsor

Follow this and additional works at: <https://scholar.uwindsor.ca/etd>

Recommended Citation

EL-SEBAKHY, IBRAHIM SAYED AHMED., "ELASTIC AND ULTIMATE BEHAVIOUR OF WAFFLE SLAB STRUCTURES." (1982). *Electronic Theses and Dissertations*. 1887.
<https://scholar.uwindsor.ca/etd/1887>

This online database contains the full-text of PhD dissertations and Masters' theses of University of Windsor students from 1954 forward. These documents are made available for personal study and research purposes only, in accordance with the Canadian Copyright Act and the Creative Commons license—CC BY-NC-ND (Attribution, Non-Commercial, No Derivative Works). Under this license, works must always be attributed to the copyright holder (original author), cannot be used for any commercial purposes, and may not be altered. Any other use would require the permission of the copyright holder. Students may inquire about withdrawing their dissertation and/or thesis from this database. For additional inquiries, please contact the repository administrator via email (scholarship@uwindsor.ca) or by telephone at 519-253-3000ext. 3208.

CANADIAN THESES ON MICROFICHE

I.S.B.N.

THESES CANADIENNES SUR MICROFICHE



National Library of Canada
Collections Development Branch

Canadian Theses on
Microfiche Service

Ottawa, Canada
K1A 0N4

Bibliothèque nationale du Canada
Direction du développement des collections

Service des thèses canadiennes
sur microfiche

NOTICE

The quality of this microfiche is heavily dependent upon the quality of the original thesis submitted for microfilming. Every effort has been made to ensure the highest quality of reproduction possible.

If pages are missing, contact the university which granted the degree.

Some pages may have indistinct print especially if the original pages were typed with a poor typewriter ribbon or if the university sent us a poor photocopy.

Previously copyrighted materials (journal articles, published tests, etc.) are not filmed.

Reproduction in full or in part of this film is governed by the Canadian Copyright Act, R.S.C. 1970, c. C-30. Please read the authorization forms which accompany this thesis.

THIS DISSERTATION
HAS BEEN MICROFILMED
EXACTLY AS RECEIVED

AVIS

La qualité de cette microfiche dépend grandement de la qualité de la thèse soumise au microfilmage. Nous avons tout fait pour assurer une qualité supérieure de reproduction.

S'il manque des pages, veuillez communiquer avec l'université qui a conféré le grade.

La qualité d'impression de certaines pages peut laisser à désirer, surtout si les pages originales ont été dactylographiées à l'aide d'un ruban usé ou si l'université nous a fait parvenir une photocopie de mauvaise qualité.

Les documents qui font déjà l'objet d'un droit d'auteur (articles de revue, examens publiés, etc.) ne sont pas microfilmés.

La reproduction, même partielle, de ce microfilm est soumise à la Loi canadienne sur le droit d'auteur, SRC 1970, c. C-30. Veuillez prendre connaissance des formules d'autorisation qui accompagnent cette thèse.

LA THÈSE A ÉTÉ
MICROFILMÉE TELLE QUE
NOUS L'AVONS REÇUE

ELASTIC AND ULTIMATE BEHAVIOUR
OF WAFFLE SLAB STRUCTURES

by



Ibrahim Sayed Ahmed El-Sebakhy
B.Sc. (Honour), M.A.Sc.

A Dissertation
submitted to the Faculty of Graduate Studies
through the Department of
Civil Engineering in Partial Fulfillment
of the requirements for the Degree of
Doctor of Philosophy at
The University of Windsor

Windsor, Ontario, Canada

1982

© Ibrahim Sayed Ahmed El-Sebakhy 1982

778101

To my parents and my wife

ABSTRACT

In this dissertation the author investigates the behaviour of reinforced and prestressed concrete waffle slabs from initial to collapse load. The theoretical treatment covering the whole range of load, is divided into three parts: elastic analysis, ultimate analysis, and progressive failure analysis. The elastic analysis part is based on a Fourier series solution for simply supported slabs and this is extended to continuous waffle slab structures. The ultimate limit state analysis is obtained by adopting the yield line theory as an upper bound solution. The progressive failure analysis is tackled by the finite element method as a numerical technique; beyond the initiation of the first crack at sections of maximum stresses, an iterative incremental procedure is adopted to take into account the reduction of rigidities with the corresponding increment of loading, thus converting the non-linear problem into a series of incrementally linear problems in the elastic-plastic range.

Comparison of results is made between skew and rectangular waffle slabs as well as between continuous slabs on isolated supports and on continuous line-supports. A study of the effect of rotating the isolated

column support line about the center of the bridge on the structural response is undertaken.

The theoretical analyses are substantiated and verified by experimental results obtained from tests on seven models of reinforced and prestressed concrete waffle slab bridges. The deflections and strains obtained from the tests are found to be in good agreement with the theoretical solutions.

From this study it is concluded that the yield-line analysis is simple and reliable in predicting the ultimate load of waffle slab structures. Furthermore, prestressed concrete waffle slab construction is well suited for use in large span structures. Also, in predicting the collapse load of waffle slab structures, it is found that the progressive failure analysis of such structures gives results which are in close agreement with those obtained from the tests as well as from the yield-line analysis.

ACKNOWLEDGEMENT

The author wishes to express his deep appreciation and sincere gratitude to his advisor, Dr. J. B. Kennedy, for his patience and continuous guidance as well as encouragement and valuable suggestions throughout the completion of this dissertation.

The author is grateful to the Civil Engineering Faculty at the University of Windsor for their indirect inspiration through their valuable courses. Also, thanks are due to the Computer staff at the University of Windsor for their assistance.

Thanks are due to the staff of the Structural Engineering Research Division at the Ontario Ministry of Transportation and Communication, for their help during the numerical analysis. The author extends his thanks to the staff of the structural engineering laboratory in the Department of Civil Engineering for their assistance in the experimental part of this study.

The author is grateful to the financial support provided by the National Sciences and Engineering Research Council.

Special appreciation is extended to Mrs. Zeleney for typing the manuscript.

Finally, the author is deeply indebted to his wife, Amal, for her moral support and encouragement.

TABLE OF CONTENTS

ABSTRACT.	v
ACKNOWLEDGEMENTS.	vii
LIST OF FIGURES	xii
LIST OF TABLES.	xxii
LIST OF APPENDICES.	xxiii
NOMENCLATURE.	xxiv
CHAPTER	
I. INTRODUCTION	1
1.1 General.	1
1.2 Object and Scope	3
II. BACKGROUND AND REVIEW OF LITERATURE.	6
2.1 General.	6
2.2 Elastic Analysis (Working Load).	7
2.2.1 Elastic Series Solution	7
2.2.1.1 Reinforced Concrete Slabs.	7
2.2.1.2 Prestressed Concrete Slabs.	9
2.2.2 Finite Element Method (Working Load).	10
2.3 Ultimate Load Analysis (Yield-Line Theory).	11
2.4 Progressive Failure Analysis	18
III. ELASTIC BEHAVIOUR OF CONCRETE WAFFLE SLAB STRUCTURES.	20
3.1 Introduction	20
3.2 Elastic Series Solution for Simply Supported Slabs	20
3.2.1 Bending Analysis.	21
3.2.1.1 Boundary Conditions.	24
3.2.1.2 Flexural and Torsional Rigidities.	26
3.2.2 In-Plane Stress Analysis.	26
3.2.2.1 In-Plane Axial Rigidities	28

3.3	Elastic Series Solution for Continuous Slabs (Influence Lines)	30
3.4	Elastic Finite Element Analysis	33
3.4.1	General	33
3.4.2	Scope and Definition of the STRAND Program	33
3.4.3	Analysis by SAADS Program	37
IV.	YIELD LINE THEORY FOR WAFFLE SLAB STRUCTURES (ULTIMATE ANALYSIS)	39
4.1	Introduction	39
4.2	Assumptions for Prediction of a Yield-Line Pattern	40
4.3	Ultimate Load Analysis	40
4.4	Yield Moment on Axes Not Perpendicular to Reinforcing	42
4.5	Correction Forces for the Equilibrium Method	43
4.6	Effect of Four Concentrated Loads on the Yield-Line Pattern (Wheel Truck)	44
4.7	Simply Supported Waffle Slabs	44
4.7.1	Skew Waffle Slab Bridge Under Uniformly Distributed Load	44
4.7.2	Skew Waffle Slab Bridge Under Concentrated Load at Center	46
4.7.3	Skew Waffle Slab Bridge Under Concentrated Load at Center of Edge Beam	48
4.8	Continuous Waffle Slab Supported by Isolated Columns	50
4.8.1	Rectangular Waffle Slab Supported by Two Isolated Columns	50
4.8.2	Skew Waffle Slab Supported by Two Isolated Columns	52
4.8.3	Effect of the Skew Angle on the Yield-line Pattern	55
V.	PROGRESSIVE FAILURE ANALYSIS	57
5.1	Introduction	57
5.2	Analysis by the Finite Element Method	57
5.3	Uncracked Rigidities for Plate Bending Analysis	61
5.4	Rigidities of Cracked Sections	61
5.4.1	Flexural Rigidities	61
5.4.2	Torsional Rigidity	63

VI.	EXPERIMENTAL INVESTIGATION.	65
6.1	Introduction.	65
6.2	Materials	67
6.2.1	Concrete	67
6.2.2	Reinforcement.	67
6.3	Formwork.	68
6.4	Description of the Two Continuous Slab Models	68
6.4.1	Continuous Rectangular Post-Tensioned Waffle Slab Model, PC3	68
6.4.2	Continuous 45° Skew Post-Tensional Waffle Slab, PC4	69
6.5	Experimental Equipment.	70
6.5.1	Prestressing Equipment	70
6.5.2	Automatic Strain Indicator	70
6.5.3	Hydraulic Jack for Lateral Loading.	71
6.6	Instrumentation	71
6.6.1	Electric Strain Gauges on the Concrete	71
6.6.2	Mechanical Dial Gauges	72
6.6.3	Load Cells	73
6.7	Construction of the Slab Models	73
6.8	Experimental Setup and Test Procedure	75
6.8.1	Rectangular Prestressed Concrete Waffle Slab	75
6.8.2	45° Skewed Prestressed Concrete Waffle Slab	76
VII.	DISCUSSION OF RESULTS	78
7.1	General	79
7.2	Elastic Solution (Working Load Condition).	79
7.2.1	Simply Supported Slab Models	79
7.2.2	Continuous Prestressed Waffle Slabs.	81
7.2.2.1	Series Solutions Using Influence Lines	81
7.2.2.2	Finite Element Method	82
7.2.2.2.1	Rectangular Concrete Waffle Slab	83
7.2.2.2.2	Skew Concrete Waffle Slab	85
7.3	Ultimate Load Solution (Yield-Line Theory).	86
7.3.1	Reinforced Concrete Waffle Slabs (Group A).	87

7.3.2	Prestressed Concrete Waffle Slabs, Simply Supported (Group B)	90
7.3.2	Continuous Prestressed Concrete Waffle Slabs (Group C)	91
7.4	Progressive Failure Analysis (Finite Element Method)	95
7.4.1	Simply Supported Waffle Slabs	95
7.4.2	Continuous Prestressed Waffle Slabs	98
7.5	Effect of Rotating the Interior-Column Line About the Center of the Slab Bridge Model.	100
7.6	Effect of Continuous Pier Line Support in a Rectangular Slab.	101
7.6.1	Rigid Pier Line Support	101
7.7	Effect of Continuous Pier Line Support in a Skew Slab	101
7.7.1	Rigid Pier Line Support	101
VIII.	SUMMARY AND CONCLUSIONS.	103
	FIGURES	106
	TABLES.	250
	APPENDICES.	256
	REFERENCES.	312
	VITA AUCTORIS	319

LIST OF FIGURES

<u>Figure</u>	<u>Page</u>
3.1 Planform of the Waffle Slab Model (RC1)	107
3.2 Cross-Sectional Geometries of Waffle Slab Model	108
3.3 Planforms of Prestressed Concrete Waffle Slab Bridge Models	109
3.4 In-Plane Prestress Loading on Skew Waffle Slab Structure	110
3.5 Flow Chart of STRAND SYSTEM.	111
3.6 Sign Convention of In-Plane and Plate Bending Stresses	114
3.7 Finite Element Mesh for a Rectangular Waffle Slab Using Triangular Elements	115
3.8 Finite Element Mesh for a Skew Waffle Slab Using Triangular Elements.	116
3.9 Triangular Elements for STRAND Analysis. . . .	117
4.1 Cracked Sections of Waffle Slab.	118
4.2 Single Yield-Line Pattern for Skew Waffle Slab Due to a Concentrated Load at the Center of the Slab	119
4.3 Yield-line Crack Patterns for Skew Waffle Slab Due to a Concentrated Load at the Center of the Edge Beam.	120
4.4 Single Yield-line Crack Pattern in Continuous Rectangular Waffle Slab.	121
4.5 Yield Lines in Continuous Skew Waffle Slab . .	122
5.1 Incremental and Iterative Procedure in STRAND Program (Modified).	123
6.1 The Tested Waffle Slabs.	124
6.2 Rectangular Prestressed Waffle Slab Model (PC3).	125
6.3 Skew Prestressed Waffle Slab Model (PC4) . . .	125

<u>Figure</u>		<u>Page</u>
6.4	Bottom Plan Layout (Rectangular Waffle Slab PC3)	126
6.5	Bottom Plan Layout (Skew, PC4)...	127
6.6	Prestressed Wire Profile for Rectangular Slab (PC3)	128 .
6.7	The Prestressing Hydraulic Jack in Position. . .	129
6.8	The Prestressing of Skew Slab Model PC3.	129
6.9	Wire Profile and Eccentricities of the Curved Tendons for Skew Slab PC4	130
6.10	The Automatic Strain Indicator	131
6.11	Concentrated Loading System.	132
6.12	The Two Bracing Steel Columns and Dial Gauges in Position.	133
6.13	Prestressed Concrete Waffle Slab PC3	134
6.14	Prestressed Concrete Waffle Slab PC4	135
6.15	Form of the Steel Bed Before Casting the Concrete	136
6.16	Set Up the Slab PC3 in the Loading Position. . .	136
6.17	In-Plane Prestressing Force for Rectangular Slab PC3	137
6.18	In-Plane Prestressing Force for Skew Slab (PC4).	138
6.19	Waffle Slab PC3 Under Two Concentrated Loads Each at the Center of Each Span.	139
6.20	Waffle Slab PC4 Under a Single Concentrated Load at the Center of the Edge Beam.	139
7.1	Load-Deflection Relationships for Rectangular Model Under Load at Center of Edge Beam (Location 3)	140
7.2	Load-Strain Relationships for Rectangular Model Under Load at Center of Edge Beam (Location 3).	141

<u>Figure</u>		<u>Page</u>
7.3	Load-Deflection Relationship for Skew Model Under Central Load (Location 1)	142
7.4	Load-Strain Relationships for Skew Model Under Central Load (Location 1)	143
7.5	Load-Strain Relationships for Skew Model at Center of Edge Beam (Location 4)	144
7.6	Upward Deflection Distribution (Camber) Due to Prestressing.	145
7.7	Strain Distribution in the Bottom Fibre for Rectangular Slab (PC3) After Prestressing.	146
7.8	Strain Distribution in the Top Fibre for Rectangular Slab (PC3) After Prestressing.	147
7.9	Distribution of Moment for the Rectangular Slab (PC3) Due to Prestressing	148
7.10	Deflection Distribution (Camber) Due to Prestressing of Skew Slab (PC4)	149
7.11	Strain Distribution for Skew Slab (PC4) in the Top Fibre Due to Prestressing.	150
7.12	Moment Distribution for the Skew Slab (PC4) Due to Prestressing.	151
7.13	Initial and Final Prestressing for the Rectangular Slab (PC3)	152
7.14	Initial and Final Prestressing for the Skew Lab	153
7.15	Load-Deflection Relationship for Rectangular Slab (PC3) at the Center of the Edge Beam (Location 3)	154
7.16	Load-Deflection Relationship for Rectangular (PC3) Slab Due to Concentrated Load at the Center of the Edge Beam.	155
7.17	Load-Deflection Relationship for the Rectangular Slab (PC3) Loading at Point 5.	156
7.18	Load-Deflection Relationship for Rectangular Slab (PC3) For Load at Point 5	157

<u>Figure</u>		<u>Page</u>
7.19	Load-Deflection Relationship for Rectangular Slab (PC3) Due to a Single Concentrated Load at Point 9.	158
7.20	Load-Deflection Relationship for Rectangular Slab (PC3) Due to Two Concentrated Loads at the Center of the Edge Beam	159
7.21	Load-Deflection Relationship for Rectangular Slab (PC3) Due to Two Concentrated Loads Each at the Center of the Edge Beam.	160
7.22	Load-Deflection Relationship for Rectangular Slab (PC3) Due to Two Concentrated Loads Each at the Center of Each Span.	161
7.23	Load-Deflection Relationship for Rectangular Slab (PC3) Due to Two Concentrated Loads Each at the Center of Each Span.	162
7.24	Deflection Distribution for Rectangular Slab (PC3) Due to 8 kN at Point 1.	163
7.25	Deflection Distribution for Rectangular Slab (PC3) Due to 18 kN at Point 5	164
7.26	Deflection Distribution for Rectangular Slab (PC3) Due to a Single Concentrated Load (18kN) at Point 9	165
7.27	Deflection Distribution for Rectangular Slab (PC3) Due to Two Concentrated Labs (36 kN) Each at the Center of the Edge Beam	166
7.28	Deflection Distribution for Rectangular Slab Due to Two Concentrated Loads (36 kN) Each at the Center of Each Span.	167
7.29	Load-Strain Relationships for Rectangular Slab (PC3) at the Center of the Edge Beam	168
7.30	Load-Strain Relationship for Rectangular Slab Loading at Point 5.	169
7.31	Load-Strain Relationship for Rectangular Slab Due to Concentrated Load at Point 9	170
7.32	Load-Strain Relationship for Rectangular Slab Due to Two Concentrated Loads at the Edge Beam.	171

<u>Figure</u>		<u>Page</u>
7.33	Load-Strain Relationship for Rectangular Slab (PC3) Due to Two Concentrated Loads Each at the Center of Each Span.	172
7.34	Moment Distribution for Rectangular Slab Due to 18 kN at Point 1.	173
7.35	Moment Distribution for Rectangular Slab Due to 18 kN at Point 5.	174
7.36	Moment Distribution for Rectangular Slab Due to a Concentrated Load (18 kN) at Point 9.	175
7.37	Moment Distribution for Rectangular Slab Due to Two Concentrated Loads (36 kN) Each at the Center of the Edge Beam	176
7.38	Moment Distribution for Rectangular Slab (PC3) Due to Two Concentrated Loads (36 kN) at the Center of Each Span	177
7.39	Load-Deflection Relationship for Skew Slab (PC4) Due to Concentrated Load at the Edge Beam Point 2	178
7.40	Load-Deflection Relationship for Skew Slab (PC4) Due to a Concentrated Load at the Edge Beam Point 2	179
7.41	Load-Deflection Relationship for Skew Slab (PC4) Due to a Concentrated Load at the Center of the Span	180
7.42	Load-Deflection Relationship for Skew Slab (PC4) Due to a Concentrated Load at the Center of the Span	181
7.43	Deflection Relationship for Skew Slab (PC4), Due to a Concentrated Load at the Center of the Edge Beam	182
7.44	Load Deflection Relationship for Skew Slab (PC4) Due to a Concentrated Load at the Center of the Edge Beam.	183
7.45	Load Deflection Relationship for Skew Slab Due to a Concentrated Load at the Center of the Slab Model PC4.	184
7.46	Load Deflection Relationship for Skew Slab Due to Two Concentrated Loads at the Center of the Edge Beam	185

<u>Figure</u>		<u>Page</u>
7.47	Load-Deflection Relationship for Skew (PC4) Slab Due to Two Concentrated Loads at the Center of the Edge Beam.	186
7.48	Load-Deflection Relationship for Skew Slab (PC4) Due to Two Concentrated Loads at the Center of Each Span	187
7.49	Deflection Distribution for Skew Slab (PC4) Due to a Concentrated Load (18 kN) at the Center of the Edge Beam	188
7.50	Deflection Distribution for Skew Slab Due to a Concentrated Load (18 kN) at the Center of the Edge Beam.	189
7.51	Deflection Distribution for Skew Slab Due to a Concentrated Load (18kN) at the Center of the Edge Beam.	190
7.52	Deflection Distribution for Skew Slab Due to a Concentrated Load (18kN) at the Center of the Slab	191
7.53	Deflection Distribution for Skew Slab (PC4) Due to Two Concentrated Loads (36 kN) Each at the Center of the Edge Beam.	192
7.54	Deflection Distribution for Skew Slab Due to Two Concentrated Loads (36kN) Each at the Center of Each Span	193
7.55	Load-Strain Relationship Due to a Concentrated Load at Point 2	194
7.56	Load-Strain Relationship for Skew Slab Due to Concentrated Load at Center of the Span.	195
7.57	Load-Strain Relationship for Skew Slab Due to a Concentrated Load at the Center of the Edge Beam	196
7.58	Load-Strain Relationship for Skew Slab (PC4) Due to a Concentrated Load at the Center of the Slab	197
7.59	Load-Strain Relationship for Skew Slab (PC4) Due to Two Concentrated Loads at the Center of the Edge Beam.	198

<u>Figure</u>		<u>Page</u>
7.60	Load-Strain Relationship for Skew Slab (PC4) Due to Two Concentrated Loads Each at the Center of the Span.	199
7.61	Moment Distribution for Skew Slab Due to Concentrated Load (18 kN) at the Center of the Edge Beam.	200
7.62	Moment Distribution for Skew Slab (PC4) Due to a Concentrated Load (18kN) at the Center of the Span	201
7.63	Moment Distribution for Skew Slab (PC4) Due to Load (18 kN) at the Center of the Edge Beam.	202
7.64	Moment Distribution for Skew Slab (PC4) Due to a Concentrated Load (18 kN) at the Center of the Slab.	203
7.65	Moment Distribution for Skew Slab Due to Two Concentrated Loads (36 kN) Each at the Center of the Edge Beam.	204
7.66	Moment Distribution for Skew Slab (PC4) Due to Two Concentrated Loads (36 kN) Each at the Center of Each Span :	205
7.67	Yield Lines in the Tested Slab Models	206
7.68	Load Versus Deflection and Strain for Rectangular Slab Model (RC1) Under Uniformly Distributed Load.	207
7.69	Single-Line Crack Pattern of Waffle Slab Model RC1	208
7.70	Load Versus Deflection and Strain for Rectangular Reinforced (RC2) and Prestressed Model (PC1) Under Concentrated Load	209
7.71	Single-Line Crack Pattern of Waffle Slab Model RC2	210
7.72	Load Versus Deflection and Strain for Reinforced Skew Slab (RC3) Under a Concentrated Load at Center	211
7.73	Cracks of Skew Waffle Slab Model RC3.	212

<u>Figure</u>		<u>Page</u>
7.74	Load Versus Deflection and Strain for Prestressed Model PC1 Under Concentrated Load at Center of Edge Beam.	213
7.75	Cracks of Waffle Slab Model PC1 Due to Edge Load.	214
7.76	Load Versus Deflection and Strain for Prestressed Skew Model Under Concentrated Load at Center	215
7.77	Single-Line Crack Pattern of Waffle Slab Model PC2.	216
7.78	Negative Single-Line Crack Pattern Joining the Two Columns in Waffle Slab Model PC3	216
7.79	Combined Flexural and Torsional Cracks in Waffle Slab PC4.	217
7.80	Yield Line in Waffle Slab PC4.	217
7.81	Rectangular Reinforced Concrete Waffle Slab RC1 Subjected to Uniformly Distributed Load.	218
7.82	Rectangular Reinforced Concrete Waffle Slab (RC2) Subjected to a Single Concentrated Load at the Center of the Slab	219
7.83	Skew Reinforced Concrete Waffle Slab (RC3) Subjected to a Single Concentrated Load at the Center of the Slab	220
7.84	Rectangular Prestressed Concrete Waffle Slab (PC1) Subjected to a Single Concentrated Load at the Center of the Edge Beam	221
7.85	Skew Prestressed Concrete Waffle Slab (PC2) Slab Subjected to a Single Concentrated Load at the Center of the Slab.	222
7.86	Rectangular Prestressed Continuous Waffle Slab (PC3) Subjected to Two Concentrated Loads of 14.96 Kips (Cracking Load) Each at the Center of Each Span Panel.	223
7.87	Rectangular Prestressed Continuous Waffle Slab (PC3) Subjected to two Concentrated Loads of 17.68 Kips acting at the Center of Each Span Panel	224

<u>Figure</u>		<u>Page</u>
7.88	Cracks at Load 19.04 Kips.	225
7.89	Cracks at Load 20.4 Kips	226
7.90	Rectangular Prestressed Continuous Waffle Slab (PC3) Subject to Two Concentrated Loads of 24.7 Kips Ultimate Load Each at the Center of Each Span Panel.	227
7.91	Skew Prestressed Continuous Waffle Slab (PC4) Subjected to two Concentrated Loads of 15.84 Kips (Cracking Load) at the Center of Each Span Panel	228
7.92	Cracks at Load = 18.44 Kips.	229
7.93	Cracks at Load = 22 Kips	230
7.94	Cracks at Load = 24 Kips	231
7.95	Cracks at Ultimate Load of 26.4 Kips	232
7.96	Load Versus Deflection for Rectangular Slab (RC1) Model Under Uniformly Distributed Load . .	233
7.97	Load Versus Deflection for Rectangular Slab Model (RC2) Under Concentrated Load at the Center	234
7.98	Load Versus Deflection for Reinforced Skew Slab (RC3) Under a Concentrated Load at Center	235
7.99	Load Versus Deflection for Prestressed Model (PC1) Concentrated Load at the Center of Edge Beam.	236
7.100	Load Versus Deflection for Prestressed Skew Model (PC2) Under Concentrated Load at the Center of the Slab	237
7.101	Deflection Relationship for Rectangular Slab Due to Two Concentrated Loads Each at the Center of Each Span.	238
7.102	Load-Deflection Relationship for Skew Slab Due to Two Concentrated Loads Each at the Center of Each Span.	239

<u>Figure</u>		<u>Page</u>
7.103	Deflection Pattern Due to Rotating the Two Columns about the Center of the Bridge Model (PC4)	240
7.104	Deflection Pattern Due to Rotating the Two Interior Columns About the Center of the Bridge Model PC4	241
7.105	Deflection Pattern Due to Rotating the Two Interior Columns About the Center of the Bridge Model (PC4)	242
7.106	The Distribution of Moment in Slab (PC4) Due to Rotating the Two Columns	243
7.107	The Distribution of Moments in Slab (PC4) Due to Rotating the Two Columns About the Center of the Slab.	244
7.108	The Distribution of the Moment in Slab (PC4) Due to Rotating the Two Columns About the Center of the Slab.	245
7.109	Deflection Pattern in Continuous Waffle Slab Due to Two Concentrated Loads	246
7.110	The Distribution of the Moment in Rectangular Slab with Continuous Pier Supports Due to Two Concentrated Loads.	247
7.111	Deflection Pattern in Continuous Skew Slab Due to Two Concentrated Loads	248
7.112	The Distribution of the Moment in Skew Slab With Continuous Pier Supports	249

LIST OF TABLES

<u>Table</u>		<u>Page</u>
3.1	Limitations of STRAND Programs.	251
6.1	Details of Test Bridge Models	252
7.1	Column Reactions Due to a Single Concentrated Load 4 Kips Acting at the Center of the Span. .	253
7.2	Column Reactions Using Finite Element Method. .	254
7.3	Comparison of Theoretical and Experimental Results for Deflections and Ultimate Loads. . .	255

++''

LIST OF APPENDICES

<u>Appendix</u>	<u>Page</u>
A Cracked and Uncracked Rigidities of Waffle Slab Structures.	258
B Theoretical Collapse Load by Yield-Line Theory.	264
C The Input Data for the STRAND Program	271
D Calibration of Load Cells and Tension Test on Wires	305

NOMENCLATURE

$[A]$	=	in-plane rigidity matrix of waffle slab;
$A_s (A'_s)$	=	area of prestressing steel in longitudinal (transverse) rib;
$2a$	=	skew width of waffle slab;
$2b$	=	skew length of waffle slab;
$b_x (b_y)$	=	width of transverse (longitudinal) rib;
$C_{1n}, \dots, C_{16n}, C_{17}, \dots, C_{24}$	=	arbitrary constants;
c	=	$\cos \theta$;
C_{ij}	=	elastic compliances;
D_i	=	flexibility of column i ;
D_x, D_y	=	flexural rigidity of waffle slab per unit length and per unit width, respectively;
D_{xy}, D_{yx}	=	transverse and longitudinal shear rigidities, respectively;
D_1, D_2	=	coupling rigidities arising from Poisson ratio effect;
d	=	total depth of section;
$E(G)$	=	elastic (shear) modulus of concrete;
EI	=	flexural rigidity of edge beam;
f'_c	=	ultimate strength of concrete at 28 days;
f_e	=	effective stress in prestressing tendon;
f_{su}	=	stress in prestressing tendon at ultimate load;
f_y	=	yield stress of steel;

- GJ = torsional rigidity of edge beam;
 $2H$ = $D_{xy} + D_{yx} + D_1 + D_2$ = torsional rigidity of waffle slab;
 h = thickness of plate deck;
 $I_{cx}(I_{cy})$ = moment of inertia of the concrete in compression about the neutral axis
 $[K]$ = element stiffness matrix;
 k = depth of compression stress block;
 k_1 = $c[(\sqrt{D_x D_y} + H)/2D_x]^{1/2}$;
 k_2 = $c[(\sqrt{D_x D_y} - H)/2D_x]^{1/2} + s$;
 k_3 = $c[(\sqrt{D_x D_y} - H)/2D_x]^{1/2} - s$;
 k_4 = $1/(k_1^2 + k_2^2)$;
 k_5 = $1/(k_1^2 + k_3^2)$;
 k_6 = $(s^4 D_x + 2s^2 c^2 H + c^4 D_y)/D_x$;
 ℓ = orthogonal width of waffle slab) bridge;
 M_B, M'_B = positive and negative ultimate moment of resistance of edge beam;
 M_x, M_y, M_{xy} = bending and twisting moments of x-y coordinate system per unit width;
 M_n = bending moment along outwardly drawn normal per unit width;
 M_1, M_2 = external bending moments due to prestressing;
 m, n = integers ≥ 1 = number of harmonics;
 $m_1(m_2)$ = ultimate positive (negative) moment of resistance about the x-axis per unit width;
 N = total number of harmonics;
 N_x, N_y, N_{xy} = in-plane forces per unit length;

$P(P_u)$	=	transverse concentrated (ultimate) load;
P_{us}	=	punching shear capacity;
p	=	Perimeter of concrete area surrounding punching collar;
$\{Q\}$	=	load vector in matrix form;
Q_x	=	shearing force of x-y coordinate system per unit width;
q	=	intensity of transverse load;
$q(q_u)$	=	intensity of transverse (ultimate load);
q_D	=	intensity of dead weight of waffle slab bridge;
R_i	=	reaction of column i;
s	=	$\sin \theta$;
$S_x(S_y)$	=	spacing of transverse (longitudinal) rib;
U	=	strain energy functional;
u, v	=	oblique coordinates;
V_x	=	reactive force of x-y coordinate system per unit width;
v_c	=	punching shear strength;
w	=	lateral displacement of waffle slab;
$w_e(w_i)$	=	external (internal) virtual work;
x, y, z	=	rectangular Cartesian coordinates;
α	=	slope of yield-line with x axis
$\bar{\alpha}$	=	the torsional rigidity parameter
$\alpha n(m)$	=	$n(m)\pi/a$;
β	=	reduction factor applied to f'_c ;
$\beta_{n(m)}$	=	$n(m)\pi/b$;
$\{\Delta\}$	=	deflection vector in matrix form;
Δ_i^s	=	prescribed settlement of column i;

- δ = virtual deflection;
 γ = length of yield line / (2b)
 m_2 (m_1) = ultimate negative (positive) moment of resistance about the y-axis per unit length;
 θ = skew angle;
 μ = Poisson's ratio of concrete;
 σ_x^*, σ_v^* = external in-plane prestressing stresses in direction of x and v axes, respectively.
 $\sigma_u, \sigma_v, \tau_{uv}$ = in-plane stress field; and
 ϕ = stress function.

xxvii

CHAPTER I

INTRODUCTION

1.1 General

In recent years reinforced concrete waffle slab constructions have been employed successfully in many buildings and other structures, resulting in reduced dead weight. The use of prestressed concrete waffle slabs for rectangular and skew decks of short and medium span bridges, as well as for marine structures, can also lead to substantial economies. Waffle slab structures possess not only aesthetic beauty but also excellent structural characteristics. Some of the most notable examples are: Houston's International Airport terminals (1) and Montreal's Olympic stadium. Comparative costing with other structural systems has demonstrated that waffle construction, among its other advantages, is economical. Recently, a feasibility study was undertaken to examine the suitability and the resulting economy thereof of adopting waffle slab construction for short and medium span bridges (2). The study showed that waffle construction is a more economical alternative to solid slab as well as to one-way girder and slab con-

struction for relatively wide bridges with skewed or irregularly shaped planform supported by randomly spaced isolated columns. A similar conclusion could be drawn, when a comparison is made between waffle and voided slab constructions.

The use of prestressed concrete waffle construction in deck bridges and marine structures can have the following advantages:

1. Reduction in dead load
2. Better live load distribution
3. Improved deck durability and considerable reduction in the cost of maintenance
4. Reduction in the dead load moment, thus minimizing the amount of secondary stresses produced by sustained loads

In modern design, with the increase in heavy vehicular loading on highway bridges, the load carrying elements of a structure are, in general, used to the limit of their capacity. This has given a stimulus to the study of cracks in waffle slab structures, which requires that the design be based on an inelastic analysis.

Available analytical methods of analysis are in conformance with the small-deflection theory of orthotropic plates. However, in order to ascertain their inherent overload-carrying capacity affected by changes in the

rigidities, redistribution of stresses and cracking of the concrete, a progressive failure analysis is required. Thus, a precise evaluation of the ultimate strength of waffle slabs will invariably enable the designer to achieve more improvements in design efficiency. It is now generally accepted that the understanding of any structure is incomplete unless its structural response beyond the elastic range is investigated.

1.2 Object and Scope

The overall objectives of this investigation are: predict the structural response of waffle slab structures in the inelastic range; to assess the effects of overloading, and to compute their ultimate load-carrying capacity. This study is concerned with the analytical and experimental investigations of reinforced and prestressed concrete waffle slab bridges, considering material nonlinearity due to concrete cracking. Simply supported and continuous slab models of rectangular and skew planforms are studied under lateral uniform and concentrated loads.

The main work embodied in this dissertation comprises:

- 1) An extension of the elastic series solution by Fourier series of simply supported slabs to waffle slab bridges continuous over interior isolated column-supports.

- 2) A verification of the elastic series solution, and the finite element method by experimental investigation on seven waffle slab bridge models.
- 3) . A prediction of the ultimate load capacity of waffle slab bridges based on the upper bound yield-line theory.
- 4) Prediction of the cracking and ultimate load as well as the crack pattern of waffle slab models by means of a progressive failure analysis using the finite element method.

The experimental investigation consisted of testing of seven one-eighth scale models of waffle bridge slabs. The first three models were reinforced concrete and simply supported on two edges; the second group were two post-tensioned concrete waffle slabs with straight tendons in two perpendicular directions. The last group were two continuous prestressed waffle slabs with curved tendons in the main direction and straight tendons in the transverse direction, supported over two interior isolated columns.

The contents of this study are arranged as follows:

Chapter II provides a background and review of some of the available literature in analyzing reinforced and prestressed concrete slab bridges subjected to working and ultimate load conditions.

Chapter III, presents two methods for the elastic analysis; the first method is based on the elastic series solution for simply supported slab bridges, and its extension for continuous slab bridges. The second method is based on the finite element method.

Chapter IV, deals with the ultimate analysis using the yield-line theory.

Chapter V, introduces the finite element approach coupled with an iterative technique for a progressive failure analysis.

Chapter VI, presents the experimental study and test procedures on seven slab bridge models.

Chapter VII, deals with the discussion of the theoretical and experimental results; and

Chapter VIII, presents the summary and conclusions.

CHAPTER II

BACKGROUND AND REVIEW OF LITERATURE

2.1 General

Load tests and analysis have been carried out on reinforced and prestressed concrete waffle slab decks for different reasons. An acceptance test, or proof loading of a new structure, has been the most common; while in some instances a structure, or part of a structure, has been loaded strictly for research purposes. In cases of proof loading of a structure, only the load and the deflections are measured. Test loadings were widely specified in the early part of the twentieth century for slab construction, because at that time there was no rational method for designing slabs.

This chapter presents the background for the present investigation which is divided mainly into three distinct analyses. One analysis is concerned with the working load behaviour, and the second with behaviour at failure (yield-line theory); the third analysis is the elastic-plastic solution (progressive failure analysis) which seeks to fill the gap between the first two analyses. Some of the problems and limitations associated with each analysis are

also described.

2.2 Elastic Analysis (Working Load)

Two methods are described herein; the first is concerned with an elastic series solution using the classical method of analysis and the second method uses the finite element analysis as a numerical approach.

2.2.1 Elastic Series Solution

2.2.1.1 Reinforced Concrete Slabs

Considerable attention has been given recently to develop methods of designing more economical concrete decks for bridges, buildings and marine structures. Concrete waffle slab structures have become quite popular in buildings (3), and deck bridges (4, 5). A recent study by Kennedy and Ghobrial (2) on waffle slab constructions, showed that waffle slab bridges, supported by isolated interior columns, are more economical, in terms of the required amount of steel reinforcement, than either the one-way ribbed or solid slab bridges. It was also concluded that the waffle slab system possesses other advantages such as: Reduction in dead load moment and deflection leading to minimizing the amount of secondary stresses, easy accessibility to parts of the structure for inspection and repair; and, the shallow depth of its cross-section.

Various methods of estimating the load distribution in concrete bridge decks have been proposed to date. In all these methods values of the effective flexural and torsional rigidities of the deck system are required before the analysis can proceed. Analysis and solution of many problems involving plates of different shapes have been proposed by Timoshenko (6), Szilard (7, 8) and Lekhnitskii (9).

In 1956, Huffington (10) investigated the method for the determination of rigidities for metallic rib-reinforced deck structures. It was applied to the case of equally spaced stiffeners, of rectangular cross-section, and symmetrically placed with respect to its middle plane.

Jackson (11) proposed a method to estimate the torsional rigidities of concrete bridge decks using the membrane analogy and the estimation of the junction effect; however, the effect of continuity of the slab was not accounted for. Recently, a study was conducted by Kennedy and Bali (12) to determine the precracking and postcracking rigidities of reinforced concrete slab structures of the waffle type.

Perry and Heins (13) presented a preliminary design for transverse floor beams in orthotropic deck bridges. The applied loads were represented in the form of a Fourier series. The method is not very accurate since it neglected the effects of the coupling rigidities that

arise from the Poisson's ratio. Cardens et al. (14, 15) investigated the in-plane and flexural stiffnesses of isotropically and nonisotropically reinforced concrete plates. While Bares and Massonnet (16) and Row (17) analyzed mathematically the grid systems with particular regard to the bridge type.

Methods of analyzing rectangular and skew deck plates with simple boundary conditions have been investigated by Kennedy et al. (18, 19, 20, 21, 22) and by El-Sebakhy (23). They solved the problem of a skew plate structure under uniform and concentrated loads using a series solution; both steel stiffened plates and concrete waffle slabs were included in the analysis; the results were verified with experiments. They observed that critical stresses often occur in the obtuse corners of such skew plate structures.

2.2.1.2 Prestressed Concrete Slabs

In the past, bridge design engineers have shied away from using prestressed waffle-slab construction simply because they considered it incompatible to the predominantly one-way supporting system of a bridge. In the late 1950's several prestressed slab research projects were undertaken. Scordelis et al., 1960 (24, 25), studied the ultimate strength of continuous prestressed slabs and

proposed several design recommendations. They investigated the load distribution between the columns and the middle strips. They concluded that the elastic plate theory may be used satisfactorily to predict the behaviour of prestressed concrete slabs loaded within the elastic limit and furthermore, that prestressed slabs can sustain a large increase in load before widespread cracking takes place.

Hondros and Smith (26) carried out a theoretical and experimental investigation of a post-tensioned diagrid flat plate simply supported on four sides; they used the Link Force Method of analysis which ignores the influence of torsion on the plate. Muspratt (27) investigated the load-carrying capacity of a prestressed waffle slab with unbonded tendons, and concluded that torsional stresses in the diagonals demand careful investigation.

Possibly the largest stride in the design of prestressed slabs was taken by Lin et al. (28, 29) who were the first to use post-tensioned waffle construction in a bridge; they used large precast concrete pans to form a waffle layout for the bridge deck; the dead load on the bridge was practically balanced by prestressing.

2.2.2 Finite Element Method (Working Load)

A variety of methods for the solution of plate problem have been used, but the most flexible one appears to be the

finite element method. It has been applied to a vast spectrum of engineering problems, including not only linear elastic problems, but also those with geometric and material nonlinearities as well as plates with irregular planforms.

A large number of publications, most of which have appeared since 1960, discuss the finite element method, particularly its application to structural mechanics [see Desai (30), and Zienkiewicz (31)].

More sophisticated finite element programs have been developed recently for solving plate problems. The most general of these is the STRAND (STRuctural ANalysis and Design) developed by University College, Swansea, Wales, U.K., and is maintained by the Highway Engineering Computer Branch, U.K. (32, 33). The program possesses only elastic analysis capability; for example, it cannot predict the ultimate load-carrying capacity as well as the cracking load of the structure. As part of this research the program was revised to accommodate a progressive failure analysis up to the ultimate load capacity of the structure.

2.3 Ultimate Load Analysis (Yield-Line Theory)

The yield-line theory was first initiated by Ingerslev (34) and substantially pioneered by Johansen (35). In 1953 Hognestad (36) summarized the development of the theory; anomalies in the theory were apparent and extensive research

continued resulting in the publications, by Wood (37), Jones (38), and Jones and Wood (39).

The yield-line theory is a limit design method which gives an upper-bound solution; therefore it is essential to ensure that the most critical collapse mechanism has been selected if the load-carrying capacity of the slab is not to be over-estimated. The method is not specifically recognized by the American Concrete Institute Code (40). However, the theory can be applied to almost any shape of slab, load and edge conditions as well as to slabs with irregular column spacing (41, 42), and slabs with edge beams (43).

The yield lines in concrete slab structures are formed by many cracks in the concrete surface. These cracks are among the most important consideration in the design of reinforced and prestressed concrete structures. Cracks of excessive width may be a source of danger due to the possibility of corrosive attack on the reinforcement especially if it is used in marine structures. In 1962-63 (44) a survey was carried out by researchers at the University of Illinois on crack formation in concrete structures. Clark (45, 46) designed slab bridges using the factored elastic moment field, and yield-line theory; from his study he concluded that, if a slab bridge is designed against collapse in accordance with the Draft British

Code of Practice (47) for Bridges then the crack widths can, in general, be controlled to values below the maximum permissible by limiting the spacing of the longitudinal reinforcement. When a high percentage of tensile reinforcement is used in slab bridges, further studies are needed to make a judicious choice of reinforcing bar spacing. Based on model studies, Clark concluded that the best qualitative similitude of the overall crack pattern is obtained when threaded rod reinforcements are used.

In 1962, Kemp (48) developed a lower bound solution to the collapse of a simply supported rectangular slab, orthotropically reinforcement and carrying a uniformly distributed load. The twisting moments were modified to produce positive yield moments at the corners. The solution was compared with the upper bound solution derived from the yield-line theory; it was found that the lower bound collapse loads were close to the upper bound values.

In 1964 Holmes (49), extended the work of Kemp and Wood by developing a lower bound solution to the collapse of a uniformly loaded isotropically-reinforced rectangular slab, with two opposite sides continuous and the other sides, simply supported. The solution was compared with the upper bound values, showing good agreement. A lower bound solution for a simply supported square slab was developed by Parkhill (50), based on the assumption of

an elastic-plastic behaviour of the slab material. It was shown that the elastic moments within the segments of a chosen yield-line pattern were everywhere statically admissible.

Wood (51) discussed the orientation of reinforcement in slabs as well as the quantity based on the predetermined field of moments. He found that using Hillerborg's rules for calculation of the reinforcement required for a slab may result in less steel than that required by the yield line theory.

Clark (52, 53, 54) extended the work of Wood and tested twelve uniformly loaded skew slabs and three skew highway bridges loaded with the Ministry of Transport Standard and Abnormal loadings (U.K.). He concluded that considerable economies in the total amount of steel required in a slab can be obtained by using an orthogonal arrangement of reinforcement. He also suggested that, if yield-line theory is to be incorporated into the limit state design of such bridges, the longitudinal steel should be designed to satisfy the limit state design of serviceability under both standard and abnormal loading; and, the transverse steel should then be designed by the yield-line theory for factored abnormal loading; see reference (55).

Some developments in yield-line theory were carried out in 1965 to determine the collapse mechanism for re-

inforced concrete slabs. Kemp (56) evaluated the nodal and edge forces for reinforced concrete slab by the yield-line theory. The forces were calculated by a differentiation process using a procedure similar to that employed in the virtual work method. Morley (57) obtained a sufficient condition for the least upper bound on the collapse load by considering upper-bound moment distributions for isotropic, homogeneous plates with eccentric square yield criterion and postulated straight-line yield mechanisms; this condition allowed a demonstration of the basis and limits of applicability of Johansen's equilibrium method. Morley concluded that the equilibrium method is not essentially confined to plates with the eccentric square criterion. Nielsen (58) presented a new nodal-force theory for isotropically reinforced slabs. He showed that agreement between the energy method, and the equilibrium method is possible in cases where a statically admissible moment field can be found in each part of the slab which satisfied the aforementioned condition. A comprehensive study on new techniques in nodal-force theory for slabs was presented by Wood (59), and a new set of rules for design was drawn up. Jones (60) discussed the work of Kemp, Morley, Nielsen and Wood to use the nodal forces in yield-line analysis with more emphasis on the differences of opinion between the four authors. He concluded that these differences were

mainly due to the discontinuity of load, discontinuous boundaries and discontinuous stress fields. Kwiecinski (61, 62) proposed a new yield criterion for reinforced concrete slabs based on partial kinking of the reinforcement. The yield criterion was verified by experimental work on sixteen model slabs with various arrangements of reinforcement. He neglected the effect of twisting moment along the yield lines, and concluded that the adopted design procedure could lead to economies in the amount of reinforcement required in some slabs. Such economies would probably be significant only in thin slabs, i.e., slabs with high span/depth ratios (recommended limit of 35). Taylor (63) studied the effect of the arrangement of reinforcement on the behaviour of reinforced concrete slabs by testing ten two-way simply supported concrete slabs. The slabs were designed to have similar ultimate loads, but different arrangements of the reinforcement were adopted. He concluded that, in slabs designed by normal plastic theories, the use of variably spaced bars would lead only to minimal economy, if any, compared with uniformly spaced bars; and, variably reinforced slabs were slightly stiffer than uniformly reinforced slabs over the load range up to the ultimate load. The influence of strength of edge beams on the formation of yield lines was also studied at the University of Illinois.

(64). Groups of tests were carried out on multiple panels of two-way slabs; a positive moment yield line developed near the mid-span in the exterior panels parallel to the outside edges and the failure extended across the interior and spandrel beams that formed perpendicular to the outside edge. However, it should be pointed out that, although the calculated failure load for this mode of failure closely matched the actual failure load, the structure did not fail in the mode the yield-line method had predicted. Failure of the individual slabs was indicated by theory at a load some 25% lower than the actual load.

In 1971, a set of tests were carried out on reinforced concrete slabs by Jain (65), at the University of Windsor to confirm the elastic-plastic solution, using the finite difference approximations. The elastic-plastic solution was applied to rectangular and skew concrete slabs. Problems of skew in bridge design were clarified by Kennedy and Tamberg (66) and the need for further research on the ultimate strength was required.

In 1976, Hughes (67), followed by Ferguson (68), presented the limit state theory for reinforced concrete design and resolved some of the earlier inconsistencies in the equilibrium methods due to the neglected membrane and corner effects.

Although an appreciable amount of work has been done

on the analysis of flat slabs, very little work is available on waffle slab construction using the yield line theory as a design method. While this approach theoretically would lead to an upper bound solution to the collapse load (35) it is shown later that the results obtained are quite close to the test results from seven bridge models.

2.4 Progressive Failure Analysis

Scanning through the aforementioned literature on the yield-line theory, it was concluded that some important aspects of the behaviour of waffle slab structures, such as deflections and the distribution of moments were left undefined, and therefore needed further exploration. The advent of the finite element method not only has made the linear analysis of such structures of general form under arbitrary loading and boundary conditions a relatively straightforward matter, but also it has inspired many successful attempts to deal with various material and geometrical nonlinear problems.

Successful application of the finite element method has been made to non-linear analyses of plates in flexure e.g., the works of Marcal et al. (69), Armen et al. (70), and Whang (71). However, these analyses were peculiar to metallic plates and specifically to metals that satisfy the Von-Mises criterion.

The earliest work on the non-linear behaviour of a concrete slab was carried out by Bhaumik and Hanley (72) who solved the plate equilibrium and moment-curvature relationships by converting them into finite difference form; the applications of Johansen's, Tresca's and Von-Mises yield criteria were examined. Later, McNeice and Kemp (73) developed an interesting technique for the analysis of reinforced concrete slabs, using a finite element approach together with the assumption of an elastic-perfectly-plastic behaviour of the concrete and using a square yield criterion. Jofriet et al. (74) used a step-by-step procedure, incorporating the change in rigidity of each region, cracked or uncracked, under increasing load. Bell et al. (75) described a theoretical model based on the use of anisotropic finite elements, and a successive approximation technique.

Przemieniecki and Desai (76, 33) presented a comprehensive study on non-linear material and geometrically nonlinear problems using the finite element technique. The question of nonlinearities arising from material properties was discussed and methods were developed to allow for the standard linear forms to be used in an iterative way to obtain solutions.

CHAPTER III

ELASTIC BEHAVIOUR OF CONCRETE WAFFLE

SLAB STRUCTURES

3.1 Introduction

To meet the design requirement for the ultimate limit states of concrete waffle slab structures, their response to load intensity causing eventual collapse should be examined and predicted. It is necessary to study first the behaviour of a structure at working load and before cracking of the concrete (serviceability limit states). This problem, applied to simply supported bridges, was investigated by the author earlier (23), however, for continuity to the present work the method of analysis used in reference (23) is presented briefly herein.

3.2 Elastic Series Solution for Simply Supported Slabs

An analytical solution to post-tensioned waffle slab bridges is obtained by superimposing a bending analysis to an in-plane stress analysis, assuming no coupling; experience has shown that such an uncoupled analysis is quite valid when the deflection of a structure is relatively small.

3.2.1 Bending Analysis

The following assumptions are made with respect to waffle-slab construction:

1. The number of ribs is large enough for the real structure to be replaced by an idealized one with continuous properties, Fig. 3.1.
2. The neutral plane in each of the two orthogonal directions coincides with the center of gravity of the total section in the corresponding direction, Fig. 3.2.
3. The area of the flange plate is magnified by the factor $1/(1-\mu^2)$ to allow for the influence of Poisson's ratio (μ).

Past experiences have shown that the foregoing assumptions are valid in practice. The differential equation governing the lateral deflection, w , of a bent orthotropic slab (6) can be expressed in skew coordinates (u, v), Fig. 3.3, as

$$\begin{aligned} D_x w_{,uuuu} - E_1 w_{,uuuv} + E_2 w_{,uuvv} - E_3 w_{,uvvv} + E_4 w_{,vvvv} \\ = c^4 q(u,v) \end{aligned} \quad (3.1)$$

in which

D_x = flexural rigidities of the slab per unit width
in the x direction.

D_y = flexural rigidities of the slab per unit width
in the y direction

$$E_1 = 4 s D_x$$

$$E_2 = 2 (3 D_x s^2 + H c^2)$$

$$E_3 = 4 s (D_x s^2 + H c^2)$$

$$E_4 = D_x s^4 + 2 H s^2 c^2 + D_y c^4$$

$$c = \cos \theta, s = \sin \theta, \theta = \text{skew angle}$$

$$u = x \sec \theta$$

$$v = y - x \tan \theta$$

$$2H = D_{xy} + D_{yx} + D_1 + D_2$$

where

D_{xy}, D_{yx} are the transverse and longitudinal torsional rigidities per unit width, respectively, D_1 and D_2 are the coupling rigidities arising from the Poisson ratio effect.

$q(u,v)$ is the intensity of lateral load.

The solution to Eq. 3.1 can be expressed in the form

(21):

$$\begin{aligned} W = & \sum_{n=1}^{\infty} [C_{1n} \text{ch } k_1 \beta_n u + C_{2n} \text{sh } k_1 \beta_n u] \cos (k_2 u + v) \beta_n \\ & + (C_{3n} \text{ch } k_1 \beta_n u + C_{4n} \text{sh } k_1 \beta_n u) \sin (k_2 u + v) \beta_n + (C_{5n} \text{ch } k_1 \beta_n u \\ & + C_{6n} \text{sh } k_1 \beta_n u) \cos (k_3 u - v) \beta_n + (C_{7n} \text{ch } k_1 \beta_n u + C_{8n} \text{sh } k_1 \beta_n u) \\ & \sin (k_3 u - v) \beta_n + (C_{9n} \text{ch } k_4 k_1 \alpha_n v + C_{10n} \text{sh } k_4 k_1 \alpha_n v) \\ & \cos (k_4 k_2 v + u) \alpha_n + (C_{11n} \text{ch } k_4 k_1 \alpha_n v \end{aligned}$$

$$\begin{aligned}
& + C_{12n} \operatorname{sh} k_4 k_1 \alpha_n v) \sin(k_4 k_2 v + u) \alpha_n + (C_{13n} \operatorname{ch} k_5 k_1 \alpha_n v \\
& + C_{14n} \operatorname{sh} k_5 k_1 \alpha_n v) \cos(k_5 k_3 v - u) \alpha_n + (C_{15n} \operatorname{ch} k_5 k_1 \alpha_n v \\
& + C_{16n} \operatorname{sh} k_5 k_1 \alpha_n v) \sin(k_5 k_3 v - u) \alpha_n] \\
& + C_{17} + C_{18} \left(\frac{u}{a}\right) + C_{19} \left(\frac{v}{b}\right) + C_{20} \left(\frac{u}{a}\right)^2 \\
& + C_{21} \left(\frac{v}{b}\right)^2 + C_{22} \left(\frac{u}{a}\right)^3 + C_{23} \left(\frac{v}{b}\right)^3 + C_{24} \left(\frac{k_6 u^4 - v^4}{b^4}\right) \\
& + c^4 a_0 \frac{\frac{v^4}{24} - \frac{v^2 b^2}{4} + \frac{5b^4}{24}}{4E_4} + \sum_{m=1}^{\infty} (T_{1m} \cos \alpha_m u \\
& + T_{2m} \sin \alpha_m u) \\
& + \sum_{n=1}^{\infty} (T_{3n} \cos \beta_n v + T_{4n} \sin \beta_n v) + \sum_{m=1}^{\infty} \sum_{n=1}^{\infty} (T_{5mn} \\
& \cos \alpha_m u \cos \beta_n v \\
& + T_{6mn} \sin \alpha_m u \cos \beta_n v + T_{7mn} \cos \alpha_m u \sin \beta_n v \\
& + T_{8mn} \sin \alpha_m u \sin \beta_n v) \tag{3.2}
\end{aligned}$$

in which $k_1 = c[(\sqrt{D_x D_y} + H)/2D_x]^{1/2}$; $k_2 = c[(\sqrt{D_x D_y} - H)/2D_x]^{1/2} + s$; $k_3 = c[(\sqrt{D_x D_y} - H)/2D_x]^{1/2} - s$; $k_4 = 1/(k_1^2 + k_2^2)$; $k_5 = 1/(k_1^2 + k_3^2)$; $k_6 = E_4/D_x$; $\operatorname{ch} \equiv \cosh$; $\operatorname{sh} \equiv \sinh$; $\alpha_n = n\pi/a$; $\beta_n = n\pi/b$; $C_{1n}, \dots, C_{16n}, C_{17}, \dots, C_{24}$ = arbitrary constants; and $a_0, T_{1m}, \dots, T_{3n}, \dots$

T_{8mn} = constants determined from the particular integral of the governing differential equation (21). The solution given by Eq. 3.2 is applicable to torsionally soft and flexurally stiff slab classification, i.e., $H^2 \leq D_x D_y$. The constants $C_{1n}, \dots, C_{16n}, C_{17}, \dots, C_{24}$ are found by satisfying the boundary conditions.

3.2.1.1 Boundary Conditions

For a simply supported post-tensioned waffle slab bridge, Fig. 1, the following boundary conditions must be satisfied:

Simply supported edges, $v = \pm b$ and $-a \leq u \leq a$

$$w = 0 \quad (3.3)$$

$$\text{and } M_n = M_1 \quad (3.4)$$

Elastically supported edges, $u = \pm a$ and $-b \leq v \leq b$

$$V_x = Q_x - M_{xy,y} = -EIw_{,yyyy} \quad (3.5)$$

$$\text{and } M_x = GJw_{,xyy} + M_2 \quad (3.6)$$

For a free edge, Eqs. (3.5) and (3.6) become

$$V_x = 0 \quad (3.7)$$

$$M_x = M_2 \quad (3.8)$$

in which M_x and M_{xy} = bending and twisting moments of the xOy coordinate system; V_x = Kirchhoff edge reaction; Q_x = shearing force of the xOy coordinate system; EI and GJ = flexural and torsional rigidities of the elastic support, respectively; M_n = the moment along the normal n to the

edges $v = \pm b$; and M_1 and M_2 = the external moments due to prestressing forces normal to the edges $v = \pm b$ and $u = \pm a$, respectively. The constants in Eq. 3.2 are found by satisfying the boundary conditions (Eqs. 3.3-3.6). Advantage is taken of quadrant symmetry by dividing any loading into polar symmetric and antisymmetric components. For a symmetric loading state, all odd terms in Eq. 3.2 vanish, while for the antisymmetric loading state, all even terms vanish. The number of constants in Eq. 3.2 is thus reduced from 24 to 12 for either of the two loading cases. For N number of harmonics in Eq. 3.2, a matrix equation of dimension $8N + 4$ is generated from the four boundary conditions along two adjacent edges. The coefficients of the solution matrix equation can be found elsewhere (23). The solution of this matrix equation for each of the two loading states yields the arbitrary constants and therefore the deflection function, w , the bending and twisting moments, and the stresses and strains can then be calculated, e.g., the bending strains ϵ_x and ϵ_y are determined from the moments M_x and M_y and in terms of the rigidities, D_x , D_y , D_1 , D_2 and M_{xy} in terms of D_{xy} as follows (23):

$$\epsilon_x = \frac{z(M_x D_y - M_y D_1)}{(D_x D_y - D_1 D_2)} \quad (3.9a)$$

$$\epsilon_y = \frac{z(M_y D_x - M_x D_2)}{(D_x D_y - D_1 D_2)} \quad (3.9b)$$

$$\gamma_{xy} = \frac{zM_{xy}}{D_{xy}} \quad (3.9c)$$

in which z = the vertical distance from a fiber to the neutral axis of the section; a typical geometry for a waffle slab construction is shown in Fig. 3.2.

3.2.1.2 Flexural and Torsional Rigidities

In order to predict accurately the response of waffle slab bridges to applied load, it is essential that the designer use realistic estimates of the rigidities of the structure (Fig. 3.2). Recently Kennedy and Bali (12) deduced analytical expressions for the various rigidities for both the precracking and postcracking stages; the results were verified by experimental tests. Such expressions for the rigidities have been employed in the analysis presented herein.

3.2.2 In-Plane Stress Analysis

Fig. 3.3a shows a waffle slab bridge subjected to external in-plane prestressing stresses at its edges, σ_x^* and σ_y^* ; these stresses can be more conveniently represented by Fourier series if they are assumed to act as shown in Fig. 3.3b. Thus one can write, for the stresses along the edges $u = 0$ and $u = 2a$

$$\sigma_x^* = \sum_{m=1}^{\infty} A_m \sin \frac{m\pi y}{l} \quad (3.10)$$

in which $\ell = 2b + 2a \sin \theta$

$$\text{and } \sigma_v^* = \sum_{n=1}^{\infty} B_n \sin \frac{n\pi u}{a} \quad (3.11)$$

for the stresses along the edges $v = 0$ and $v = 2b$. The in-plane stress field in skew coordinates u, v can be represented as

$$\sigma_u^* = \sigma_u^0 + \sigma_x^* \sec \theta \quad (3.12a)$$

$$\sigma_v = \sigma_v^0 + \sigma_v^* + \sigma_x^* \sin \theta \tan \theta \quad (3.12b)$$

$$\tau_{uv} = \tau_{uv}^0 - \sigma_x^* \tan \theta \quad (3.12c)$$

in which the stress system $[\sigma_u^0, \sigma_v^0, \tau_{uv}^0]$ is determined from

$$\sigma_u^0 = \phi_{,vv}; \quad \sigma_v^0 = \phi_{,uu}; \quad \tau_{uv}^0 = -\phi_{,uv} \quad (3.13)$$

where ϕ = an appropriate stress function, found by applying the virtual work principle to the strain energy functional

$$U = \frac{1}{2} \int_0^{2a} \int_0^{2b} [c_{11}\sigma_u^2 + 2c_{12}\sigma_u\sigma_v + 2c_{13}\sigma_u\tau_{uv} + c_{22}\sigma_v^2 + 2c_{23}\sigma_v\tau_{uv} + c_{33}\tau_{uv}^2] du dv \quad (3.14)$$

in which c_{ij} = the elastic compliances referred to the u - v system of axes and which can be found in terms of the waffle slab in-plane stiffnesses in the x - y system by applying the usual transformations. Once the stresses σ_u , σ_v and τ_{uv} are

found, the inplane stresses σ_x , σ_y and τ_{xy} are determined by the following transformation:

$$\begin{Bmatrix} \sigma_x \\ \sigma_y \\ \tau_{xy} \end{Bmatrix} = \begin{bmatrix} \sec \theta & \sin \theta \cos \theta & 2 \tan \theta \\ 0 & \cos \theta & 0 \\ 1 & \sin \theta & 1 \end{bmatrix} \begin{Bmatrix} \sigma_u \\ \sigma_v \\ \tau_{uv} \end{Bmatrix} \quad (3.15)$$

The corresponding strains are found from

$$\epsilon_x = \frac{(A_{22}\sigma_x - A_{12}\sigma_y)}{(A_{11}A_{22} - A_{12}^2)} \quad (3.16a)$$

$$\epsilon_y = \frac{(A_{11}\sigma_y - A_{12}\sigma_x)}{(A_{11}A_{22} - A_{12}^2)} \quad (3.16b)$$

$$\text{and } \tau_{xy} = \frac{\tau_{xy}}{A_{33}} \quad (3.16c)$$

in which $[A]$ = the equivalent in-plane rigidity matrix of the waffle slab in the x-y system.

3.2.2.1 In-Plane Axial Rigidities

To deduce the rigidity matrix $[A]$, it is assumed that:

- (1) The in-plane strains in the flange plate element (deck) are equal to those in the ribs (beams); and (2) the in-plane shearing stresses are resisted by the flange plate element alone. Thus the in-plane forces per unit length in the flange plate of thickness h , Fig. 3.2 are

$$(N_x)_p = h\sigma_x = \frac{hE(\epsilon_x + \mu\epsilon_y)}{(1-\mu^2)} \quad (3.17a)$$

$$(N_y)_p = h\sigma_y = \frac{hE(\epsilon_y + \mu\epsilon_x)}{(1-\mu^2)} \quad (3.17b)$$

$$(N_{xy})_p = h\tau_{xy} = hG\gamma_{xy} \quad (3.17c)$$

in which E and G = the elastic and shear moduli of the concrete, respectively.

For the same strains in the ribs (beams), the in-plane forces in the ribs (Fig. 3.2) per unit length can be written as:

$$(N_x)_r = \frac{Eb_x(d-h)\epsilon_x}{S_x} \quad (3.18a)$$

$$= \frac{Eb_y(d-h)\epsilon_y}{S_y} \quad (3.18b)$$

$$(N_{xy})_r = 0 \quad (3.18c)$$

in which \bar{d} = total depth of the section; $b_y(b_x)$ = width of longitudinal (transverse) rib; and $S_y(S_x)$ = spacing of longitudinal (transverse) rib.

Thus, the total in-plane forces per unit length of the section become

$$N_x = (N_x)_p + (N_x)_r, \text{ etc.} \quad (3.19)$$

or, in matrix notation

$$\begin{Bmatrix} N_x \\ N_y \\ N_{xy} \end{Bmatrix} = h \begin{bmatrix} A_{11} & A_{12} & 0 \\ A_{21} & A_{22} & 0 \\ 0 & 0 & A_{33} \end{bmatrix} \begin{Bmatrix} \epsilon_x \\ \epsilon_y \\ \gamma_{xy} \end{Bmatrix} \quad (3.20)$$

in which $[A]$ = the equivalent in-plane rigidity matrix of the waffle slab given by: $A_{11} = E[(1/l - \nu^2) + b_x(d - h)/(h S_x)]$; $A_{12} = A_{21} = (\nu E)/(1 - \nu^2)$; $A_{22} = E[1/(1 - \nu^2) + b_y(d - h)/(h S_y)]$; and $A_{33} = G$.

The final results for post-tensioned waffle slabs are obtained by appropriate superposition, thus, deflections and moments are found from the bending analysis alone (by virtue of the uncoupling assumption), while total stresses and strains are derived from the bending and in-plane analyses, e.g., total strains are found by combining Eqs. 3.9 and 3.16.

3.3 Elastic Series Solution for Continuous Slabs (Influence Lines)

The analytical solution presented herein for simply supported slab of rectangular and skew plan form can be readily extended to prestressed concrete waffle slab bridges continuous over line piers by superimposing the in-plane solution, in Section 3.2.2, and the bending solution for continuous orthotropic slab bridges presen-

ted by Gupta and Kennedy (77); this latter solution is adjusted to accommodate the boundary conditions for the moments at the simply supported edges and at the free edges due to the prestressing, as well as to account for the varying profile of prestressing steel by means of equivalent uniformly distributed loading (2).

For several reasons, waffle slab construction in highway bridges, buildings and marine structures are quite often supported by isolated interior columns. To arrive at a solution for such bridges of prestressed waffle slab construction, the column reactions need to be evaluated first; this can be performed as follows:

(a) Remove all column reactions, R_i ($i = 1, \dots, r$); apply the external load, q , to the simply supported prestressed waffle slab bridge and calculate the slab deflections at the center of the column positions, i.e., calculate $w_1^q, w_2^q, \dots, w_r^q$ from Eq. (3.2). The load q may be due to dead load plus the equivalent load due to prestressing or it may include also the applied live load. If the transverse and longitudinal prestress along the edges are eccentric, then the edge moments due to prestressing, M_1 and M_2 , will appear in the boundary Equations (3.4) and (3.6)

(b) Apply consecutively a unit load over the area of each column, say j , and determine by means of Eq. 3.2,

in each of such loading, the deflection of the waffle slab at the center of column i , i.e., w_{ij} , putting $M_1 = 0$ in Eq. (3.4) and $M_2 = 0$ in Eq. (3.6).

(c) Allow for prescribed settlement Δ_i^s of column i , and for its elastic deformation $R_i D_i$, in which

D_i = the specified flexibility of column i .

(d) Write the following compatibility equation for deflection of the waffle slab at the center of column i position:

$$\sum_{i=1}^r \sum_{j=1}^r [R_j (w_{ij} + D_i \delta_{ij}) + \Delta_i^s - w_i^q] = 0 \quad (3.21)$$

in which

δ_{ij} = the Kronecker delta, i.e., $\delta_{ij} = 1$ when $i = j$ and $\delta_{ij} = 0$ when $i \neq j$ or, in matrix form

$$\begin{bmatrix} (w_{11}+D_1) & w_{12} & w_{1r} \\ w_{21} & (w_{22}+D_2) & w_{2r} \\ \vdots & \vdots & \vdots \\ w_{r1} & w_{r2} & (w_{rr}+D_r) \end{bmatrix} \begin{bmatrix} R_1 \\ R_2 \\ \vdots \\ R_r \end{bmatrix} = \begin{bmatrix} w_1^q - \Delta_1^s \\ w_2^q - \Delta_2^s \\ \vdots \\ w_r^q - \Delta_r^s \end{bmatrix} \quad (3.22)$$

Solving the above equation will yield the column reactions, R_1, \dots, R_r . Having found the reactions, the pre-

stressed waffle slab bridge can be analyzed for the effect of total loading, e.g., dead load + equivalent load due to the prestressing steel profile + live load + column load treated as upward patch loads; or, dead load + equivalent load due to the prestressing steel profile + upward patch loads due to the column reactions. Once the bending solution is obtained it is superimposed on the in-plane stress solution to yield the final stresses for design.

3.4 Elastic Finite Element Analysis

3.4.1 General

The use of the digital computer has greatly widened the scope of the analytic techniques available such as the finite element method. The finite element program STRAND, which has been tested extensively and is available at the Ministry of Transportation and Communication, Ontario, analyzes reinforced and prestressed concrete slab bridge structures. The user has to specify the percentage losses due to wobble, friction, etc., at various positions along the cable. However, in this work, prestressing losses are not considered.

3.4.2 Scope and Definition of the STRAND Program

The STRAND program is written in FORTRAN IV and is designed to operate on computers having a core equivalent

of 32K (24 bit word) or greater. It is a complex computer program for the analysis and design of isotropic and orthotropic slab systems; the analysis is based on the finite element technique using triangular elements. The STRAND program consists of seven sub-programs: FECK2, IPUT2, LOAD, SAADS, OPUT2, PPUT and SPUT. These sub-programs are combined together with a flexible flow chart that can accommodate readily different paths depending on the nature of the problem at hand. These sub-programs are described below:

FECK2: Checks the input data for IPUT2

IPUT2: Generates binary or formatted data files for analysis by SAADS

LOAD: Calculates equivalent nodal load data for uniformly distributed loads, beam loads, knife edge loads, and concentrated loads. It also can produce the equivalent nodal load data either on punched cards or as a full binary file of all the finite element data.

SAADS: Carries out finite element plate bending and plane stress analysis due to lateral and in-plane loads. It also carries out finite element plate bending and plane stress analysis due to prestressing loads using triangular plate elements. The input data may be a formatted set of data or

in the form of a binary file. A binary file of results may be made.

OPUT2: Used for the design of reinforced concrete slabs. Produces the reactions accompanying the moment fields.

PPUT: Generates a binary file of finite element data from prestressing cable loading data and the finite element mesh data OUTPUT by IPUT2. Two distinct sets of data are prepared, one for an in-plane analysis and the other for a plate-bending analysis.

SPUT: Used for the design of prestressed concrete slab structures and processes the results file of either a prestressing analysis by SAADS or the file of both a prestressing analysis and normal loading analysis produced by SAADS. Factored combination of prestressing and normal loadings can be made.

The program IPUT2 automatically generates the finite element mesh and nodal co-ordinates for regular deck shapes or any shape which can be defined by a series of straight lines called generators. The program also generates the nodal loading data for different loading cases.

The effect of prestressing upon a waffle slab structure can be separated into two independent effects. These

are the out-of-plane bending due to the cable eccentricities in elevation and the in-plane stresses due to the cable forces. The STRAND program can deal with straight and curved tendons in the elevation, and the prestressing forces are taken as external forces at the nodes. The analysis of the structure under the in-plane and out-of-plane prestressing loads is carried out by program SAADS using triangular and beam elements, Fig. 3.4 for both the plane stress and plate bending analysis. The program SAADS also carries out the plate bending analysis due to normal loadings such as dead weight, live load, etc. A feature of SAADS is its ability to store the element stiffnesses of the structure for future runs.

Fig. 3.5 shows the flow chart of the STRAND program and the relationships of the various programs to each other. Table 3.1 shows the limitations on the size of problem which may be handled by the STRAND program.

The program assumes the right-handed global coordinate system, Fig. 3.6a, which is usually oriented so that the origin is at one corner of the bridge deck. The positive x-direction is then usually taken as being parallel or tangential to the length of the bridge, and the y-direction is taken across the bridge deck. The z-direction is then defined as being positive downwards. The sign conventions adopted for the nodal forces and displacements

and stress resultants for plate bending and plane stress analysis are shown in Fig. 3.6b.

3.4.3 Analysis by SAADS Program

The finite element method is an approximate analytical tool. Its accuracy depends on the mesh size and the type of element used as the basic unit of the mesh. Figures 3.7 and 3.8 show some typical meshes that are generated throughout this study to analyze different problems in slab structures.

The analysis is performed by using non-conforming triangular plate bending or plane stress elements. Beam elements can also be included in both types of analysis but these are assumed to be concentric with the neutral axis of the slab. In the plate bending analysis three degrees of freedom are considered at each node, namely W , W_x , and W_y ; for the plane stress analysis two degrees of freedom u and v are assumed at each node; see Figs. 3.9a and 3.9b.

If the problem involves the analysis of a prestressed concrete structure, then PPUT may be used in addition to generate the loads from the prestressing cables. The data required when using SAADS includes the nodal coordinates and element topology, material properties, boundary conditions and applied loads.

The output from SAADS is similar for both plate bending and plane stress and consists of the nodal displacements and reactions at both fixed and elastic boundaries for each load case. For plate bending the centroidal or nodal averaged moments and principal moments are produced, while for plane stress it is the in-plane stresses and principal stress which are printed out.

Once the input data has been read in, the computer forms the element stiffnesses which are then transferred into global coordinates and stored. The solution procedure recalls the element stiffnesses from disk and forms the overall structural stiffness matrix and then carries out a banded Gaussian elimination process. During this operation the boundary conditions are imposed and the equations are modified and stored on file ready for back substitution. The current load vector is modified and multiplied by the modified stiffness equations and thus the nodal displacements and reactions are found. From these displacements the stresses and moments, etc., in each element are calculated.

CHAPTER IV

YIELD LINE THEORY FOR WAFFLE SLAB STRUCTURES (ULTIMATE ANALYSIS)

4.1 Introduction

The yield line theory is a plastic theory for the prediction of ultimate flexural strength of concrete slab structures, and can be successfully applied even to complex slabs, with limited mathematical effort. The yield lines, or the crack pattern locations depend on the loading position as well as on the boundary conditions.

The terms positive and negative yield lines are often used to distinguish between yield lines giving tension in the bottom fibre of a slab and those giving tension in the top fibre of a slab.

When such a slab is overloaded beyond the cracking load, yielding will begin in regions of high stresses, and as loading continues, yield lines will form and spread into a crack pattern. The load carrying capacity of the slab will be reached when the yield line has spread to the slab edges, at which load the slab reaches a state of neutral equilibrium.

4.2 Assumptions for Prediction of a Yield-Line Pattern

The following general assumptions assist in the prediction of the yield-line pattern for any slab:

1. Yield lines terminate at a slab boundary.
2. Yield lines are straight (it should be noted, however, that for some systems of concentrated loads or circular supports a multiple system of yield lines can approximate a single curved yield line, in the form of a fan mechanism).
3. Yield lines pass through the intersection of the axes of rotation of adjacent slab elements, and,
4. Axes of rotation generally lie along lines of supports and pass over columns.

4.3 Ultimate Load Analysis

The Ultimate Load Method of analysis is extremely useful as:

1. A check on the elastic analysis and hence the derivation of a load factor for the design loads.
2. A design procedure to determine the cross-sectional geometry and reinforcing or prestressing steel requirements for the structure.

The ultimate load analysis is based on a postulated yield-line pattern with the application of either the virtual work or Johansen's "equilibrium" method. In this

dissertation the virtual work method has been adopted and the results checked by the equilibrium method.

When an admissible yield-line pattern is completely formed only an "infinitesimal" increase in load is required to cause the structure to collapse. By the principle of virtual work, the work done on the slab by the loads equals the work done against the yield lines as they rotate. Hence, if a point on the slab is given a virtual deflection, δ , displacements in the form of rotations compatible with this deflection must take place along the yield lines. The internal work done on the slab is the sum of the rotations in the yield lines multiplied by the resisting collapse moments. The external work done by the loads is the sum of the loads multiplied by their respective deflections. Equating the internal and external work gives the relation between the collapse resistance moments in the slab and the collapse load.

The ultimate moment can be readily calculated if the position and magnitude of the center of pressure of the compressive stress block can be defined. According to the ACI code and Ferguson (68), the stress distribution is taken as shown in Fig. 4.1. Equating the longitudinal forces in Fig. 4.1 yields:

$$A_s f_y = \beta f'_c (S) (k)$$

$$k = A_s f_y / \beta f'_c S \quad (4.1)$$

$$M_u = A_s f_y (d - k/2) \quad (4.2)$$

where

$\beta = 0.85$ for $f'_c = 30$ MPa (4 ksi) or less for $f'_c > 30$ MPa (4 ksi), the factor β is reduced linearly at the rate of 0.05 per 7 MPa (1 ksi) excess over 30 MPa (4 ksi), but not to any value less than 0.65

A_s = area of steel in mm^2

f_y = yield stress of the steel in MPa

f'_c = ultimate strength of concrete at 28 days in MPa

M_u = ultimate moment of the section in MPa.

S = spacing between the ribs in mm, and

k = the depth of the compression stress block in mm.

It should be noted that the primary cause of failure is either the yielding of the steel or the crushing of the concrete. Any given failure mechanism establishes an upper limit on the collapse load and the real collapse load is the smallest one that can be found from all possible mechanisms.

4.4 Yield Moment on Axes Not Perpendicular to Reinforcing

When there is no twisting moment and the yield moments in the two perpendicular directions are equal, the yield moments in all directions are equal. Hognestad (36) showed [following Johansen's demonstration (35)] that when the

reinforcement in one direction differs from that in a perpendicular direction by some constant ratio, the slab dimensions can be modified to permit analysis as an isotropic slab. Such cases will not be considered in this work.

If m_x is the yield moment about the x-axis and m_y about the y-axis, the yield moment about an axis at an angle α with the x-axis will be

$$\begin{aligned} m_\alpha &= m_x \cos^2 \alpha + m_y \cos^2 (90 - \alpha) \\ &= m_x \cos^2 \alpha + m_y \sin^2 \alpha \end{aligned} \quad (4.3)$$

when $m_x = m_y = m$,

$m_\alpha = m$ as stated before.

4.5 Correction Forces for the Equilibrium Method

Correction forces appear when a yield line intersects a free edge at other than a 90° angle. These correction forces substitute for twisting moments along assumed yield lines and for normal shears which exist at negative moment yield lines. They are internal forces, appearing on the free body diagram only, and act normal to the plane of the slab with magnitude

$$m_t = m \cot \alpha \quad (4.4)$$

where

α = is the angle between the yield line and the free edge.

4.6 Effect of Four Concentrated Loads on the Yield-Line Pattern (Wheel Truck)

It is obvious that a single concentrated load is more critical than four concentrated loads. Under the action of several concentrated loads there will be at least more than a single yield-line, resulting in a higher ultimate moment capacity for the slab. However, the study in this dissertation is based on a single concentrated load.

Based on previous experience and on the test results from seven concrete waffle slab bridge models, it was possible to consider the most probable yield-line crack patterns of failure for the most common and critical loading conditions on the deck. While this approach theoretically would lead to an upper bound solution to the collapse load (35), it is shown later that the results obtained are quite close to the test results.

4.7 Simply Supported Waffle Slabs

4.7.1 Skew Waffle Slab Bridge Under Uniformly Distributed Load

Figure 4.2 shows a simply supported skew waffle slab bridge with relatively weak edge beams; the assumed single line failure crack pattern (fg), intercepting the edge

beams is also shown. Past experience and observations of the crack patterns of the tested models suggest that the failure line (fg) will be inclined to the x-axis an angle of approximately $\theta/2$. At collapse it is assumed that the failure line (fg) deflects downward a distance δ ; while this assumption leads to variable rotations of the parts of the bridge at failure, however, working with average rotations will give the correct answer. It can be shown that the external and internal virtual works, W_e and W_i , respectively, are

$$W_e = (2b\ell)q \left[\left(3b - \frac{\ell}{2} \tan \frac{\theta}{2} \right) \delta / 6b \right] \quad (4.5)$$

$$\begin{aligned} W_i = & 2m_1 (\ell) (\delta/b \cos \theta) \cos \theta/2 + 2 \, vm_1 \\ & (\ell \tan \frac{\theta}{2}) (\delta/b \cos \theta) \sin \frac{\theta}{2} \\ & + 2M_B \left[\frac{\delta}{b - \frac{\ell}{2} \tan \frac{\theta}{2}} + \frac{\delta}{b + \frac{\ell}{2} \tan \frac{\theta}{2}} \right] \end{aligned} \quad (4.6)$$

in which m_1 (vm_1) = ultimate positive moment of resistance per unit width (length) about the x-axis (y-axis); $(2b)$ and ℓ are, respectively, the span and orthogonal width of the waffle slab bridge; and, M_B = ultimate moment of resistance of the edge beam (resisting a sagging moment).

Equating W_e to W_i and rearranging will yield the fol-

lowing expression for the ultimate collapse load q_u :

$$q_u = 6 [m_1 (\cos^2 \frac{\theta}{2} + \nu \sin^2 \frac{\theta}{2}) / b \cos \theta \cos \frac{\theta}{2} + 2 M_B b / \ell (b^2 - \frac{\ell^2}{4} \tan^2 \frac{\theta}{2})] / (3b - \frac{\ell}{2} \tan \frac{\theta}{2}) \quad (4.7)$$

For a rectangular bridge, with $\theta = 0$, Eq. 4.7 reduces to

$$q_u = 2(m_1 + 2M_B/\ell)/b^2 \quad (4.8)$$

It should be noted that in waffle slab bridge construction, generally the edge beams are relatively weak; however, for relatively strong edge beams an X-type failure pattern is more likely to develop (38). For no edge beams, Eq. 4.7 yields

$$q_u = 6m_1 (\cos^2 \frac{\theta}{2} + \nu \sin^2 \frac{\theta}{2}) / [b \cos \theta \cos \frac{\theta}{2} (3b - \frac{\ell}{2} \tan \frac{\theta}{2})]; \quad (4.9)$$

and, for a rectangular bridge with no edge beams, Eq. 4.8 reduces to

$$q_u = 2m_1/b^2 \quad (4.10)$$

4.7.2 Skew Waffle Slab Bridge Under Concentrated Load at Center

For this case it is assumed that the failure pattern

is that of Fig. 4.2. Taking q_D as the superimposed load (including dead load) on the bridge per unit area, and P_u as the ultimate concentrated load at center causing collapse, the external and internal virtual works due to the various loads and displacement δ can be shown to be:

$$W_e = P_u \delta + 2b\ell q_D \left[\left(3b - \frac{\ell}{2} \tan \frac{\theta}{2} \right) \delta / 6b \right] \quad (4.11)$$

$$\begin{aligned} W_i = 2m_1 \ell \left(\delta / b \cos \theta \right) & \left\{ \cos \frac{\theta}{2} + 2m_1 \left(\ell \tan \frac{\theta}{2} \right) \right. \\ & \left. \left(\delta / b \cos \theta \right) \left[\sin \frac{\theta}{2} + 2M_B \left[\frac{\delta}{b - \frac{\ell}{2} \tan \frac{\theta}{2}} \right] \right. \right. \\ & \left. \left. + \frac{\delta}{b + \frac{\ell}{2} \tan \frac{\theta}{2}} \right] \right\} \quad (4.12) \end{aligned}$$

Equating W_e to W_i yields:

$$\begin{aligned} P_u = \frac{2\ell}{b(\cos \theta \cos \frac{\theta}{2})} [m_1 (\cos^2 \frac{\theta}{2} + v \sin^2 \frac{\theta}{2})] \\ + \frac{4bM_B}{(b^2 - \frac{\ell^2}{4} \tan^2 \frac{\theta}{2})} - \ell q_D \left(b - \frac{\ell}{6} \tan \frac{\theta}{2} \right) \quad (4.13) \end{aligned}$$

For a rectangular bridge, with $\theta = 0$, Eq. 4.13 reduces to:

$$P_u = (2m_1 \ell + 4M_B - \ell b^2 q_D) / b \quad (4.14)$$

For no edge beams, Eqs. 4.13 and 4.14 reduce, respectively to:



$$P_u = \frac{2\ell}{b(\cos \theta \cos \frac{\theta}{2})} [m_1 (\cos^2 \frac{\theta}{2} + \nu \sin^2 \frac{\theta}{2})] - \ell q_D (b - \frac{\ell}{6} \tan \frac{\theta}{2}) \quad (4.15)$$

and,

$$P_u = (2m_1 - b^2 q_D) \ell / b \quad (4.16)$$

It should be noted that the case of vehicle loads on the bridge would lead to a higher ultimate load; thus, for a conservative design and simplicity only the case of a concentrated load at center is treated herein.

4.7.3 Skew Waffle Slab Bridge Under Concentrated Load at Center of Edge Beam

The observed crack patterns of the tested bridge models confirm that for this case of loading the most likely failure crack pattern is the one shown in Fig. 4.3; the yield line (fg) is positive, corresponding to sagging moment condition, and the negative yield lines (gg') and (gg'') correspond to hogging moment conditions. Assuming that the concentrated load P at location f deflects downward a distance δ , then the external and internal virtual works can be shown to be

$$W_e = P(\delta) + 2 \gamma b^2 q_D \cos \theta (\delta)/3 \quad (4.17)$$

and

$$W_i = m_1 (2\gamma b \cos \theta) (2\delta/b) + \nu m_1 (2\gamma b \sin \theta)$$

$$\begin{aligned}
& [\delta/(\gamma b \cos \theta)] + 2 \{m_2 (2\gamma b \cos \theta) (\delta/b) \\
& + nm_2 b [\delta/(2\gamma b \cos \theta)]\} + M_B (2\delta/b) \quad (4.18)
\end{aligned}$$

in which m_2 = ultimate negative moment of resistance per unit width about the x-axis; nm_2 = ultimate negative moment of resistance per unit length about the y-axis.

Equating W_e to W_i yields the collapse load P:

$$\begin{aligned}
P = 4 \gamma (m_1 + m_2) \cos \theta + 2 \gamma m_1 \tan \theta + nm_2/(\gamma \cos \theta) \\
- 2\gamma b^2 \cos \theta q_D/3 + 2 M_B/b \quad (4.19)
\end{aligned}$$

For the least collapse load, $\frac{\partial P}{\partial \gamma} = 0$; or,

$$\gamma = \frac{1}{\cos \theta} \{nm_2/[4 (m_1 + m_2) - 2b^2 q_D/3]\}^{1/2} \quad (4.20)$$

Using Eq. 4.20 in Eq. 4.19 the ultimate collapse load P_u becomes:

$$\begin{aligned}
P_u = 2\{\gamma m_1 \tan \theta + M_B/b \\
+ \sqrt{nm_2 [4 (m_1 + m_2) - 2b^2 q_D/3]}\} \quad (4.21)
\end{aligned}$$

For a rectangular bridge $\theta = 0$, Eq. 4.21 reduces to

$$P_u = 2 \{M_B/b + \sqrt{nm_2 [4 (m_1 + m_2) - 2b^2 q_D/3]}\} \quad (4.22)$$

For a bridge with no edge beams, Eqs. 4.21 and 4.22 become:

$$P_u = 2 \{ \nu m_1 \tan \theta + \sqrt{\eta m_2 [4(m_1 + m_2) - 2b^2 q_D / 3]} \} \quad (4.23)$$

for a skew bridge, and

$$P_u = 2 \sqrt{\eta m_2 [4m_1 + m_2] - 2b^2 q_D / 3} \quad (4.24)$$

for a rectangular bridge.

4.8 Continuous Waffle Slab Supported by Isolated Columns

An outline is presented in this investigation of the yield-line theory for continuous prestressed waffle slabs, supported over interior isolated columns, simply supported at both ends, and with free edges.

4.8.1 Rectangular Waffle Slab Supported by Two Isolated Columns

Figure 4.4 shows a rectangular prestressed waffle slab model supported by two isolated interior columns with relatively weak edge beams (the stiffness of the beam is less than 1/8 of the slab stiffness). Both ends of the slab are simply supported, and the two column supports can allow rotation of the slab in the x and y directions. The aspect ratio of this model is 2 to 1 and is subjected to two concentrated loads, $2 P_u$, with P_u acting at the center of each span as well as the self weight of the slab, q_D . Past experience and observations of the crack patterns of the tested slabs

suggest that the failure lines ff' , gg' and ii' will be parallel to the supports, since the two simple supports and the line connecting the two columns are parallel.

At collapse it is assumed that the failure line ff' and ii' deflect downward a distance δ . The external virtual work in the slab due to the concentrated loads and self-weight is

$$\begin{aligned} W_e &= 2 P_u \delta + 4 (bl/2) (\delta/2) q_D \\ &= (2P_u \delta + bl\delta q_D) \end{aligned} \quad (4.25)$$

in which

δ = unit deflection under lines ff' , ii' .

The internal virtual work is

$$\begin{aligned} W_i &= 4 m_1 \ell (2\delta/b) + 8 M_B (2\delta/b) + 2 m_2 \ell (2\delta/b) + \\ &\quad 4 M'_B (2\delta/b) \end{aligned} \quad (4.26)$$

in which

M'_B = ultimate moment of resistance of the edge beam, resisting a hogging (negative) moment.

Equating W_e to W_i and rearranging yield the following expression for the ultimate collapse load P_u :

$$P_u = (\ell/b) [4 m_1 + 2 m_2 + (4/\ell) (2 M_B + M'_B) - q_D b^2/2] \quad (4.27)$$

4.8.2 Skew Waffle Slab Supported by Two Isolated Columns

This is the most complex slab type in bridges, since it is skewed as well as supported over isolated interior columns. In addition, this type serves to emphasize that moments are in fact vector quantities and as such may need to be resolved into components. Experience is needed with this type of bridge in order to predict accurately the crack pattern in the top and bottom surfaces of the concrete and the relative lateral displacement of the slab surface.

Figure 4.5 shows a 45° skewed waffle slab having the same volume of concrete, amount of steel, total thickness and rigidities in the x and y directions as the aforementioned rectangular slab; here the two isolated columns are positioned off the transverse centerline of the model.

Based on the assumptions mentioned earlier and observing the crack patterns of the tested slab models, the failure lines for this skew model are assumed as shown in Fig. 4.5. The assumed crack pattern is confirmed by a finite element analysis as will be explained later in Chapter V.

For this waffle slab system, the slab model transmits the load to the supports by means of two-way action. The crack pattern in this slab type is different from the pattern of the rectangular slab model. The line connecting

the two supporting columns is not parallel to the supports. To find the center of rotation, \bar{O} , of the yield-line ii' , both lines gg' and $J'T'$ are extended and the point of intersection \bar{O} is then determined and connected to point T (where the load is applied). Unit deflection is assumed along line iT except point i' which is assumed to deflect only half the unit deflection of point T. This assumption is made on the basis of rotation of the two columns about the center of the bridge and observing that the length of the edge beam $g'T'$ is close to half the length of gJ' . However, if the two columns are positioned on the center line of the bridge, the assumed deflection of line ii' which is parallel to the supports will be uniform along its length. Previous practice and study of skew slabs at working load, suggest that the downward deflection of point o , the center of the bridge, can be taken as 0.25δ (δ is the assumed unit deflection under the concentrated load). Once the downward deflections of point i , T and o are determined, all the other lateral deflections can be determined.

The external virtual work in the slab due to two concentrated loads, P_u , at the centre of each span and due to the self-weight of the slab (q_D) is

$$W_e = 2 P_u \delta + \sum_{i=1}^{i=n} q_{Di} \delta_i \quad (4.28)$$

in which

q_{Di} = self-weight of each segment of the cracked planes of the slab (assumed uniformly distributed load acting on that plane)

δ_i = the corresponding deflection of each cracked segment under its center of gravity

n = maximum number of cracked segment of the slab.

The internal virtual work is

$$\begin{aligned}
 W_i = & 2 \left[m_1 \left(\frac{\ell}{2} \right) \frac{\left(\frac{\delta}{x_2} + \frac{\delta}{x_6} \right)}{2} + m_1 \left(\frac{\ell}{2} \right) \frac{\left(\frac{.75\delta}{x_1} + \frac{1.25\delta}{x_5} \right)}{2} \right. \\
 & + m_1 \left(\frac{\ell}{2} \right) \frac{\left(\frac{.5\delta}{x_4} + 0 \right)}{2} + m_1 \left(\frac{\ell}{2} \right) \frac{\left(\frac{.75\delta}{x_3} + \frac{.75\delta}{x_1} \right)}{2} \\
 & + m_1 \left(\frac{\ell}{2} \right) \left(0 + \frac{.5\delta}{x_4} \right) + m_1 \left(\frac{\ell}{2} \right) \left(0 + \frac{\delta}{x_2} \right) \\
 & + 2 \left[m_2 \left(\frac{\ell}{2} \right) \frac{\left(\frac{1.25\delta}{x_5} + \frac{.75\delta}{x_1} \right)}{2} + m_2 \left(\frac{\ell}{2} \right) \frac{\left(\frac{.75\delta}{x_1} + \frac{.75\delta}{x_3} \right)}{2} \right. \\
 & + 2 \left[vm_1 (x_1) \frac{\left(\frac{0.5\delta}{(\ell/2)} + 0 \right)}{2} + vm_1 (x_1) \frac{\left(\frac{0.5\delta}{\ell/2} + \frac{0.5\delta}{\ell/2} \right)}{2} \right. \\
 & + vm_1 \frac{(\ell \tan \alpha_2)}{2} (2) \left(\frac{.5\delta}{\ell/2} \right) + vm_1 \left(\ell/2 \tan \alpha_1 \right) (2) \left(\frac{\delta}{\ell/2} \right) \\
 & \left. + 2 \left[2vm_2 \left(\ell/2 \tan \alpha_1 \right) \left(\frac{.50\delta}{\ell/2} \right) \right] \right]
 \end{aligned}$$

$$\begin{aligned}
 & + [M_B \left(\frac{\delta}{x_6}\right) + M_B \left(\frac{1.25\delta}{x_5}\right) + M'_B \left(\frac{1.25\delta}{x_5}\right) \\
 & + M_B \left(\frac{.5\delta}{x_4}\right) + M_B \left(\frac{.75\delta}{x_3}\right) + M'_B \left(\frac{.75\delta}{x_3}\right) \quad (4.29)
 \end{aligned}$$

in which

α_1 = slope of the line $\bar{O} g'$ with the X axis;

α_2 = slope of the line $\bar{O} i'$ with the X-axis;

θ = the skew angle with the y axis;

θ_1 = slope of crack pattern TT'; and

$x_1, x_2, x_3, x_4, x_5, x_6$, = distances as shown in

Fig. 4.5.

Equating Eqs. 4.28 and 4.29, the ultimate collapse load (P_u) is obtained as

$$(P_u) = (W_i - \sum_{i=1}^{i=n} q_{Di} \delta_i) / 2\delta \quad (4.30)$$

4.8.3 Effect of the Skew Angle on the Yield-line Pattern

From the analytical study of the tested seven slab models, and from observation of the crack pattern in each slab model, it is found that the skew angle plays a major role on the propagation of the crack pattern. In the rectangular slab models, i.e., when the skew angle = 0, the crack pattern includes a single crack line parallel to the supports; this crack pattern follows lines of maximum stress as mentioned earlier. For bridges with

skew angles up to approximately 20° it is expected that the crack pattern will be similar to that of rectangular bridges. Thus, for such small skew angles its effect on the crack pattern is not very pronounced. However, it is expected that for bridges with skew angles between 20° to 45° , say, the yield-line ff' , in Figure 4.5, will form making an angle $\theta/2$ with the x-axis; additionally, a new crack line QQ' (Figure 4.5) will start forming between the loaded point on the bridge and the nearest obtuse corner to the load. For bridges with skew angles exceeding 45° , it is expected that cracks will start under the load, say @ Q' , and will propagate only to points f' and Q' , causing failure; i.e., the crack line $Q'f$ will not form in this case.

It is interesting to note that in bridge model PC4, locating the two columns off the transverse center line of the model introduces two way slab action in both panels of the bridge model; for this reason, the longitudinal crack $Q'OT$ (Fig. 4.5) forms joining the two loaded points Q' and T and intersecting the mid-point of the negative yield line gg' .

CHAPTER V

PROGRESSIVE FAILURE ANALYSIS

5.1 Introduction

While the STRAND program is an extremely powerful analytical tool in solving reinforced and prestressed concrete slab bridges, it cannot predict the ultimate load-carrying capacity of the structure. In Chapter III a linear elastic analysis was presented for slab structures using the STRAND program; the analysis was based on the finite element technique. In Chapter IV the ultimate method of analysis was adopted based on yield-line theory. The present chapter describes a progressive failure analysis of the structure by the method of successive approximation technique; such an analysis, affected by modifying the STRAND Program described in Chapter III, provides complete information on the behaviour of concrete waffle slabs as the load level is increased from zero to failure. The yield-criterion of maximum stress theory is adopted in this analysis.

5.2 Analysis by the Finite Element Method

Finite element analysis for material nonlinearity is still under intensive research. One of the principal

limitations in this area, as far as reinforced and pre-stressed concrete structures are concerned, is the difficulty in adequately representing the material properties. In other words, better techniques of computing material parameters and utilizing experimental data must be devised. Relatively little information for two-dimensional nonlinear material behaviour is available. Moreover, few analytical and experimental results are available for comparison with finite element solution for two-dimensional problems involving material nonlinearity.

The procedure used in the analysis herein is shown in the flow diagram of Fig. 5.1. The first step is to calculate the uncracked and cracked rigidities of the concrete slab, assuming that if the element is cracked it has reached its limiting capacity (neglecting tension in the concrete, see Appendix A). The second step is to idealize the slab into a suitable mesh of triangular finite elements of uniform size. However, in areas of high stress concentrations, such as isolated columns under concentrated loads, and at the obtuse corners in skew slabs, a finer mesh is required.

The analysis is started by assigning the appropriate initial orthotropic elastic constants to the finite elements and then carrying out a linear elastic analysis. For each element, the centroidal deflection, moments,

maximum principal moments, and their directions are found: such moments are assumed to apply uniformly over the element. Further assumption is made that membrane action is neglected, which means that a confined slab will be less stiff than expected. Large displacement effects and tension membrane action are likewise neglected; although these could be taken into account, they only lead to a greater complexity which is not warranted. It is also assumed that, when cracks occur, the cracked area extends uniformly over an entire element, i.e., an element is either uncracked or cracked. Beyond the initiation of first crack, an iterative incremental procedure is adopted to take into account the reduction of stiffnesses with the corresponding increment of loading. The equilibrium equation for a single element is

$$\begin{array}{ccccc}
 & [K] & \{\Delta\} & = & \{Q\} & (5.1) \\
 \swarrow & & | & & \swarrow \\
 \text{stiff-} & & \text{deflec-} & & \text{load} \\
 \text{ness} & & \text{tion} & &
 \end{array}$$

where nonlinearity occurs in the stiffness matrix $[K]$, which is a function of the nonlinear material properties.

The basis of the incremental procedure is the subdivision of the load into many small load increments. Usually these load increments are of equal magnitude, but in general they need not be equal. The load is applied one increment

at a time, and during the application of each increment Eq. (5.1) is assumed to be linear. In other words, a fixed value of $[K]$ is assumed throughout each increment, but $[K]$ may take different values during different load increments. Essentially, the incremental procedure approximates the nonlinear problem as a series of linear problems.

An initial value of the load can be given before cracking the concrete, so the total effective load becomes

$$\{Q\} = \{Q_0\} + \sum_{i=1}^n \{\Delta Q_i\} \quad (5.2)$$

in which

$\{Q\}$ = is the total load vector;

$\{Q_0\}$ = is the initial load vector; and

$\{\Delta Q_i\}$ = is the load increment vector.

The increment in the load can be chosen with different values depending on the accuracy of the solution and the computer time required. If the cracking load is approximately known, the solution can be started with the initial load $\{Q_0\}$ just below the cracking load to save some computer time.

Once the first crack is located, the incremental procedures for the load is stopped and the iterative procedure for the reduced stiffness is started. The iterative procedure continue under the same load until there is no change in the number of cracked elements; the incremental procedure

is then started again. At the end of each load increment the failure of the slab is checked against either yielding of the steel or crushing of the concrete.

At every stage of the iterative procedure, new element stiffness matrices are computed for each cracked element. Past experience and test results from the seven waffle slab concrete bridge models, show that the cracked rigidity of a waffle concrete section is less than one tenth of uncracked rigidity. For this reason it is assumed that the modulus of elasticity for concrete is the same for cracked and uncracked sections.

5.3 Uncracked Rigidities for Plate Bending Analysis

For proper design it is essential that the designer should use realistic estimates for the rigidities of a waffle slab structure. Estimates of these rigidities (flexural and torsional) are given in References (12, 23)

5.4 Rigidities of Cracked Sections

5.4.1 Flexural Rigidities

After the concrete starts to crack, the waffle section continues to behave elastically, provided the steel stress is below its yield point and the compressive stress in the concrete does not exceed $0.5 f'_c$. For simplicity, it is assumed that the tension cracks have progressed to the neutral axis (assumed to be in the top flange-plate, which

is generally the case), and that plane sections before bending remain plane after bending. The transformed section of concrete is used for computing the rigidities, [considering the compression steel area times (n-1) and tension steel area times (n)]. Based on the above assumptions, the rigidities of the cracked section of a waffle slab can be expressed as:

$$D_x = E (I_{sx} + I_{cx}/(1 - \mu^2)) / S_x \quad (5.3a)$$

$$D_y = E (I_{sy} + I_{cy}/(1 - \mu^2)) / S_y \quad (5.3b)$$

$$D_1 = \mu D'_x \quad (5.3c)$$

$$D_2 = \mu D'_y \quad (5.3d)$$

in which

I_{cx} (I_{cy}) = moment of inertia of the concrete [and (n-1) times area of compression steel, if any] in compression about the neutral axis for bending about an axis perpendicular to the x-(y-) direction, i.e., for the neutral axis lying in the top flange plate,

$$I_{cx} = S_x (kd_x)^3 / 3 \quad (5.4a)$$

$$I_{cy} = S_y (kd_y)^3 / 3 \quad (5.4b)$$

I_{sx} (I_{sy}) = moment of inertia of the transformed steel section about the neutral axis for bending about an axis perpendicular to the x-(y-)

direction, i.e.,

$$I_{sx} = nA_s ((h + d_x - d') - Kd_x)^2 \quad (5.5a)$$

$$I_{sy} = nA'_s ((h + d_y - d'') - Kd_y)^2 \quad (5.5b)$$

$D'_x(D'_y)$ = flexural rigidity of the top flange-plate with respect to the neutral plane of the gross cracked section associated with bending about an axis perpendicular to the x-(y-) direction. The location of the neutral axis Kd_x (or Kd_y) is determined by equating the compression force to the tension force on the section.

Thus, when the neutral axis lies in the top flange-plate, Kd_x is given by

$$nA_s ((h + d_x - d') - Kd_x) - s_x (Kd_x)^2 / 2(1 - \nu^2) = 0 \quad (5.6a)$$

and Kd_y by

$$nA'_s ((h + d_y - d'') - Kd_y) - s_y (Kd_y)^2 / 2(1 - \nu^2) = 0 \quad (5.6b)$$

5.4.2 Torsional Rigidity

For a waffle-type slab the parameter $\bar{\alpha}$, defined in reference (11), can be expressed as:

$$\bar{\alpha} = (D_{xy} + D_{yx} + D_1 + D_2) / 2(D_x D_y)^{0.5} \quad (5.7)$$

Experimental test results have shown (22) that for this type of slab $D_{xy} = D_{yx}$.

Thus Eq. (5.7) becomes

$$\bar{\alpha} = (2D_{xy} + D_1 + D_2) / 2(D_x D_y)^{0.5} \quad (5.8)$$

hence

$$D_{xy} = \bar{\alpha} (D_x D_y)^{0.5} - (D_1 + D_2) / 2 \quad (5.9)$$

It is assumed that the parameter $\bar{\alpha}$ remains the same before and after cracking of the concrete. Thus by calculating $\bar{\alpha}$ from Eq. 5.8, using the precracking flexural and torsional rigidities (12, 23), the postcracking torsional rigidity D_{xy} can be estimated from Eq. 5.9, in which D_x , D_y , D_1 and D_2 are estimated from Eq. 5.3 for the postcracking condition. Since D_1 and D_2 are small compared to D_x and D_y in a waffle slab dropping D_1 and D_2 from Eq. 5.7, will yield another form for the parameter $\bar{\alpha}$:

$$\bar{\alpha} = (D_{xy} + D_{yx}) / 2(D_x D_y)^{0.5} \quad (5.10)$$

or

$$\bar{\alpha} = D_{xy} / (D_x D_y)^{0.5} \quad (5.11)$$

Thus, the torsional rigidity can now be represented as:

$$D_{xy} = \bar{\alpha} (D_x D_y)^{0.5} \quad (5.12)$$

in which D_x and D_y are determined from Eq. 5.3.

CHAPTER VI

EXPERIMENTAL INVESTIGATION

6.1 Introduction

In order to verify the analytical formulation and the modified computer program, a series of experimental tests were carried out on seven concrete waffle slab bridge models. Five slab models were simply supported and the remaining two were continuous over two interior isolated column supports. The first three models (RC1, RC2, RC3) were reinforced concrete waffle slabs, the second four models (PC1, PC2, PC3, PC4) were prestressed post-tensioned concrete waffle slabs. Two of the reinforced concrete models, RC1 and RC2, were rectangular in plan and the third one, RC3 was skewed 45° , while two of the prestressed concrete models, PC1 and PC3, were rectangular in plan and the remaining two prestressed concrete models, PC2 and PC4 were skewed 45° in plan. The reinforced concrete models were free along the sides, parallel to the traffic flow, while the prestressed ones were elastically supported by relatively weak edge beams due to construction requirements. The prestressing wires in slab models PC1 and PC2, were straight tendons in the x and y directions, while in slab

models PC3 and PC4 they were curved in the longitudinal direction, and straight in the transverse direction. Details on the testing of the five simply supported slab bridge models can be found in reference (23).

All bridge models were one-to-eight in scale since this scale was judged to be the most suitable taking into account the heterogeneity of concrete, fabrication and casting of the concrete models as well as the reliability in assessing their rigidities. The elastic material properties of the slab models were determined according to the American Society for testing and material specifications. Details of the test bridge models are presented in Table 6.1.

The ultimate load and the orientation of yield lines were observed and compared with the predicted analytical results. Load versus deflection behaviours were also obtained as well as stresses and moments at different locations of the slab models. Tests were conducted in two distinct sequences:

First: The waffle slab models were tested at different points in the elastic stress domain (with no cracks in concrete) under a lateral concentrated loading applied symmetrically and anti-symmetrically, and

Second: the slab models were tested to failure with two symmetrically placed concentrated loads.

6.2 Materials

6.2.1 Concrete

High early strength Portland cement manufactured by the Canada Cement Company was used in the two continuous prestressed waffle slabs, PC3 and PC4; this provided a 7-day concrete strength of 48 MPa (7 ksi). The maximum size of aggregate was 6 mm (0.25 in) due to the narrow dimensions between the sides of the formwork. The combined aggregate was prepared according to the ACI code (40) by mixing 40 to 60% fine aggregates of the total aggregates. This gave a well graded combined aggregate with a fineness modulus equal to 2.50. Crushed stones with hard, and durable properties were used for the coarse aggregate. Mixing of concrete was performed in an Eerich Counter Current Mixer, Model EA2(2W) with five cu. ft. charging capacity.

6.2.2 Reinforcement

High tensile steel wires of 5 mm (0.2 in) diameter were used for prestressing the two waffle slab models. Tensile tests on the wires gave an ~~average~~ ultimate strength of 1550 MPa (225 ksi), and a yield stress of 1200 MPa (175 ksi). The wire had a smooth surface which helped in providing good control on the amount of prestressing force required in each wire during the pre-

stressing operation; only minimum friction was expected to occur between the concrete and the curved steel tendon during the prestressing operation as well as during loading of the slab.

6.3 Formwork

Two forms were made from plywood, 19 mm (0.75 in) thick, with wood joist, 51 x 152 mm (2 x 6 ins.) in cross-section used as stiffeners. The first form was rectangular in plan and used for casting the slab model, PC3, Fig. 6.4. The second form was skewed 45° in plan and used for the skew slab model, PC4, Fig. 6.5. Styrofoam cubes were used for producing the waffle shapes, Figs 6.2 and 6.3, and were fixed on the wood surface by a water-resistant glue.

6.4 Description of the Two Continuous Slab Models

6.4.1 Continuous Rectangular Post-Tensioned Waffle Slab Model, PC3

The overall dimension of this slab model was 1.257 m x 2.514 m (49.5 in. x 99 in.) and of mass 500 kg (1100 lbs.). The waffle shape and dimensions are shown in Fig. 3.2. Solid drop panels were formed around regions of maximum shear, located at the two interior column positions and at the two ends of the slab model. The model was prestressed by 27 high tensile steel wires in both directions; nine curved

wires were used in the longitudinal direction, with 18 straight wires used in the transverse direction. The wire profiles and the eccentricities in the x and y directions are shown in Fig. 6.6.

To study the slab model under the working-load condition (i.e., before cracking of the concrete), ten tests were carried out by means of a movable loading jig; seven tests were with a single concentrated load, and three tests were with two concentrated loads, each acting on one span. Finally, the slab model was tested under two concentrated loads symmetrically placed at the center of each span with the load being increased from zero to collapse.

6.4.2 Continuous 45° Skew Post-Tensioned Waffle Slab, PC4

In this model the longitudinal ribs were perpendicular to the transverse ribs. The steel bearing plates used in prestressing were fitted into specially-formed grooves along the edges (Figs. 6.7 and 6.8); the plates were provided with two perpendicular eccentric holes to accommodate the prestressing wires in the two directions. The number of prestressing wires were increased to 34 wires due to the skewness of the slab. The center line joining the two isolated columns was inclined to the transverse center line of the bridge model by an angle $\psi = 11^\circ$ as shown in Fig. 6.5.

The loading procedure and the sequence in applying the lateral load on this model were the same as that in the rectangular model. Figure 6.9 shows the profile of the longitudinal prestressing wire and its eccentricities measured from the bottom fibre of the model.

6.5 Experimental Equipment

6.5.1 Prestressing Equipment

A prestressing hydraulic jack of 89 KN (20 kips) capacity was used for post-tensioning as shown in Fig. 6.7. Mechanical gripping devices with open grip type were employed. End bearing steel plates and washers were used at both ends of the wires to transfer and distribute the prestressing force from the steel to the concrete.

6.5.2 Automatic Strain Indicator

Figure 6.10 shows the automatic strain indicator which was used in recording the strains during the experiment. This model was manufactured by Vishy Intertechnology, Inc., Malvern, Penna, U.S.A. The strain indicator includes mainly four devices: the V/E-21 Switch Balance, the V/E-20 Digital Strain Indicator, Scan Controller V/E-25, and the Automatic Printer V/E-22. The V/E-21 Strain Indicator provides a method of sequentially reading the outputs of up to ten channels of strain gauge information. Eight V/E-21's were

connected to the same indicator which gave a capability of recording readings from 80 strain gauges.

6.5.3 Hydraulic Jack for Lateral Loading

A 178 KN (40 kips) hydraulic jack was used for testing the slab models at various points. The length of the jack was 490 mm (20 in.) with a 430-mm-travel (17 in.) piston. The jack was attached to a heavy steel beam by means of Heavy C clamps and fixed in such a way that it could be readily moved in both the longitudinal and transverse directions; see Fig. 6.11.

6.6 Instrumentation

6.6.1 Electric Strain Gauges on the Concrete


The concrete strains were measured on the top and bottom surfaces of the slab model, using electric strain gauges of type EA-06-500BH-120. Rosette 45° electric strain gauges of type EA-06-250RA-120 were used at the obtuse corners of the skew model. The two models were instrumented at various locations and especially around the loaded area, the interior column supports, and, in the case of the skew model, at the obtuse corners.

The gauge locations on the concrete surfaces were smoothed using fine sand paper; all dust was removed using compressed air and then the surfaces were cleaned

with acetone; all cavities were then filled by applying an epoxy of high strength (RTC). This epoxy was mixed by one volume activator B, and the same volume of resin A. After the surfaces were dry, they were again smoothened with fine silicon carbide paper and the gauges were mounted using Eastman 910 cement. After soldering the wires to the gauges, the latter were moisture-proofed using coating epoxy Bean Gakote #3, and cured for 24 hours under room temperature. The gauges were then connected to the strain indicator, balanced to zero and made ready for testing.

6.6.2 Mechanical Dial Gauges

The lateral deflections resulting from the prestressing and lateral loading were measured using mechanical dial gauges with a sensitivity of 0.025 mm (0.001 in.). In the two slab models PC3 and PC4, all the dial gauges were placed at the top surface of the slabs, and supported on a steel frame separated from the slab as shown in Fig. 6.12. In the area(s) where the load(s) was applied the dial gauge(s) was placed on top of the loading steel plate(s), as shown in Fig. 6.12. The location of the dial gauges are shown in Figs. 6.13 and 6.14 for the rectangular and skew models, respectively.



6.6.3 Load Cells

A universal flat load cell having a capacity of 222 KN (50 kips), was used in the two slab models to measure the lateral load transferred to the slab through the hydraulic jack. Thirty-four cylindrical load cells were used to measure the prestressing forces in the wires. The readings from these cylindrical load cells were monitored throughout the test, first to measure the initial and after-losses prestressing force before applying the lateral load on the model, and finally, the prestressing force in the wires at collapse of the model. The calibrations of all the load cells are given in Appendix D. Two universal flat load cells having a capacity of 111 KN (25 kips), were used at the top of the two columns to measure the reactions, ~~pro-~~duced by prestressing as well as the lateral load.

6.7 Construction of the Slab Models

The dimensions of the two slab models are shown in Figs. 6.4 and 6.5. The required wood forms were prepared as shown in Fig. 6.15, and the styrofoams were placed into position by glue. Rubber hoses having an inner diameter of 6.4 mm (0.25 in.) and 1.66 mm (0.062 in.) thick were used to cover the steel wires during casting of the concrete and to prevent bonding between the steel and the concrete. The longitudinal steels were inserted in the

rubber hoses having a curved profile to accommodate the negative moment at the interior column support region. The wires were supported on 3 mm (0.125 in.) steel wires (chairs) which provided a varying eccentricity of 25 mm (1 in.) to 82 mm (3.25 in.) from the soffit of the models, as shown in Figs. 6.8 and 6.9. The straight transverse prestressing steels were located at the center of gravity of the section.

One hour before mixing the concrete, the inside of the forms were painted with grease material, Vitrea oil 150, for easy form release after setting of the concrete. The form was placed on a special steel bed, having an attached vibrator, Fig. 6.15. Care was taken during casting and vibrating to ensure that no segregation occurred. The top surface of the slab was leveled and troweled smooth after casting then covered with a plastic sheet. After six hours, water-curing of the slab was started and continued for 7 days; the slab was then allowed to dry 2 days before applying the epoxy to the surface and mounting the strain gauges.

To determine the compressive strength of the concrete, six 76 mm x 152 mm (3 in. x 6 in.) cylinders were cast with each model. They were cured in the same way as the slab model.

6.8 Experimental Setup and Test Procedure

6.8.1 Rectangular Prestressed Concrete Waffle Slab

Extreme care and adequate precautions were taken in moving the forms out and during transfer of the slab from the casting bed, to its supports; this was necessary since the slab was still plain concrete and not yet prestressed. The slab model was supported at both ends on 38 mm (1.50 in.) diameter steel rollers, and supported in the interior region on two isolated columns, each being composed of 101 x 101 x 25 mm (4 x 4 x 1 in.) steel plate, resting on a universal flat load cell supported by a mechanical screw jack for adjusting the level of the support column with the end supports. Steel and rubber shims were used between the supports and the concrete surface to give full contact between the slab and its supports. The slab was mounted with forty-five strain gauges to measure the strain on the top and bottom surfaces of the concrete, and sixteen mechanical dial gauges to measure the lateral deflection produced by prestressing as well as the lateral load. Fig. 6.13 shows the locations of both the strain and dial gauges. The slab under two-concentrated loads applied at the center of each span is shown in Fig. 6.19.

The slab model was prestressed by 27 high tensile steel wires; adequate precautions were taken during the prestressing operation by installing steel bearings on

the four sides of the slab and following a certain sequence in post-tensioning the wires (23). To protect the slab from premature cracking as well as uplift due to the vertical component of the prestressing force, two steel columns were used as bracings on the top surface of the slab, Fig. 6.16; these steel columns were located in line with the column supports to prevent any coupling that might have occurred otherwise; the steel columns were supported on two spherical bearings to allow rotation.

Before commencing the test the slab was subjected to a small load and then unloaded; this was repeated several times to minimize the residual stresses and to insure good seating of the model on its supports. The slab was tested by a single-concentrated load at seven various positions, and tested by two-concentrated loads at three different positions before cracking the concrete. Finally, the slab was loaded by two concentrated loads, each load at the center of the span, up to failure; it was subsequently reloaded to examine its response after failure.

6.8.2 45° Skewed Prestressed Concrete Waffle Slab

The experimental procedures for this slab were similar to the ones for the rectangular model. This 45° skewed slab was mounted with forty-five strain gauges to measure the strain on the concrete surfaces and sixteen dial gauges to measure the deflections as shown in Fig. 6.14. The slab

was prestressed by thirty-four high tensile steel wires in both directions, i.e., nine curved wires in the longitudinal direction and twenty-five straight wires in the transverse directions.

This slab was subjected to six concentrated single-loads and five concentrated double-loads at various locations; the same sequence in loading was followed as for the rectangular slab model. The cracking as well as the ultimate loads were recorded; cracks, forming the yield lines at the top and bottom surfaces of the slab model, were traced. Figure 6.20 shows the slab model in position.

CHAPTER VII

DISCUSSION OF RESULTS

7.1 General

To demonstrate the application of the analytical methods developed earlier in this dissertation, test results from seven 1/8-scale waffle slab models are presented. The test results are compared with results from the finite element method and the series solution in the elastic domain. The study and the comparison between the experimental and theoretical results are extended beyond the elastic domain, to include the ultimate load as well as the progressive failure analysis solutions.

The efficiency of continuous waffle slab construction in transmitting the load through the interior column supports is examined. A comparison is made between the structural response of slabs supported on continuous pier line support and that of slabs supported on two isolated interior columns; the effect of rotating the interior column supports about the center of the bridge is also studied.

7.2 Elastic Solution (Working Load Condition)

7.2.1 Simply Supported Slab Models

The matrix solution equation resulting from the bending analysis and containing the unknown constants in Eq. 3.2, was solved by the Gauss-Jordan elimination method. The matrix elements were subjected to the usual scaling operation and stability checks indicating that the generated matrices are stable. The use of double precision improved the results only in cases involving large matrices. The average execution time on an IBM 360/65 computer was 50 seconds to analyze one structure with double precision. It was found that eight harmonics in the elastic series solution provided sufficient accuracy for engineering applications for various skew angles and for both uniform and concentrated wheel loads. The accuracy of the solutions, including static moment equilibrium checks, has been well established and details can be found elsewhere (21). The solution to the matrix equation for the in-plane analysis was obtained by a standard Gaussian elimination method. Convergency study indicated that eleven harmonics were sufficient to yield the required engineering accuracy for the in-plane stresses given by Eq. 3.14; the execution time on an IBM 360/65 computer was approximately 6 minutes to analyze one structure.

The results from the bending and in-plane stress

analyses were superimposed and then compared to the experimental test results; the rigidities of the test models were first determined (12); the deflection function w was then found from Eq. 3.2 after satisfying the boundary conditions, Eqs. 3.3 - 3.6; the moments M_x , M_y , and M_{xy} were then calculated (6), and thus the bending and torsional strains from Eq. 3.9; these strains were combined with the in-plane strains from Eq. 3.16 to yield the total strains.

The execution time on an IBM 370/3031 computer using the finite element program STRAND for one structure was 3 minutes. To check the accuracy of the STRAND program, a comparison between the theoretical and experimental results for deflection and strains was made for the two prestressed concrete waffle slabs, PC1 and PC2. Figure 7.1 shows a comparison between the test results and those from the STRAND program as well as the series solution for the center deflection of the rectangular model and deflection at the center of the edge beams. The results from the STRAND solution slightly underestimate these deflections; the results for strains, shown in Fig. 7.2 show the same tendency. A close agreement is shown in Fig. 7.3 between the test results and those from the STRAND program for the center deflection of the skew prestressed model, PC2. Figures 7.4 and 7.5 present comparisons of results for strains in the skew slab model when subjected to a load

at the center of the slab, and at the center of the edge beam, respectively. Good agreement is shown for the strains at the center of the model and fair agreement can be observed in Fig. 7.5 for the strains near the obtuse corner where the strains are difficult to predict accurately due to the steep stress gradient in this region. In using the STRAND program, a finer mesh around the obtuse corner and in the vicinity of the concentrated load was used.

Notwithstanding the differences noted between the STRAND and the test results, it can be concluded that the solution by the STRAND program, utilizing the rigidities derived in reference (12), is reliable to predict the response of prestressed concrete waffle slab bridges under load.

7.2.2 Continuous Prestressed Waffle Slabs

7.2.2.1 Series Solutions Using Influence Lines

The analytical solution presented earlier using Fourier Series for simply supported slabs is adjusted to accommodate continuous prestressed slab bridges with varying profiles of prestressing steel. The method is applied to the rectangular and skew prestressed slab models, each supported by two interior isolated columns. The column reactions are compared with those obtained from the experiment as well as from the STRAND program. The results, shown in Table 7.1

and 7.2 indicate good agreement; the solution by the STRAND program overestimates the column reaction of the skew slab model by 15%. It should be noted that the series solution method for continuous slabs requires a lengthy procedure in finding a complete solution to a bridge problem and may not be suitable for the design office.

7.2.2.2 Finite Element Method

Figures 7.6 to 7.12 show the theoretical and experimental results for deflections, strains and moments due to the prestressing of the rectangular and skew slab models. Figure 7.6 shows the distribution of the upward deflection (Camber) due to prestressing, with good correspondence between theory and experiment. The distribution of the deflection along the transverse direction is almost uniform; this confirms that a waffle slab structure when subjected to uniform load, acts as a wide beam. This uniform load, due to the applied prestressing force is more or less uniform as shown in Figs. 7.13 and 7.14.

Figures 7.7 and 7.8 show the resulting strains at the bottom and top surfaces of the slab, due to prestressing. Close agreement is obtained between the theoretical and experimental strains. The distribution of moment due to prestressing is shown in Fig. 7.9; one can notice that the moments in the longitudinal direction are relatively large

in comparison to those in the transverse direction.

Figure 7.10 shows the camber of the skew slab model due to prestressing. Close agreement is observed between the theoretical and experimental results; there is more variation in the deflection profile of this model than in the rectangular model; this is due to: (i) skew, and (ii) the inclination of the line connecting the interior supports, to the transverse center line of the bridge model. The corresponding strains are compared with the theoretical ones in Fig. 7.11 and show fair agreement. A compressive strain is observed along the side of the slab due to the transverse prestressing force while a tension strain of $70 \mu\text{mm/mm}$ is present at the obtuse corner. Figure 7.12 shows the resulting moments due to prestressing a skew slab model; Eq. 3.9 is used to calculate the moments from the experimentally measured strains; the good correspondence between the theoretical and experimental results confirms that if a suitable and more refined mesh is chosen for the finite element method, the designer can rely on this method for analyzing slab bridges.

7.2.2.2.1 Rectangular Concrete Waffle Slab

Figures 7.15 to 7.19 show the load deflection relationship due to a single load, applied at different positions on the slab model; while Figs. 7.20 to 7.23 show the same

load-deflection relationship due to a pair of equal loads (the two-load system). A study of these figures reveal good correspondence between the theoretical and experimental results before cracking of the concrete.

Figures 7.24 to 7.28 show the deflection profiles due to the single- and two-load systems. It is observed that deflection due to a single concentrated load at the center of the edge beam, equals almost three times the resulting deflection for the same load acting at the center of the slab. Also, the deflection at the center of the slab due to the two-load system, equals 80% of the resulting deflection due to the single-load system applied at the slab center.

Figures 7.29 to 7.33 present comparisons between the theoretical and experimental load-strain relationships in both the x and y directions. Good agreements are noted between the two results; it may be said that the strain gauges are more sensitive and reliable than the mechanical dial gauges, especially when small-deflections prevail.

Figures 7.34 to 7.38 show the distributions of the moments resulting from a single concentrated load of 36 kN (8 kips). It can be observed that the critical stresses are under the load for the single-load system, whereas for the two-load system they occur at the interior column support region. It can also be noticed that the

moment decreases rapidly moving away from the loading point.

7.2.2.2.2 Skew Concrete Waffle Slab

It may be recalled that the skew waffle slab model was constructed with the same volume of concrete, thickness and rib spacings as the rectangular slab model. Such similarity makes it possible to study the effect of skew on the design parameters.

Figures 7.39 to 7.45 show the load-deflection relationships in the working stage (before cracking of the concrete) due to single concentrated load applied at different locations on the model. While Figures 7.46 to 7.48 show the load-deflection relationships for the two-load system. Although each prestressed concrete slab model was tested more than ten times at different loading positions, the results show that the response of the structure to load continued to be linear elastic. To ensure such response, the slab models were tested at half the cracking load to guarantee that there was no microcracking in the models; again it can be observed that there is close agreement between the theoretical and experimental results.

The deflection distribution patterns due to lateral load are given in Figs. 7.49 to 7.54. It can be observed that the maximum deflection occurs under the load when

applied at the center of the edge beam for both the single- and two-load systems.

Figs. 7.55 to 7.60 show the load-strain relationships for the two-load system applied at different positions. Good correspondence is shown between the theoretical and experimental results. When these results are compared with the corresponding ones for the rectangular slab model, it is observed that the transverse ribs in the skew model are working more effectively with the longitudinal ribs, to transmit the load to the supports.

The distribution of the moments for the skew slab model due to the single- and two-load systems at different positions are given in Figs. 7.61 to 7.66. The moments were calculated at the points where the experimental strains are measured; comparison with the theoretical moments shows fair agreement. It is observed that the critical stresses in the skew slab occur near the obtuse corners near the interior column supports, as well as under the load as shown in Fig. 7.61, 7.63 and 7.65.

7.3 Ultimate Load Solution (Yield-Line Theory)

Figure 7.67 shows the tested concrete waffle slab models, and the proposed crack pattern for each slab model. To discuss the results from testing these slab models, the latter are divided into three groups: Group A, consisting

of three slab models, RC1, RC2 and RC3; Group B, consisting of two slab models, PC1 and PC2; and Group C, consisting of two slab models, PC3 and PC4.

7.3.1 Reinforced Concrete Waffle Slabs (Group A)

The relationships between load and deflection as well as between load and strain at the center of the uniformly loaded reinforced concrete model RC1 are shown in Fig.

7.68. Comparison of the theoretical and experimental results shows close agreement up to the cracking load; as expected, the results begin to diverge at the start of microcracking. It is interesting to note that the measured strains near the free edge in the y-direction were sensibly the same as those in the same direction at the center of the bridge, which confirms that when subjected to uniformly distributed load, such a bridge would behave as a wide beam in carrying the load. Figure 7.69 shows the single-line crack pattern intercepting the longitudinal ribs with no visible cracks in the transverse ribs; this crack pattern is further evidenced by the relatively large measured strains in the longitudinal ribs and the small measured strains in the transverse ribs. The ultimate load of 7.6 kPa (1.1 psi), was reached after extensive yielding of the reinforcing steel followed by crushing of the concrete plate deck. The theoretical

collapse load was 5.6 kPa (0.81 psi) (see Appendix B), on the basis of the single-line crack pattern. The micro-cracking load was approximately one-third the ultimate load.

The second reinforced concrete bridge model, RC2, was tested to collapse by a concentrated load at the center. The results for deflection and strains at the center of the slab model, presented in Fig. 7.70, indicate good agreement between theory and experiment up to the cracking load. It should be observed here that, unlike the case of bridge model RC1, the measured strains in the transverse ribs were relatively significant; this shows that when a waffle slab bridge is subjected to a concentrated wheel load, it will exhibit excellent transverse load distribution characteristics. The measured strain results indicated that the first yield of the reinforcing steel occurred at the center of the model in the longitudinal direction and subsequently propagated across the width of the bridge model through the transverse ribs. The model finally collapsed at a load of 12.4 kN (2.80 kips) after the concrete plate deck had crushed. All the longitudinal ribs were severely cracked across the center line of the bridge model while the transverse ribs suffered only hairline cracks at the bottom, as shown in Fig. 7.71. This model also exhibited a single-line crack pattern

similar to that of model RC1 (Fig. 7.69). The theoretical collapse load was 10.9 kN (2.45 kips). For the purpose of comparison, results of strains at the center of the prestressed concrete bridge model PC1 of group B are plotted also in Fig. 7.70. It is observed that even for a central concentrated load of more than twice the collapse load of model RC2, the response of model PC1 is linear with close agreement between theory and experiment.

Bridge Model RC3, with a skew of 45° , was failed with a concentrated load at center. Results for load versus deflection and load versus strain are presented in Fig. 7.72, showing good agreement between theory and experiment up to the cracking load. The measured strains in the transverse ribs were substantial, indicating excellent transverse-load distribution capability. The cracking at the bottom of this model is shown in Fig. 7.73 with cracks inclined to the axes of the ribs; this is due to the presence of combined flexure and torsion, in contrast to the rectangular models, RC1 and RC2, where the cracks were normal to the longitudinal ribs and due predominately to flexure. In model RC3 cracking of the concrete occurred first, followed by yielding of the reinforcing steel at the center of the middle longitudinal rib; with increased load cracks progressed toward the free edges along an inclined line, as shown in Fig. 7.73. The model finally

collapsed under a central concentrated load of 19.8 kN (4.5 kips) compared to a theoretical value of 17.8 kN (4.0 kips). The experimental crack pattern agrees well with the assumed theoretical yield-line crack pattern shown in Fig. 4.2.

7.3.2 Prestressed Concrete Waffle Slabs, Simply Supported (Group B)

The post-tensioned rectangular waffle slab bridge model PC1 was loaded near the center of the edge beam to failure. Results for deflection and strain, presented in Fig. 7.74, show close correspondence between theory and experiment up to the cracking load. First, cracks occurred under the load, followed by cracks along a curved boundary as shown in Fig. 7.75. The final collapse load of 26.7 kN (6.0 kips) was reached after some punching shear failure of the flange plate deck had taken place around the loading plate. The theoretical collapse load of 25.3 kN (5.69 kips) was derived (see Appendix B) adopting the simplified yield-line crack pattern of Fig. 4.3; the closeness of the two results gives verification to this assumed crack pattern. If the magnitude of the load required to punch through the plate deck is added the theoretical collapse load increases to 26.8 kN (6.04 kips).

The 45° skewed post-tensioned waffle slab bridge

model PC2 was tested to failure by a concentrated load at the center. Deflection and strain results are presented in Fig. 7.76; close correspondence between theory and experiment can be observed for loads prior to cracking. The first crack appeared at the bottom of the central longitudinal rib due to a concentrated load of approximately 26.6 kN (6 kips); upon further loading large cracks, caused by severe twisting, appeared at the top of the deck around the obtuse corners, Fig. 7.77. The model failed at a load of 53.8 kN (12.10 kips) precipitated by punching shear failure through the concrete plate deck; the failure crack pattern was similar to that for model RC3, Fig. 7.73. The calculated theoretical collapse load of 46.5 kN (10.44 kips) was based on the assumed yield-line pattern of Fig. 4.2 which corresponds closely to the actual failure crack pattern of the model. The theoretical collapse load increases to 54.6 kN (12.27 kips) when the punching shear capacity of the plate deck is included.

7.3.3 Continuous Prestressed Concrete Waffle Slabs (Group C)

The continuous rectangular post-tensioned waffle slab bridge model PC3 supported by two interior isolated columns, was tested to failure by a two-load system, with

a concentrated load at the center of each span. Close agreement is observed between the theoretical and experimental results, as shown in Figs. 7.15 to 7.33, prior to cracking of the concrete. First cracks occurred around the two column supports in the top surface of the slab model, followed by other cracks under the applied load in the bottom surface of the model. Upon increasing the loading further, the cracks propagated across the width of the slab model through the transverse ribs. All the longitudinal ribs were cracked across the center line of each span panel at the bottom surface; furthermore, the top surface of the concrete flange plate was also cracked along the line connecting the two interior support columns, as shown in Fig. 7.78. This continuous slab model exhibited three single-line crack patterns parallel to the supports, one in each span panel (positive yield-line) and one along the line joining the two interior support columns (negative yield-line); see Fig. 4.4.

The experimental collapse load was 108.7 kN (24 kips), reached after punching shear failure of the plate deck had taken place around the loading plates. The theoretical collapse load was 109 kN (24.5 kips), derived by adopting the simplified yield-line crack pattern of Fig. 4.4 (see Appendix B). The closeness of the theoretical and experimental results gives verification to the assumed

crack pattern. The simplicity of the yield line method in solving a complicated problem is quite evident.

The 45° skewed continuous prestressed waffle slab bridge model PC4 was tested to failure by two concentrated loads as in slab model PC3. Deflection and strain results in the elastic stage and before cracking of the concrete were presented earlier in Figs. 7.39 to 7.60; close correspondence can be observed between the theoretical results obtained by the finite element method and by experiment.

Experience is required with this type of structure to predict the crack propagation and the formation of the yield-line, since the slab is skewed 45° and supported by two isolated staggered columns around the center of the slab model. Based on past experience and from studying this slab model under different load conditions, the proposed crack pattern in Fig. 4.5 is used to estimate the theoretical collapse load. The first crack appeared at the top surface around the two support columns, due to two-concentrated loads of approximately 72 kN (16 kips); upon further loading, cracks appeared under the two loads at the bottom surface of the slab model (Fig. 7.79) and extended along a path of maximum stress to the free edges (Fig. 7.80), lines Q'f' and Ti in Fig. 4.5; upon increasing the load further, severe cracks, due mainly to twisting,

extended to the obtuse corners and to the center of the slab as well as along $3/4$ the lengths of lines Q'f and Ti'. For simplicity in design the crack pattern is assumed along the full lengths of lines Q'f and Ti' as shown in Fig. 4.5; this assumption is confirmed by the progressive failure analysis as will be discussed later.

The calculated theoretical collapse load of 115.7 kN (26.0 kips), which is close to the experimental failure load of 119 kN (26.7 kips), was derived adopting the yield-line crack pattern of Fig. 4.5, (see Appendix B). The assumed crack pattern correspond closely to the actual failure crack pattern of the slab model.

A summary of results for the ultimate collapse loads as well as the central deflection corresponding to the cracking load for the seven bridge models are presented in Table 7.3. It can be observed that there is close agreement between theory and experiment, and that the prestressed concrete bridge models are much stiffer and stronger than the reinforced concrete models. As was mentioned earlier punching shear failure of the deck was evident in bridge models PC1, PC2, PC3, and PC4. Punching shear capacity is influenced by many factors such as: concrete area resisting punching, shape of section, strength of concrete, percentage of steel and the effective prestress in the steel.

7.4 Progressive Failure Analysis (Finite Element Method)

7.4.1 Simply Supported Waffle Slabs

Figure 7.81 shows the crack propagation of the simply supported rectangular reinforced concrete waffle slab (RC1) by means of the Progressive Failure Analysis. The slab model was subjected to a uniformly distributed load. The first cracks appeared at the bottom surface and along the line of symmetry of the slab model due to a uniform load of 2.6 kN/m^2 (0.38 psi) as shown in Fig. 7.81a. More cracks appeared around the center line of the slab model upon increasing the uniform load. The final theoretical collapse load of 5.7 kN/m^2 (0.82 psi) based on the Progressive Failure Analysis is below the experimental collapse load of 7.6 kN/m^2 (1.1 psi). It can be noted that this model exhibited a single-line crack pattern which is identical to the one used in the ultimate load method. It can also be noted that this slab model acts as a wide beam under the uniform load; notice that in Fig. 7.81a all the elements along the transverse center-line cracked simultaneously. Figure 7.96 shows the load-deflection relationship for the rectangular model due to uniform load. Close agreement is observed between theory and experiment.

Figure 7.82 shows the crack propagation of the rec-

tangular slab model (RC2) due to a single concentrated load at the center of the slab model. The first crack appeared directly under the load at the bottom surface of the slab model due to a load of 5 kN (1.12 kip). Upon increasing the load other elements in the region of the initial crack began to crack to form a single-line crack pattern extending towards the free edges of the model. The ultimate collapse load by the Progressive Failure Analysis is 10.3 kN (2.32 kips), which is close to the actual failure load as well as the theoretical ultimate load based on the yield-line theory. The comparison is shown in Table 7.3. Figure 7.97 shows the load-deflection relationship for the rectangular slab model (RC2) due to a single concentrated load at the center of the model. Good agreement is again observed between theory and experiment.

Figure 7.83 shows the propagation of cracks in the skew slab model (RC3) due to a single concentrated load applied at the center of the slab model. The first cracks occurred at the bottom surface under a load of 17.4 kN (3.90 kips), and they extended along a line making an angle of approximately $\theta/2$ with the x axis, and intersecting the two free edges. The final crack pattern of the model, shown in Fig. 7.83d, due to a load of approximately 17 kN (3.84 kips) agrees closely

with the one derived by the yield-line analysis as shown in Fig. 4.2. The load deflection relationship for this model is shown in Fig. 7.98 and close agreement is noted between the theoretical and experimental results.

Figure 7.84 shows the crack propagation of the rectangular prestressed waffle slab (PC1) due to a lateral concentrated load applied at the center of the edge beam. The first crack occurred at the bottom surface under a load of 9.6 kN (2.16 kips) and extended along the center-line of the model; this was followed by the appearance of another crack at the top surface of the model as shown in Fig. 7.84d. The final collapse load of 24 kN (5.4 kips) obtained by the Progressive Failure Analysis is in good agreement with the actual failure load, as well as with the collapse load estimated by the yield-line analysis as shown in Table 7.3. Results for the load-deflection relationship are presented in Fig. 7.99, and good agreement is noted between theory and experiment.

The 45° skewed post-tensioned waffle slab model (PC2) was tested to failure by a concentrated load at the center. Crack propagation is presented in Fig. 7.85, and is similar to that of the reinforced skew slab shown in Fig. 7.83. However, with model PC2 the first crack occurred at a load of 16 kN (6.6 kips) and the model failed at a load of 28 kN (11.4 kips), which corresponds closely to the

actual failure load. Figure 7.100 shows the load-deflection relationship for the skew slab model due to a concentrated load at the center; again, close agreement is shown between theory and experiment. It is observed that the maximum central deflections of the prestressed models are much smaller than the maximum central deflections of the reinforced concrete models. This is due to the fact that the causes of failure in the two types are different; in the prestressed waffle system the failure is due to crushing of the relatively thin concrete flange plate, while in the reinforced waffle system failure is due to yielding of the steel reinforcing.

7.4.2 Continuous Prestressed Waffle Slabs

Figures 7.86 to 7.90 show the crack propagation of the rectangular prestressed continuous waffle slab (PC3) by means of the Progressive Failure Analysis. The first crack appeared at the top surface around the two interior support columns due to two concentrated loads of approximately 67.5 kN (14.96 kips) applied at the center of each span; upon further loading further elements cracked under the load at the bottom surface and subsequently the cracks extended to the free edges of the slab model. The corresponding theoretical collapse load was 110 kN (24.7 kips) which is close to the actual failure load as well as the

theoretical collapse load calculated on the basis of an assumed yield-line pattern. It can be observed that the final crack pattern of the model corresponds closely to the assumed yield-line crack pattern.

Figure 7.101 shows the load-deflection relationship for the continuous rectangular prestressed slab model, subjected to two concentrated loads, applied at the center of each span panel. Close agreement is observed between the theory and experiment.

Figures 7.91 to 7.95 show the crack propagation of the continuous prestressed skew waffle slab model (PC4) by means of the Progressive Failure Analysis. The first cracks occurred at the two interior column supports due to a load of 71 kN (15.84 kips); this was followed by cracks under the two concentrated loads. Cracks were also formed at the top surface along the line joining the two interior column supports, forming a negative yield line, and intersecting the two free edges; similarly, cracks under the loads extended at the bottom surface to form positive yield lines. The final cracked pattern of the model in Fig. 7.95 closely resembles that assumed in the yield-line analysis. The theoretical collapse load by Progressive Failure Analysis was 117.5 kN (26.4 kips), which is in good agreement with that calculated using the yield line analysis. Figure 7.102 shows the load-

deflection relationship for the skew model (PC4); close correspondence is shown between theory and experiment.

7.5 Effect of Rotating the Interior-Column Line About the Center of the Slab Bridge Model

Figure 7.54 and Figs. 7.103 to 7.105 show the deflection distribution for the continuous skew slab model subjected to two concentrated loads each of 35.6 kN (8 kips) capacity, and applied at the center of each span panel. Upon rotating the column-line, keeping their x distance constant from the longitudinal center line of the slab model, the deflection pattern changes gradually to become almost flat at the middle of the longitudinal center line; the central deflection of the slab model increases from 0.05 mm (0.002 in.) to 0.127 mm (0.005 in.) due to the increased distance between the two columns. Figure 7.66 and Figs. 7.106 to 7.108 show the corresponding moment distribution for the same slab model. It can be observed that the longitudinal moment decreases whereas the transverse moment increases. Study of these figures indicates that the best location for the two interior columns will be as shown in Fig. 7.106, in which the transverse and longitudinal moments at the center of each span panel are almost equal, i.e., both the transverse and the longitudinal ribs will be working effectively together in carrying the load.

7.6 Effect of Continuous Pier Line Support in a Rectangular Slab

7.6.1 Rigid Pier Line Support

Figure 7.109 shows the deflection distribution for a rectangular prestressed waffle slab due to two concentrated loads each of 35.6 kN (8 kips) acting at the center of each span panel. The slab is supported by a rigid continuous pier line support. Figure 7.110 shows the corresponding moment distribution for the same slab. Comparing these deflections with these in a similar slab supported by two isolated rigid interior columns, it is noted that the latter deflections are about 5% greater than the former. The same conclusion can be drawn when comparing the resulting moments in both slab models as shown in Figs. 7.110 and 7.38.

7.7 Effect of Continuous Pier Line Support in a Skew Slab

7.7.1 Rigid Pier Line Support

Figures 7.111 and 7.112 show the deflection and moment distributions, respectively, for a skew waffle slab due to two concentrated loads applied at the center of each span panel; the slab is supported by a rigid continuous pier line support. Comparing the deflection values with those in Fig. 7.104 for a skew slab with two isolated

rigid column supports, shows that the latter are approximately 10% greater than the former. The same observation is obtained when comparing the moment distributions for both slabs.

CHAPTER VIII

SUMMARY AND CONCLUSIONS

A study of the behaviour of reinforced and prestressed concrete waffle slab structures, loaded to failure, has been presented. The elastic response of such structures, of rectangular or skew planform, is predicted by means of a Fourier series solution based on an orthotropic plate theory using realistic estimates for the orthotropic rigidities. The solution is formulated by the superposition of results from a bending analysis to those from an in-plane stress analysis, and applied to single span as well as to continuous waffle slab bridges.

The results obtained from the series solution in the elastic range are compared with the results obtained from a finite element solution; furthermore, the ultimate collapse loads of such structures are estimated by means of the yield-line theory.

The intermediate stage after the cracking of the concrete and before collapse of the structure is studied by means of a progressive failure analysis using the finite element technique. Modified flexural and torsional rigidities of cracked regions are used in the

analysis.

Test results were obtained from an experimental program on seven reinforced and prestressed waffle slab models. Five slab models were simply supported, while the remaining two were continuous over interior isolated column supports. The experimental results verify and substantiate the elastic, ultimate load and progressive failure analyses.

A comparison is presented between the behaviour of waffle slab structures supported on interior isolated columns, and those supported on a continuous pier. A study of the effect of rotating the column support line about the center of the bridge on the structural response of a waffle slab bridge are also made.

Based on the experimental work and in conjunction with the analytical studies undertaken, the following conclusions can be drawn:

1. The elastic behaviour of concrete waffle slab structures can be accurately predicted by means of the classical orthotropic plate theory.
2. The reliability of the estimates of the orthotropic ~~flexural~~ flexural, torsional, and axial rigidities of waffle slab construction is confirmed.
3. A waffle slab bridge has an excellent transverse load distribution characteristic due to its signi-

ficant transverse and torsional rigidities.

4. The elastic response of a prestressed concrete waffle slab bridge can be predicted more accurately than a reinforced concrete one, due to the absence of local cracking and microcracking.
5. the yield-line analysis is simple and reliable in predicting the collapse load of rectangular and skew waffle slab bridges in reinforced and prestressed concrete construction.
6. Prestressed concrete waffle slab construction is much stiffer and stronger than one in reinforced concrete, and therefore, it is well suited for use in large-span structures, as well as in marine structures.
7. A progressive failure analysis using a finite element approach, and variable rigidities is shown to predict collapse loads of reinforced and prestressed waffle slabs very close to those obtained by the yield-line analysis.
8. The progressive failure analysis provides the designer with reliable information regarding the serviceability and ultimate limit states of reinforced and prestressed waffle slab structures.

FIGURES

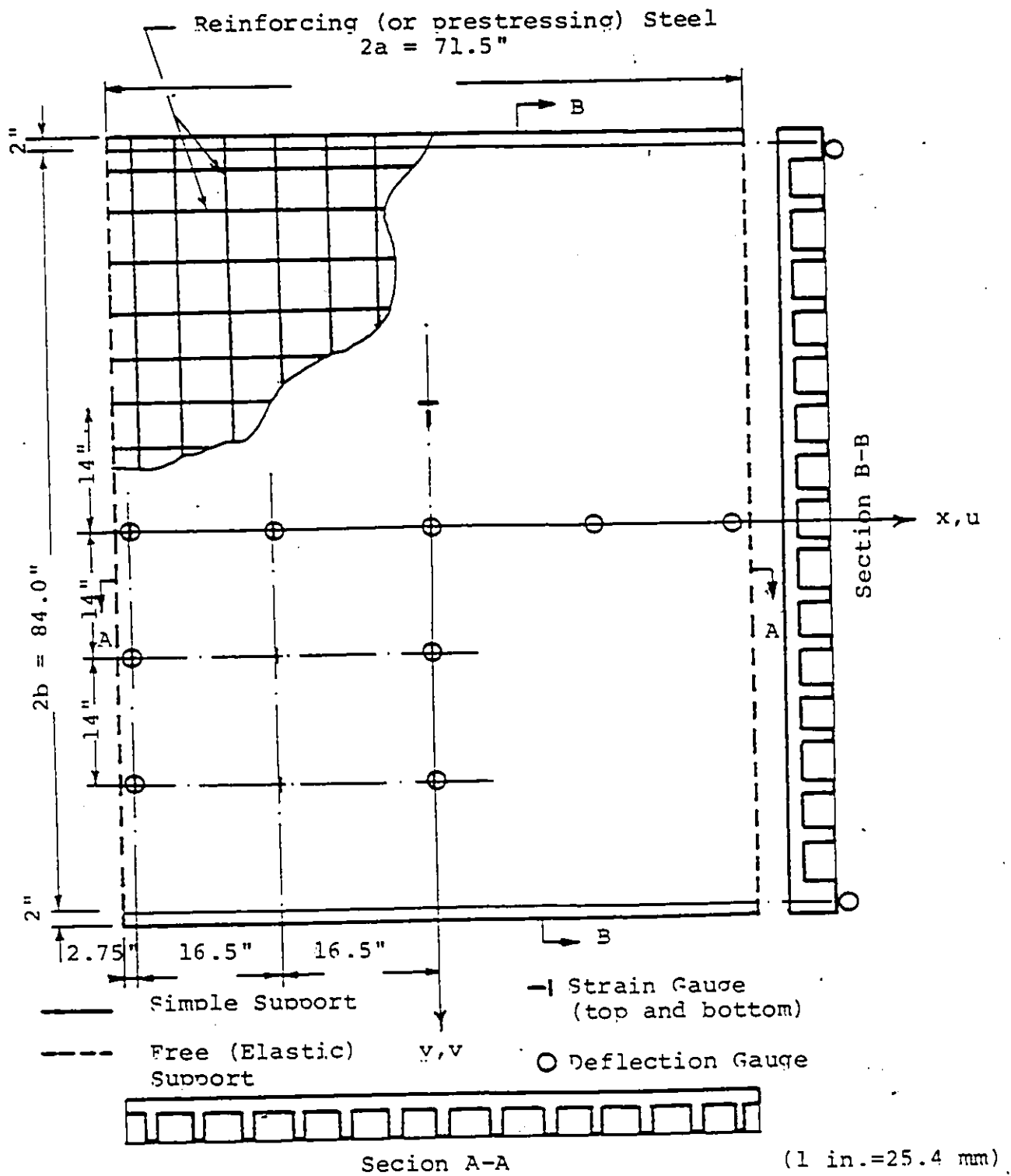


FIGURE 3.1 PLANFORM OF THE WAFFLE SLAB MODEL (RC1)

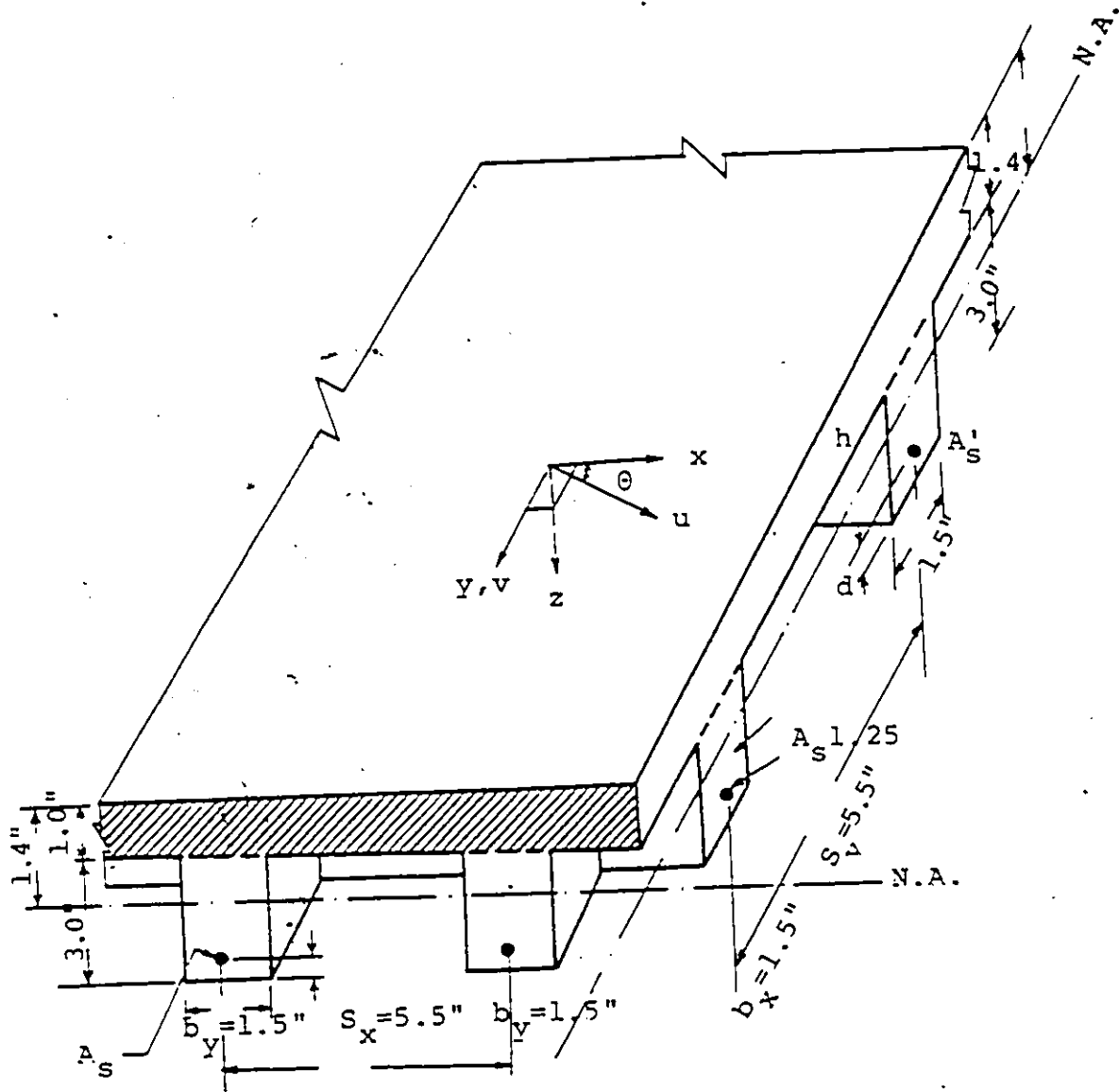


FIGURE 3.2 CROSS-SECTIONAL GEOMETRIES OF WAFFLE SLAB
MODEL (1 inch = 25.4 mm)

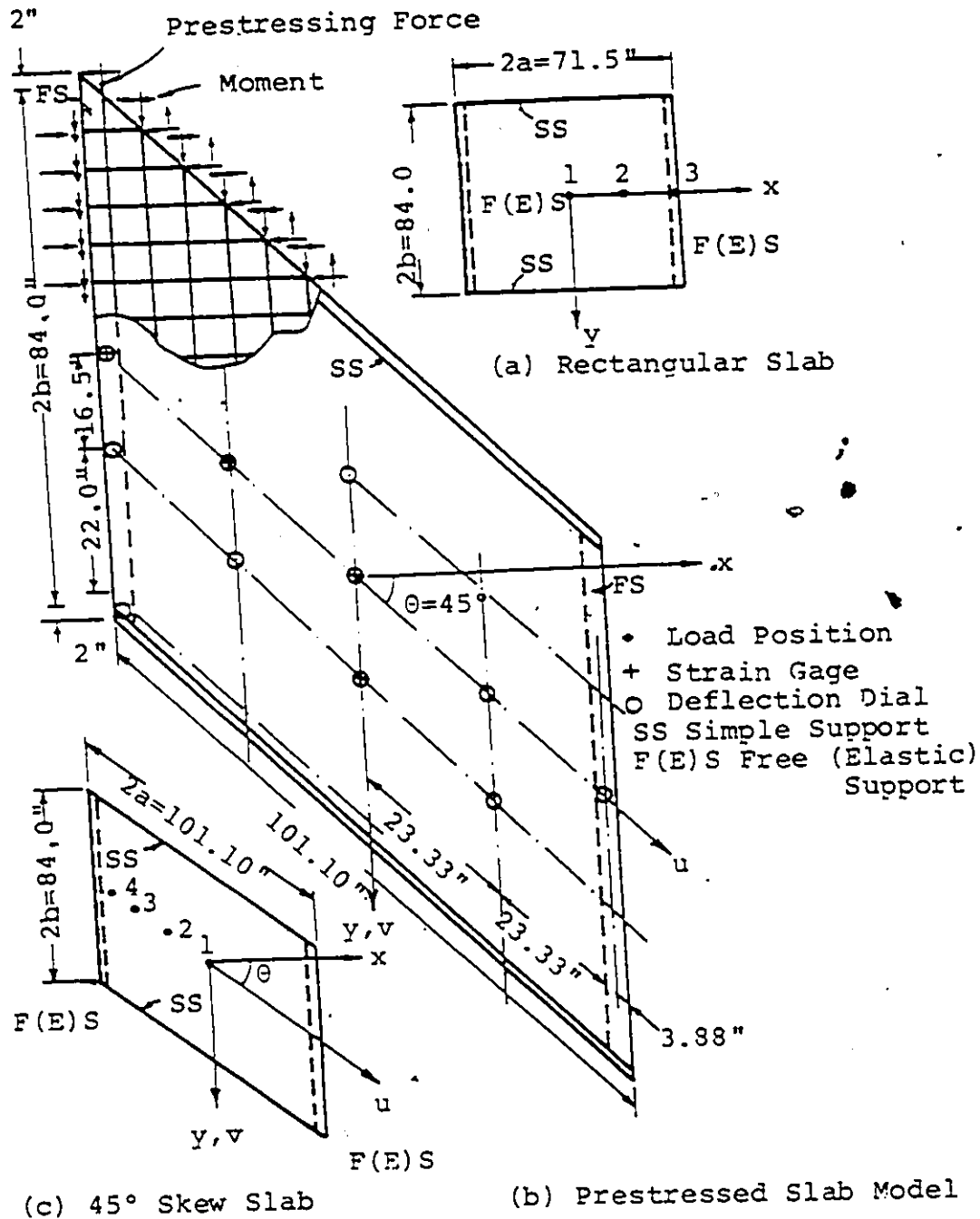


FIGURE 3.3 PLANFORMS OF PRESTRESSED CONCRETE WAFFLE SLAB BRIDGE MODELS (1 inch = 25.4 mm)

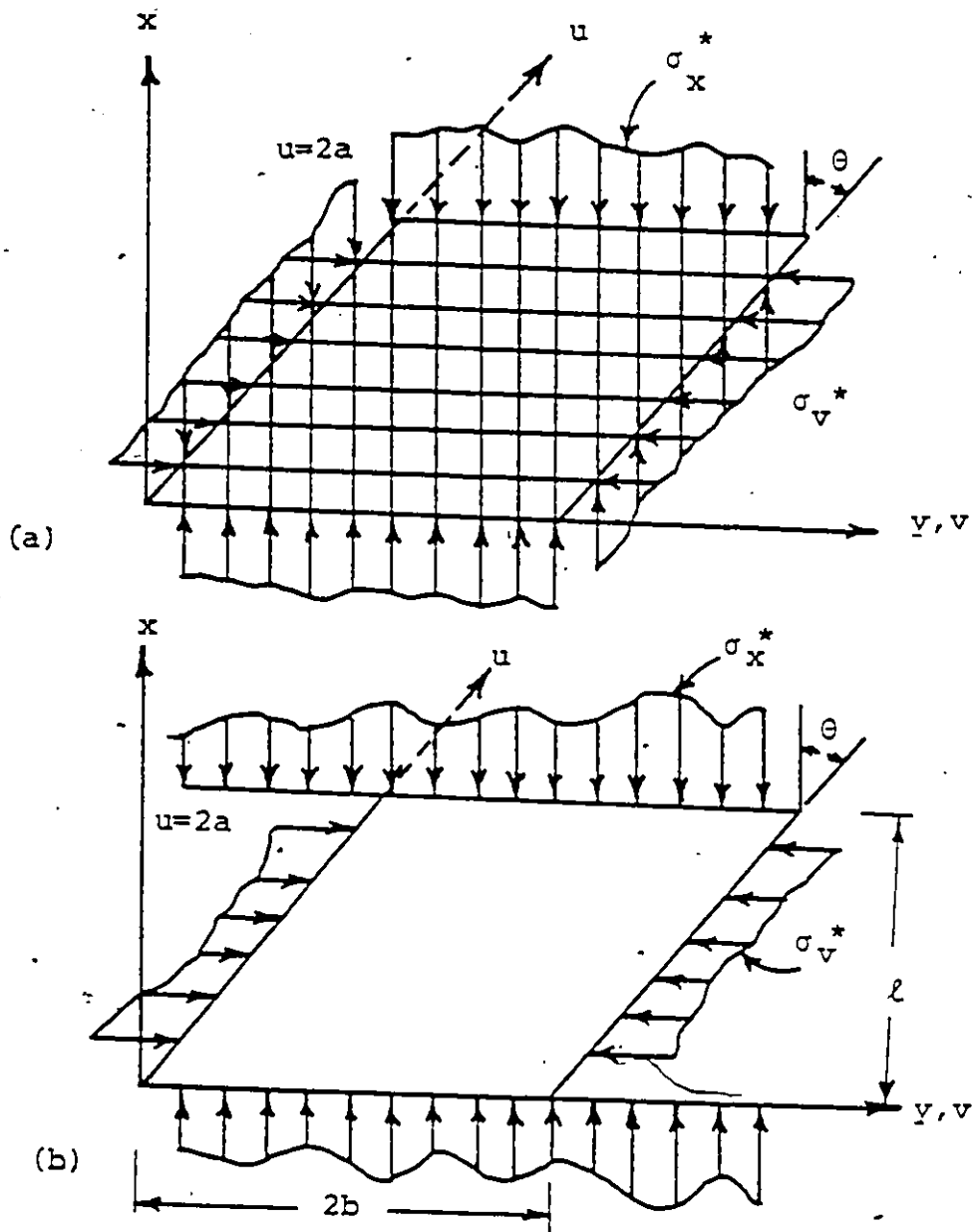


FIGURE 3.4 IN-PLANE PRESTRESS LOADING ON SKEW WAFFLE SLAB STRUCTURE

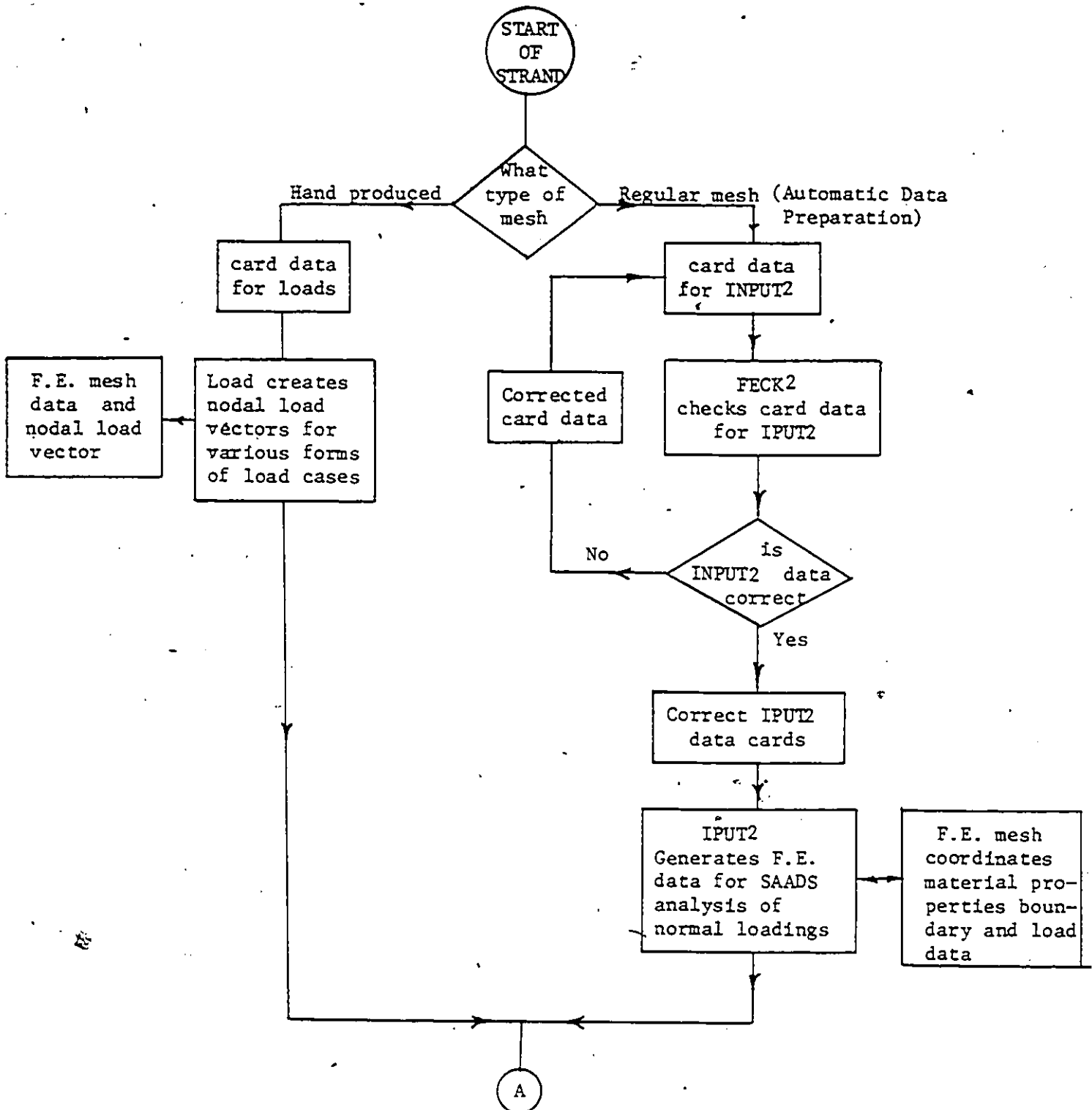


FIGURE 3.5 FLOW CHART OF STRAND SYSTEM

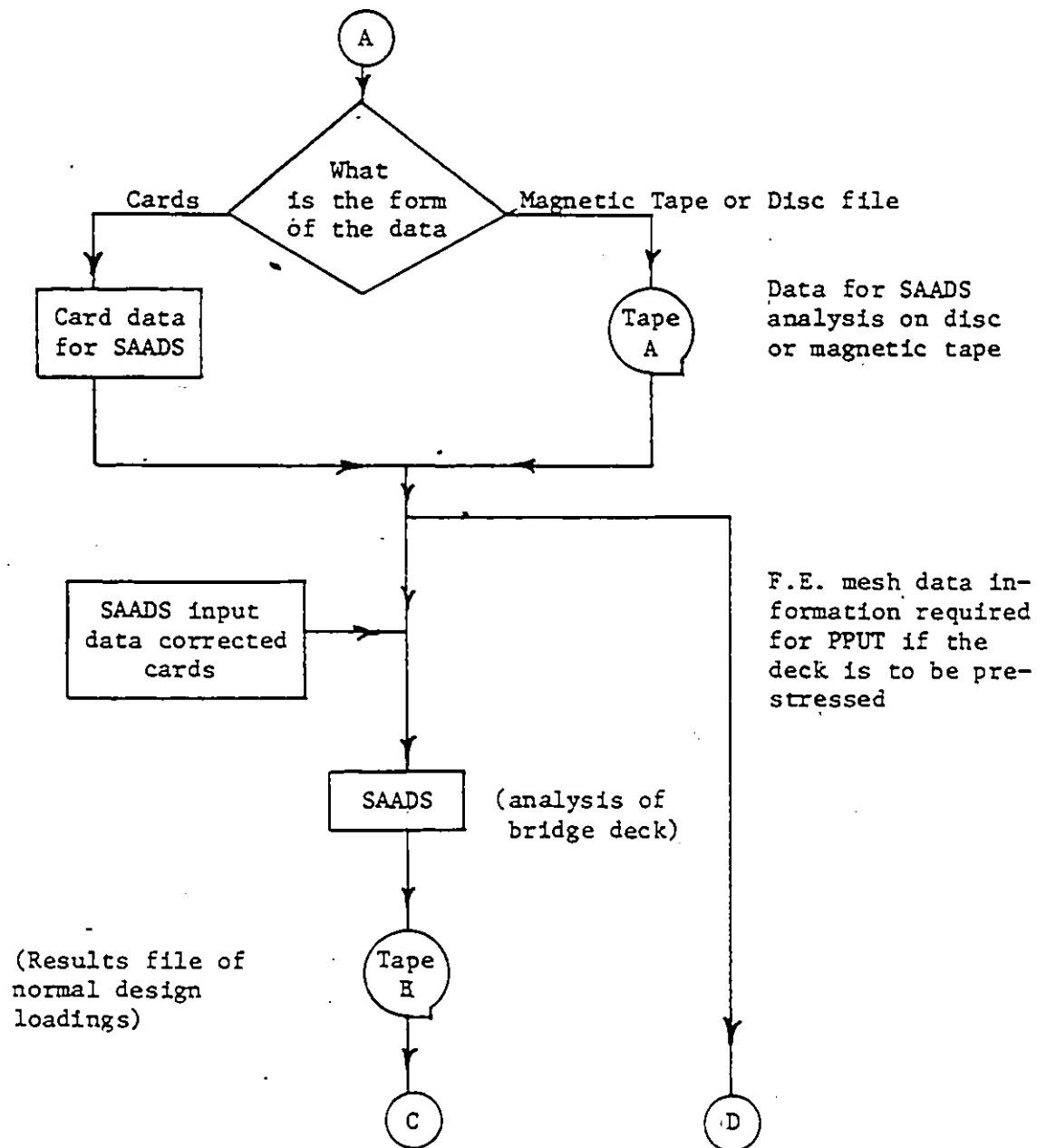
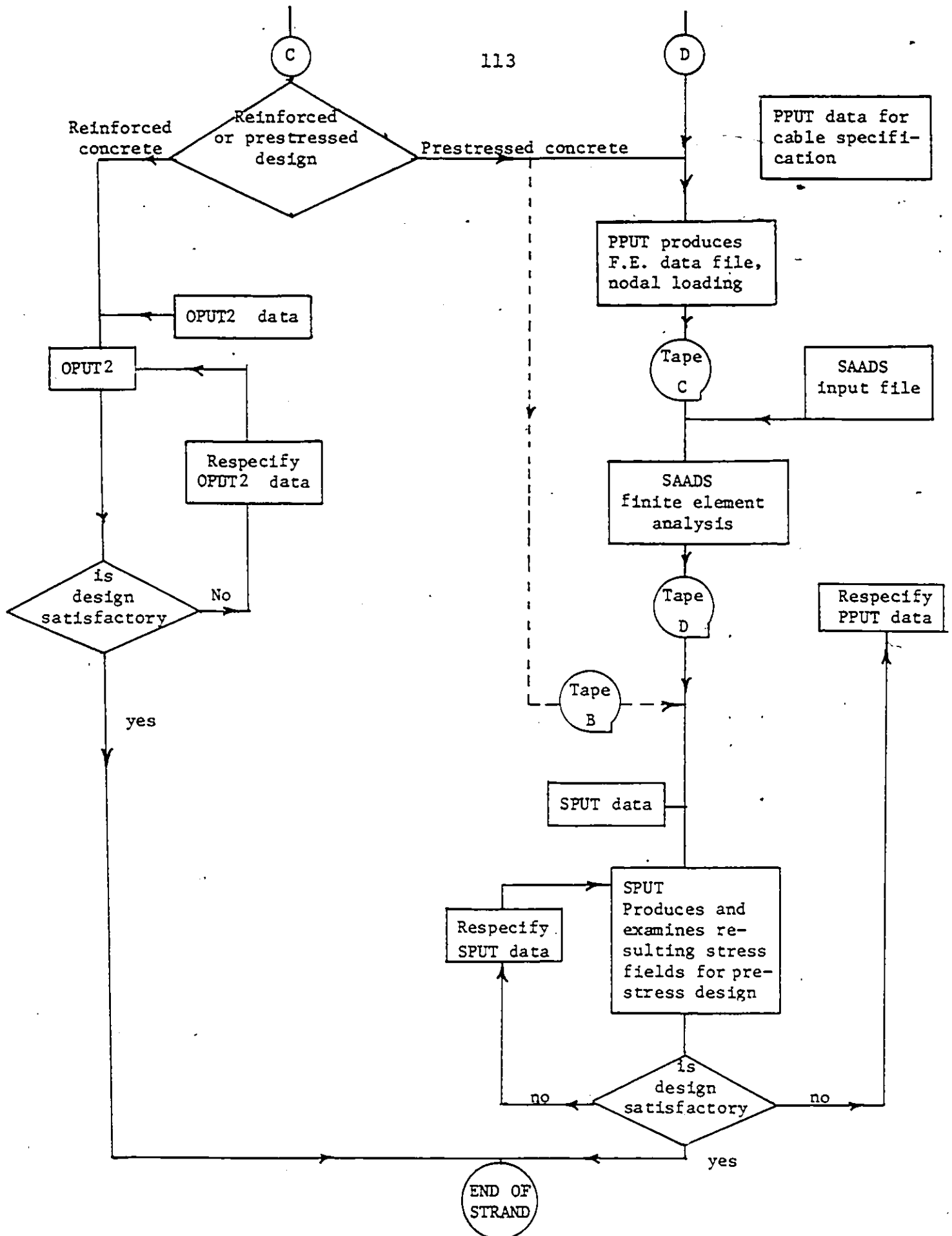
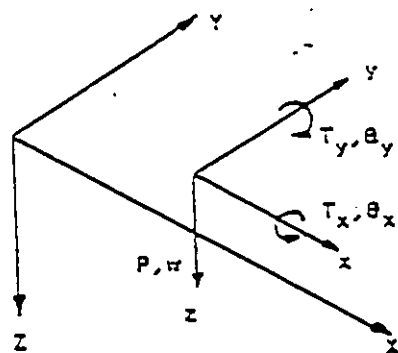


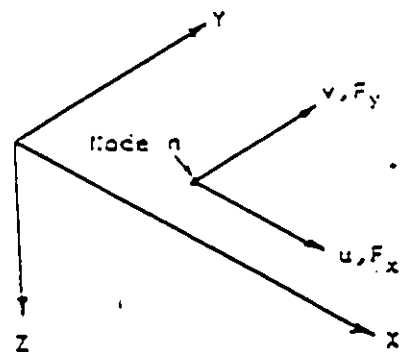
FIGURE 3-5 continued





NODAL FORCES AND DISPLACEMENTS
(plate)

(a)



NODAL FORCES AND DISPLACEMENTS
(plane stress)

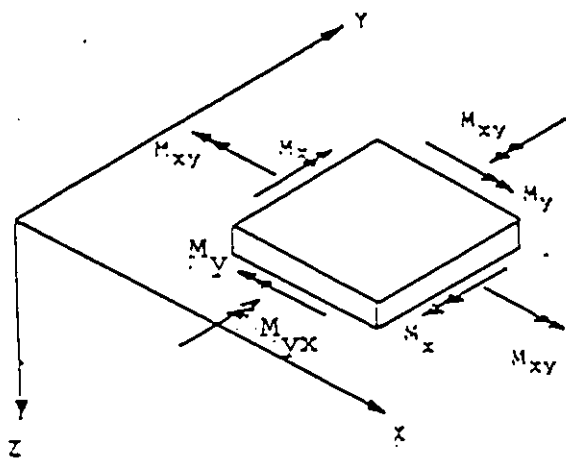
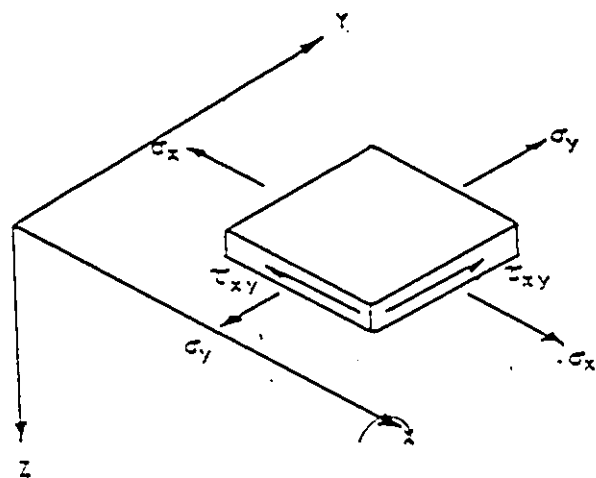
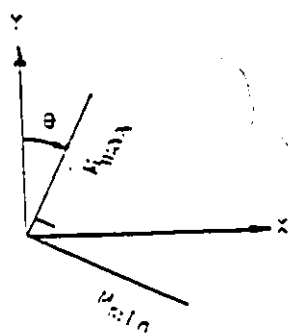


Plate bending stress

(b)

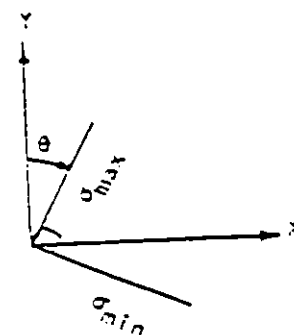


In-plane stresses



PRINCIPAL STRESSES

(c)



PRINCIPAL STRESSES

FIGURE 3.6 SIGN CONVENTION OF IN-PLANE AND PLATE BENDING STRESSES

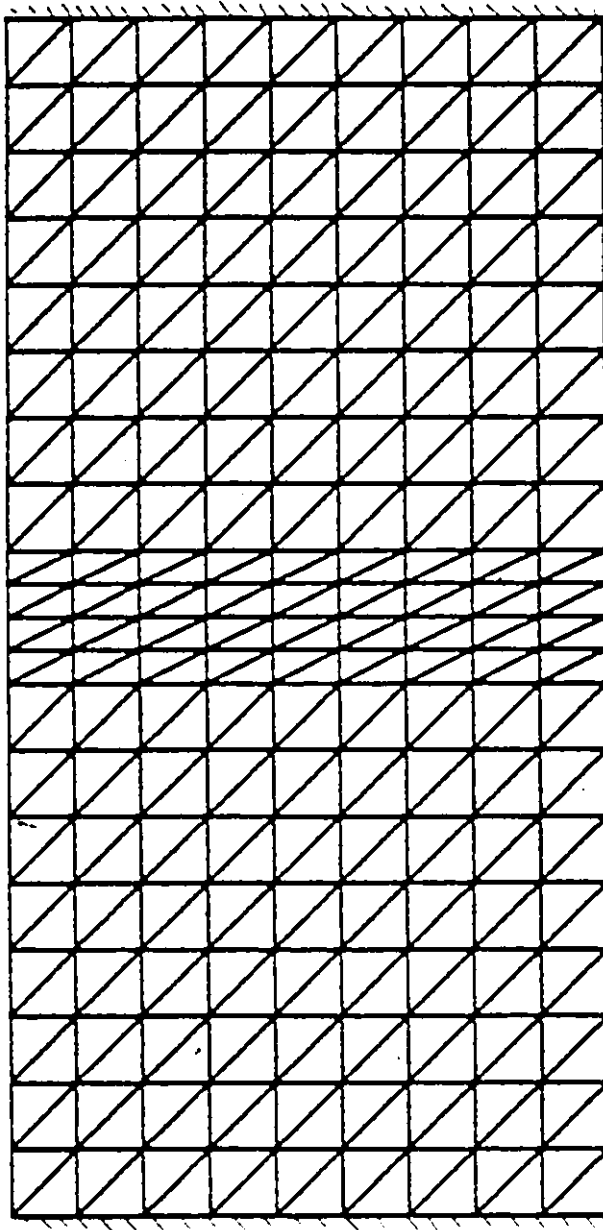


FIGURE 3.7 FINITE ELEMENT MESH FOR A RECTANGULAR WAFFLE SLAB
USING TRIANGULAR ELEMENTS

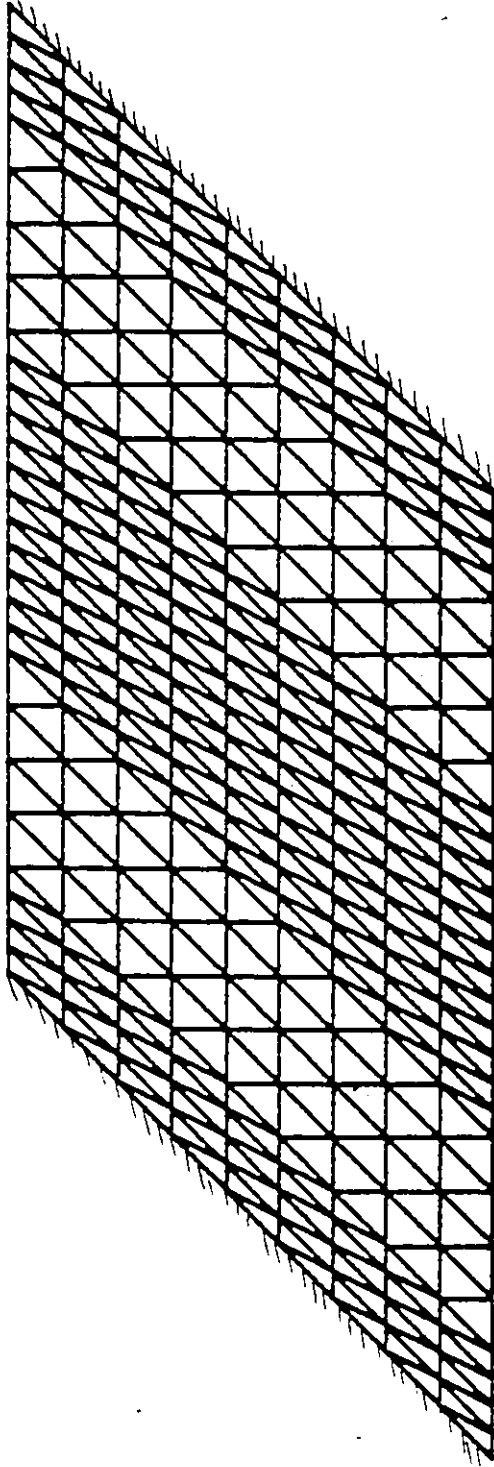
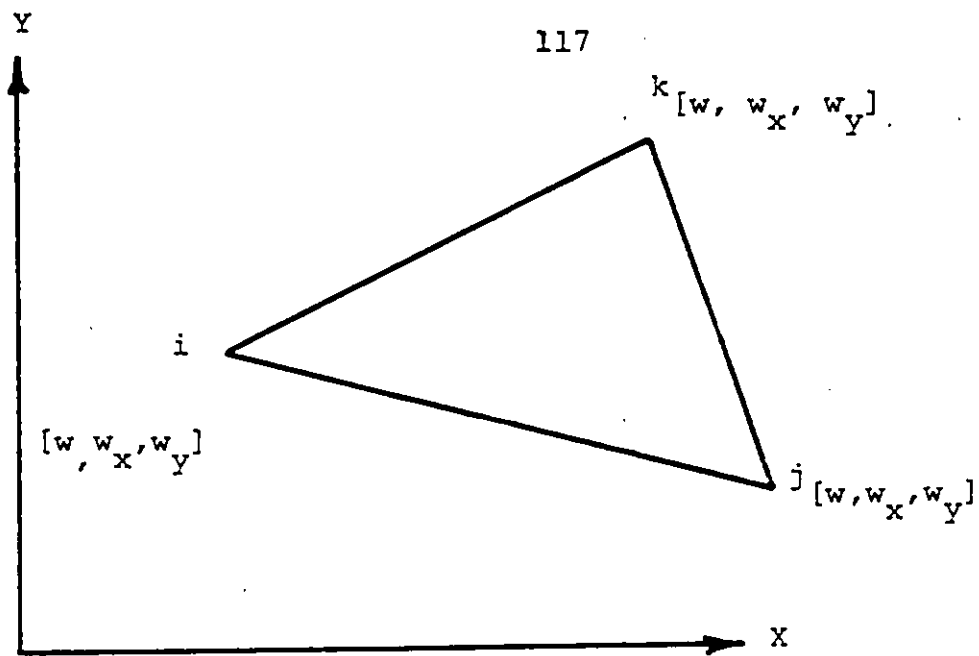
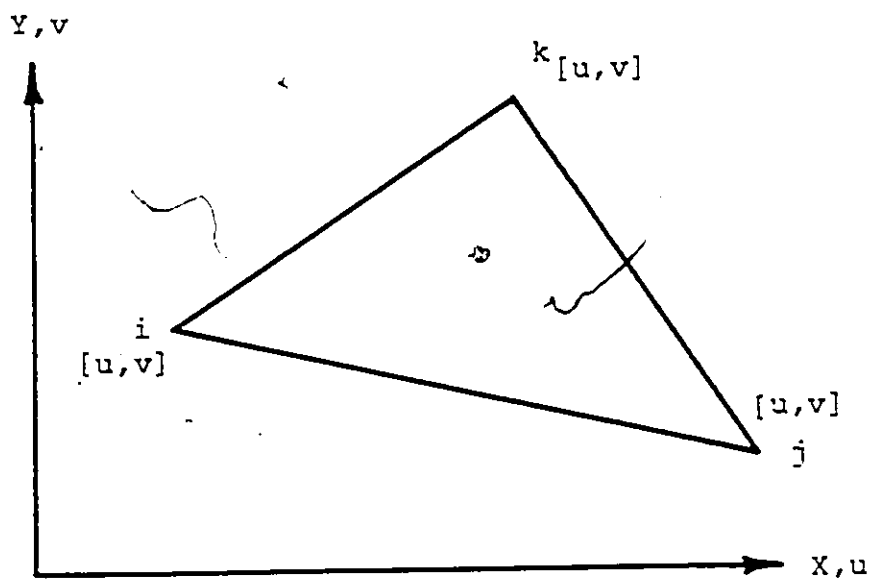


FIGURE 3.8 FINITE ELEMENT MESH FOR A SKEW WAFFLE SLAB USING TRIANGULAR ELEMENTS



a. PLATE ELEMENT



b. PLANE STRESS ELEMENT

FIGURE 3.9 TRIANGULAR ELEMENTS FOR STRAND ANALYSIS

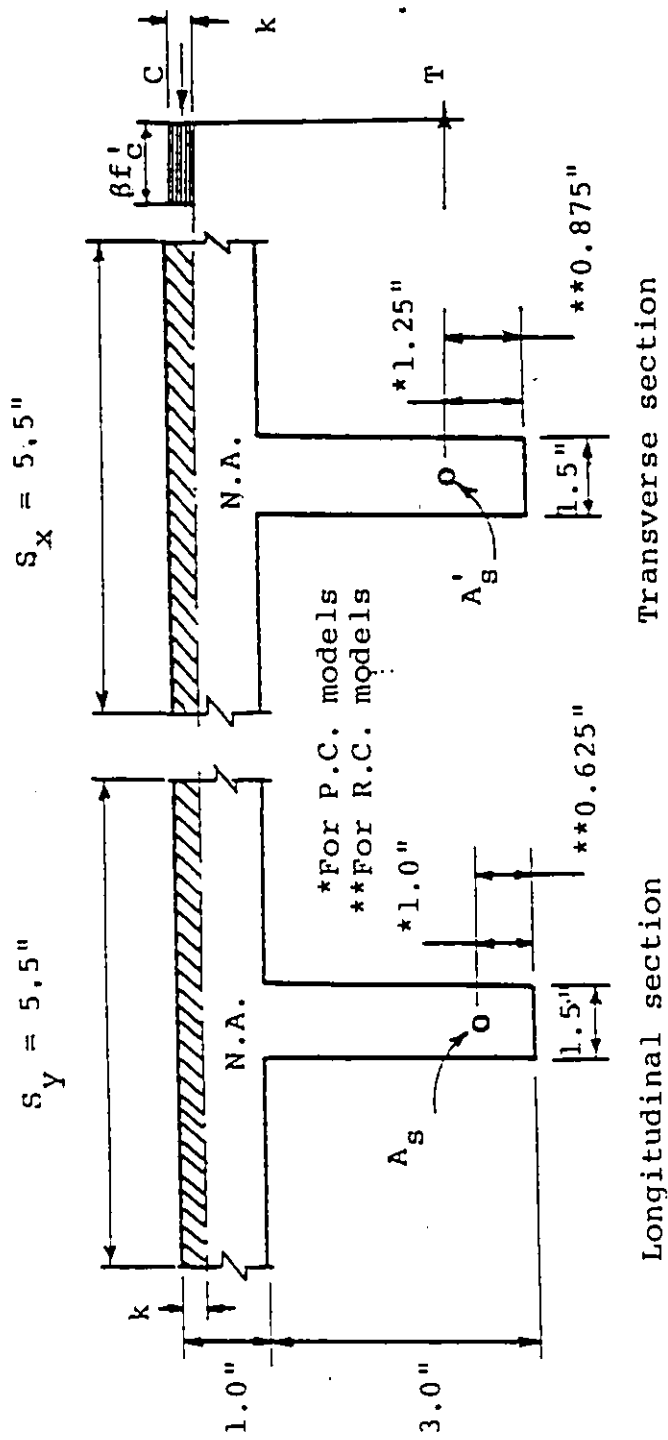


FIGURE 4.1 CRACKED SECTIONS OF WAFFLE SLAB

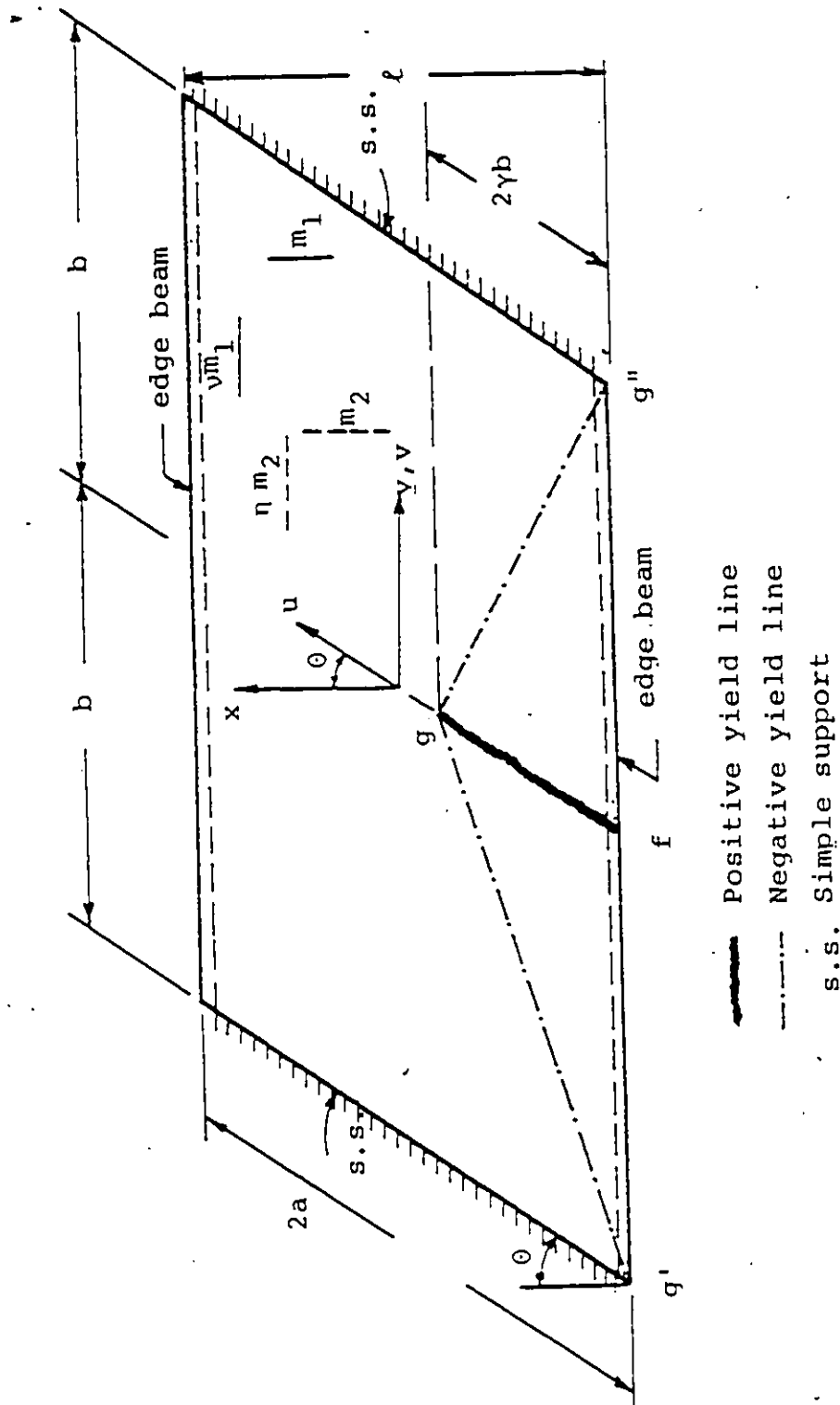


FIGURE 4.3 YIELD-LINE CRACK PATTERNS FOR SKEW WAFFLE SLAB DUE TO A CONCENTRATED LOAD AT THE CENTER OF THE EDGE BEAM

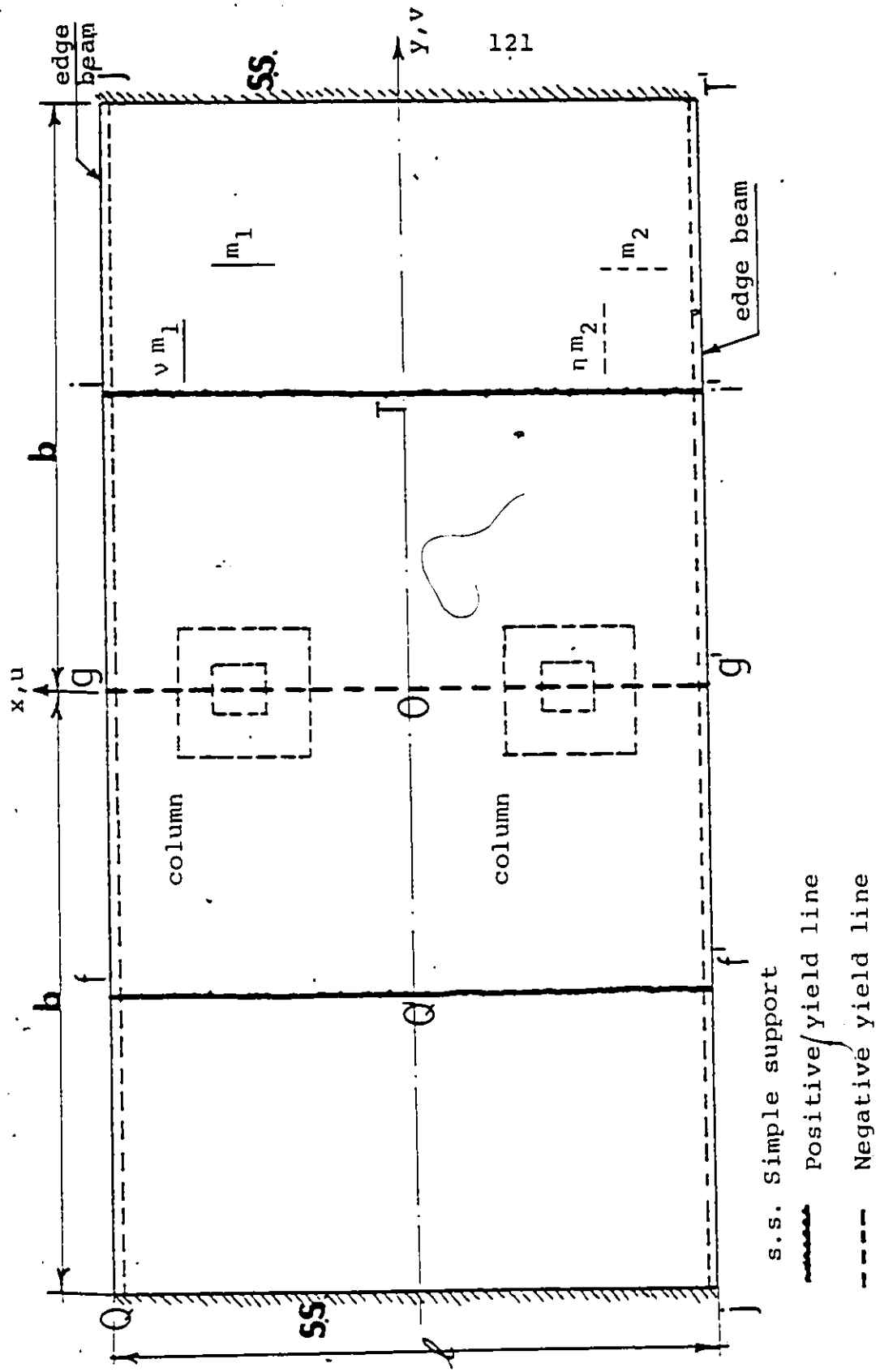


FIGURE 4.4 SINGLE YIELD-LINE CRACK PATTERN IN CONTINUOUS RECTANGULAR WAFFLE SLAB.

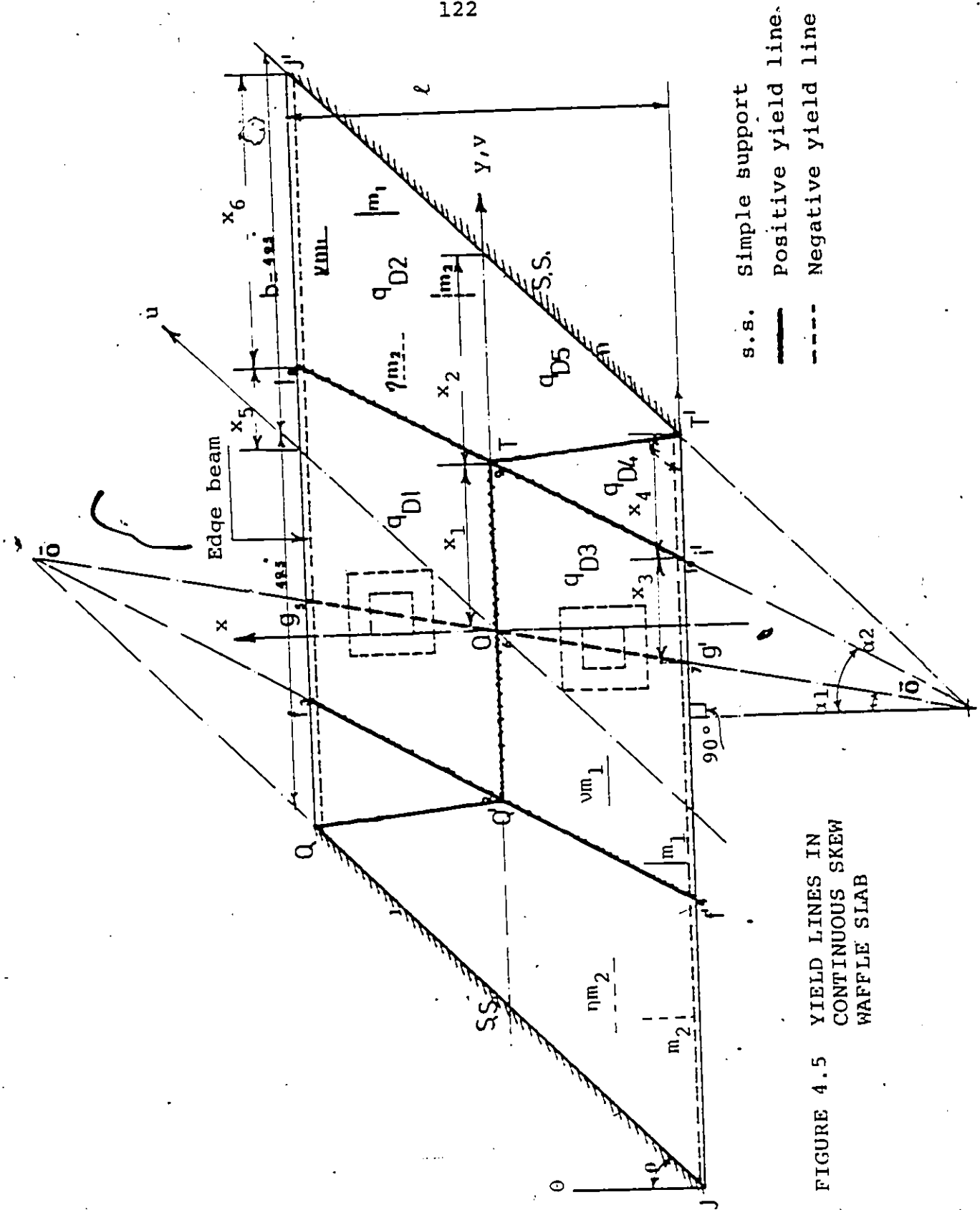


FIGURE 4.5 YIELD LINES IN CONTINUOUS SKEW WAFFLE SLAB

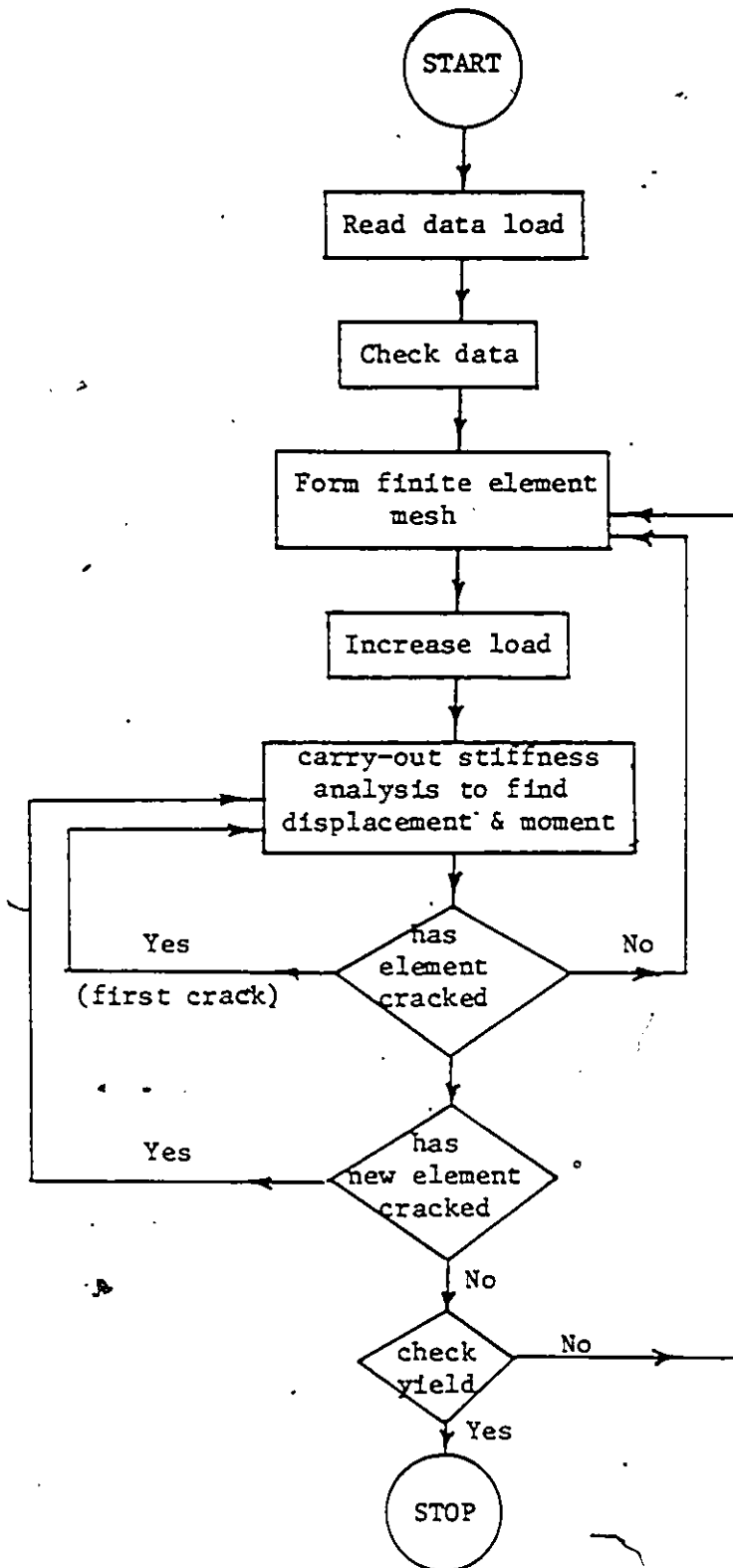


FIGURE 5.1 INCREMENTAL AND ITERATIVE PROCEDURE IN STRAND PROGRAM (MODIFIED)

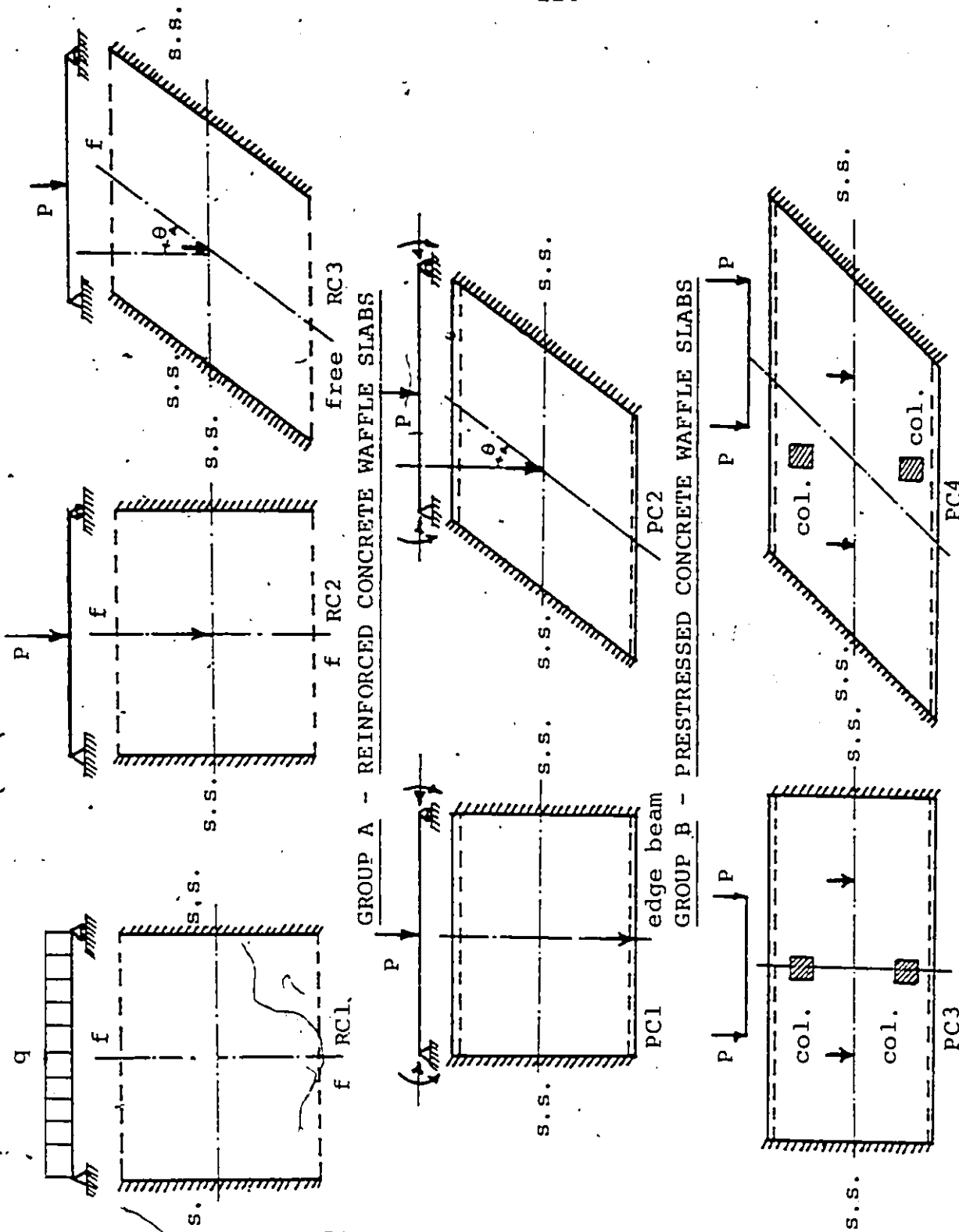


FIGURE 6.1 THE TESTED WAFFLE SLABS

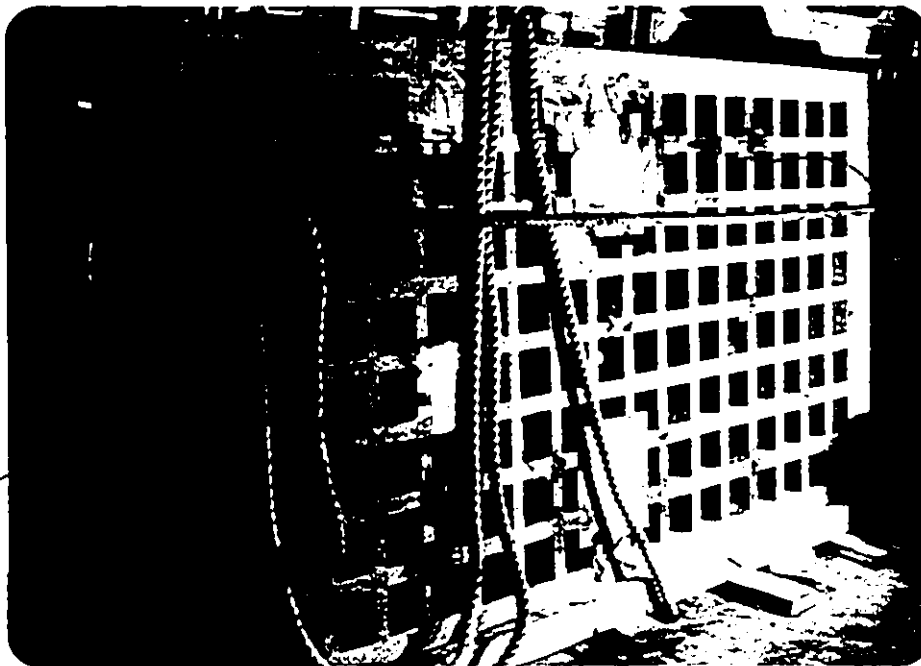


FIGURE 6.2 RECTANGULAR PRESTRESSED WAFFLE SLAB
MODEL (PC3)

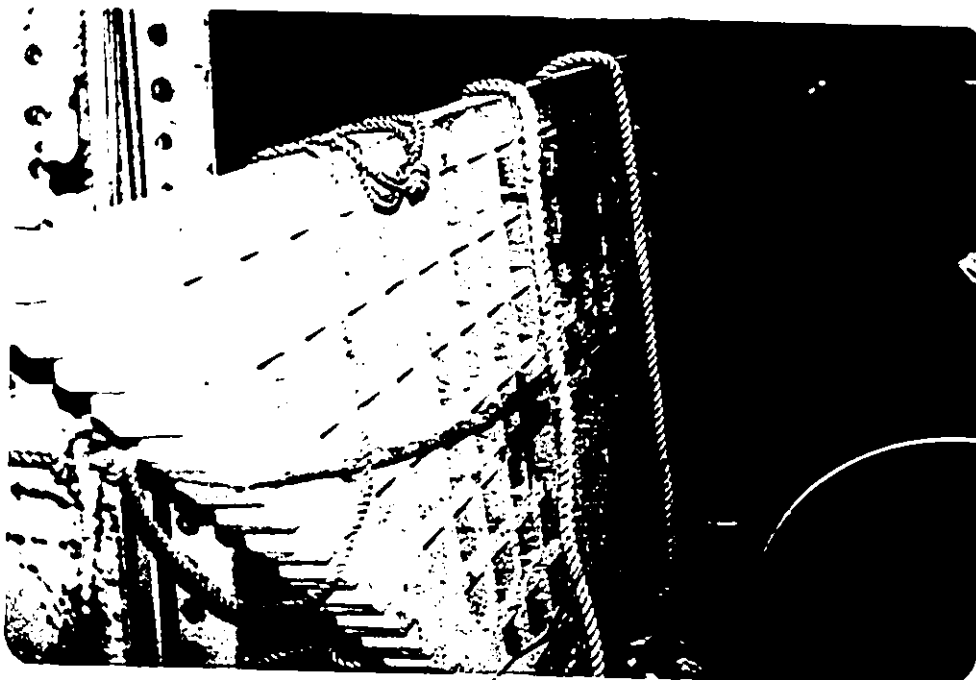


FIGURE 6.3 SKEW PRESTRESSED WAFFLE SLAB
MODEL (PC4)

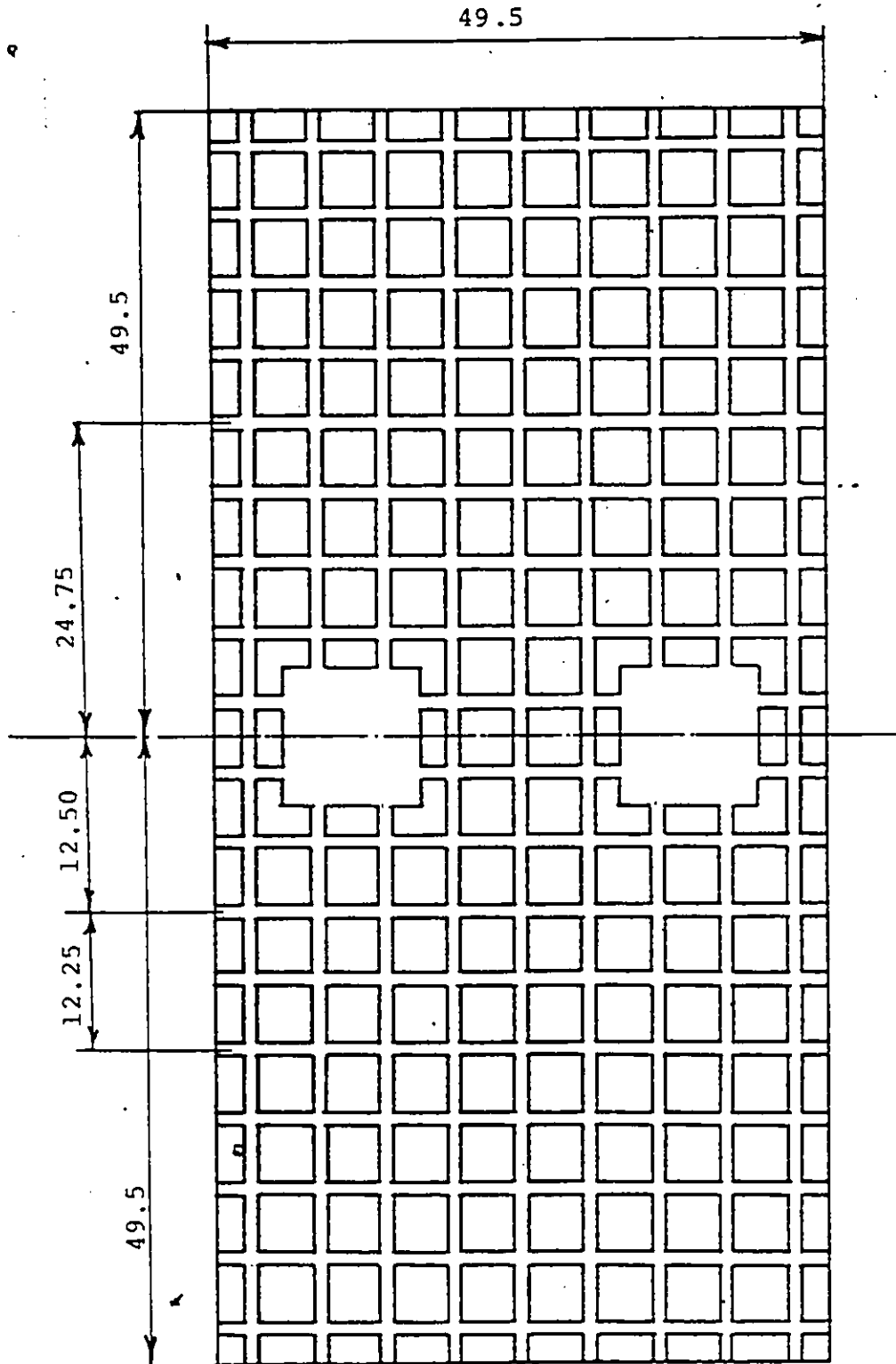


FIGURE 6.4 BOTTOM PLAN LAYOUT (RECTANGULAR WAFFLE SLAB PC3)

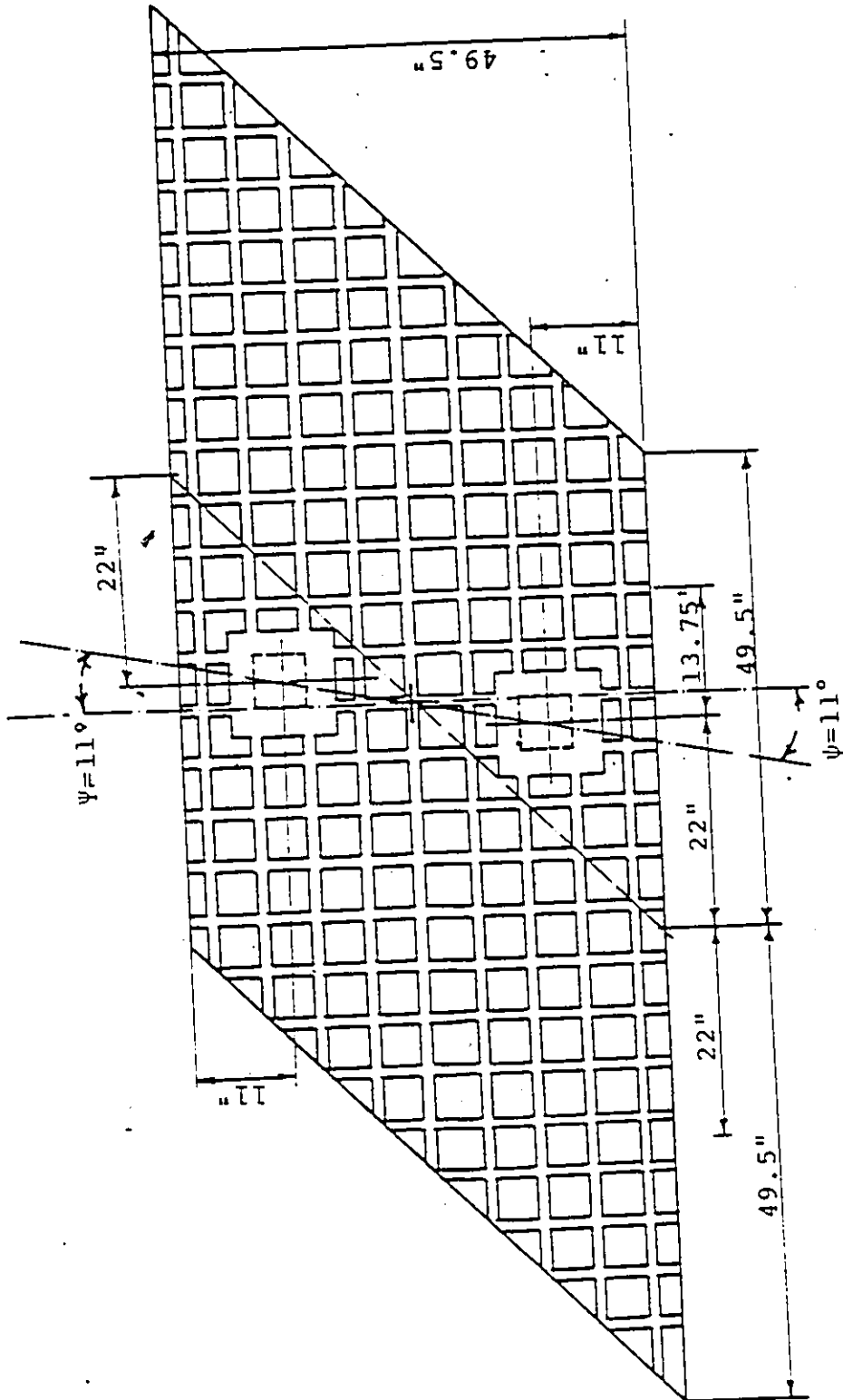


FIGURE 6.5 BOTTOM PLAN LAYOUT (SKEW, PC4).

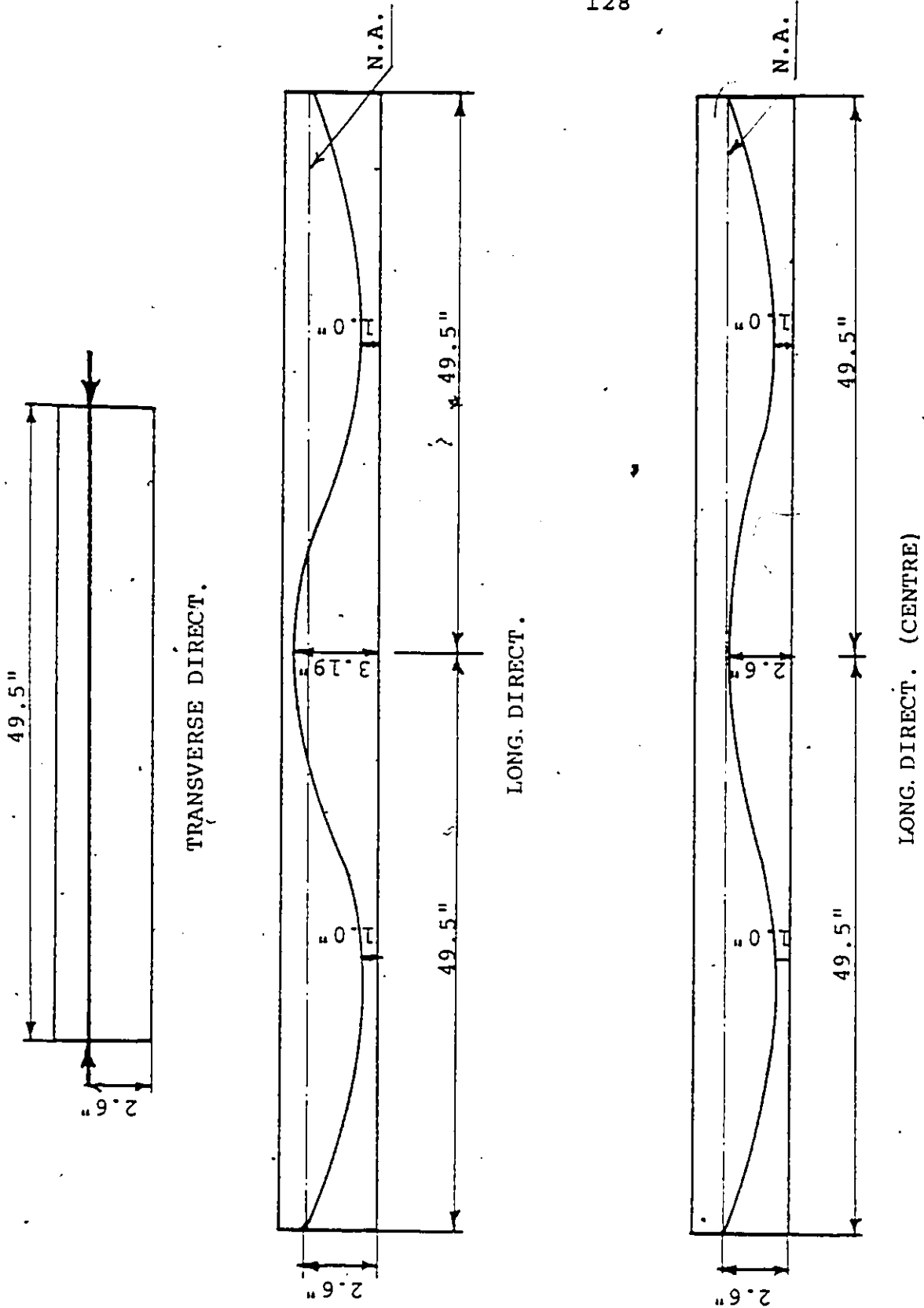


FIGURE 6.6 PRESTRESSED WIRE PROFILE FOR RECTANGULAR SLAB PC3 (1 in. = 25.4 mm)

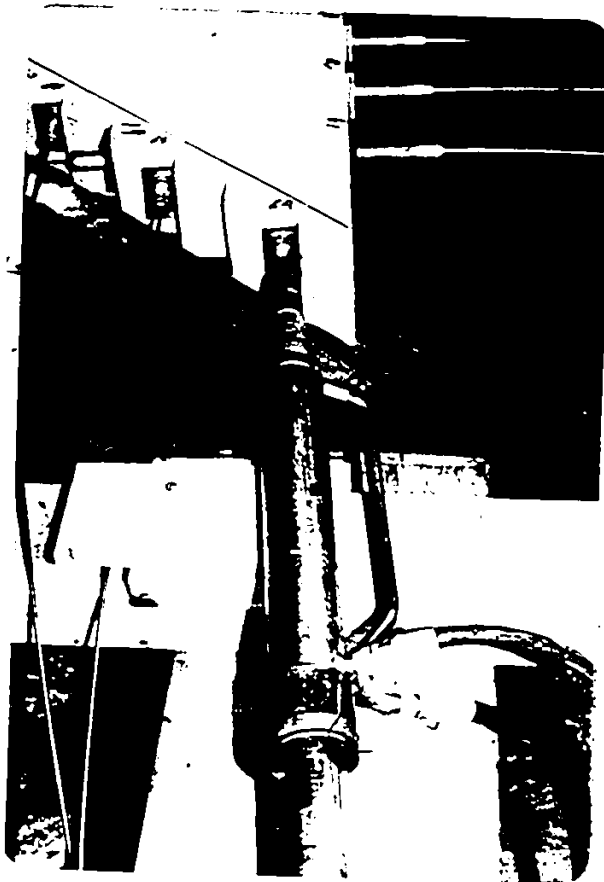


FIGURE 6.7 THE PRESTRESSING HYDRAULIC JACK IN POSITION

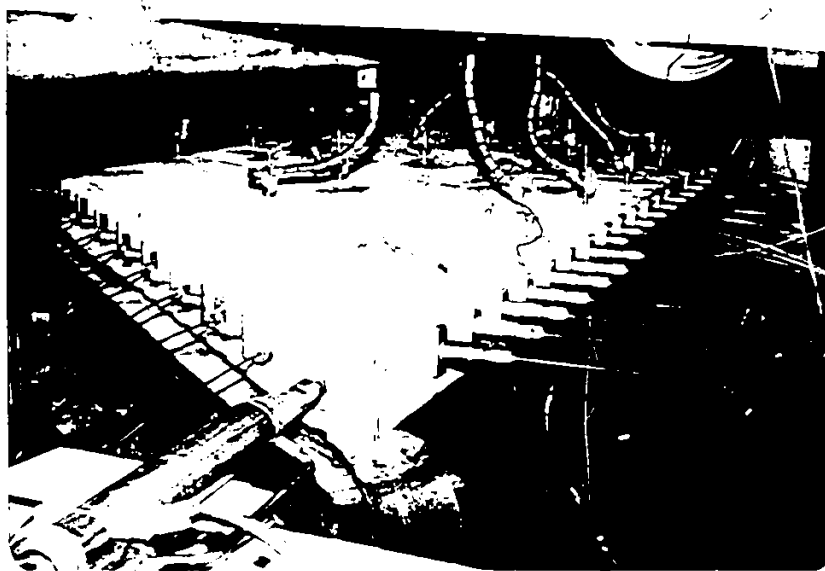


FIGURE 6.8 THE PRESTRESSING OF SKEW SLAB MODEL PC3

Cable
No.

Eccentricities

	1	2	3	4	5	6	7	8	9	e
1	66	66	66	66	66	66	66	66	66	1
2	57	55	55	58	60	60	57	50	50	2
3	50	46	44	50	50	50	38	35	33	3
4	42	38	38	44	44	31	25	25	25	4
5	36	35	33	41	28	31	25	25	28	5
6	31	28	28	36	28	29	28	41	50	6
7	25	27	25	30	34	34	44	60	84	7
8	25	25	28	31	47	50	66	76	85	8
9	33	30	39	44	60	69	79	82	84	9
10	50	44	60	63	68	88	82	76	71	10
11	66	60	76	79	60	80	73	61	50	11
12	80	76	82	82	50	63	57	41	33	12
13	84	82	79	73	31	44	38	28	25	13
14	76	79	63	52	28	31	25	25	25	14
15	52	63	47	36	29	25	25	28	28	15
16	31	41	31	25	33	31	25	31	38	16
17	25	25	25	25	41	34	31	34	44	17
18	33	25	28	36	58	42	41	41	50	18
19	52	37	38	44	66	50	44	44	57	19
20	57	53	53	57	66	60	57	57	58	20
21	66	66	66	66	66	66	66	66	66	21

FIGURE 6.9 WIRE PROFILE AND ECCENTRICITIES OF THE CURVED TENDONS FOR SKEW SLAB PC4
(in mm)

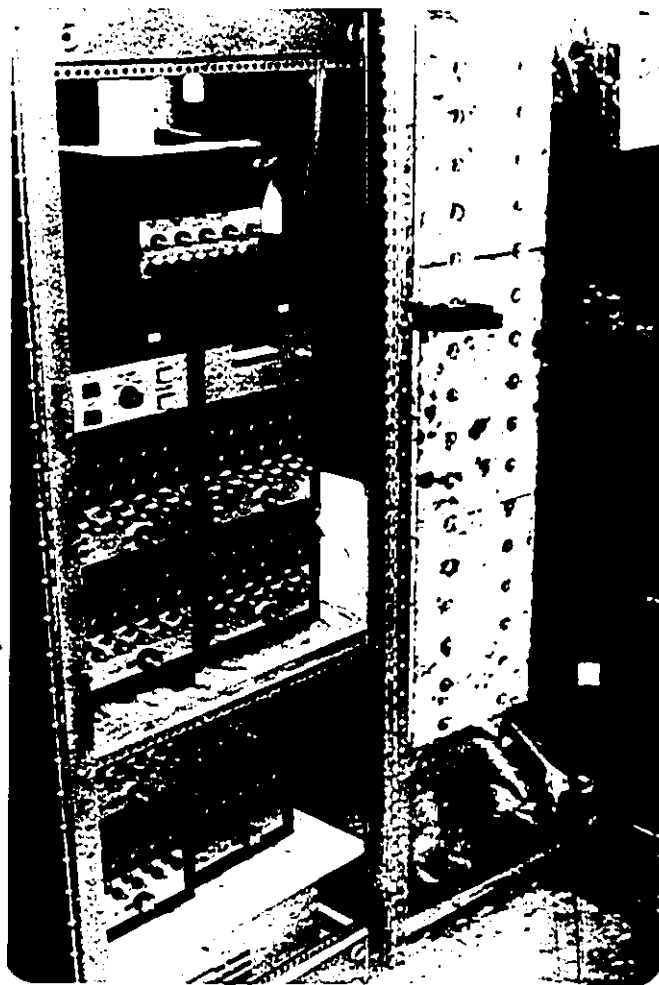


FIGURE 6.10 THE AUTOMATIC STRAIN
INDICATOR

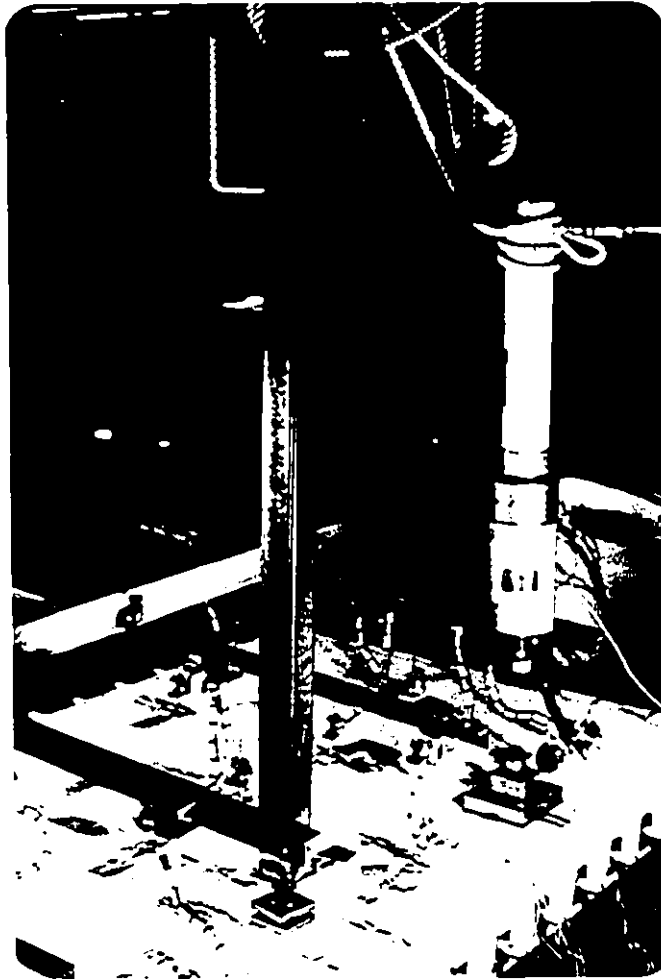


FIGURE 6.11 CONCENTRATED LOADING SYSTEM

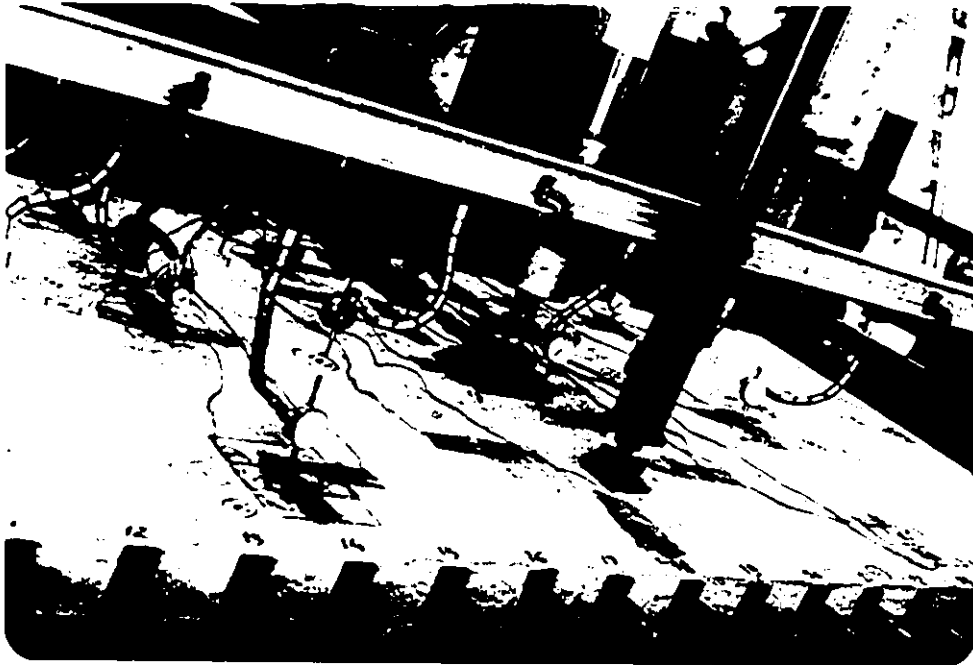
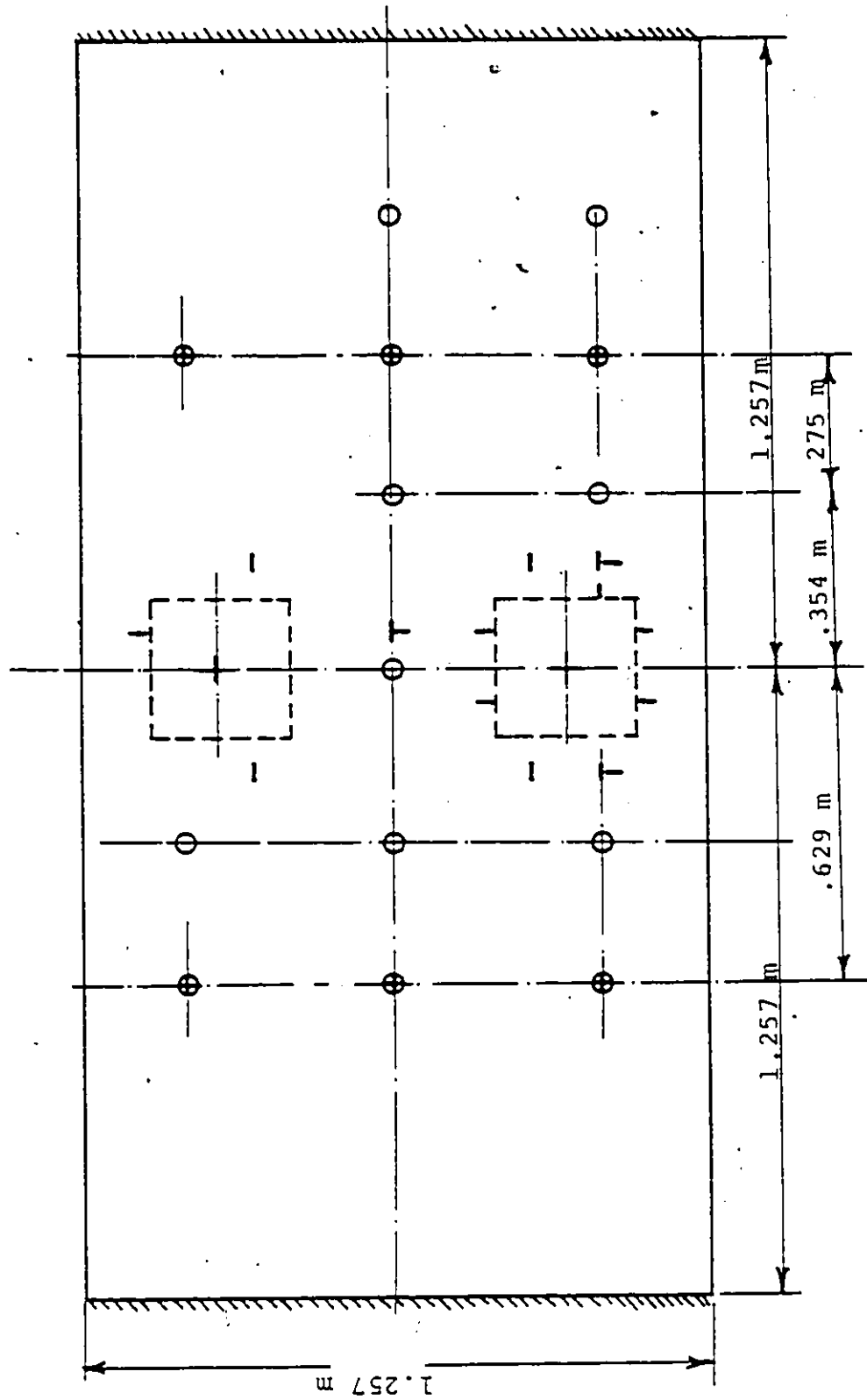


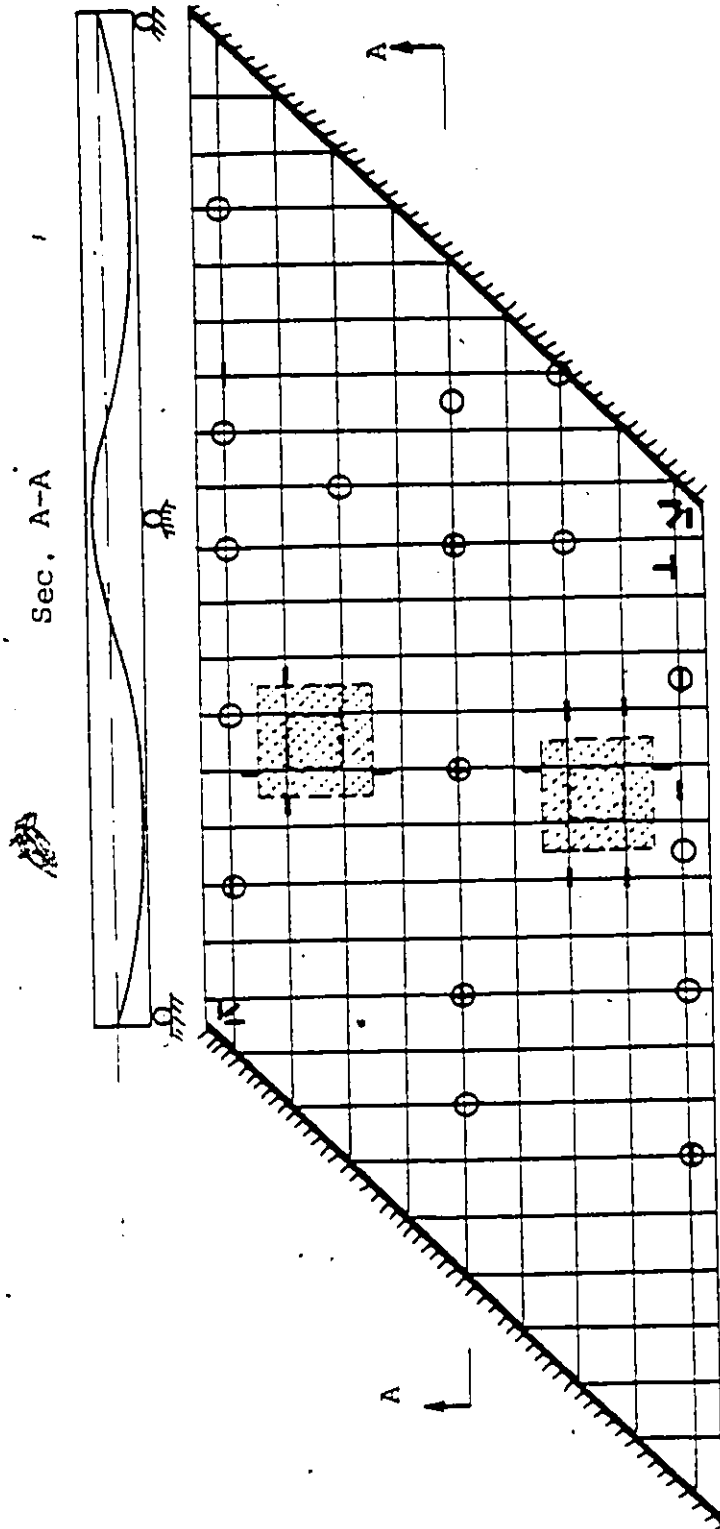
FIGURE 6.12 THE TWO BRACING STEEL COLUMNS AND
DIAL GAUGES IN POSITION



○ Dial gauges

— Strain gauges
(top and bottom)

FIGURE 6.13 PRESTRESSED CONCRETE WAFFLE SLAB PC3



O Dial gauges
 — Strain gauges
 (top and bottom)

FIGURE 6.14 PRESTRESSED CONCRETE WAFFLE SLAB PC4

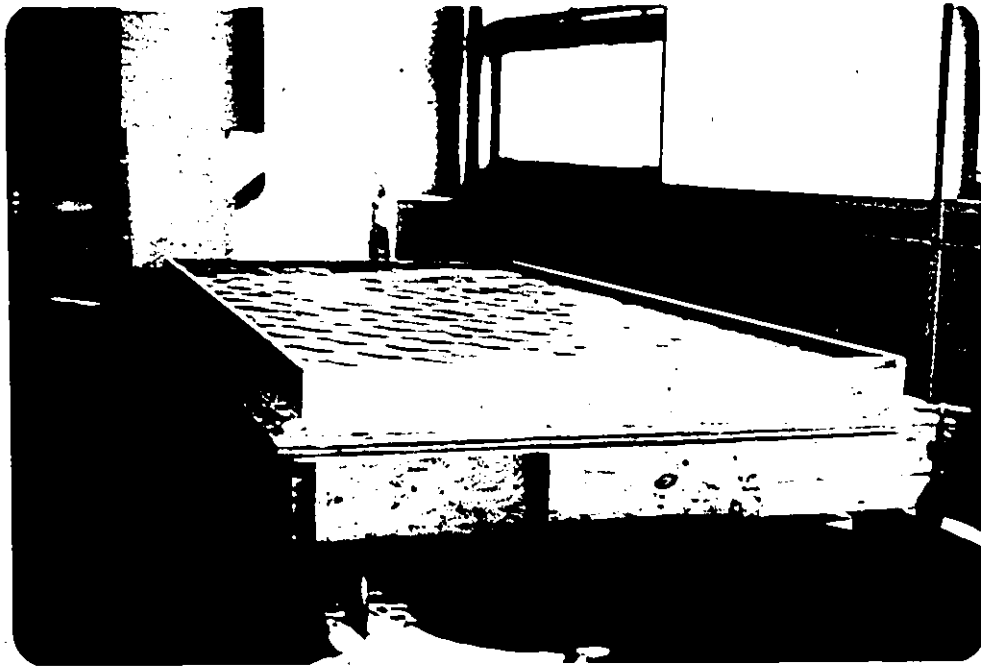


FIGURE 6.15 FORM ON THE STEEL BED BEFORE CASTING THE CONCRETE

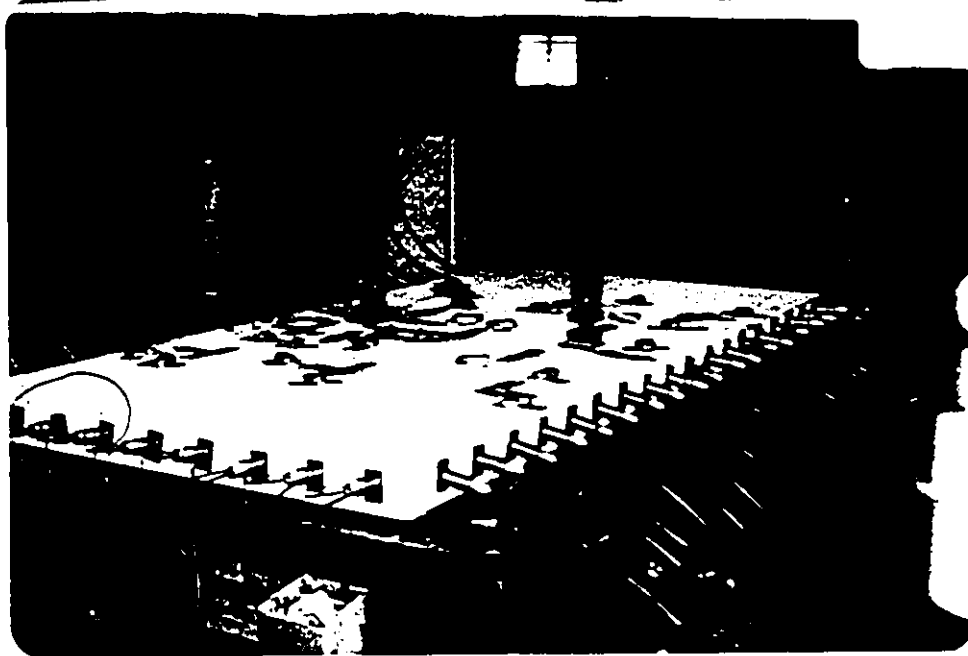


FIGURE 6.16 SET UP THE SLAB PC3 IN THE LOADING POSITION

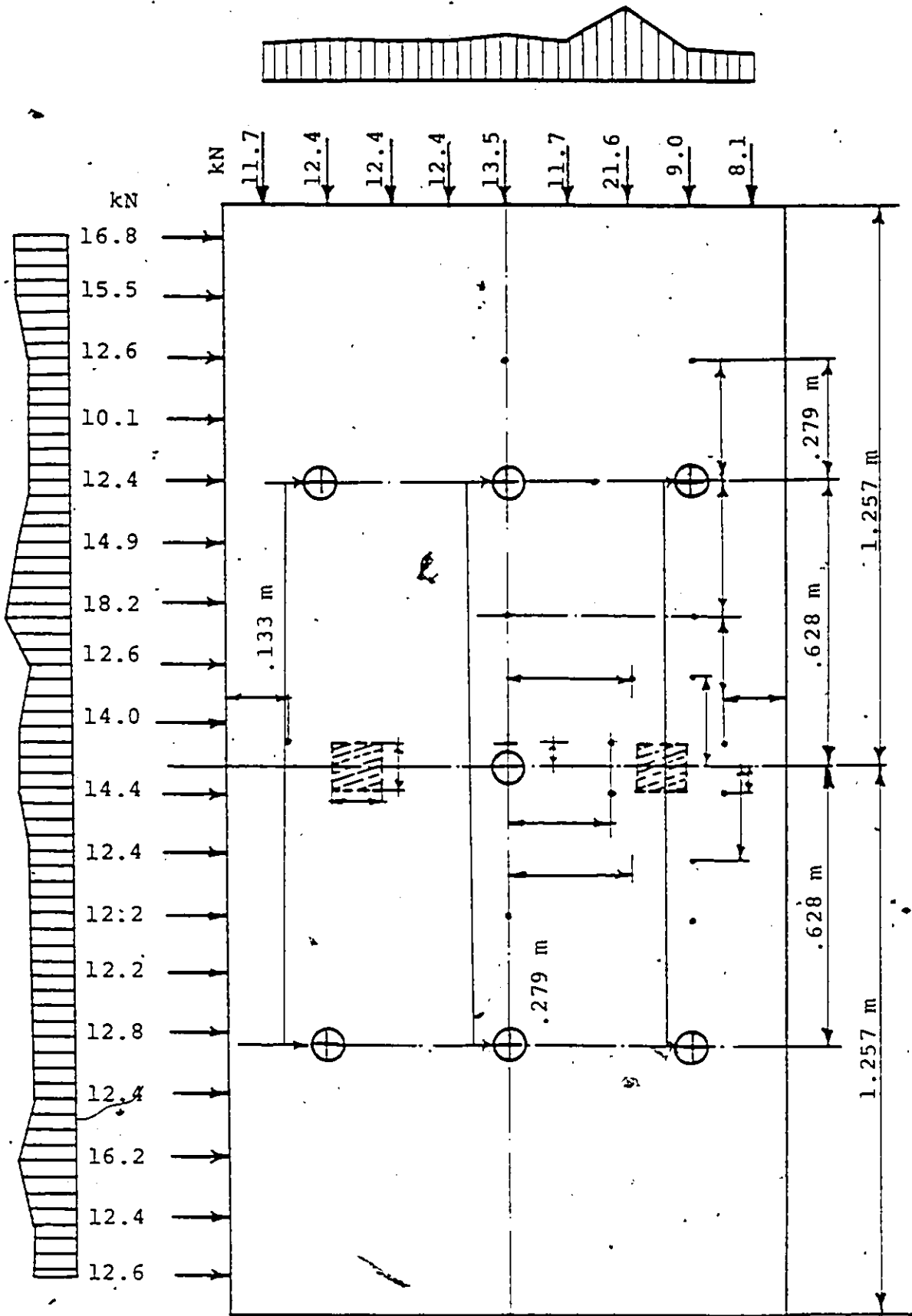
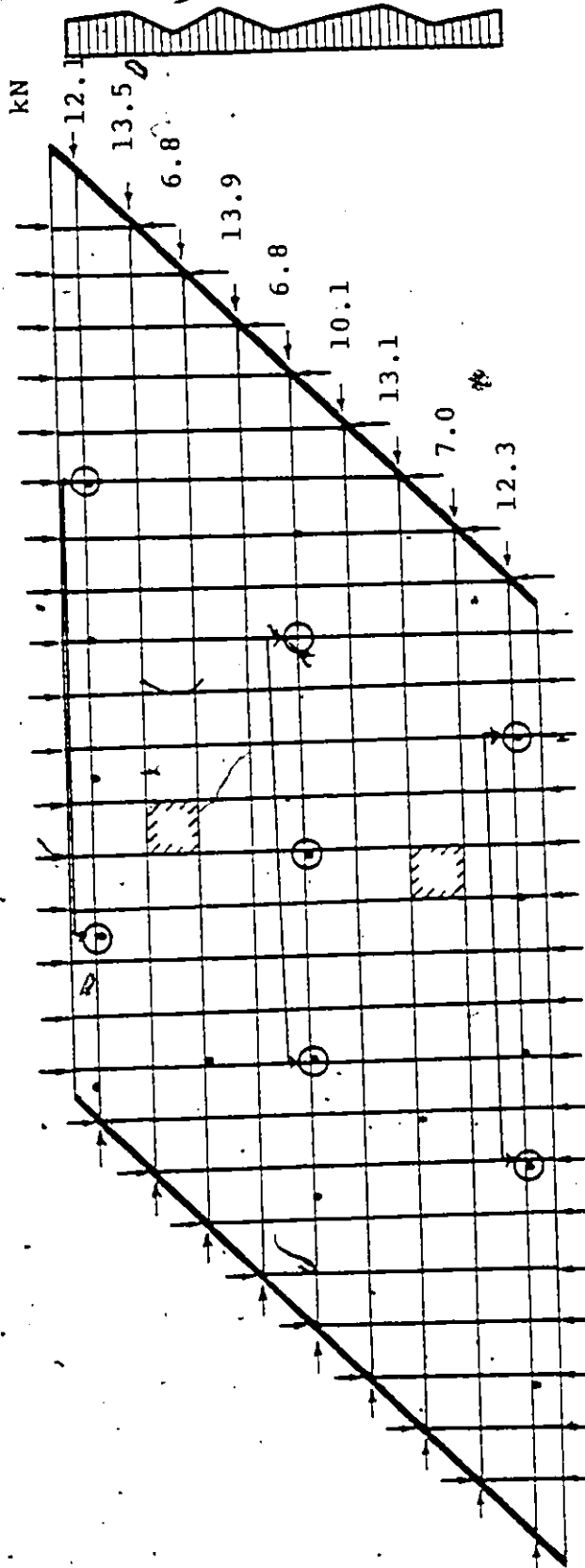


FIGURE 6.17 IN-PLANE PRESTRESSING FORCE
FOR RECTANGULAR SLAB PC3



7 kN
9.75

10.

10.0

12.5

12.5

10.75

11.5

11.3

13.7

11.9

20.4

11.7

12.1

12.6

12.4

13.0

11.7

13.7

12.4

12.2

9.67

7.2

10.6

9.2

10.35

FIGURE 6.18 IN-PLANE PRESTRESSING FORCE FOR SKEW SLAB (PC4).

Double concentrated loads

Single concentrated loads

Double-concentrated loads

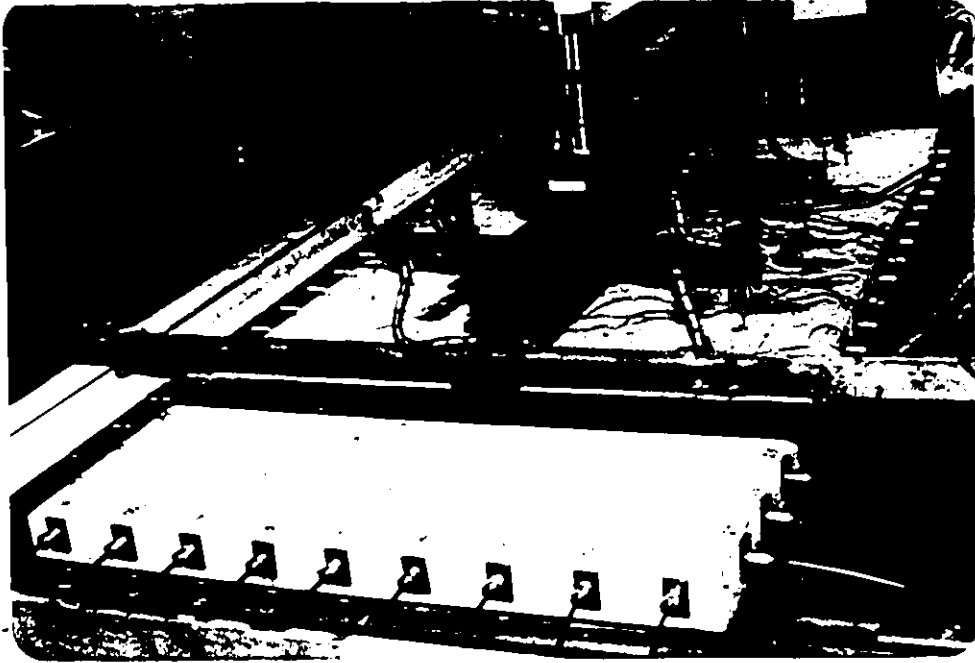


FIGURE 6.19 WAFFLE SLAB PC3 UNDER TWO CONCENTRATED LOADS EACH AT THE CENTER OF EACH SPAN

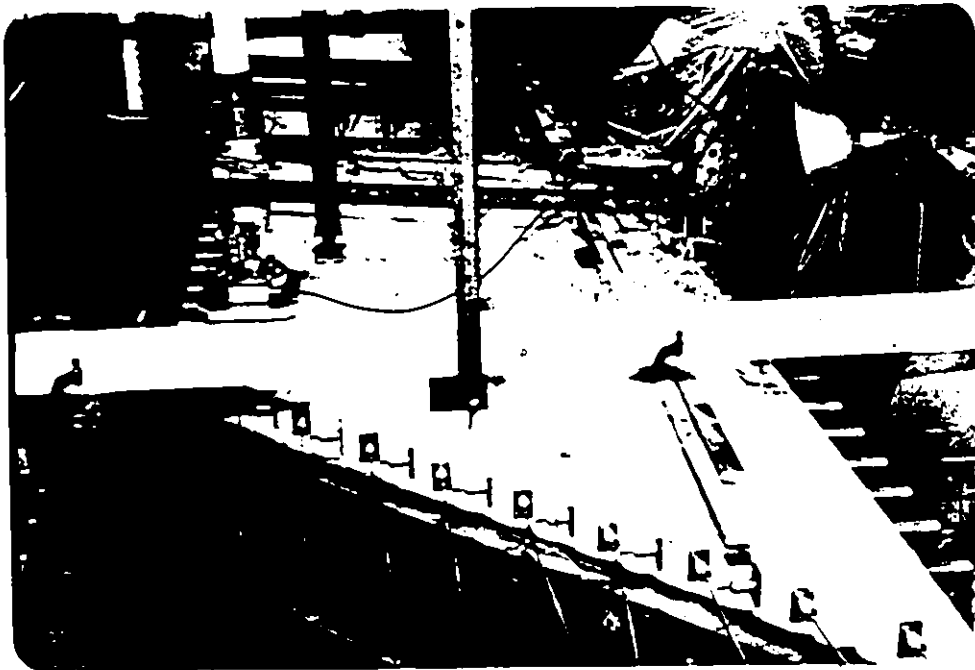


FIGURE 6.20 WAFFLE SLAB PC4 UNDER A SINGLE CONCENTRATED LOAD AT THE CENTER OF THE EDGE BEAM

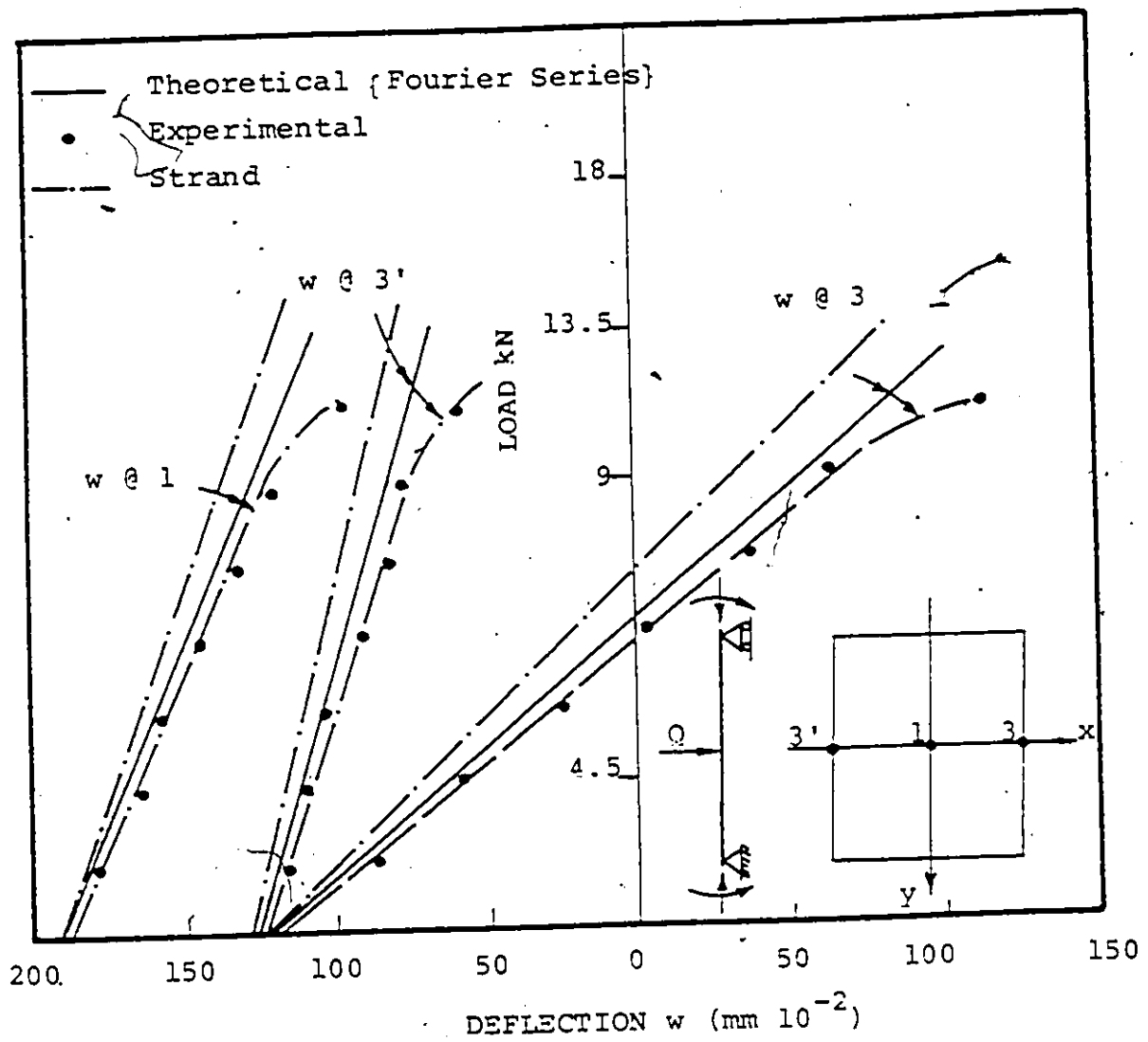


FIG. 7.1 LOAD-DEFLECTION RELATIONSHIPS FOR RECTANGULAR MODEL UNDER LOAD AT CENTER OF EDGE BEAM (LOCATION 3)

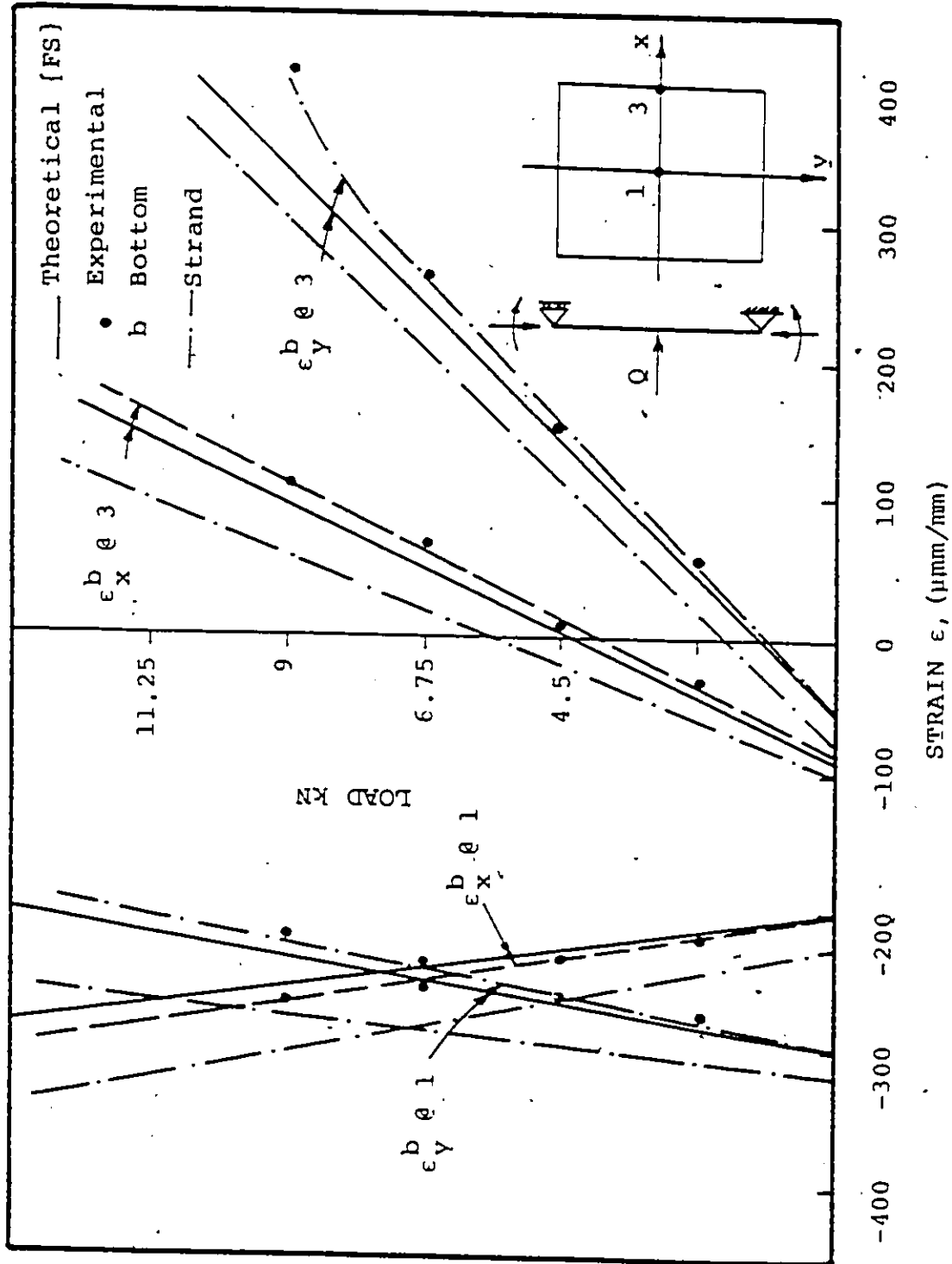


FIGURE 7.2 LOAD-STRAIN RELATIONSHIPS FOR RECTANGULAR MODEL UNDER LOAD AT CENTER OF EDGE BEAM (LOCATION 3)

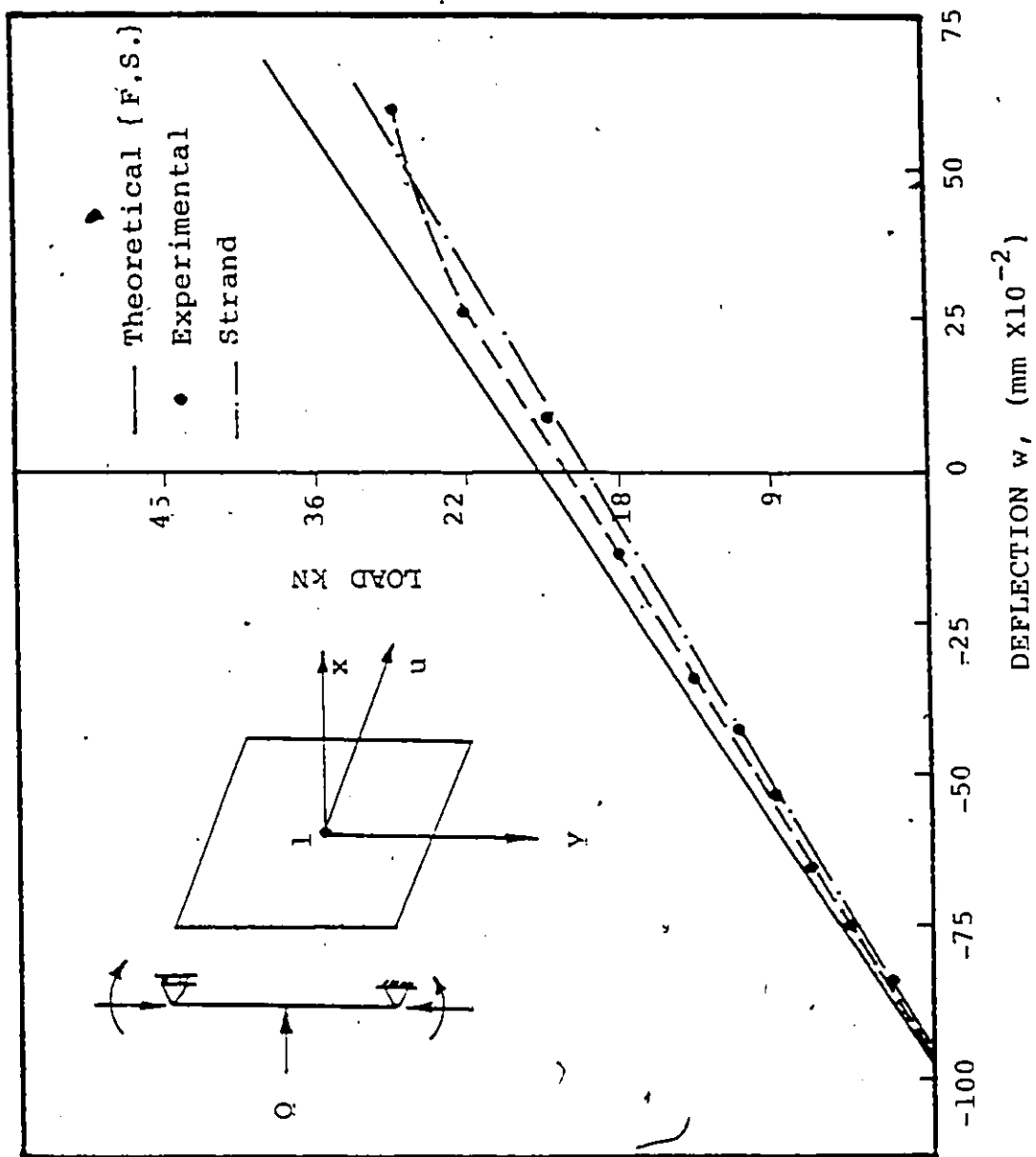


FIGURE 7.3 LOAD-DEFLECTION RELATIONSHIP FOR SKEW MODEL UNDER CENTRAL LOAD (LOCATION 1)

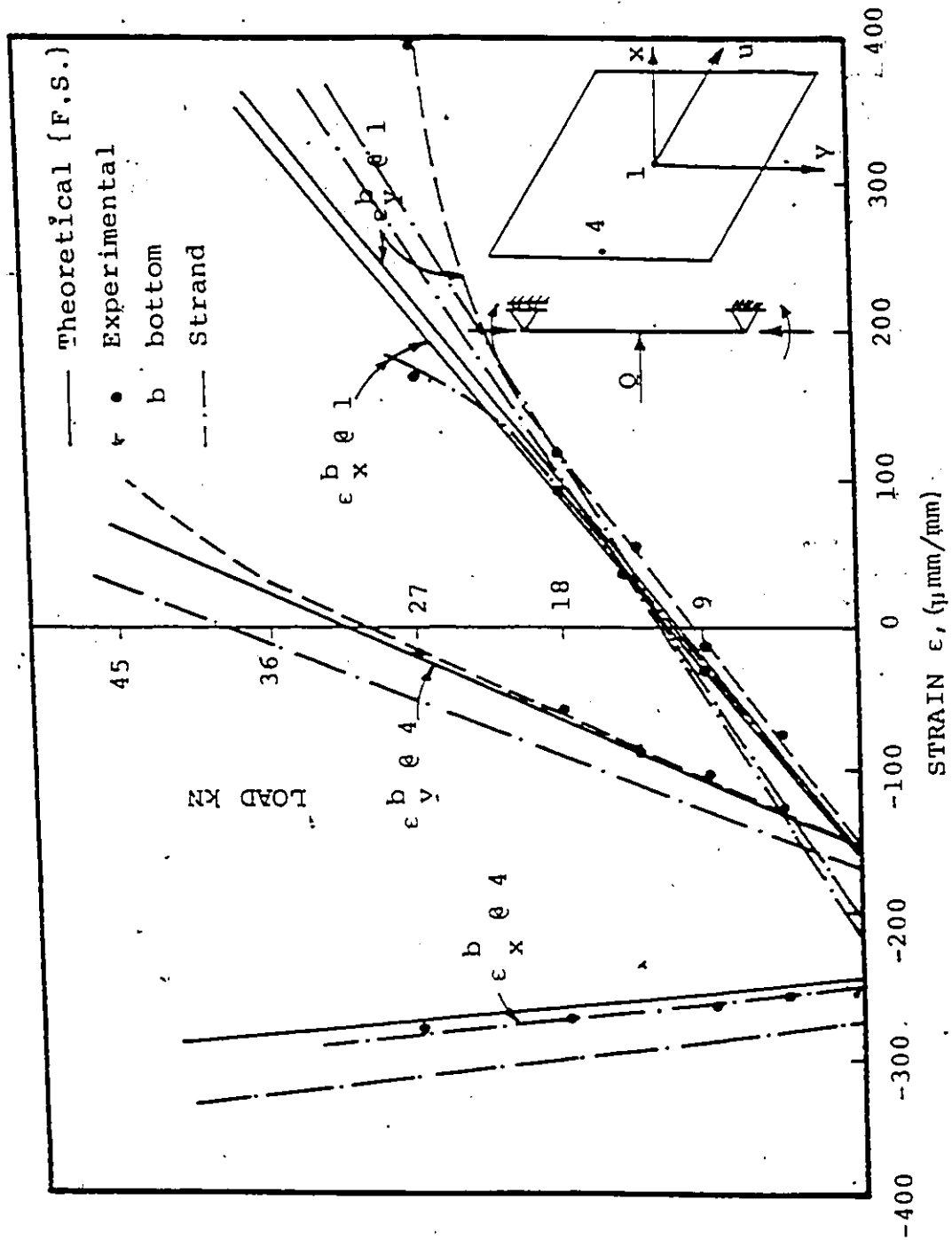


FIGURE 7.4 LOAD-STRAIN RELATIONSHIPS FOR SKEW MODEL UNDER CENTRAL LOAD (LOCATION 1)

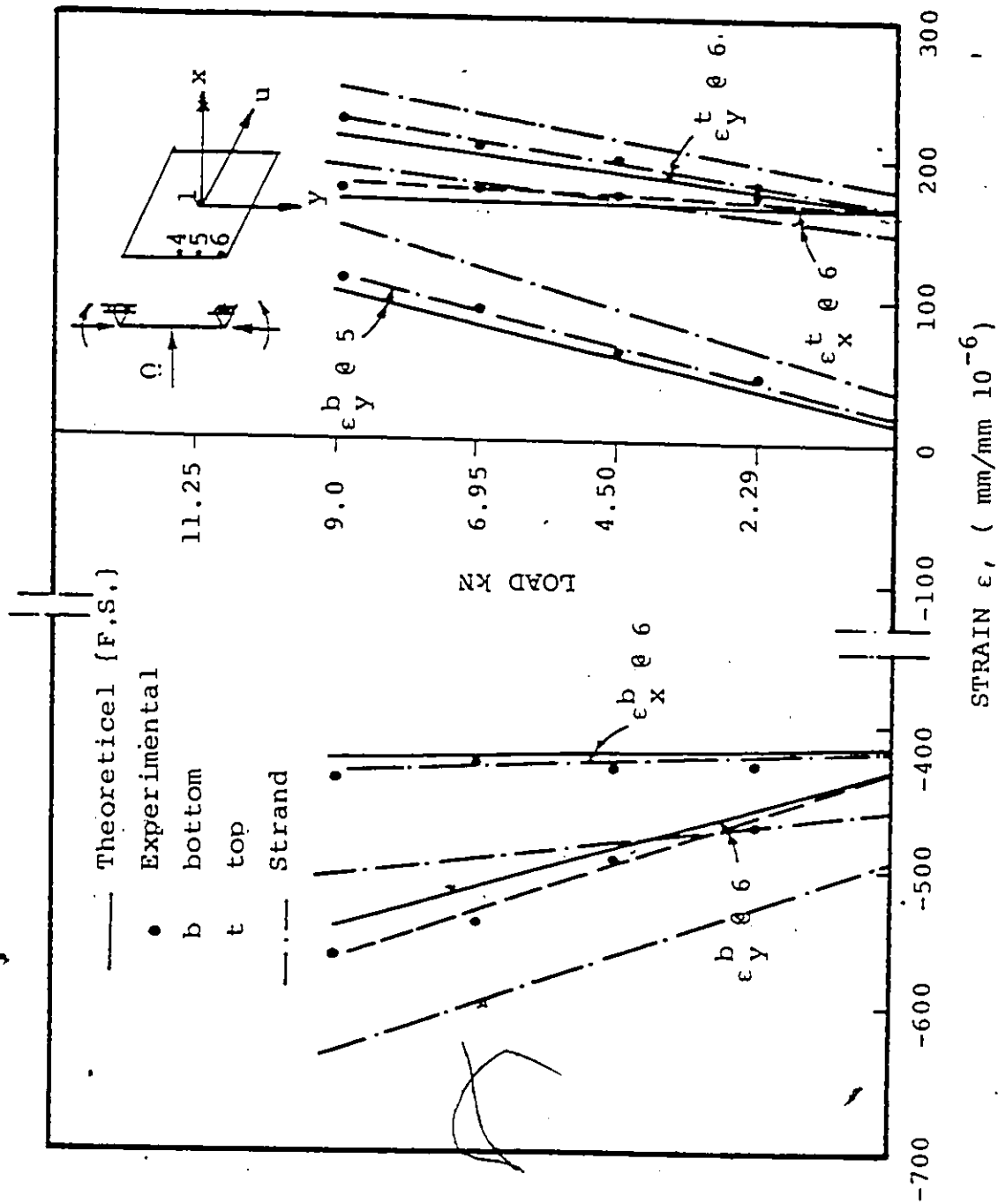


FIGURE 7.5 LOAD-STRAIN RELATIONSHIPS FOR SKEW MODEL UNDER LOAD AT CENTER OF EDGE BEAM (LOCATION 4)

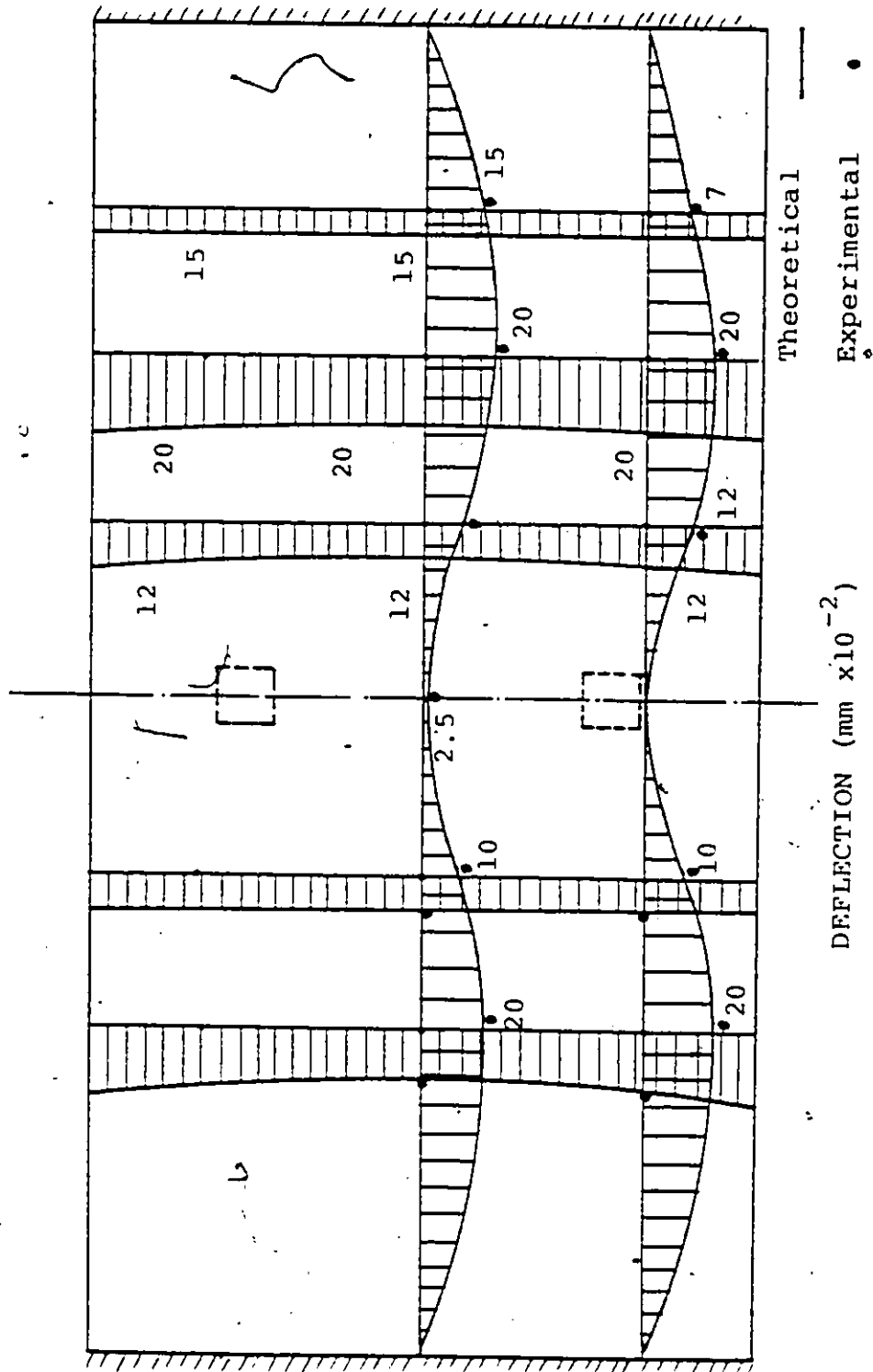


FIGURE 7.6 UPWARD DEFLECTION DISTRIBUTION (CAMBER) DUE TO PRESTRESSING.

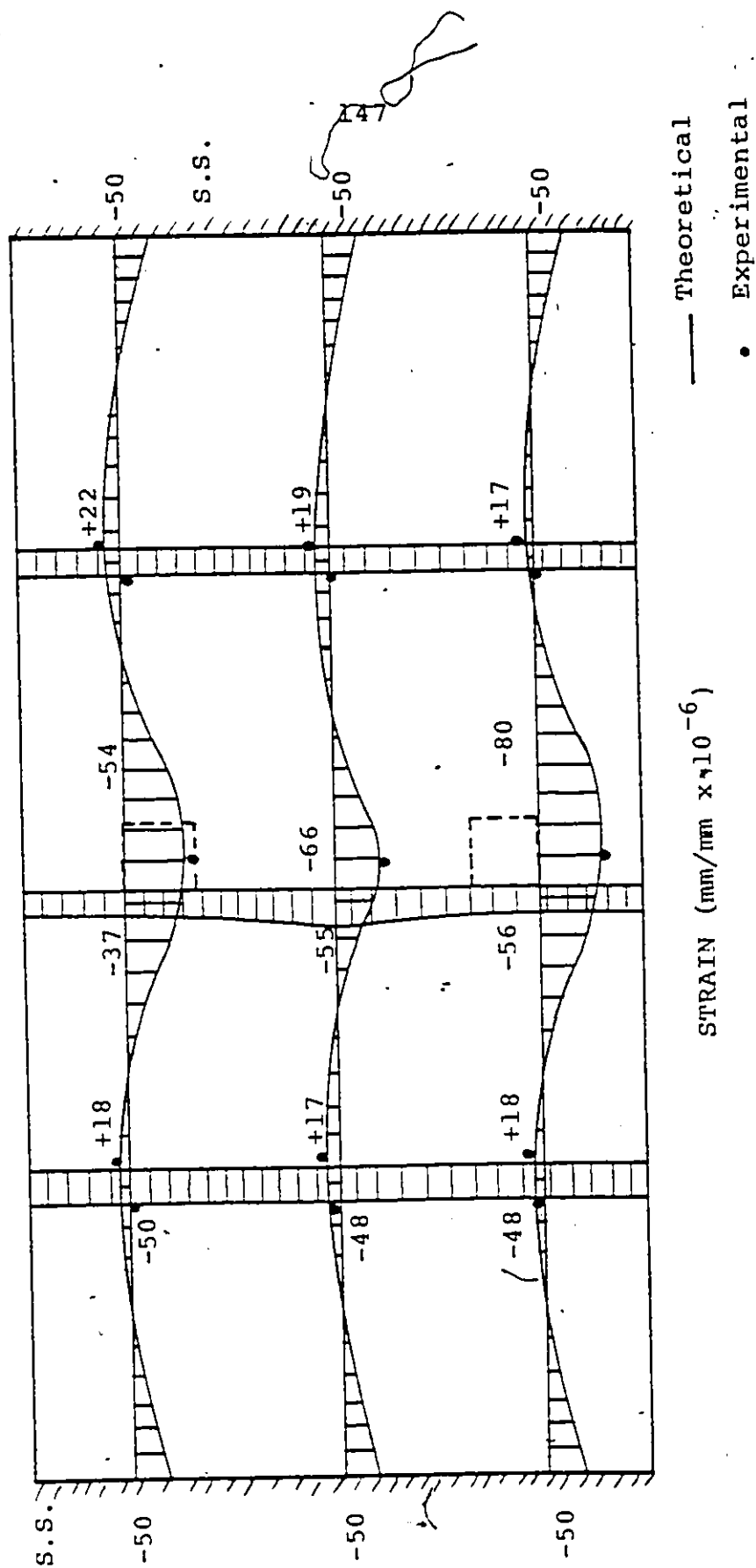


FIGURE 7.8 STRAIN DISTRIBUTION IN THE TOP FIBRE FOR RECTANGULAR SLAB (PC3) AFTER PRESTRESSING

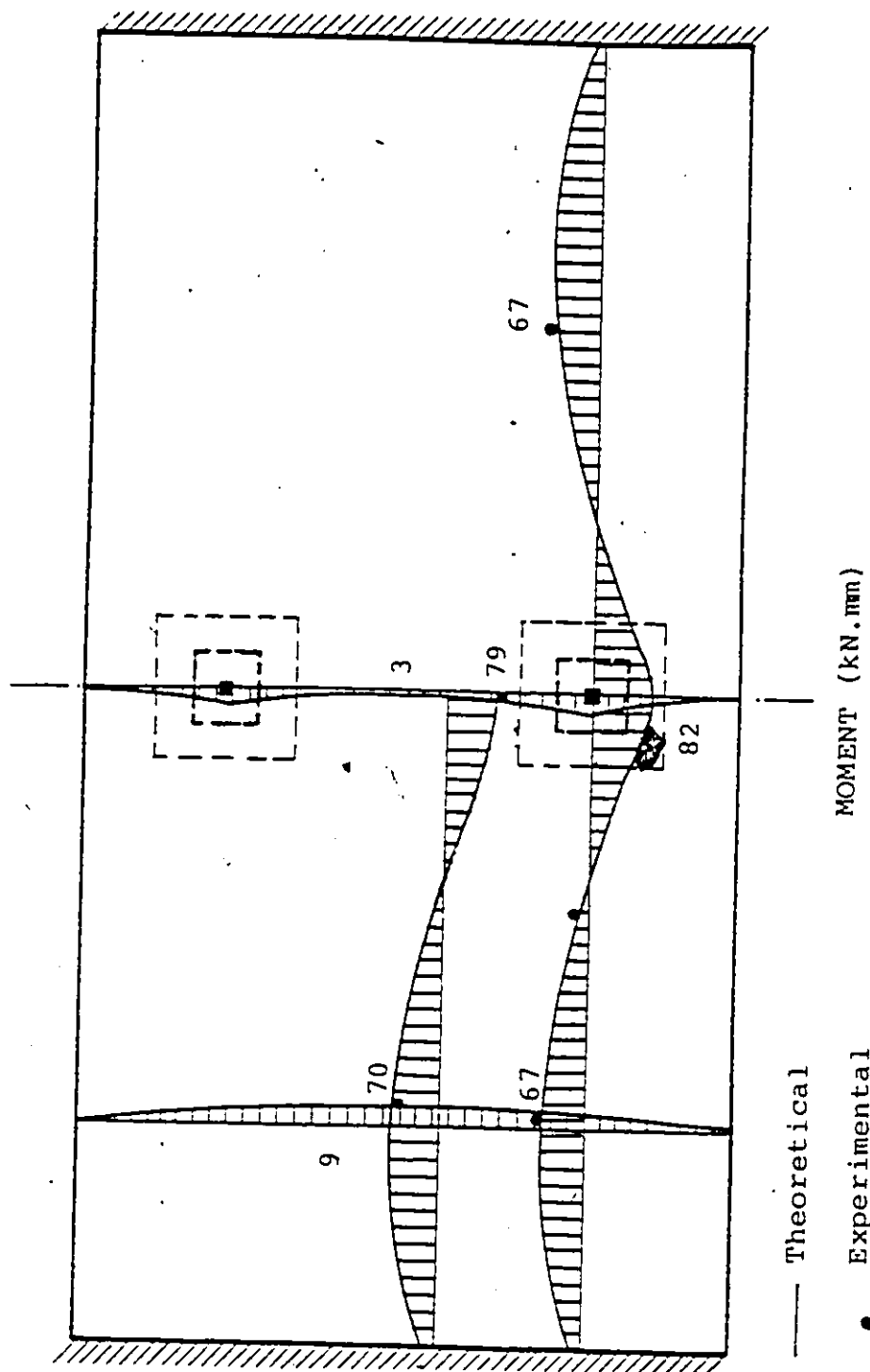


FIGURE 7.9 DISTRIBUTION OF MOMENT FOR THE RECTANGULAR SLAB (PC3) DUE TO PRESTRESSING.

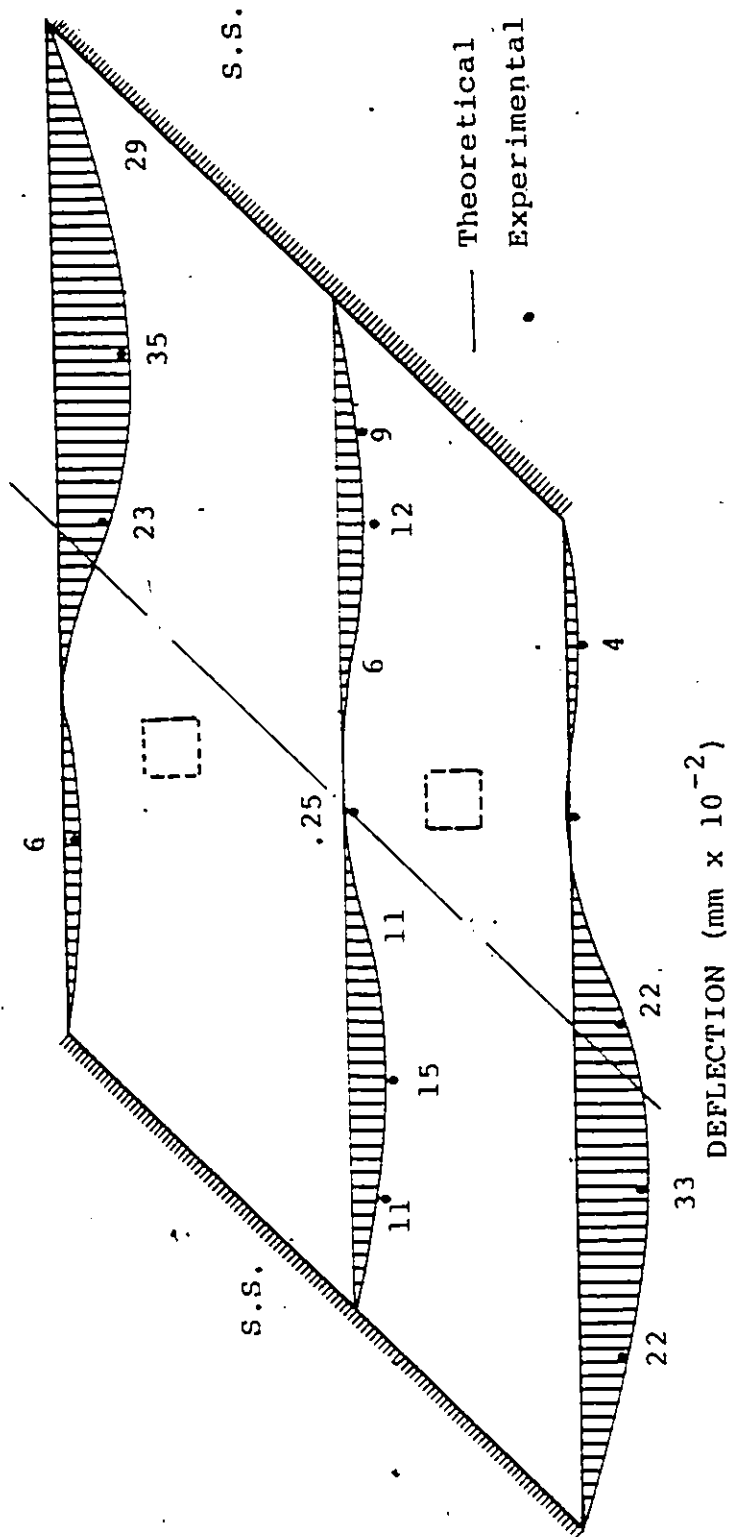


FIGURE 7.16 DEFLECTION DISTRIBUTION (CAMBER) DUE TO PRESTRESSING OF SKEW SLAB (PC4)

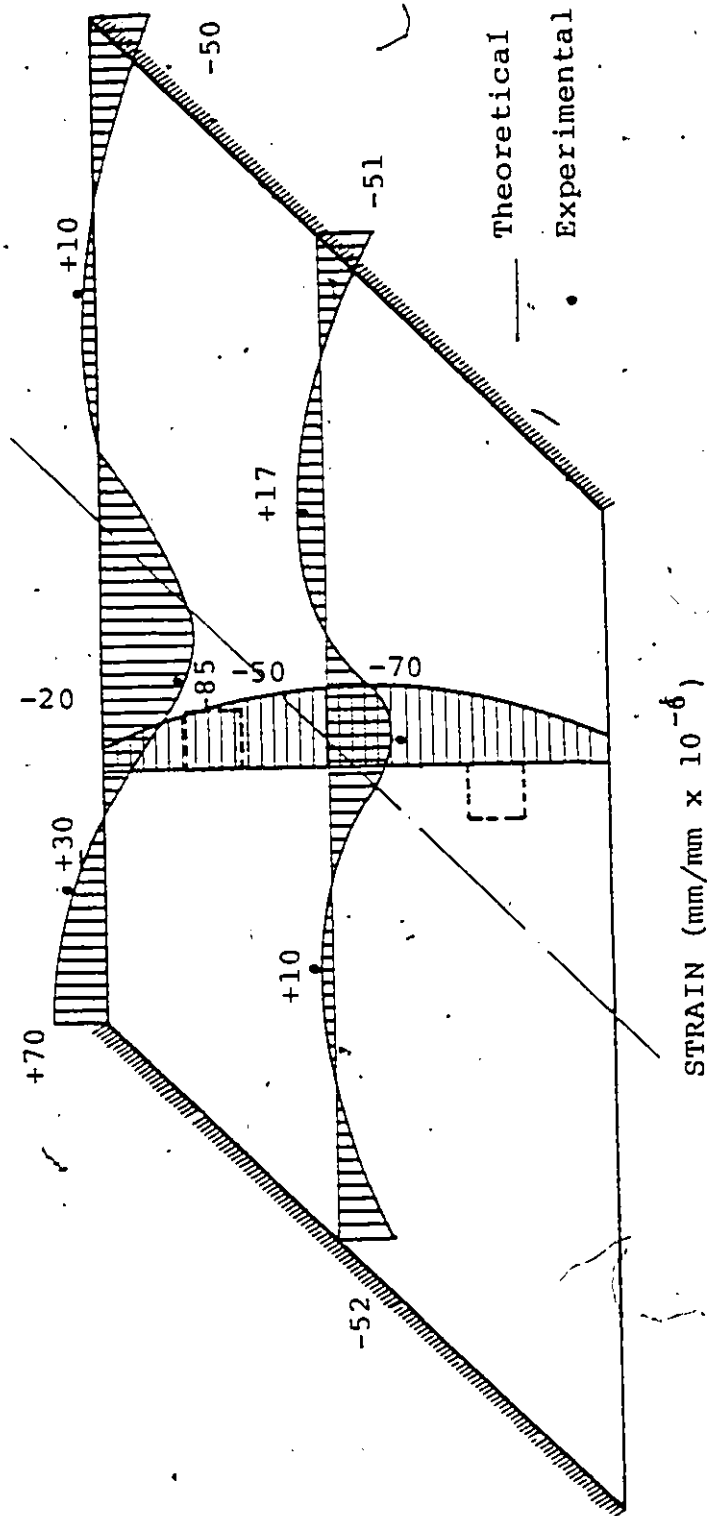


FIGURE 7.11 STRAIN DISTRIBUTION FOR SKEW SLAB (PC4) IN THE TOP FIBRE DUE TO PRESTRESSING

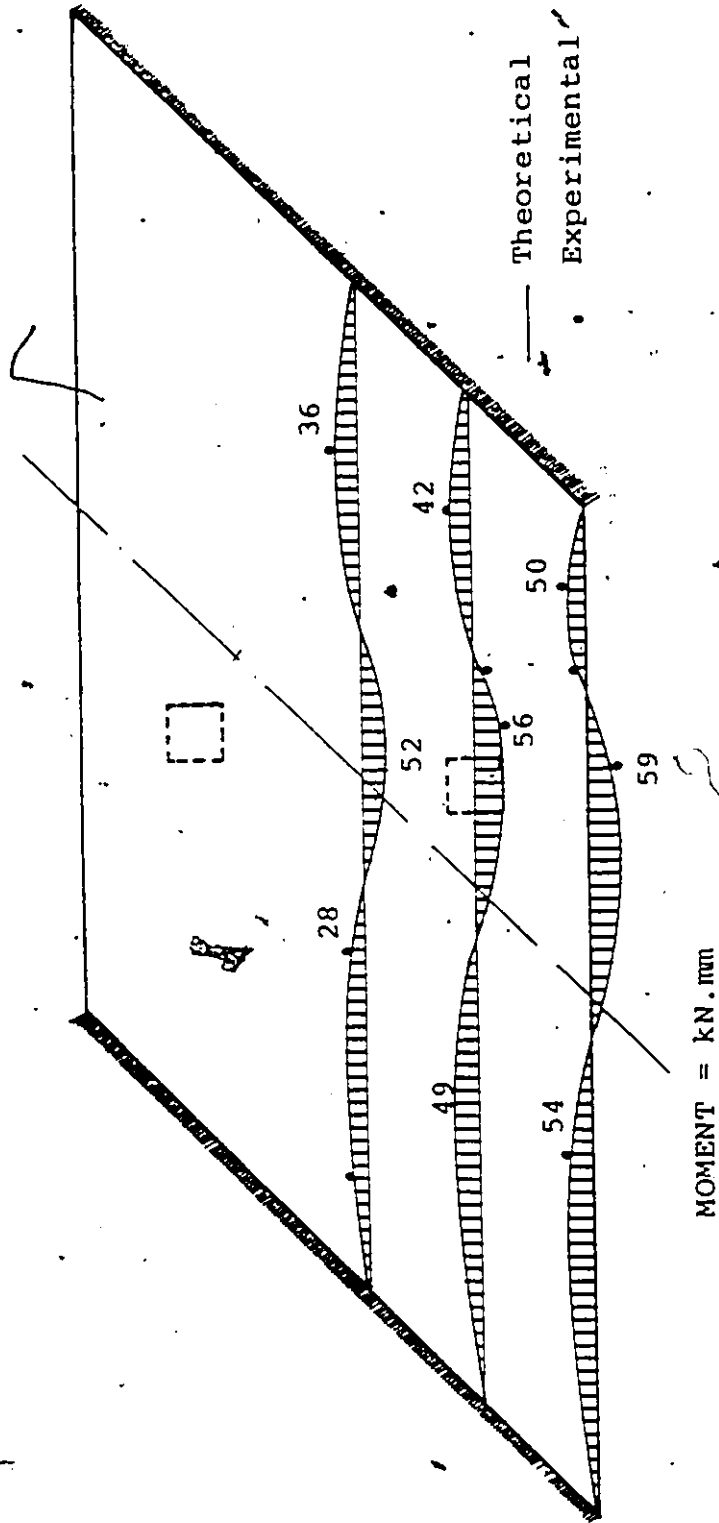
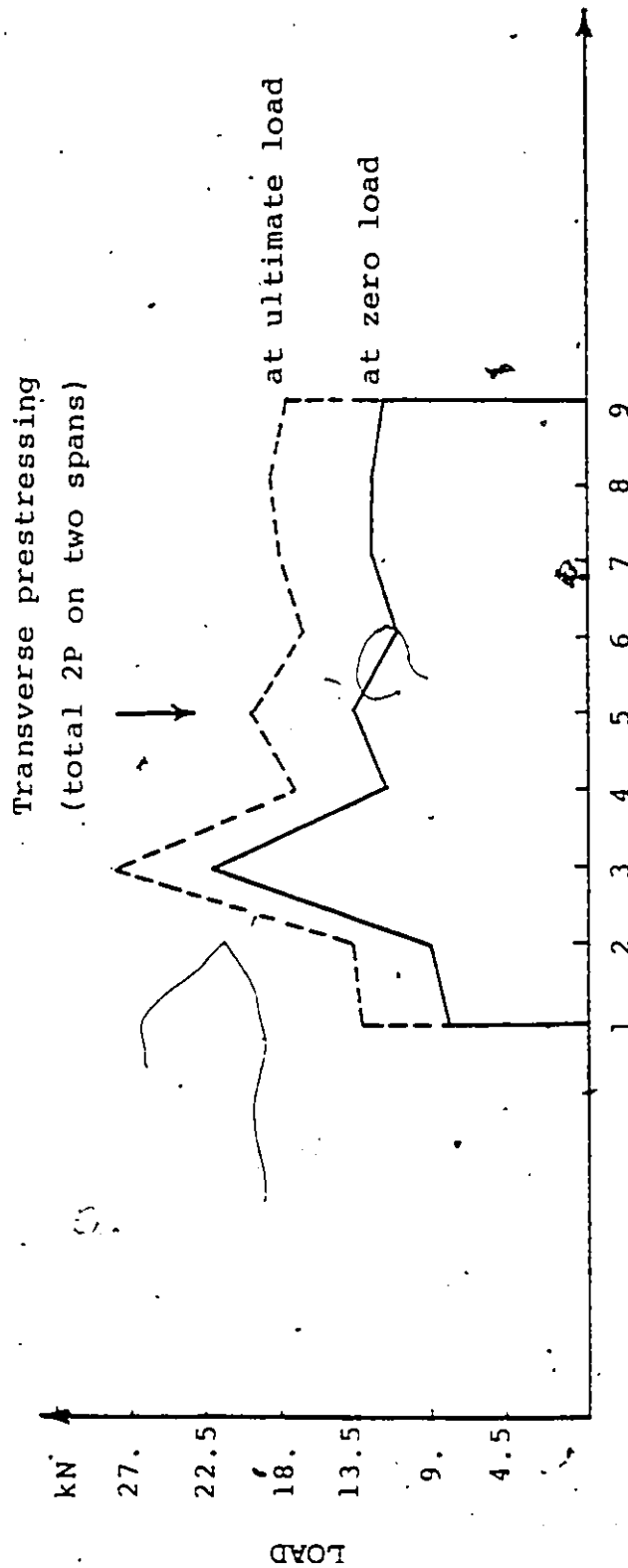
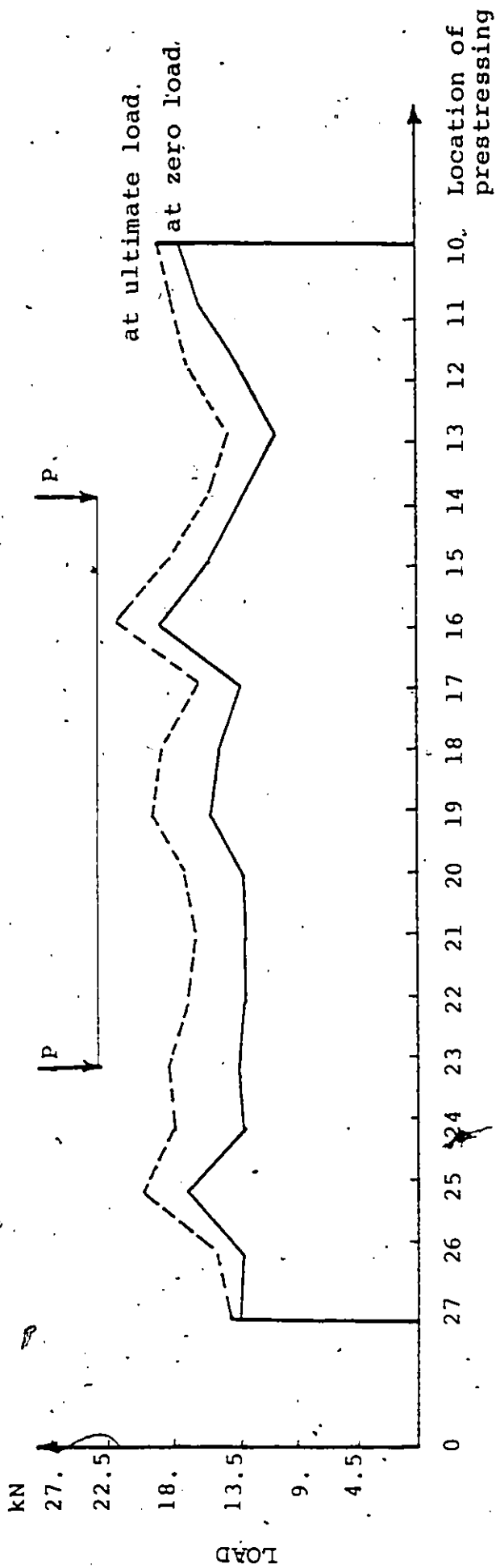
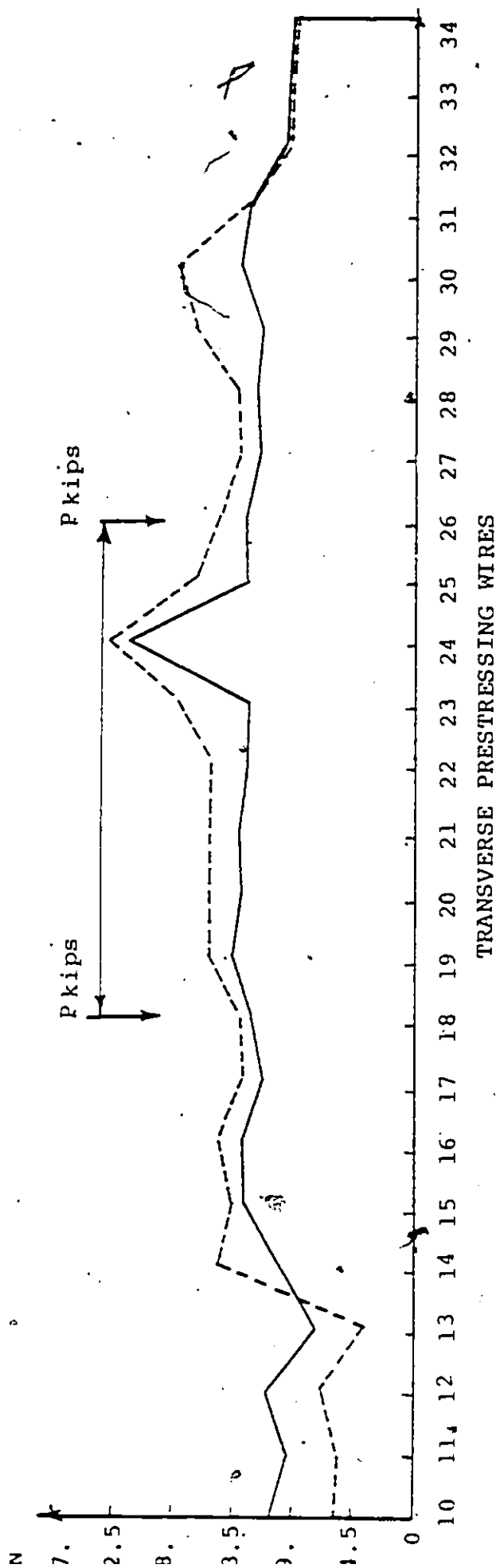


FIGURE 7.12 MOMENT DISTRIBUTION FOR THE SKEW SLAB (PC4) DUE TO PRESTRESSING



LONGITUDINAL PRESTRESSING

FIGURE 7.13 INITIAL AND FINAL PRESTRESSING FOR THE RECTANGULAR SLAB (PC3).



153

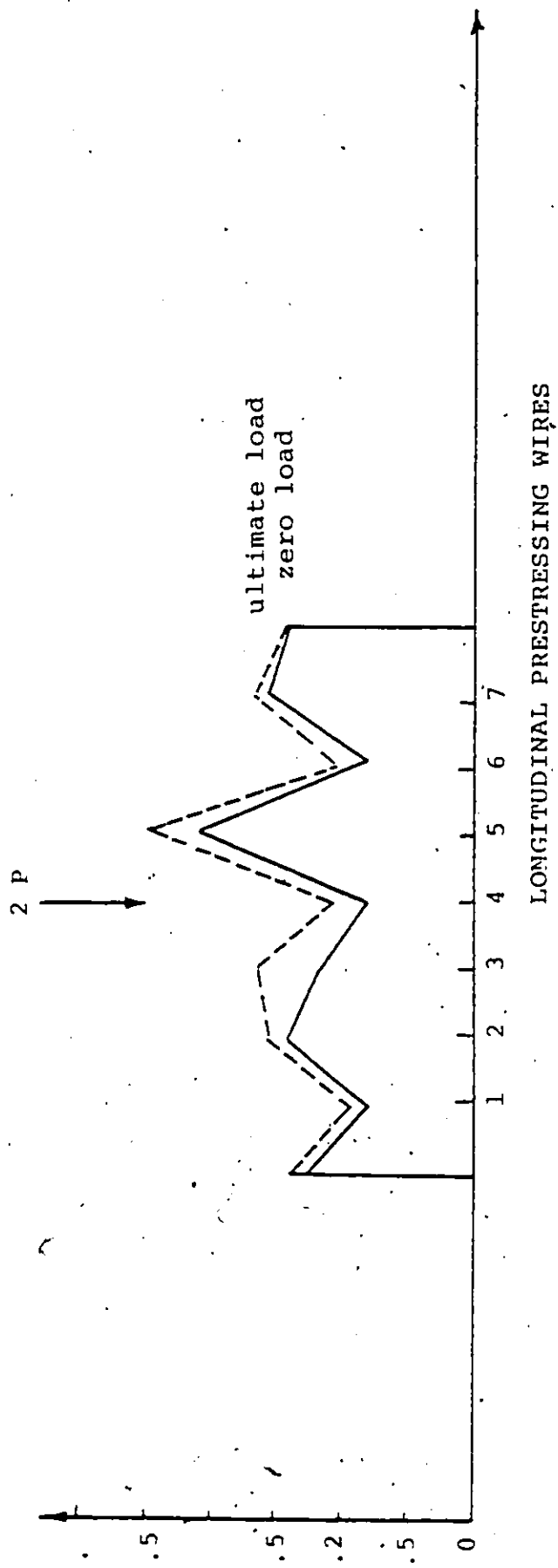


FIGURE 7.14 INITIAL AND FINAL PRESTRESSING FOR THE SKEW SLAB

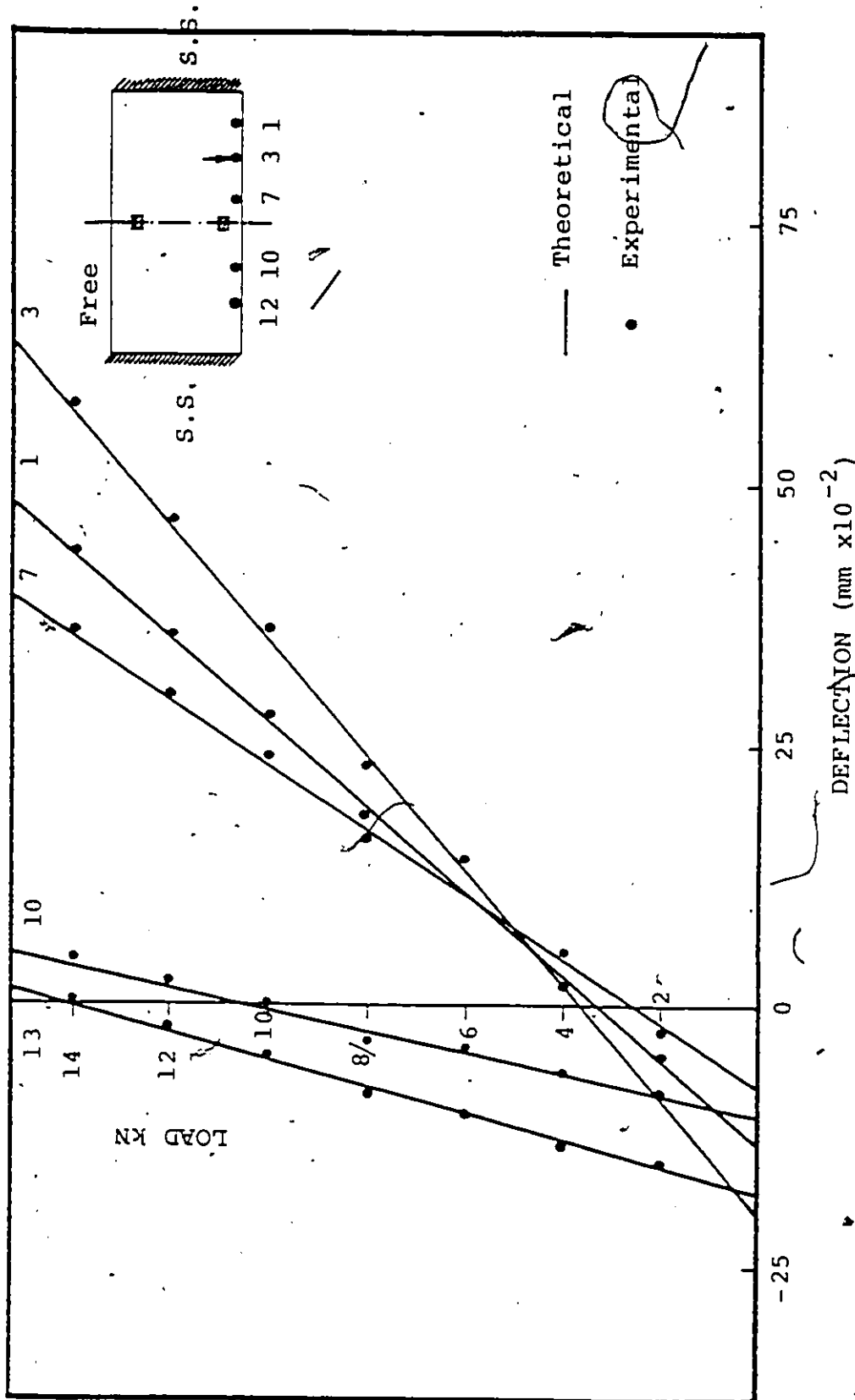


FIGURE 7.15 LOAD-DEFLECTION RELATIONSHIP FOR RECTANGULAR SLAB (PC3) AT THE CENTER OF THE EDGE BEAM (LOCATION 3)

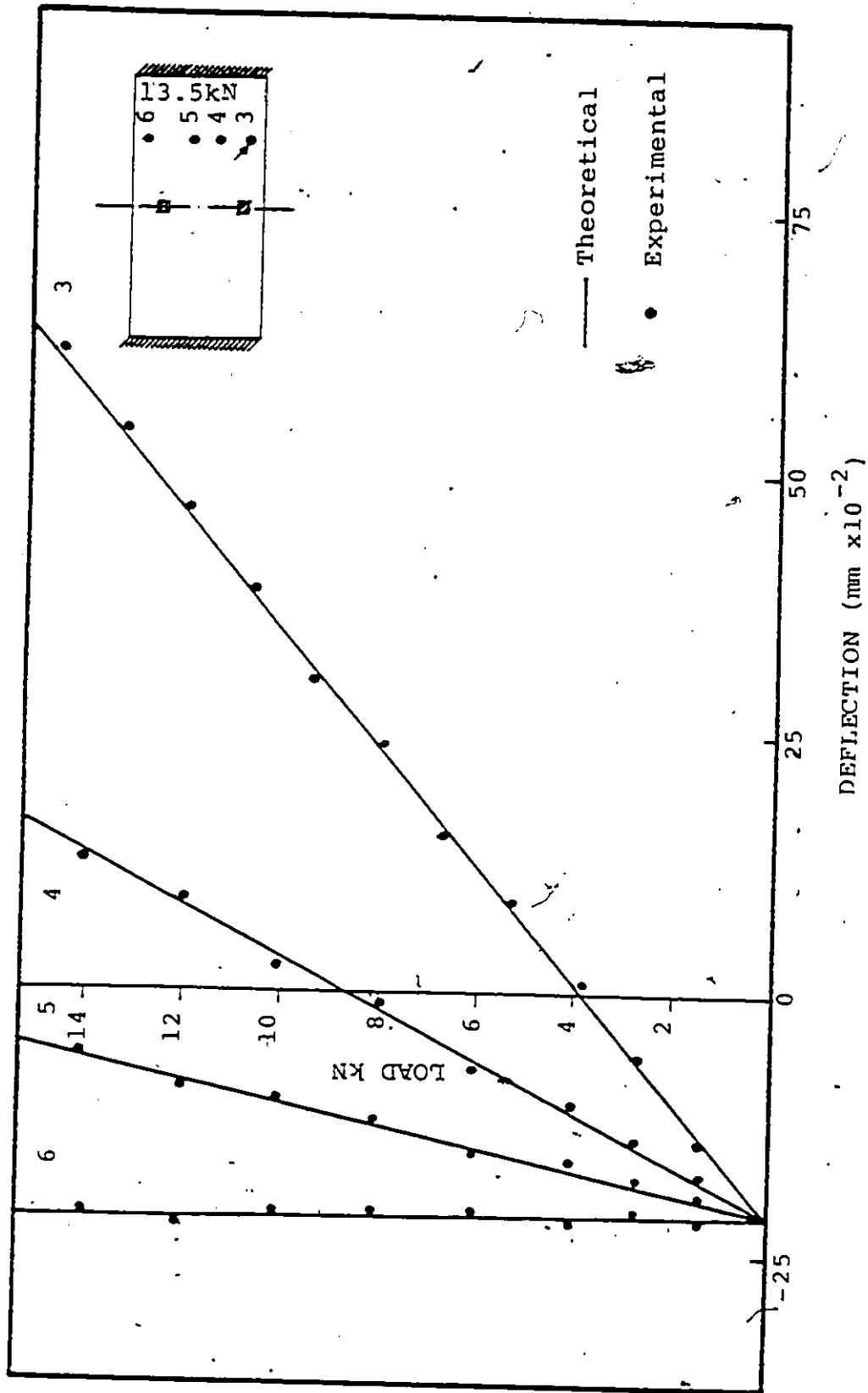


FIGURE 7.16 LOAD-DEFLECTION RELATIONSHIP FOR RECTANGULAR (PC3) SLAB DUE TO CONCENTRATED LOAD AT THE CENTER OF THE EDGE BEAM

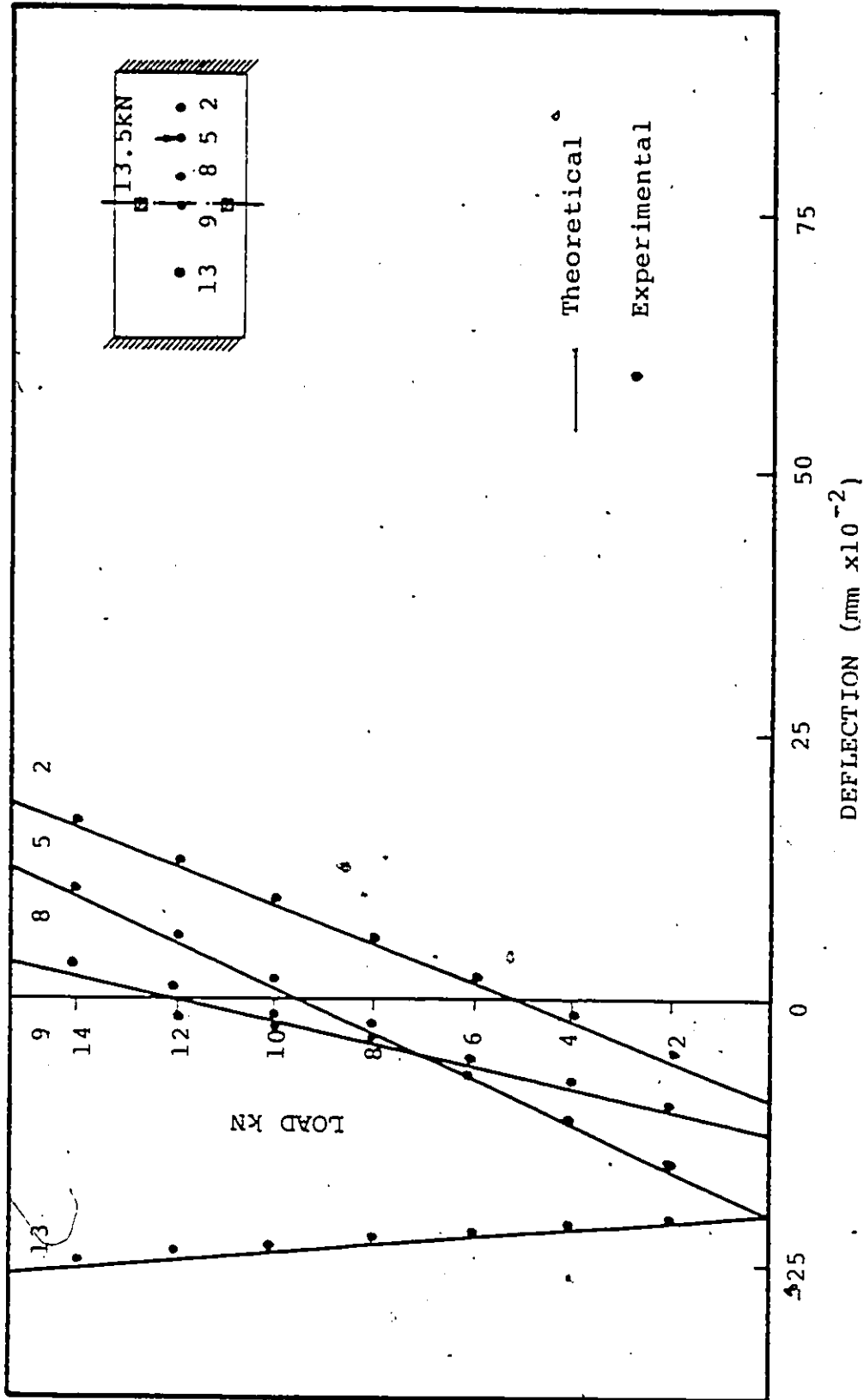


FIGURE 7.17 LOAD-DEFLECTION RELATIONSHIP FOR THE RECTANGULAR SLAB (PC3) LOADING AT POINT 5

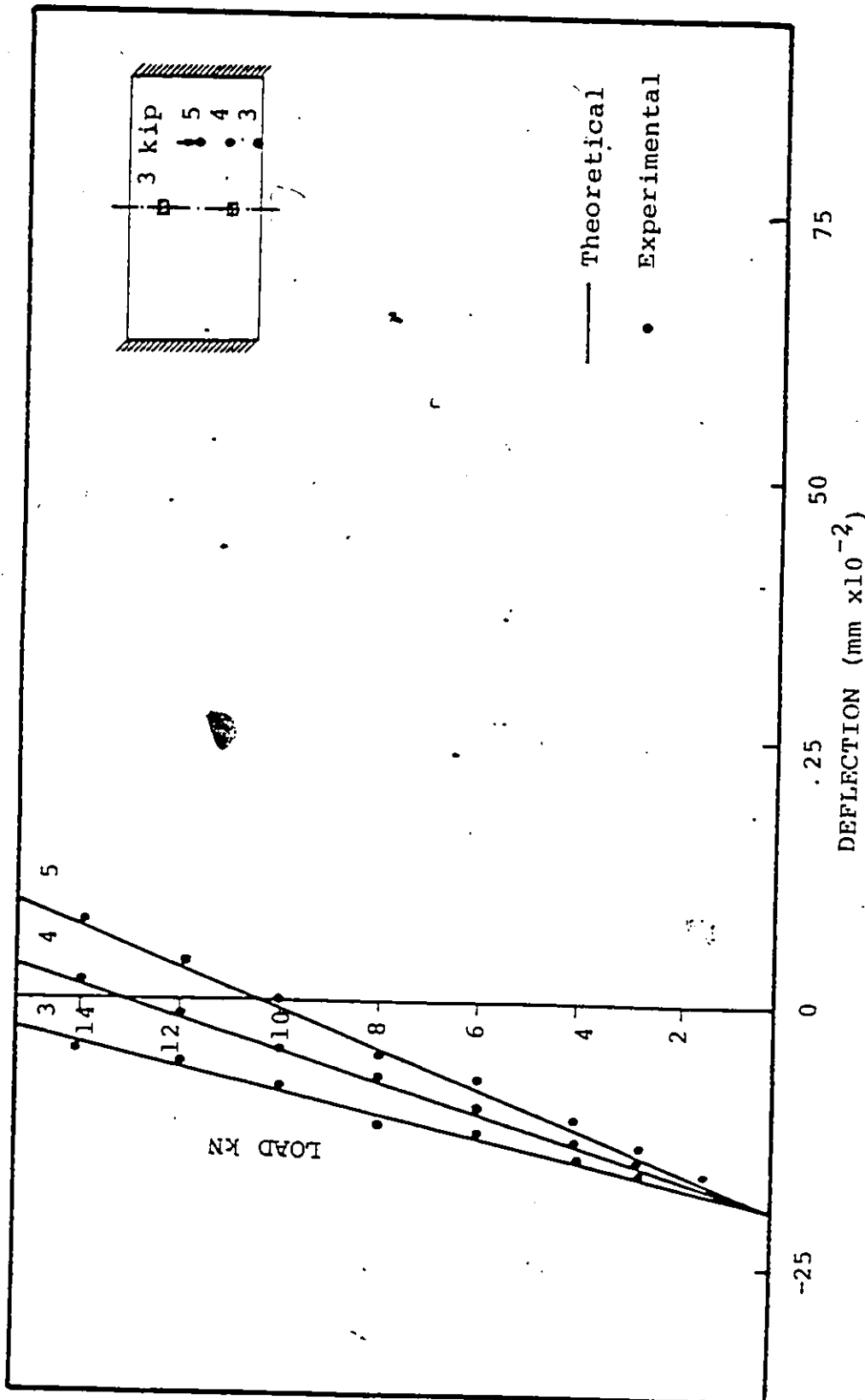


FIGURE 7.18 LOAD-DEFLECTION RELATIONSHIP FOR RECTANGULAR SLAB (PC3), FOR LOAD AT POINT 5.

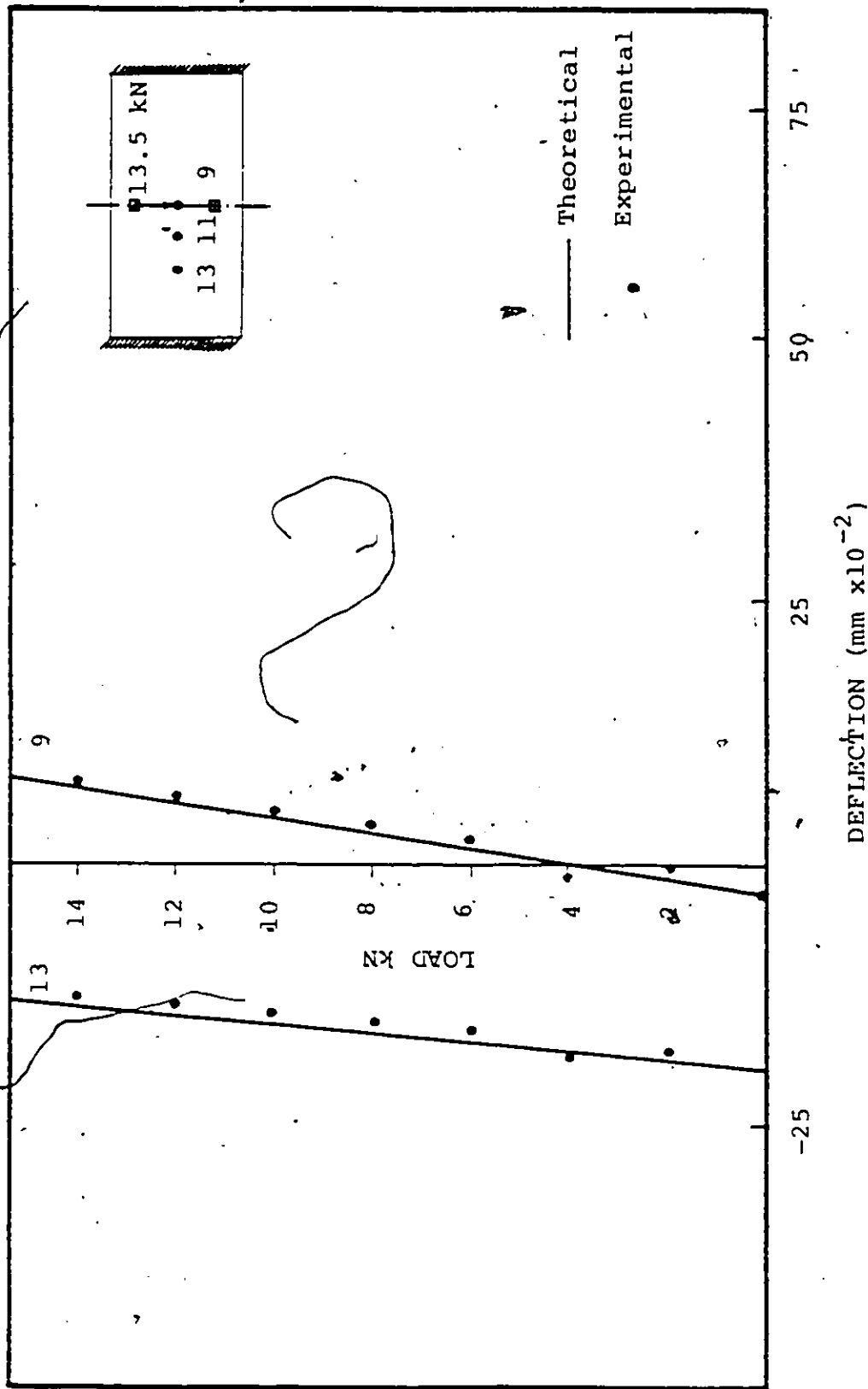


FIGURE 7.19 LOAD-DEFLECTION RELATIONSHIP FOR RECTANGULAR SLAB (PC3) DUE TO A SINGLE CONCENTRATED LOAD AT POINT 9

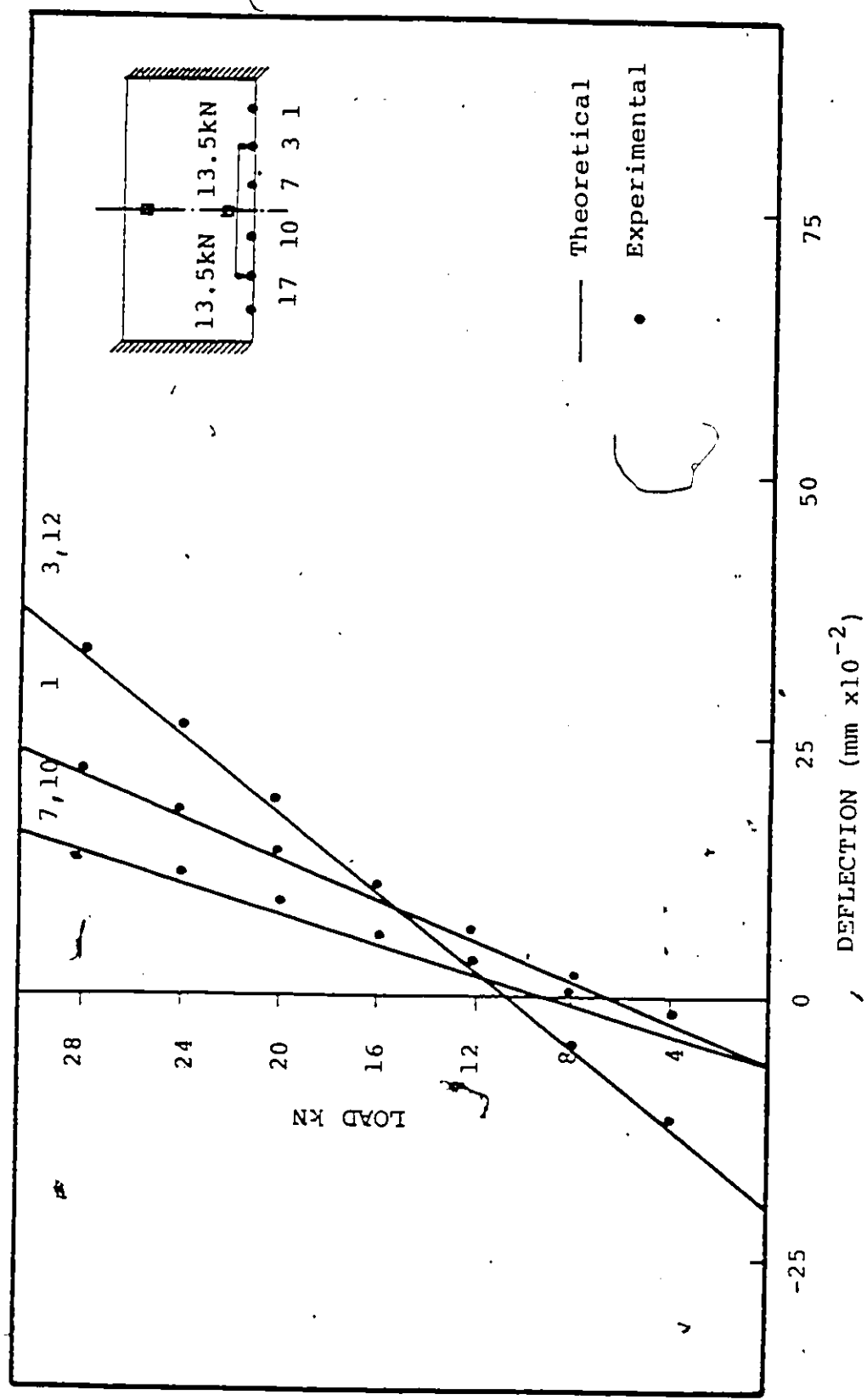


FIGURE 7.20 LOAD-DEFLECTION RELATIONSHIP FOR RECTANGULAR SLAB (PC3) DUE TO TWO CONCENTRATED LOADS AT THE CENTER OF THE EDGE BEAM

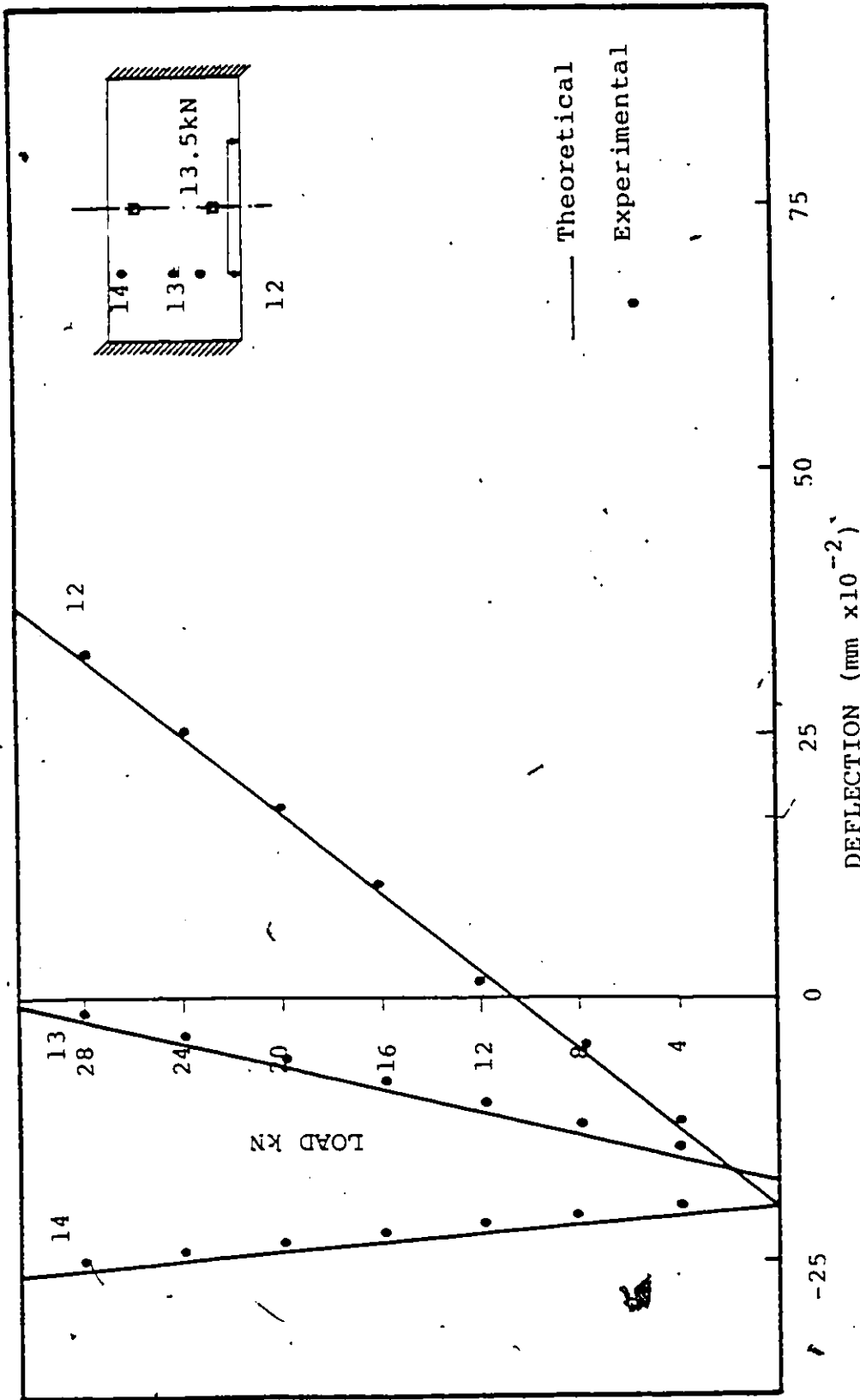


FIGURE 7.21 LOAD-DEFLECTION RELATIONSHIP FOR RECTANGULAR SLAB (PC3) DUE TO TWO CONCENTRATED LOADS EACH AT THE CENTER OF THE EDGE BEAM

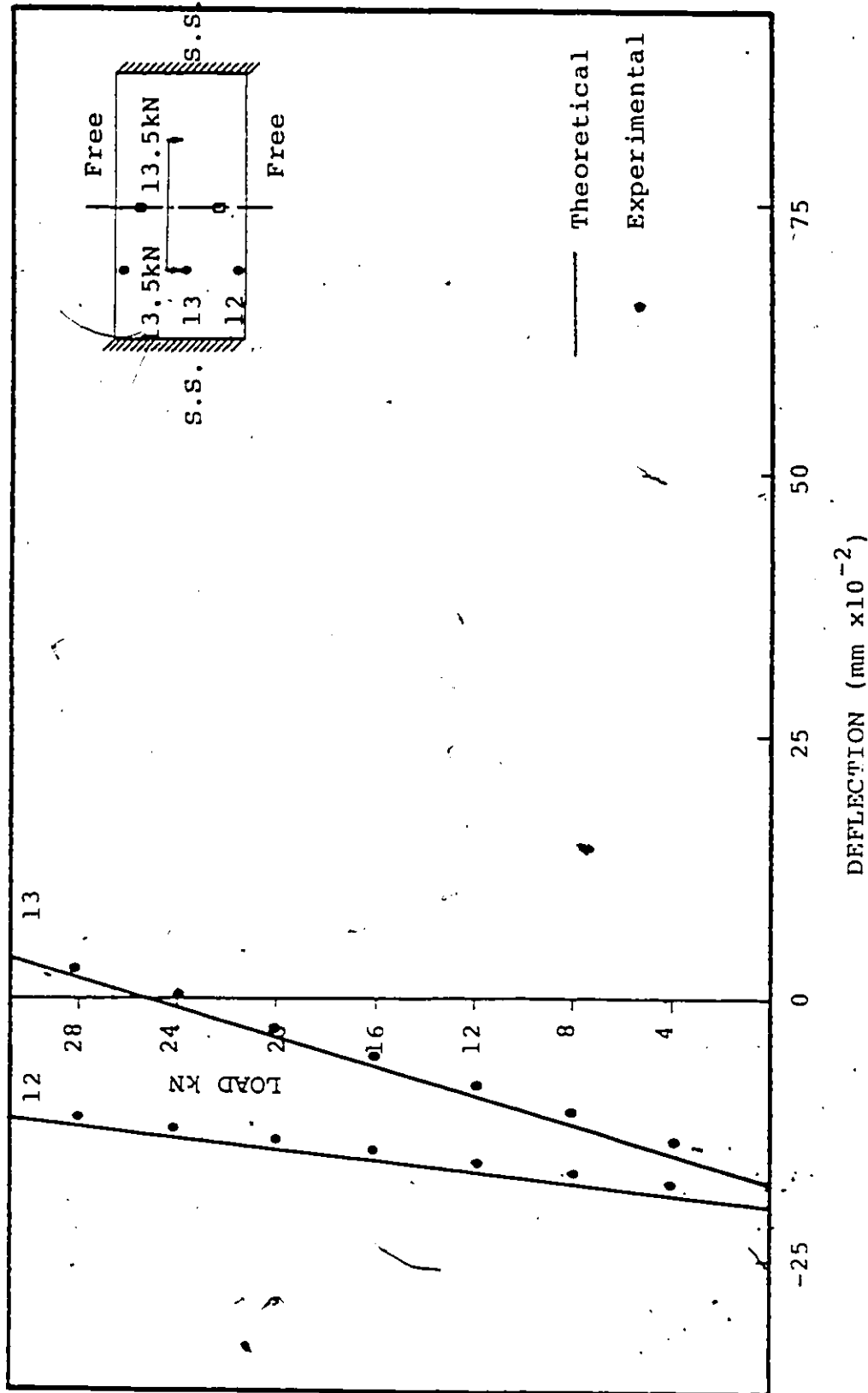


FIGURE 7.22 LOAD-DEFLECTION RELATIONSHIP FOR RECTANGULAR SLAB (PC3) DUE TO TWO CONCENTRATED LOADS EACH AT THE CENTER OF EACH SPAN

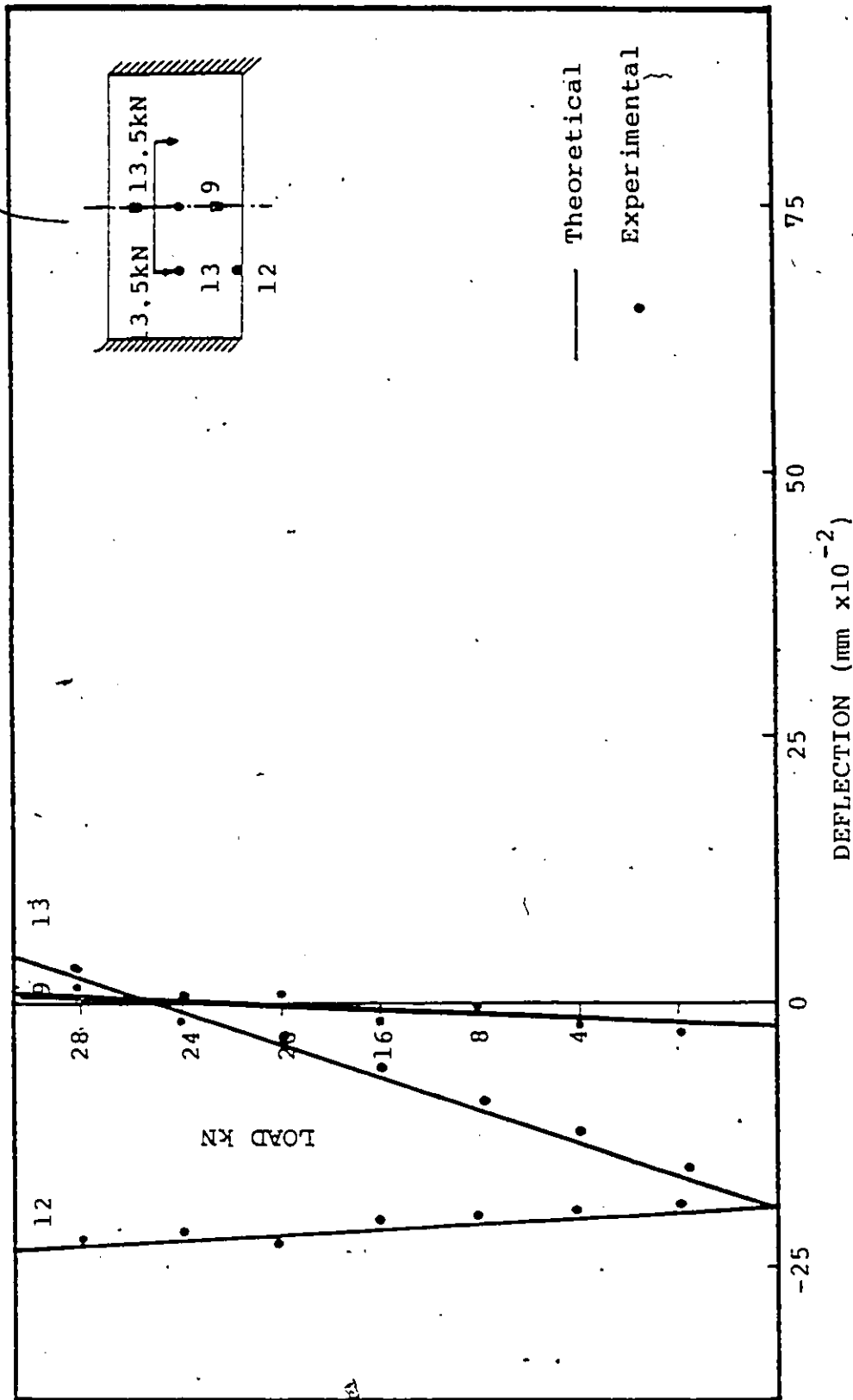


FIGURE 7.23 LOAD-DEFLECTION RELATIONSHIP FOR RECTANGULAR SLAB (PC3) DUE TO TWO CONCENTRATED LOADS EACH AT THE CENTER OF EACH SPAN

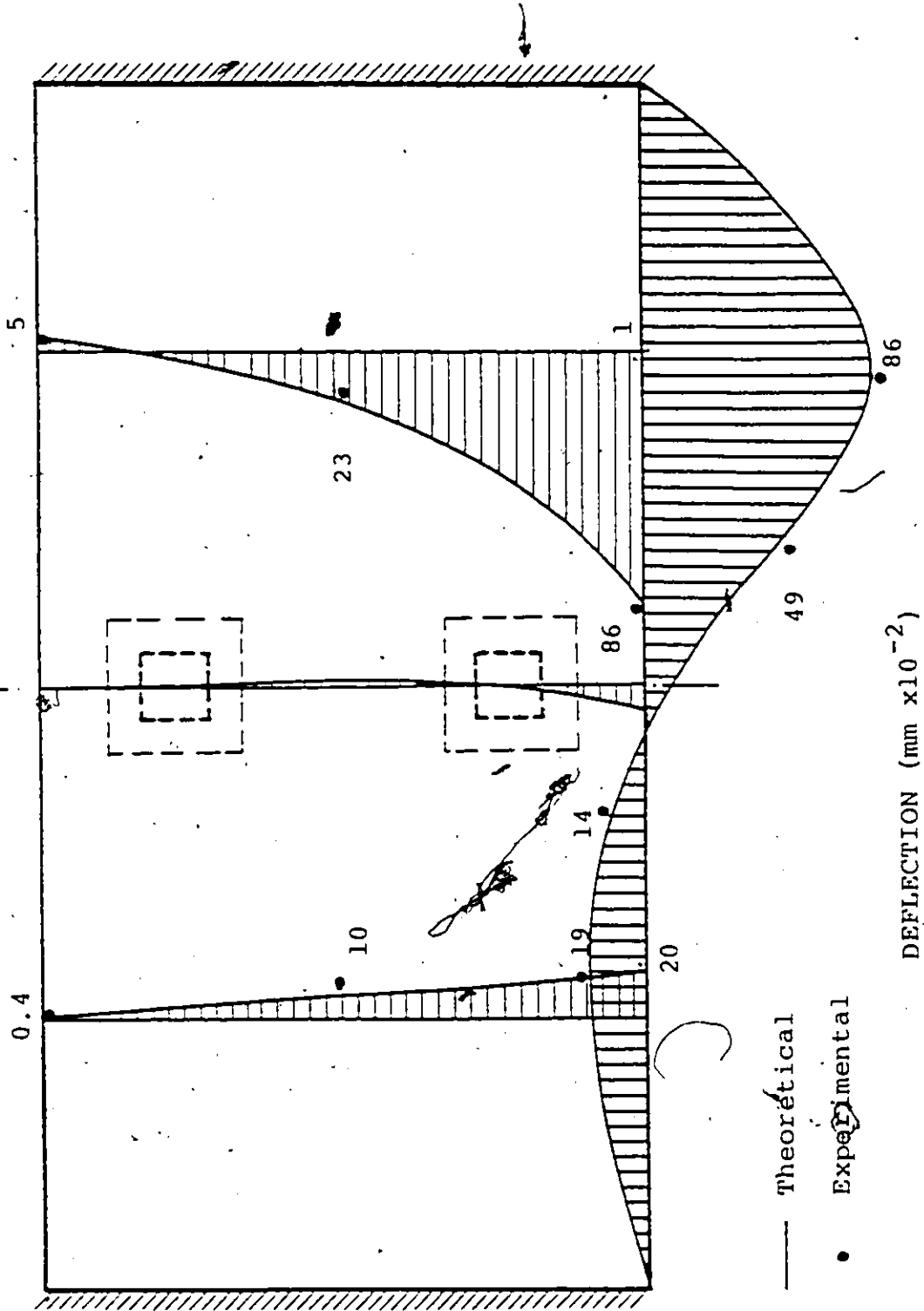


FIGURE 7.24 DEFLECTION DISTRIBUTION FOR RECTANGULAR SLAB (PC3) DUE TO 8 kN AT POINT 1

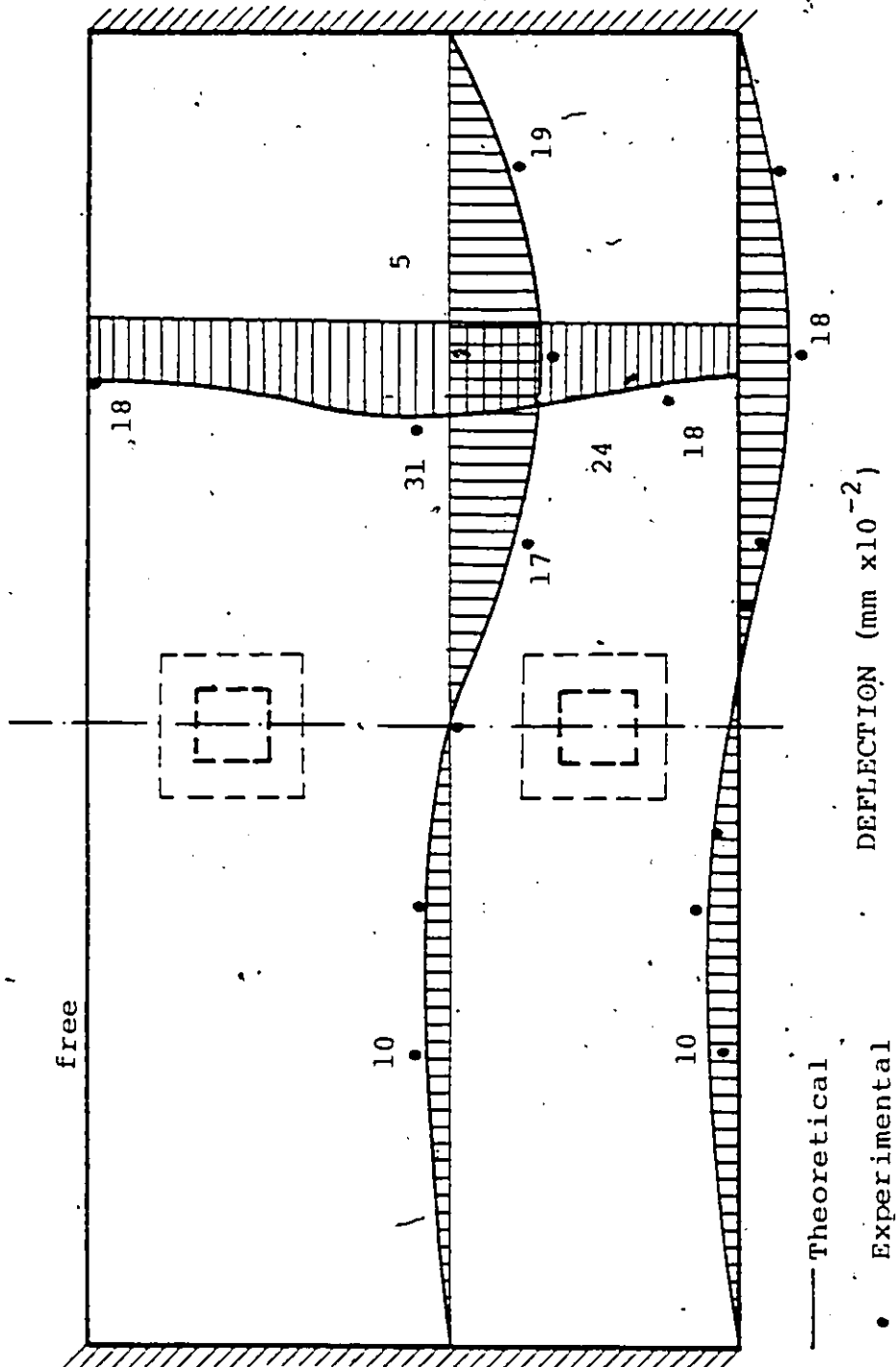


FIGURE 7.25 DEFLECTION DISTRIBUTION FOR RECTANGULAR SLAB (PC3) DUE TO 18 kN AT POINT 5

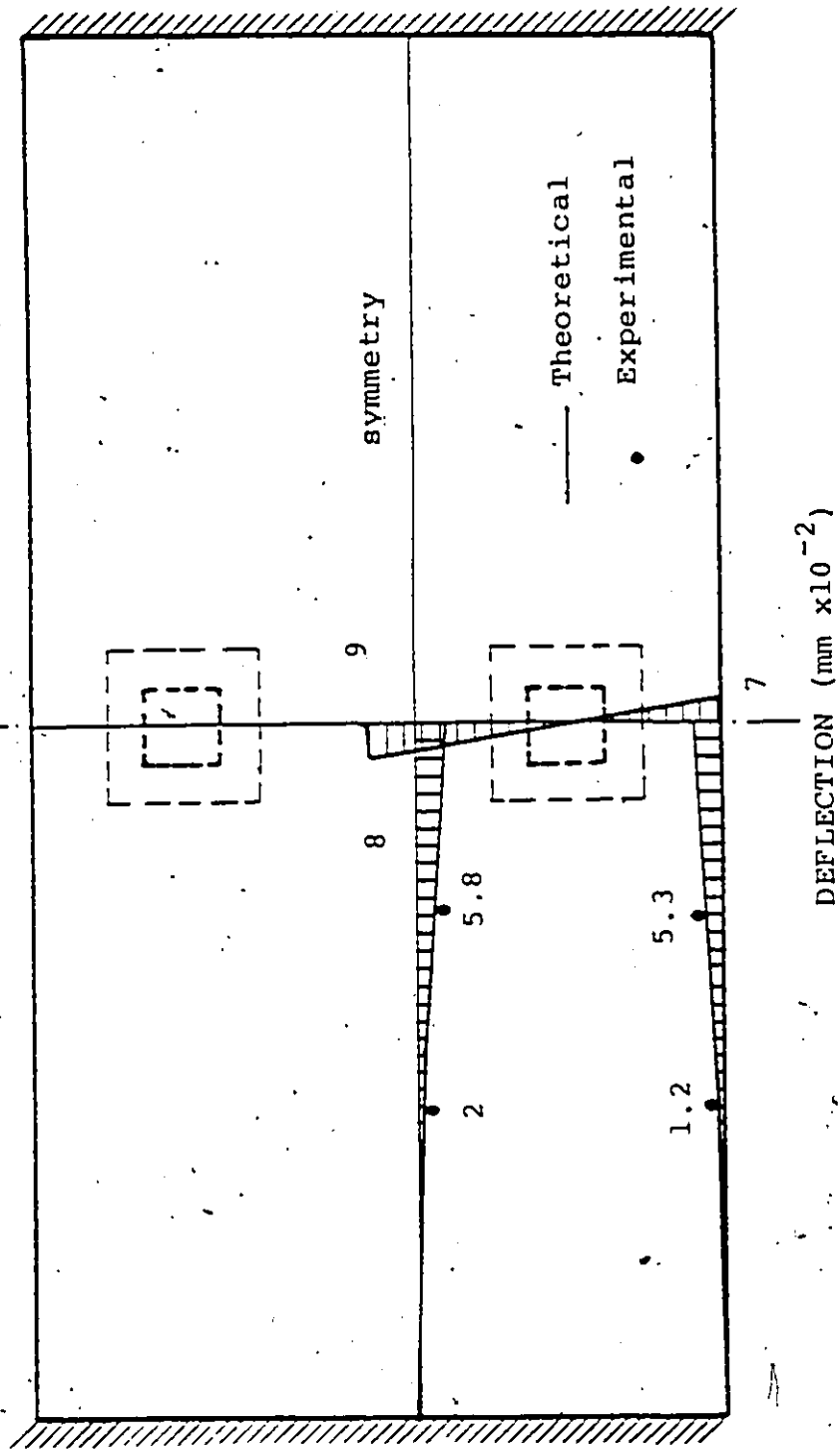
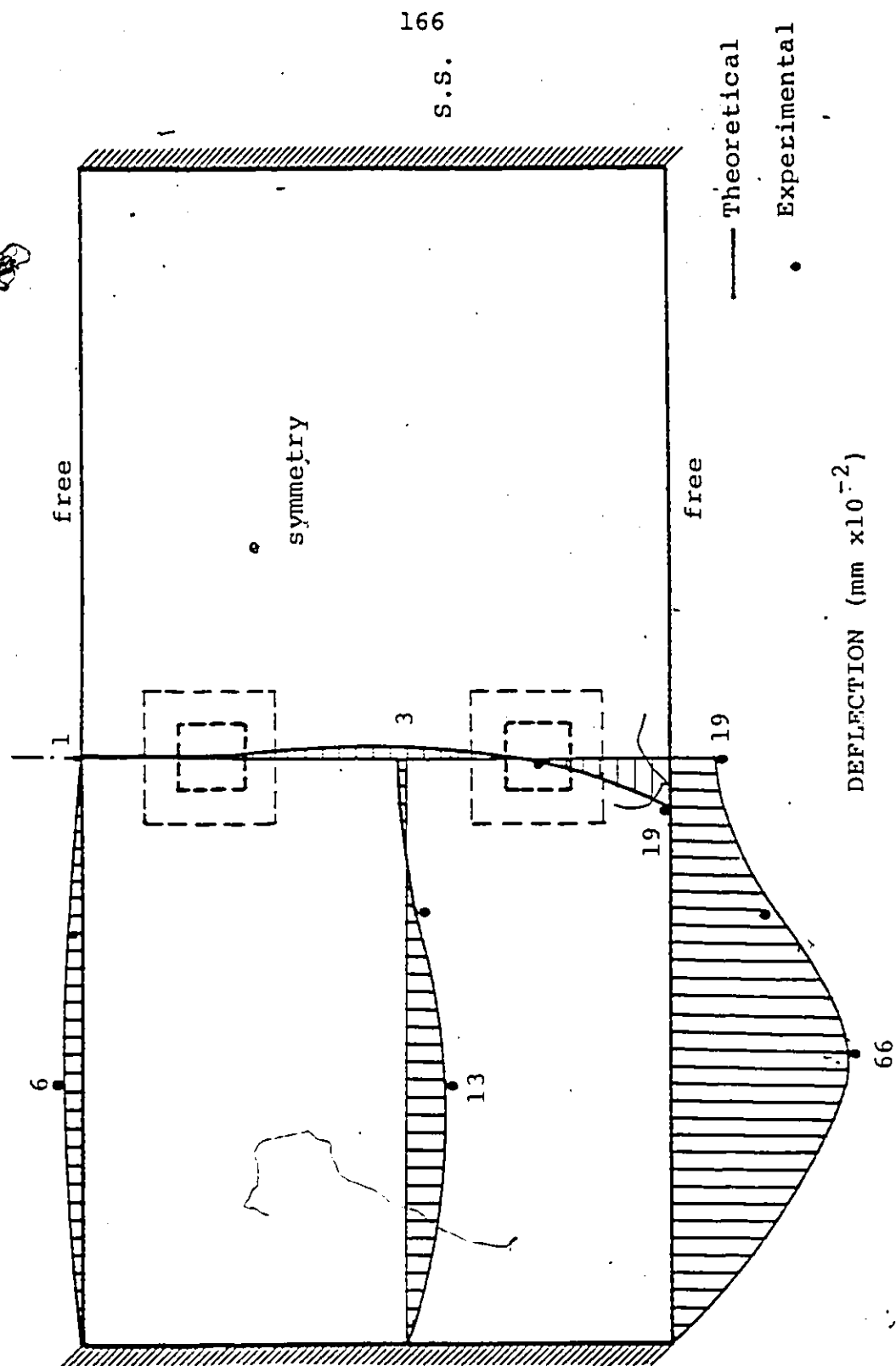


FIGURE 7.26 DEFLECTION DISTRIBUTION FOR RECTANGULAR SLAB (PC3) DUE TO A SINGLE CONCENTRATED LOAD (18kN) AT POINT 9



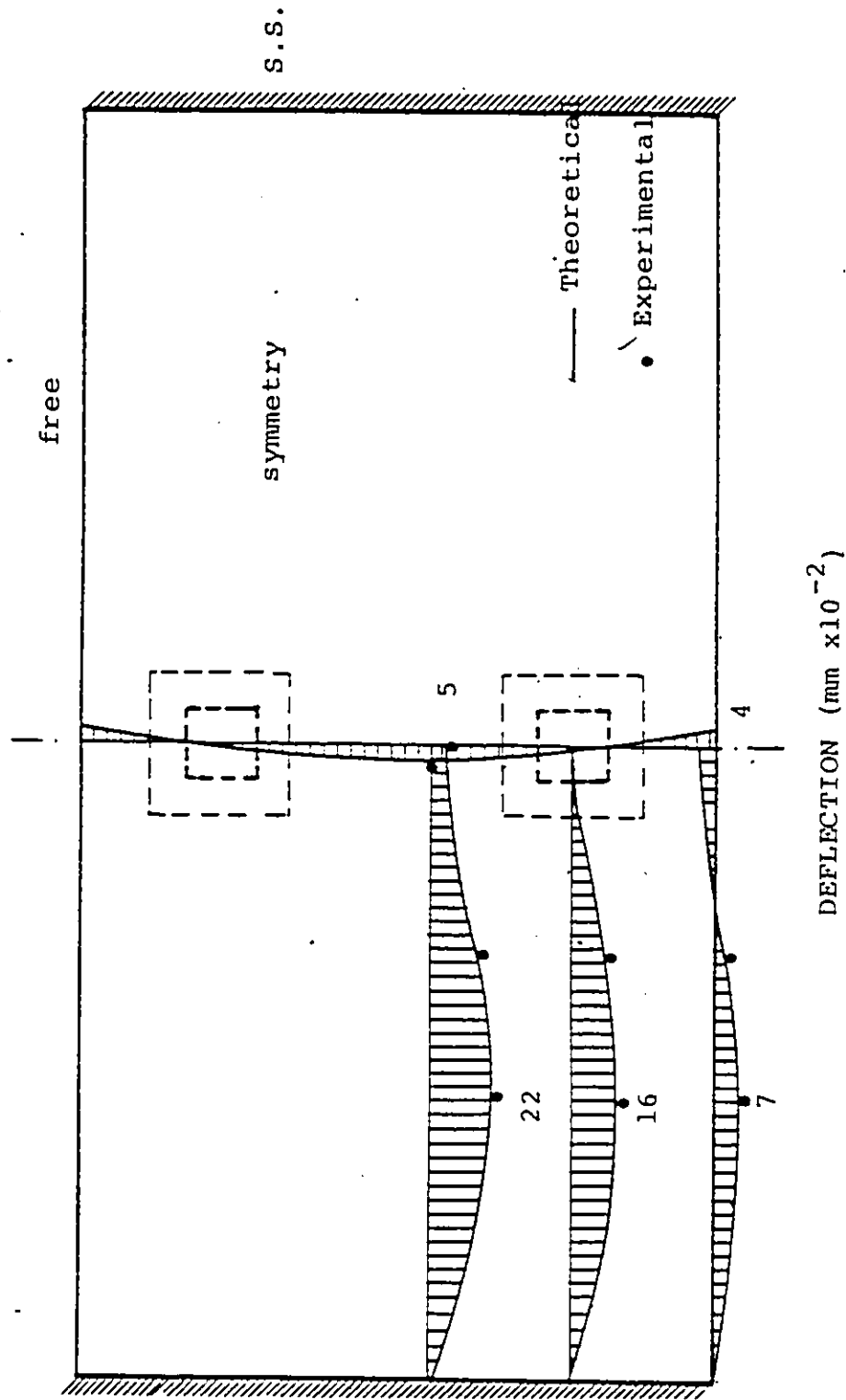


FIGURE 7.28 DEFLECTION DISTRIBUTION FOR RECTANGULAR SLAB DUE TO TWO CONCENTRATED LOADS (36 kN) EACH AT THE CENTER OF EACH SPAN

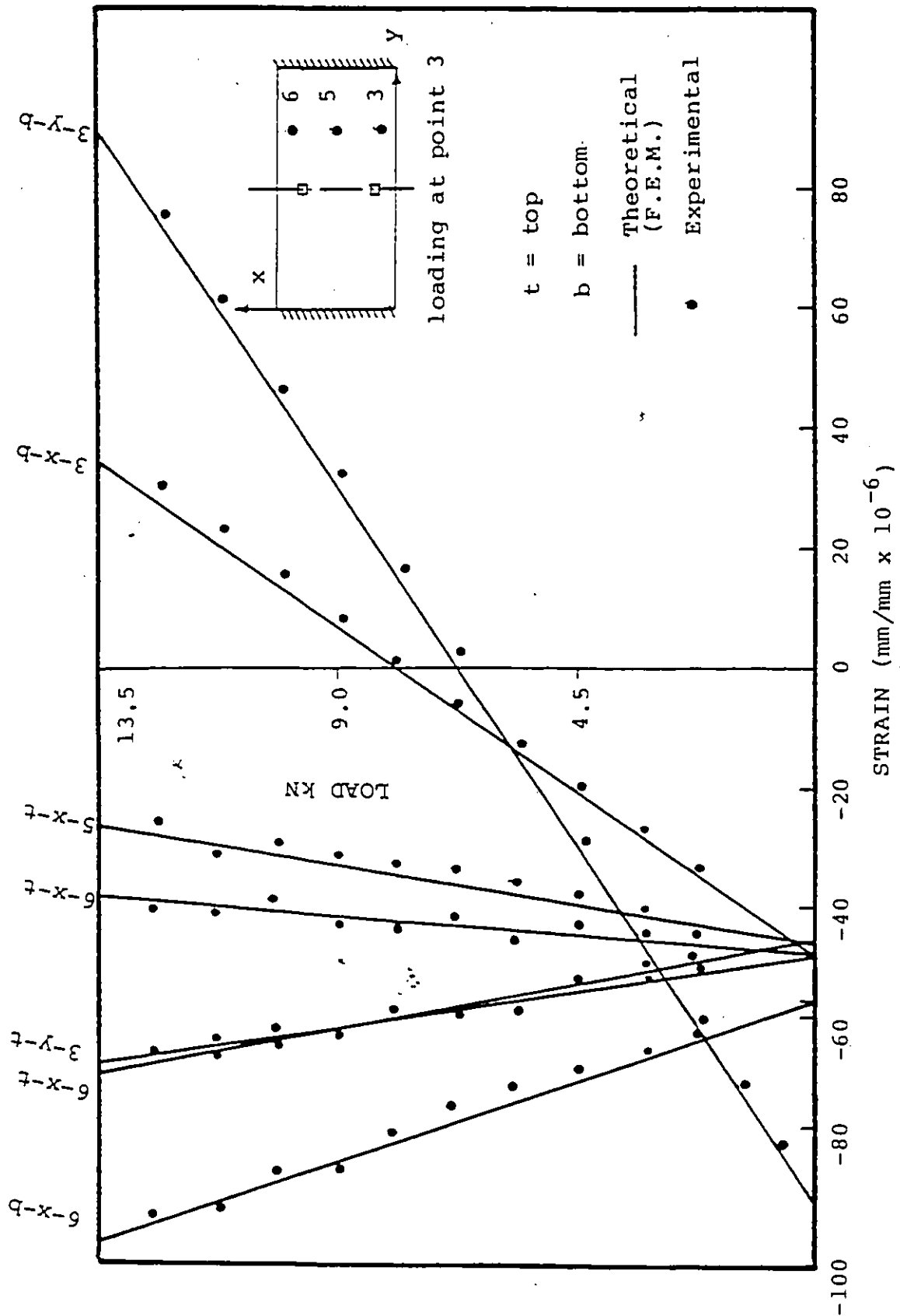


FIGURE 7.29 LOAD-STRAIN RELATIONSHIPS FOR RECTANGULAR SLAB (PC3) AT THE CENTER OF THE EDGE BEAM

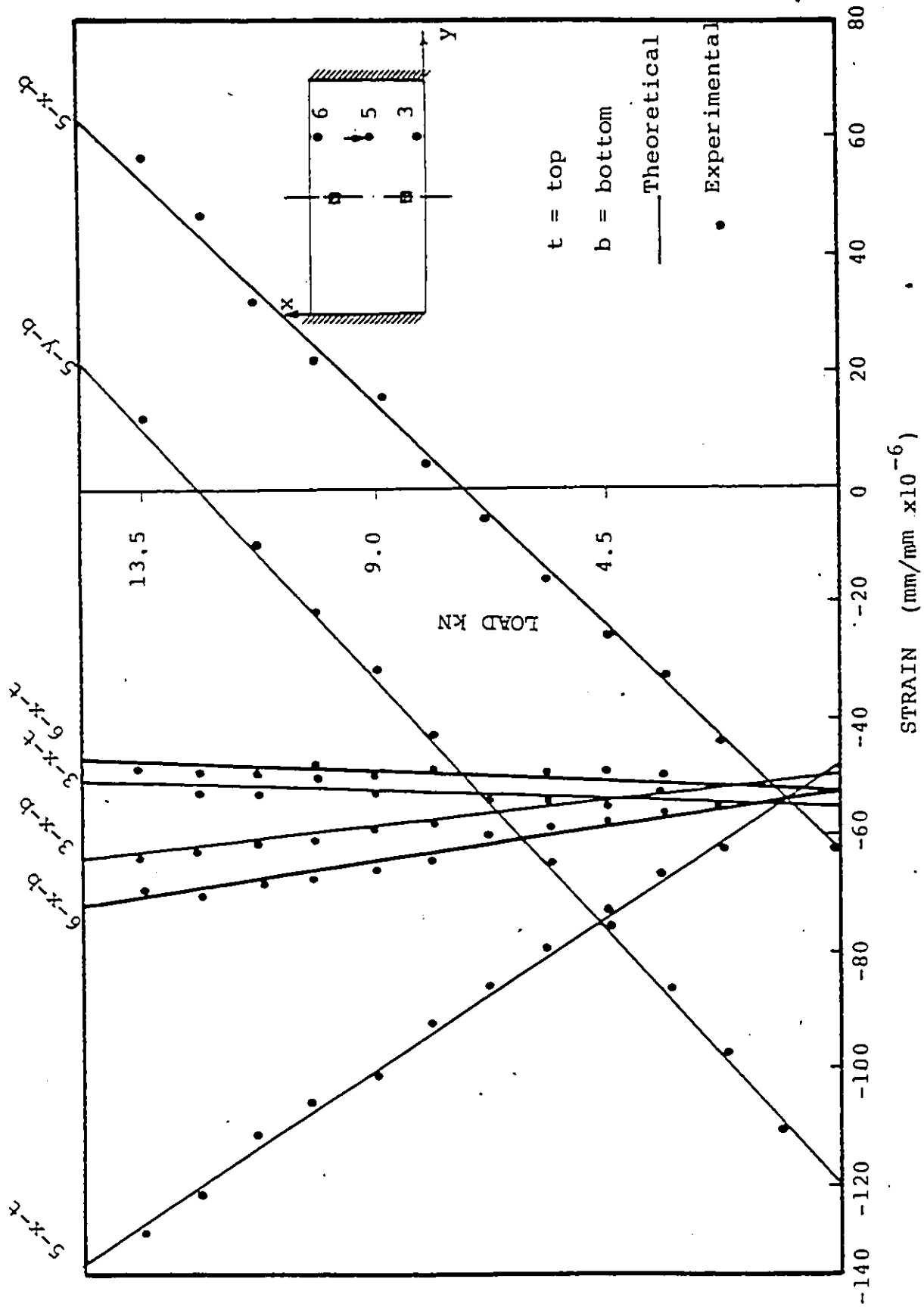


FIGURE 7.30 LOAD-STRAIN RELATIONSHIP FOR RECTANGULAR SLAB LOADING AT POINT 5

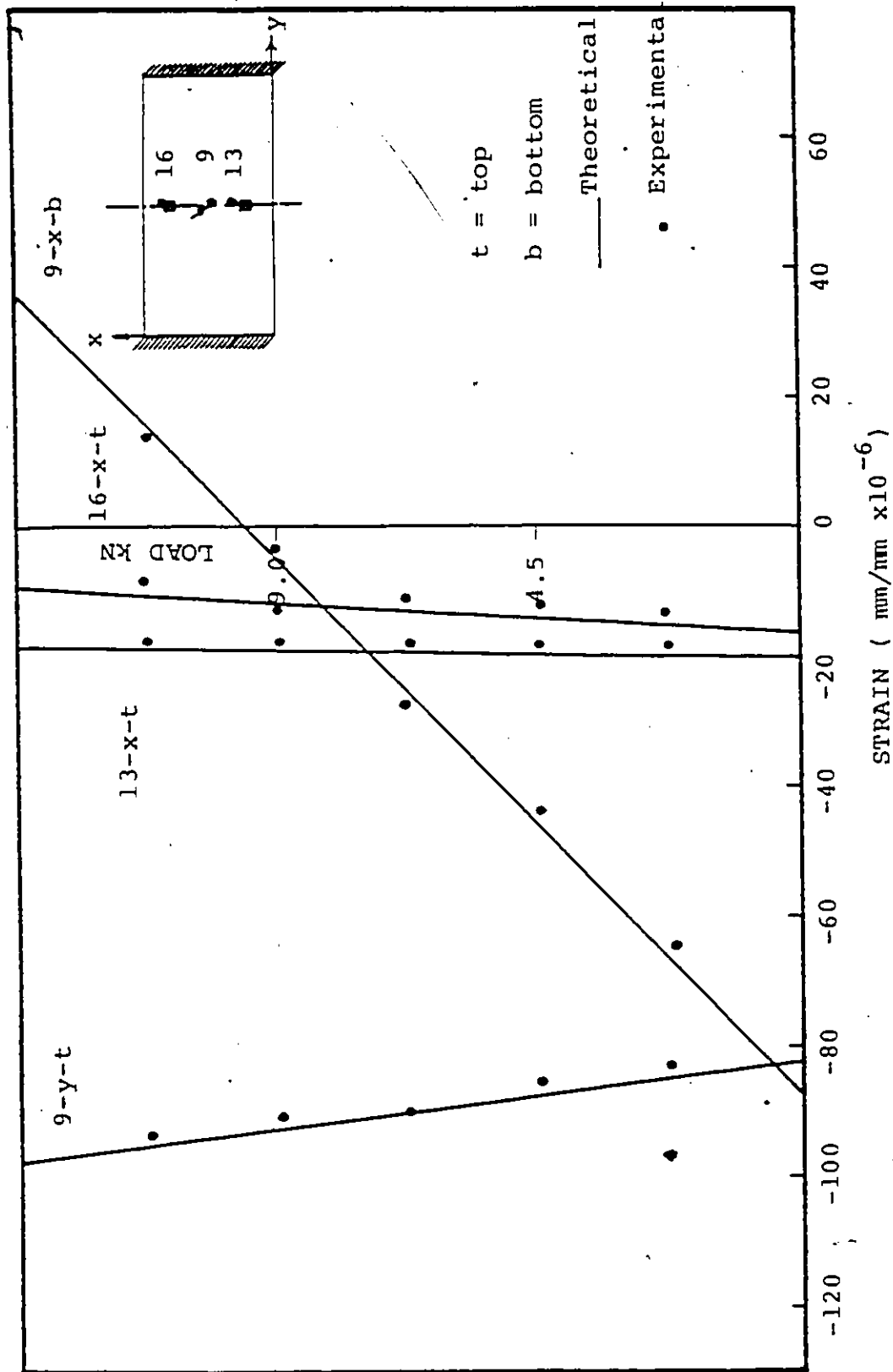


FIGURE 7.31 LOAD-STRAIN RELATIONSHIP FOR RECTANGULAR SLAB DUE TO CONCENTRATED LOAD AT POINT 9

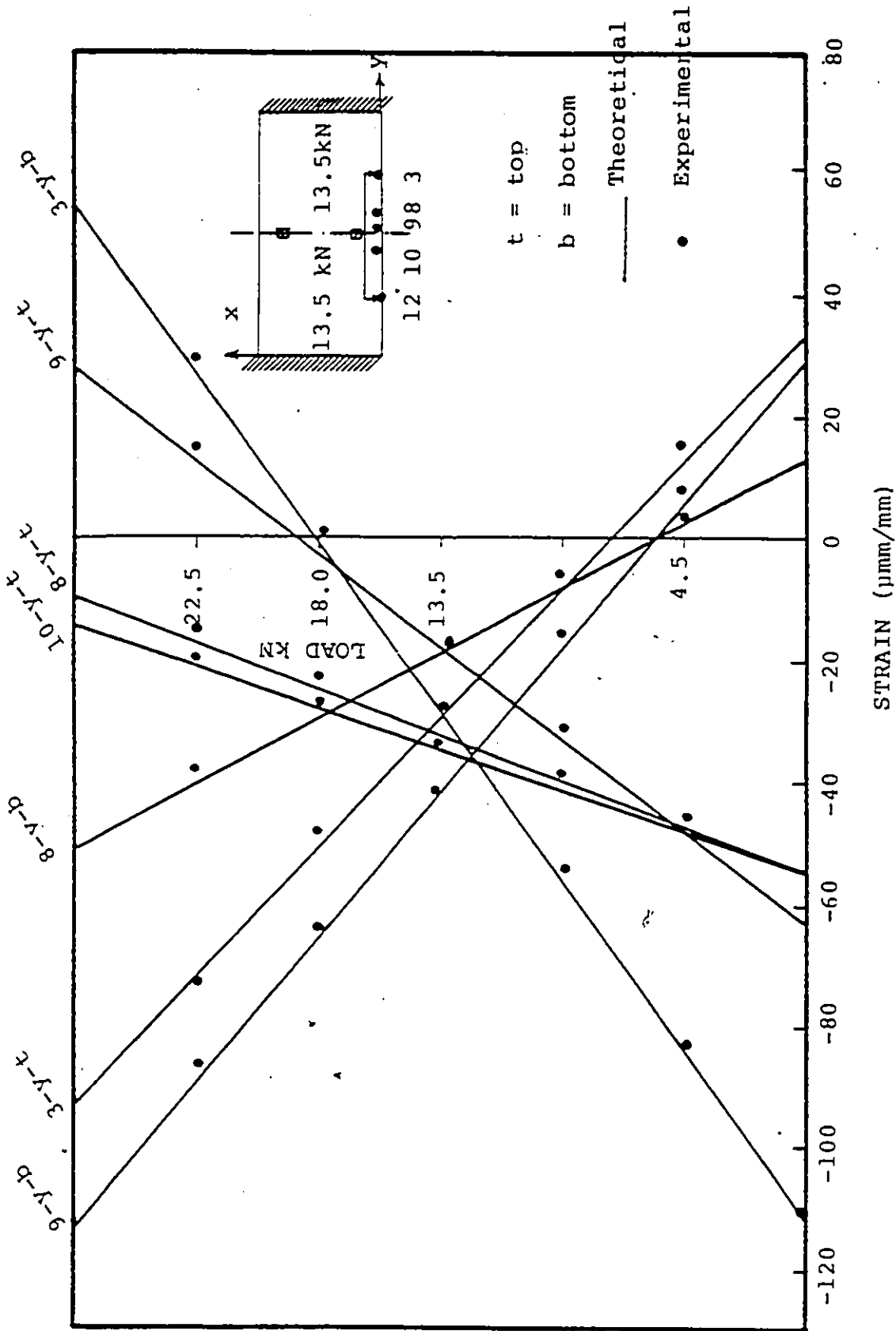


FIGURE 7.32 LOAD-STRAIN RELATIONSHIP FOR RECTANGULAR SLAB DUE TO TWO CONCENTRATED LOADS AT THE EDGE BEAM

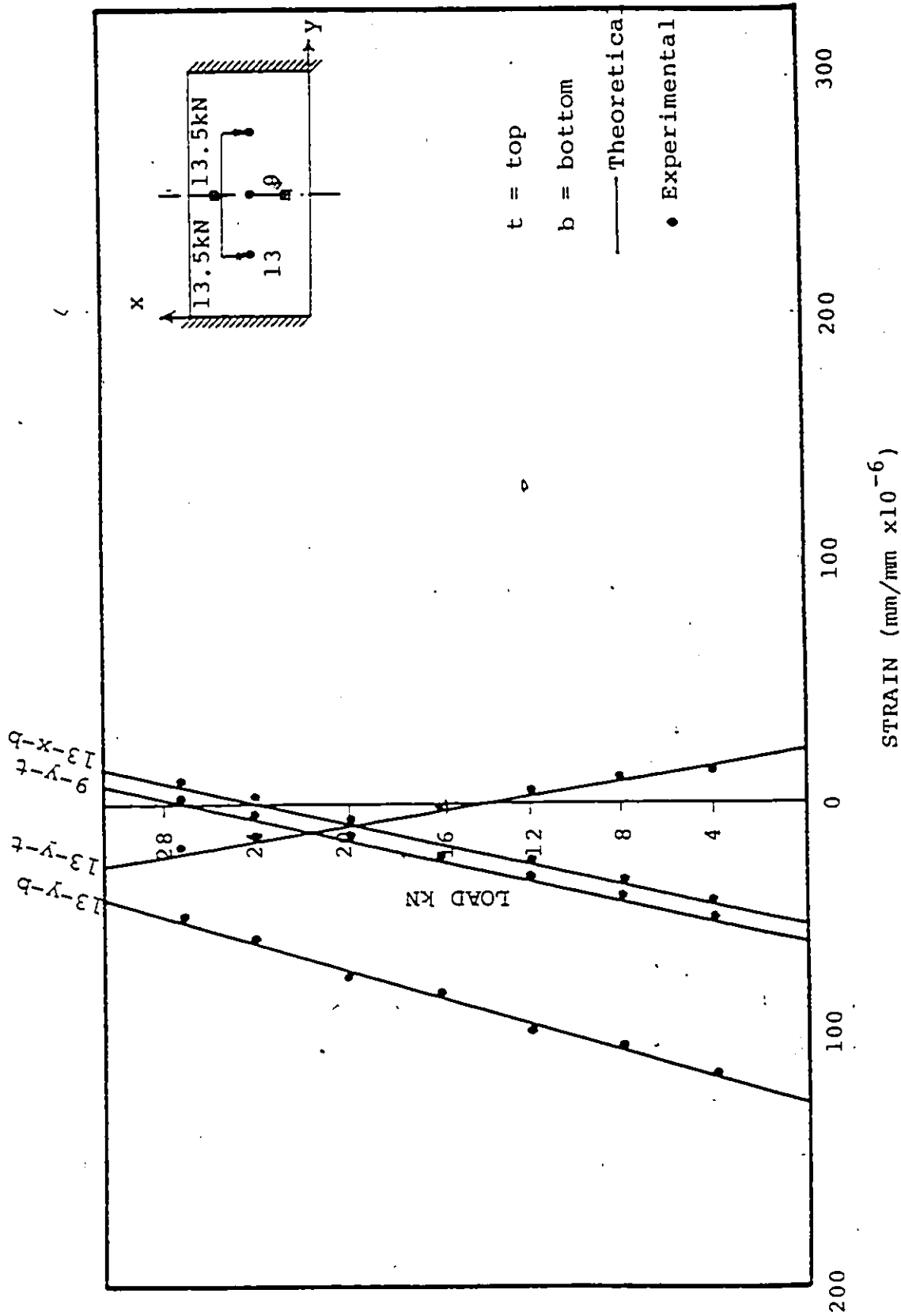


FIGURE 7.33 LOAD-STRAIN RELATIONSHIP FOR RECTANGULAR SLAB (PC3) DUE TO TWO CONCENTRATED LOADS EACH AT THE CENTER OF EACH SPAN

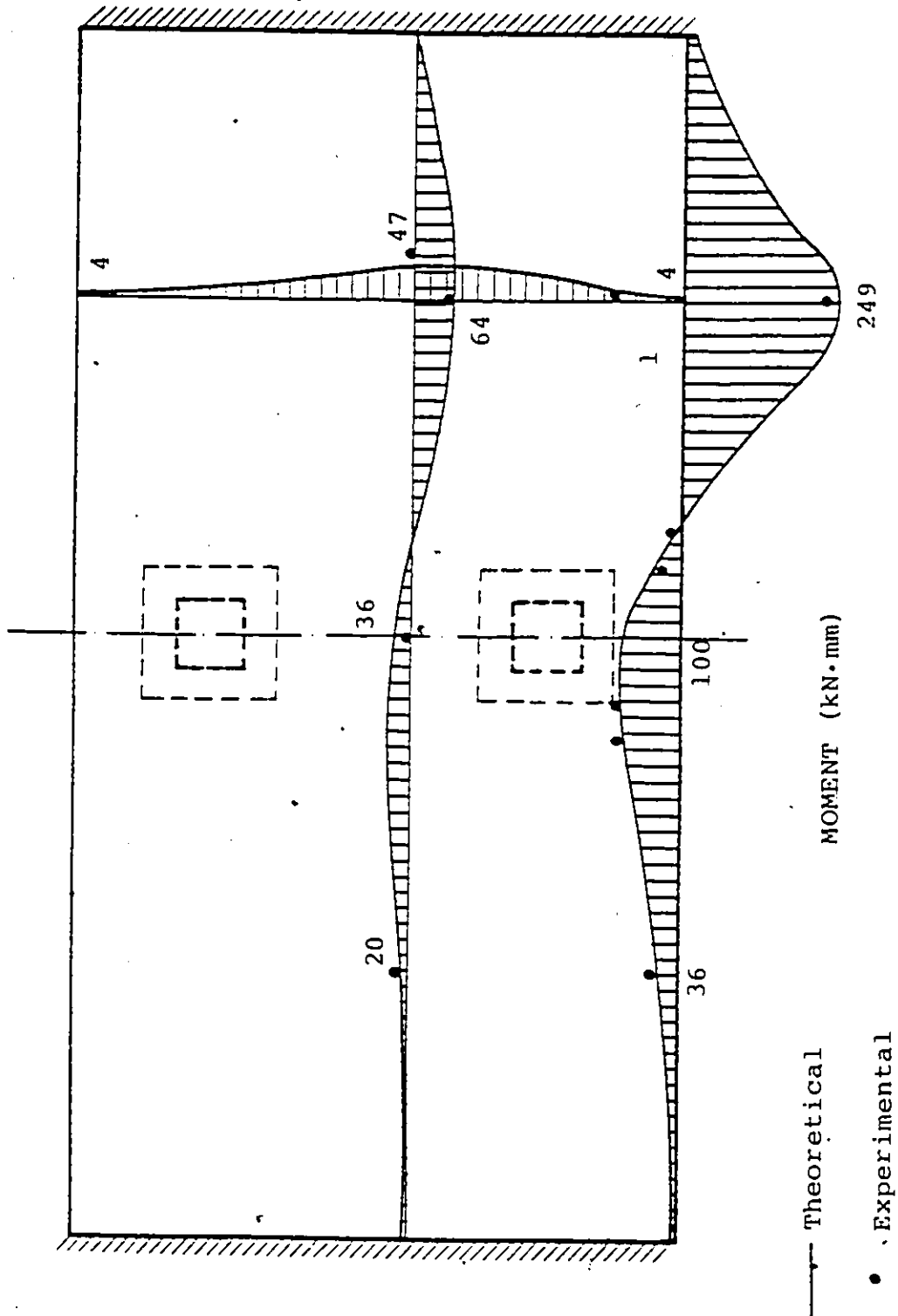


FIGURE 7.34 MOMENT DISTRIBUTION FOR RECTANGULAR SLAB DUE TO 18 kN AT POINT 1

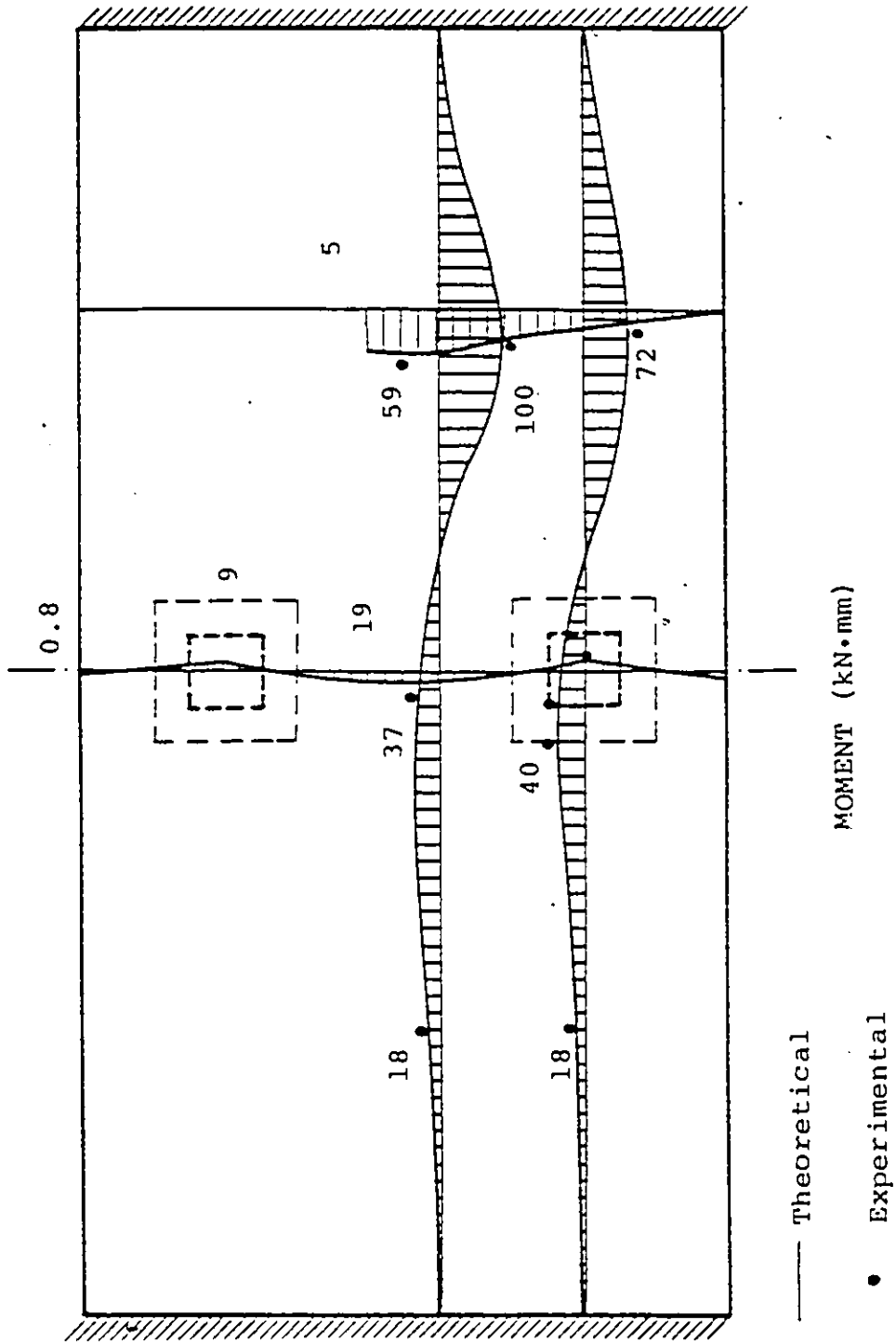


FIGURE 7.35 MOMENT DISTRIBUTION FOR RECTANGULAR SLAB DUE TO 18 kN AT POINT 5

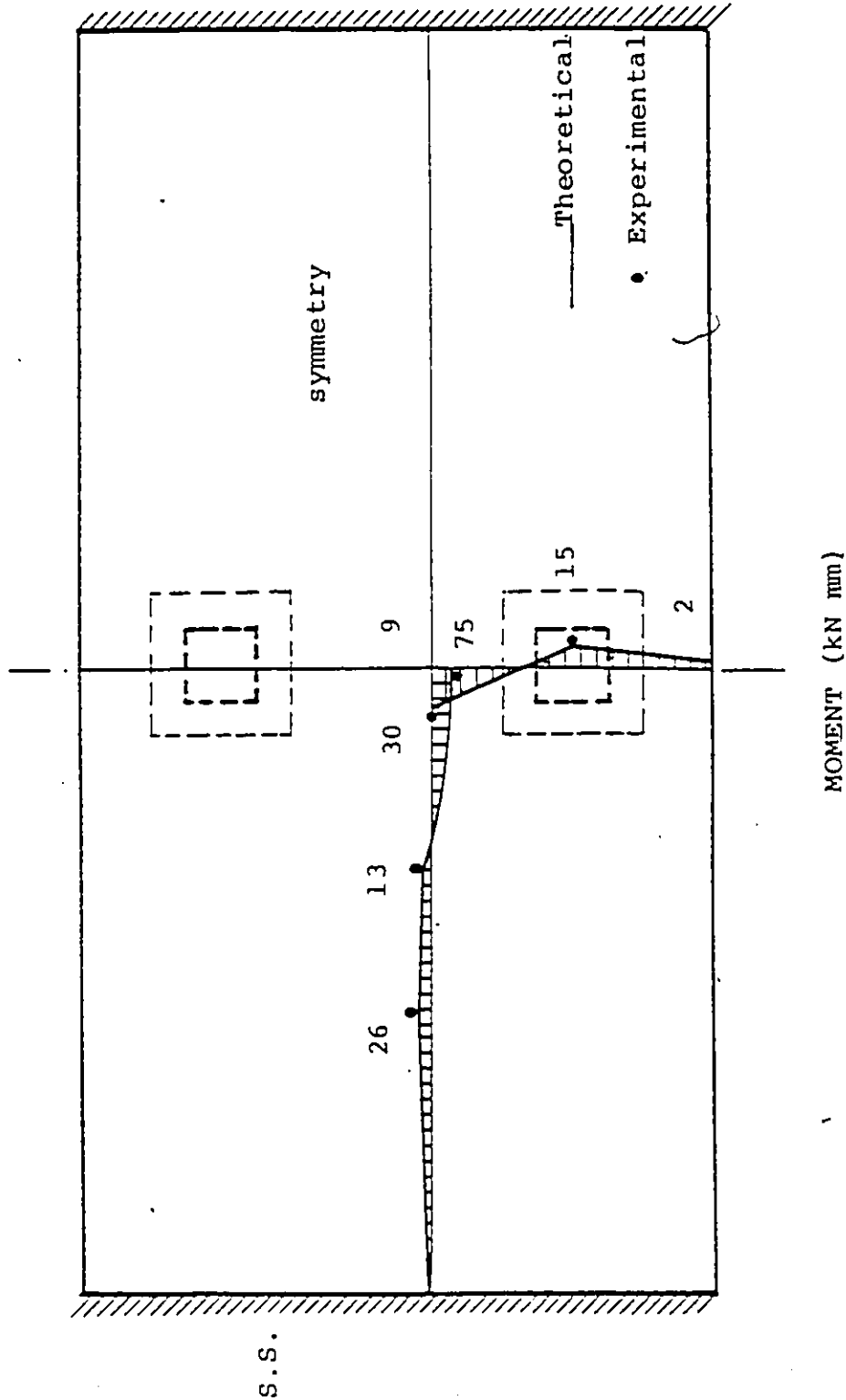


FIGURE 7.36 MOMENT DISTRIBUTION FOR RECTANGULAR SLAB DUE TO A CONCENTRATED LOAD (18 kN) AT POINT 9

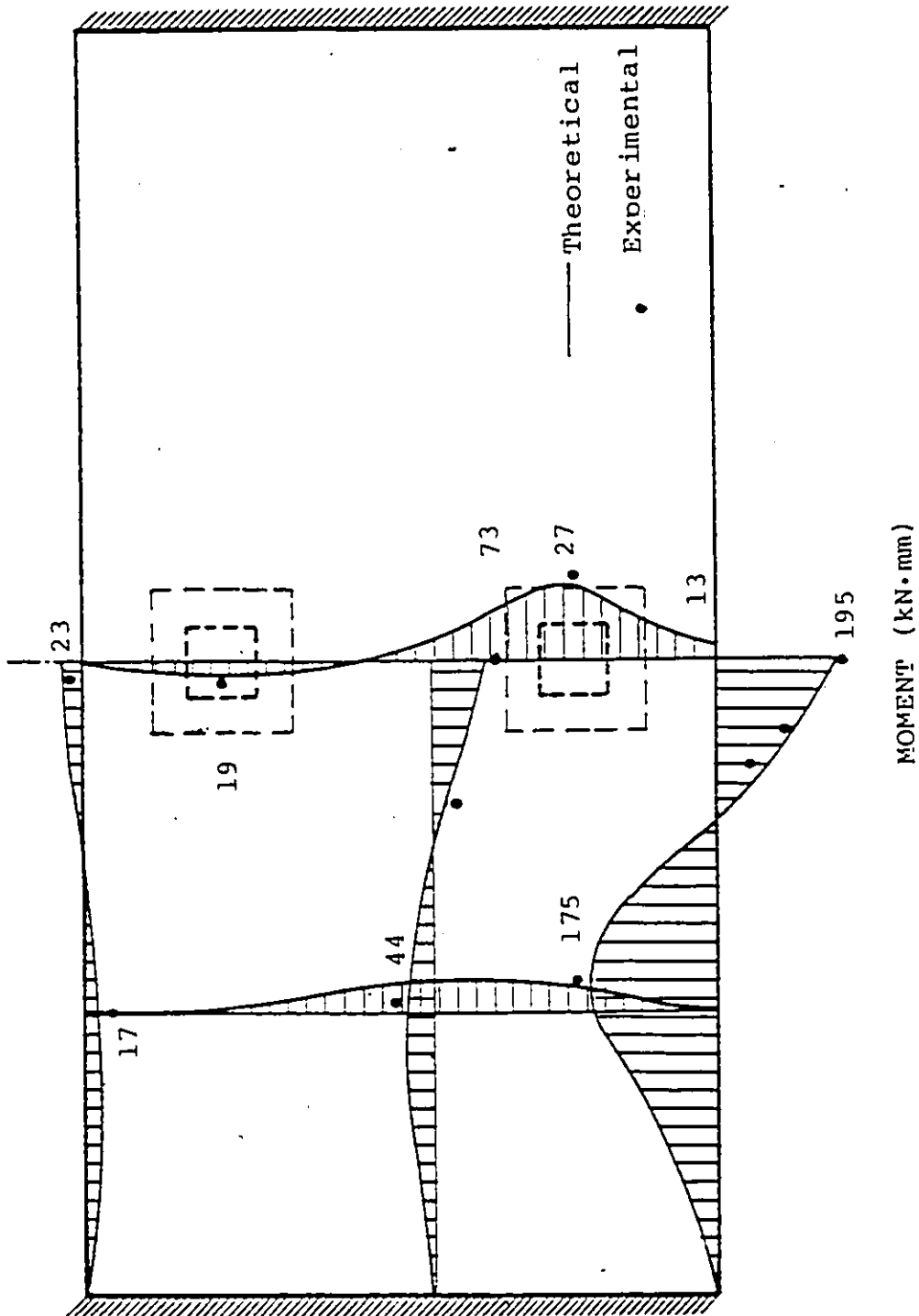


FIGURE 7.37 MOMENT DISTRIBUTION FOR RECTANGULAR SLAB DUE TO TWO CONCENTRATED LOADS (36 kN) EACH AT THE CENTER OF THE EDGE BEAM

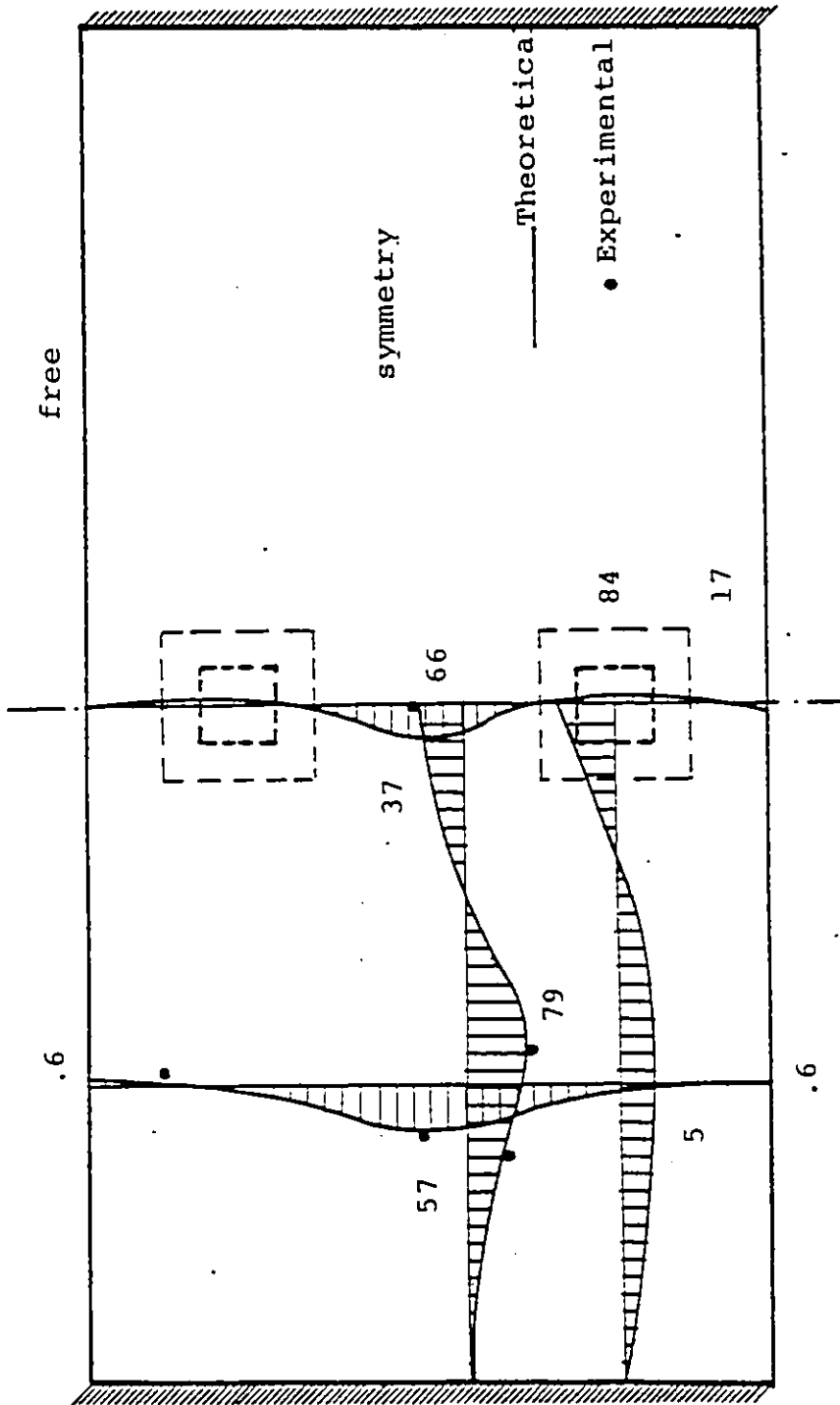


FIGURE 7.38 MOMENT DISTRIBUTION FOR RECTANGULAR SLAB (PC3) DUE TO TWO CONCENTRATED LOADS (36 kN) AT THE CENTER OF EACH SPAN

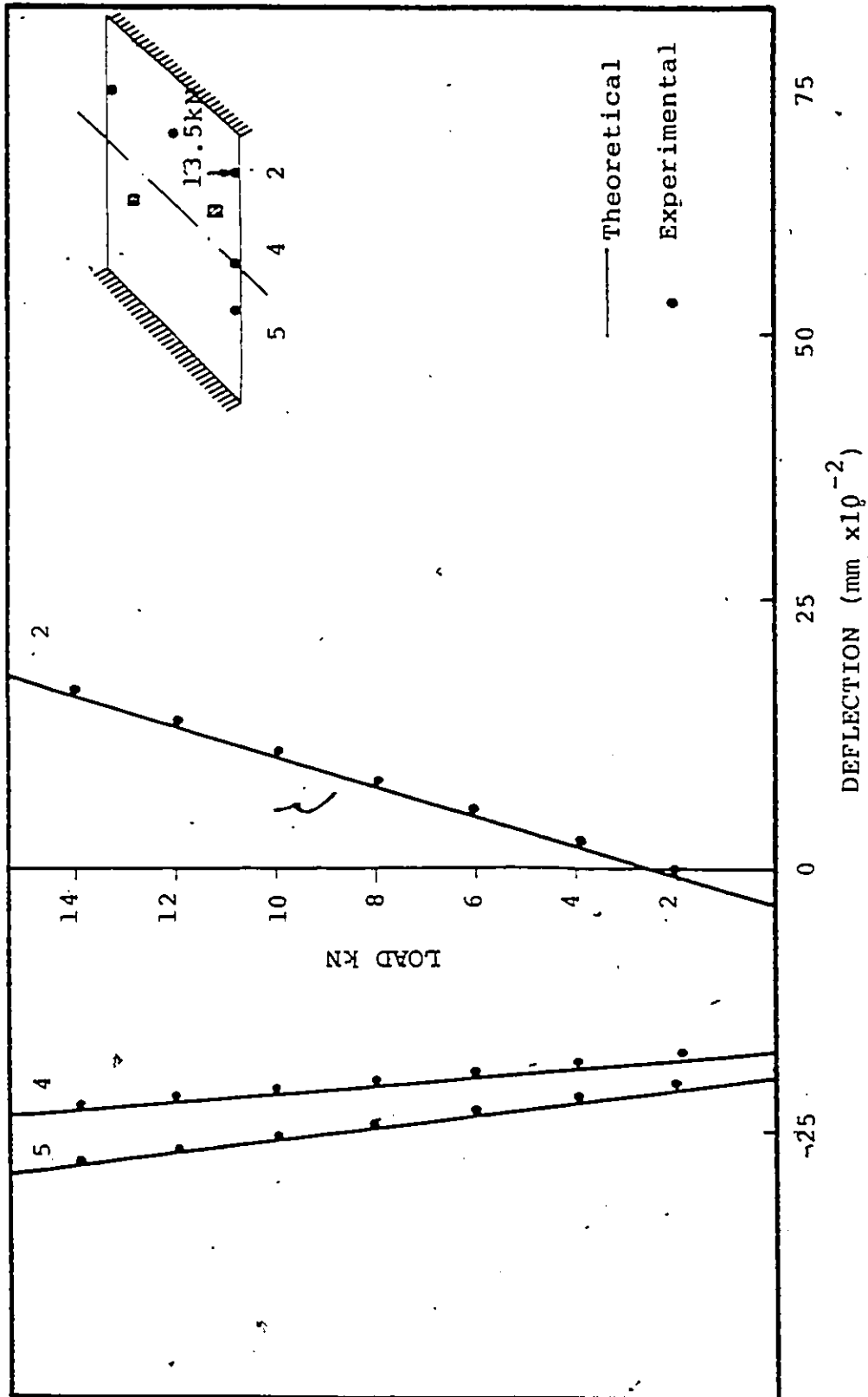


FIGURE 7.39 LOAD-DEFLECTION RELATIONSHIP FOR SKEW SLAB (PC4) DUE TO CONCENTRATED LOAD AT THE EDGE BEAM POINT 2

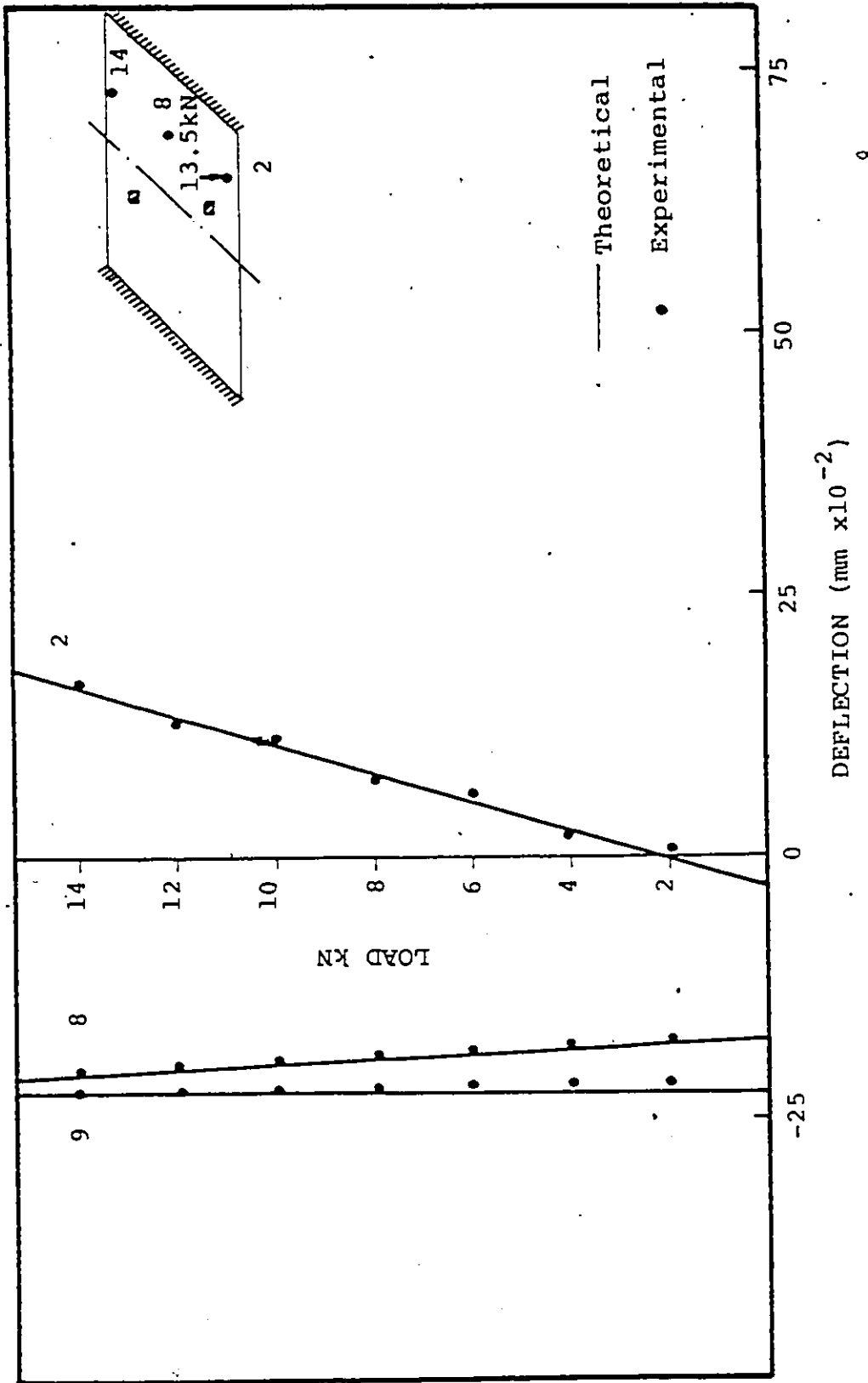


FIGURE 7.40 LOAD-DEFLECTION RELATIONSHIP FOR SKEW SLAB (PC4) DUE TO A CONCENTRATED LOAD AT THE EDGE BEAM, POINT 2

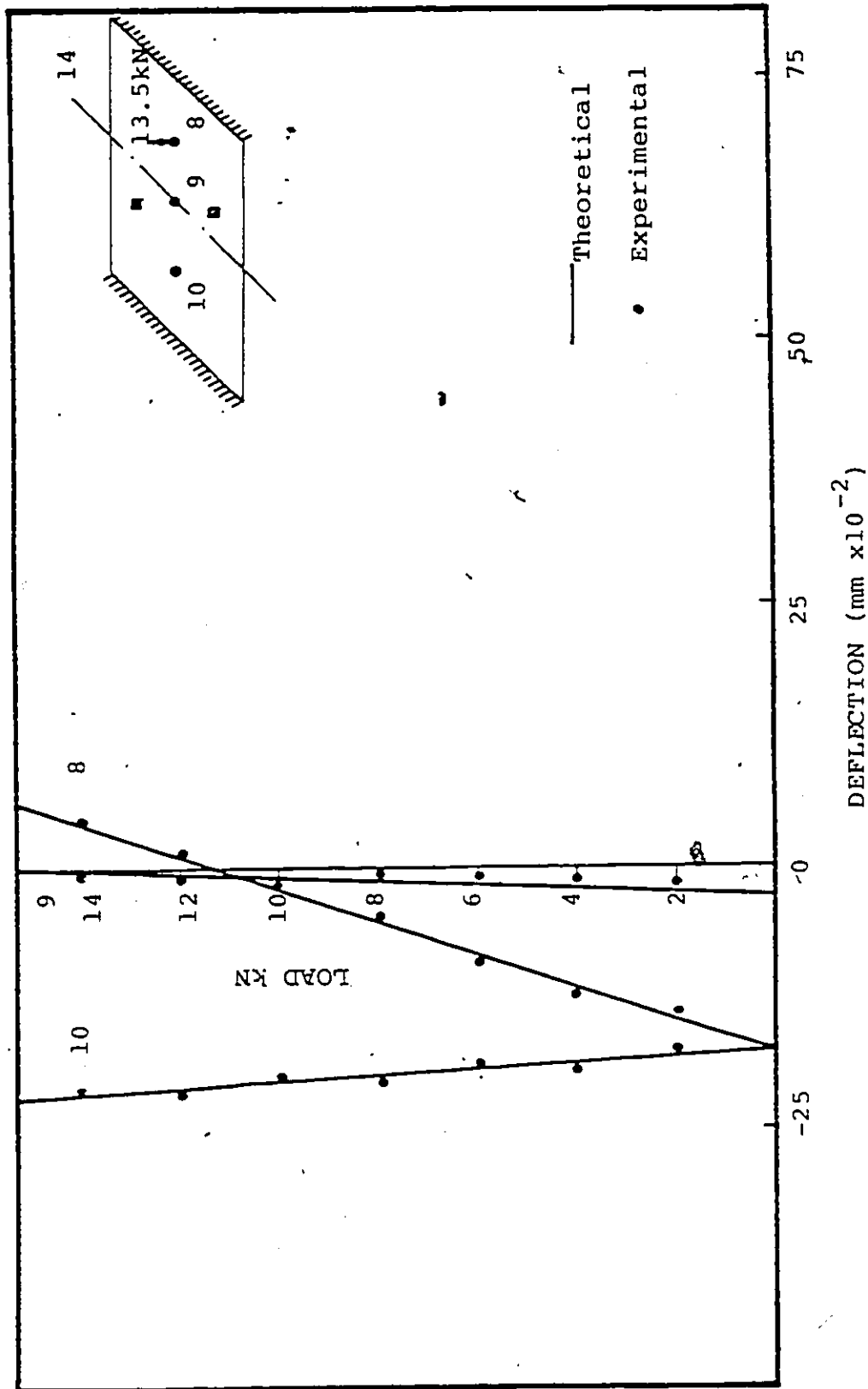


FIGURE 7.41 LOAD DEFLECTION RELATIONSHIP FOR SKEW SLAB (PC4) DUE TO A CONCENTRATED LOAD AT THE CENTER OF THE SPAN.

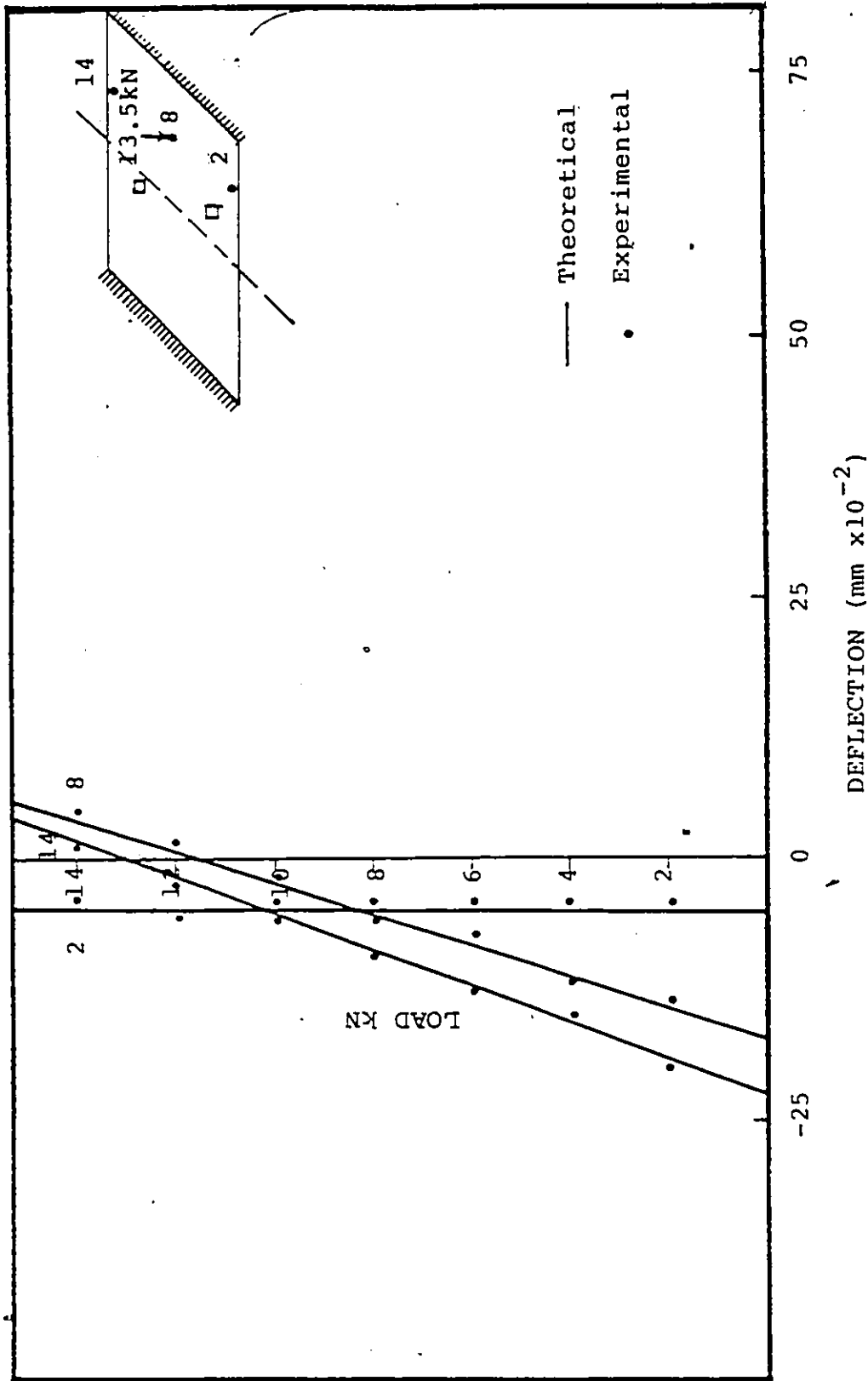


FIGURE 7.42 LOAD DEFLECTION RELATIONSHIP FOR SKEW SLAB (PC4) DUE TO A CONCENTRATED LOAD AT THE CENTER OF THE SPAN,

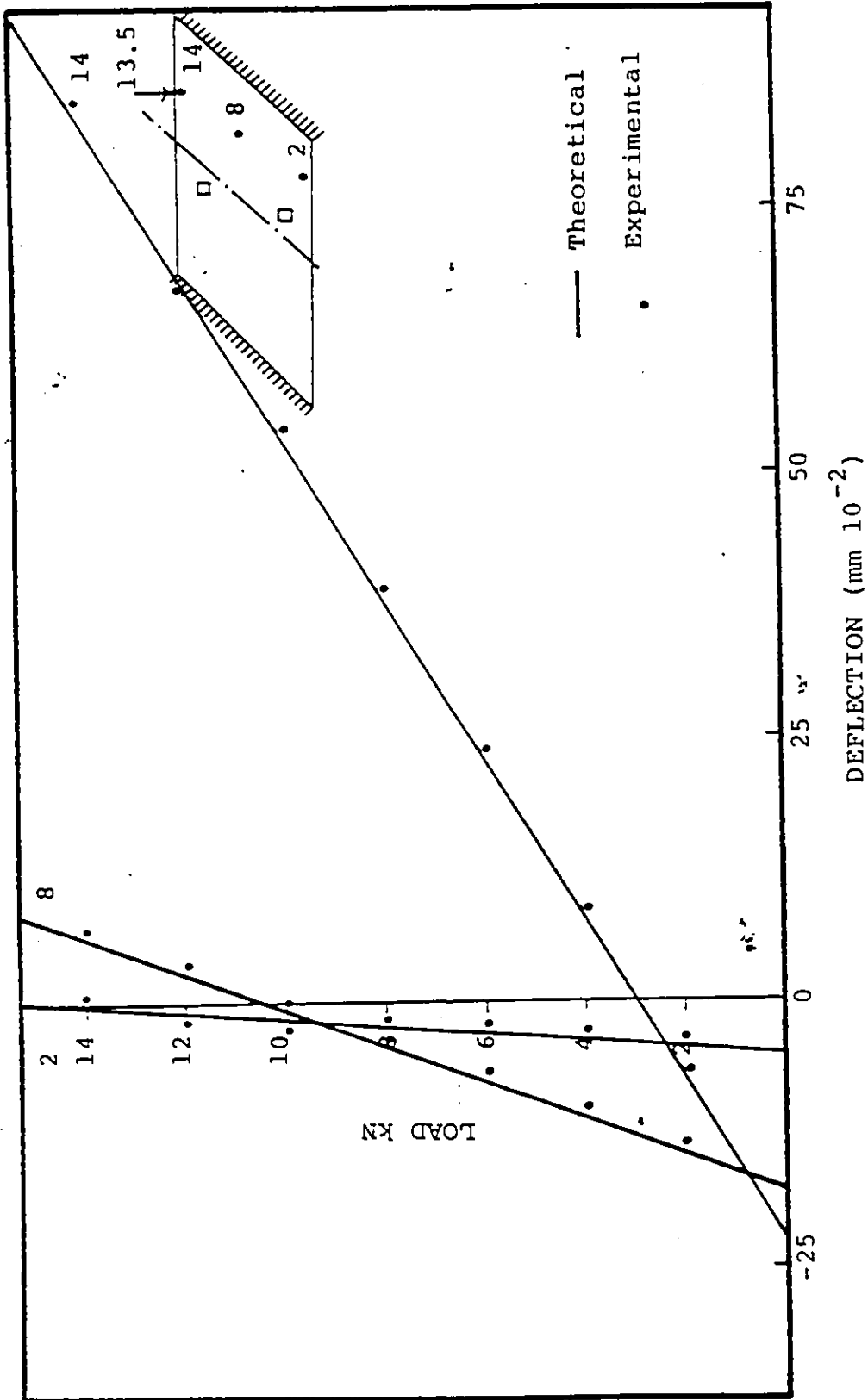


FIGURE 7.43 DEFLECTION RELATIONSHIP FOR SKEW SLAB (PC4) DUE TO A CONCENTRATED LOAD AT THE CENTER OF THE EDGE BEAM

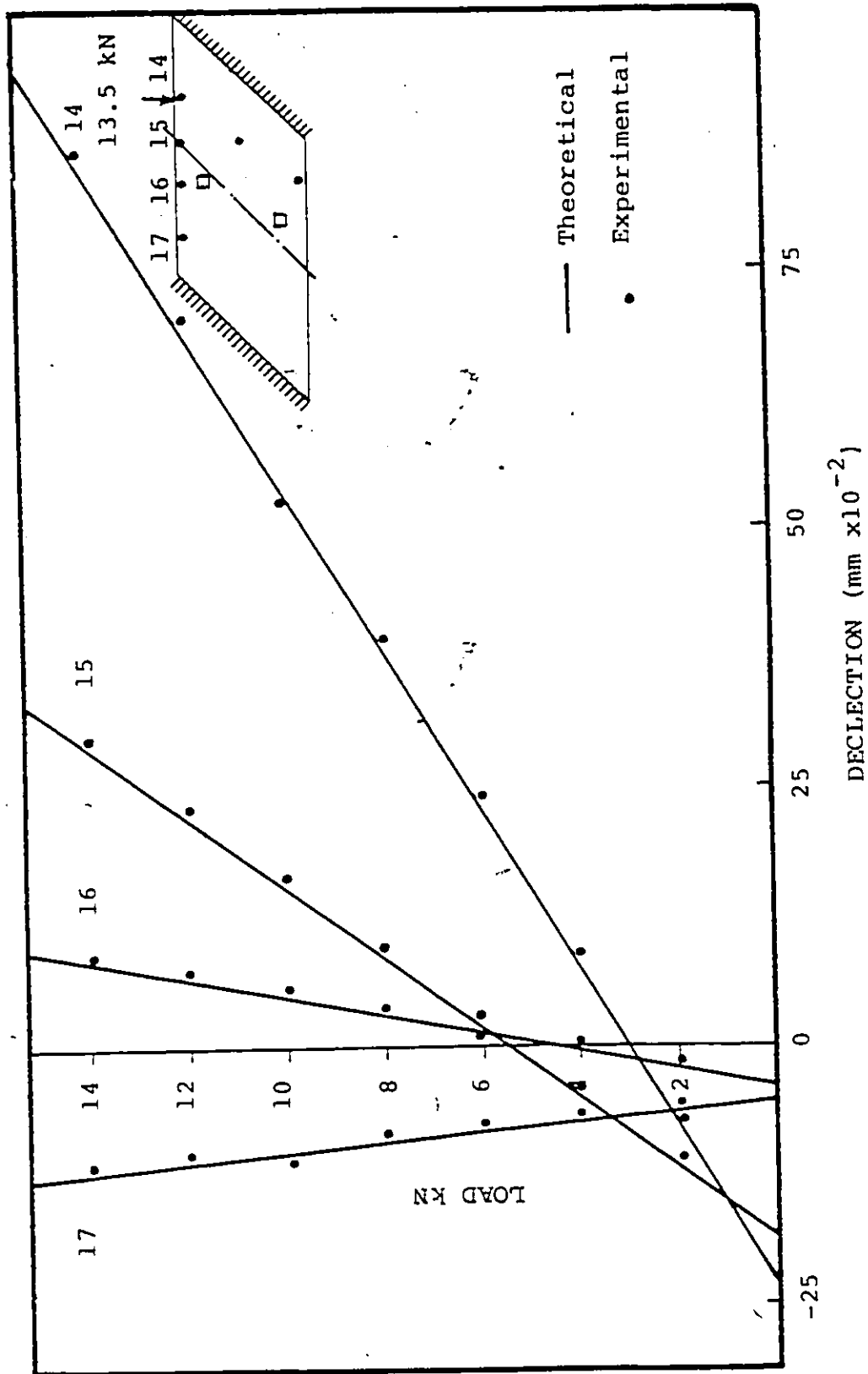


FIGURE 7.44 LOAD DEFLECTION RELATIONSHIP FOR SKEW SLAB (PC4) DUE TO A CONCENTRATED LOAD AT THE CENTRE OF THE EDGE BEAM

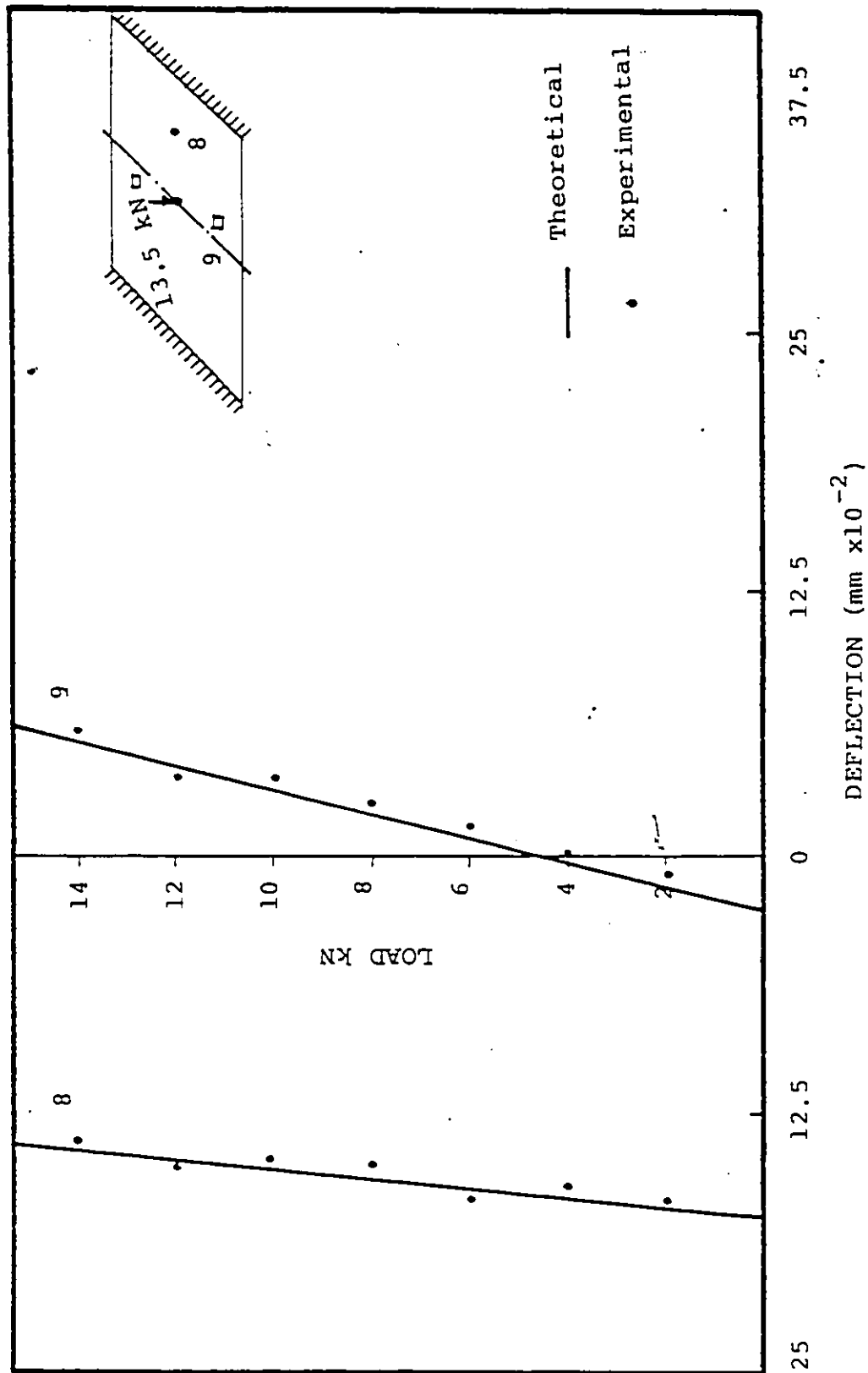


FIGURE 7.45 LOAD DEFLECTION RELATIONSHIP FOR SKEW SLAB DUE TO A CONCENTRATED LOAD AT THE CENTER OF THE SLAB MODEL PC4

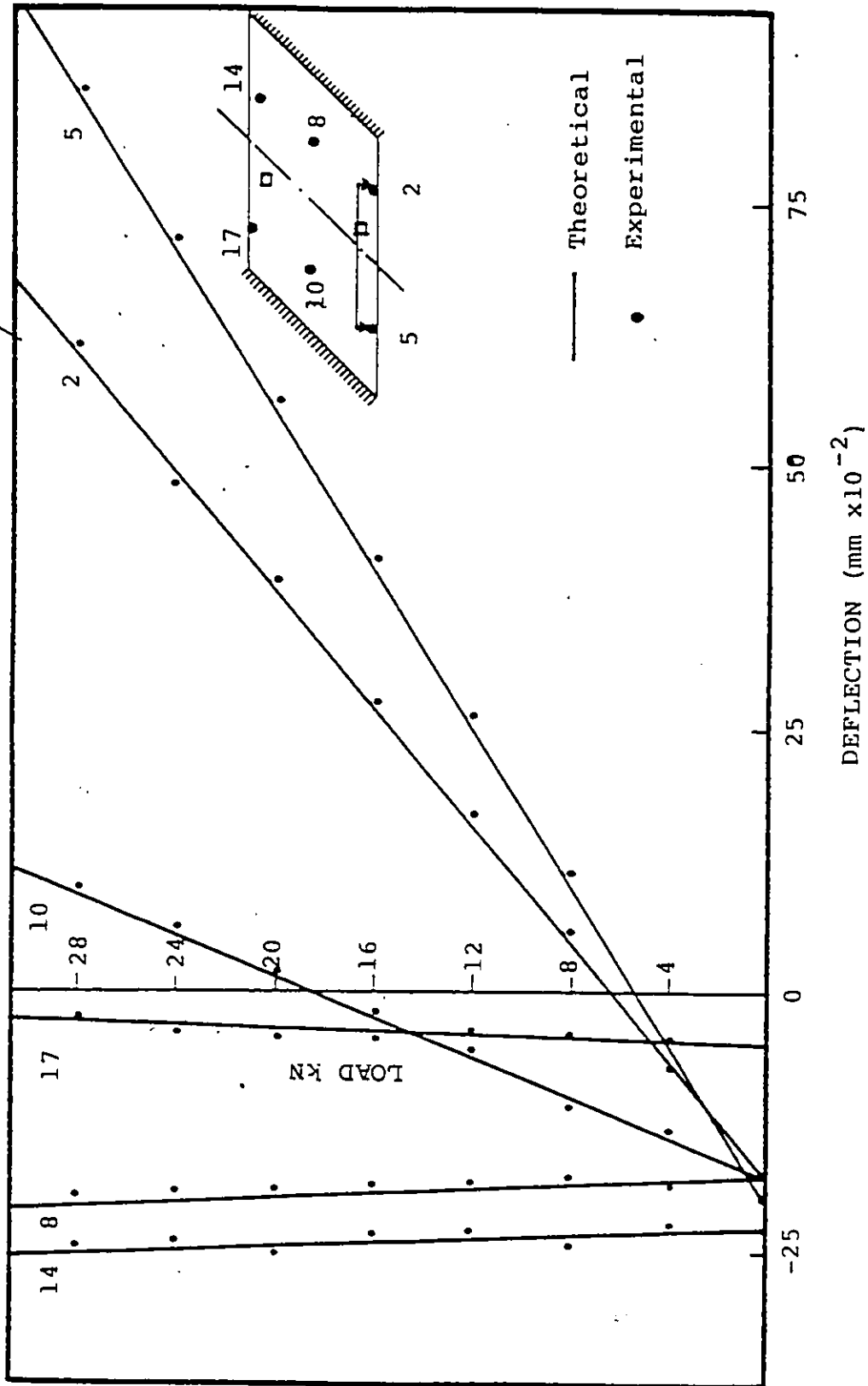


FIGURE 7.46 LOAD DEFLECTION RELATIONSHIP FOR SKEW SLAB DUE TO TWO CONCENTRATED LOADS AT THE CENTER OF THE EDGE BEAM

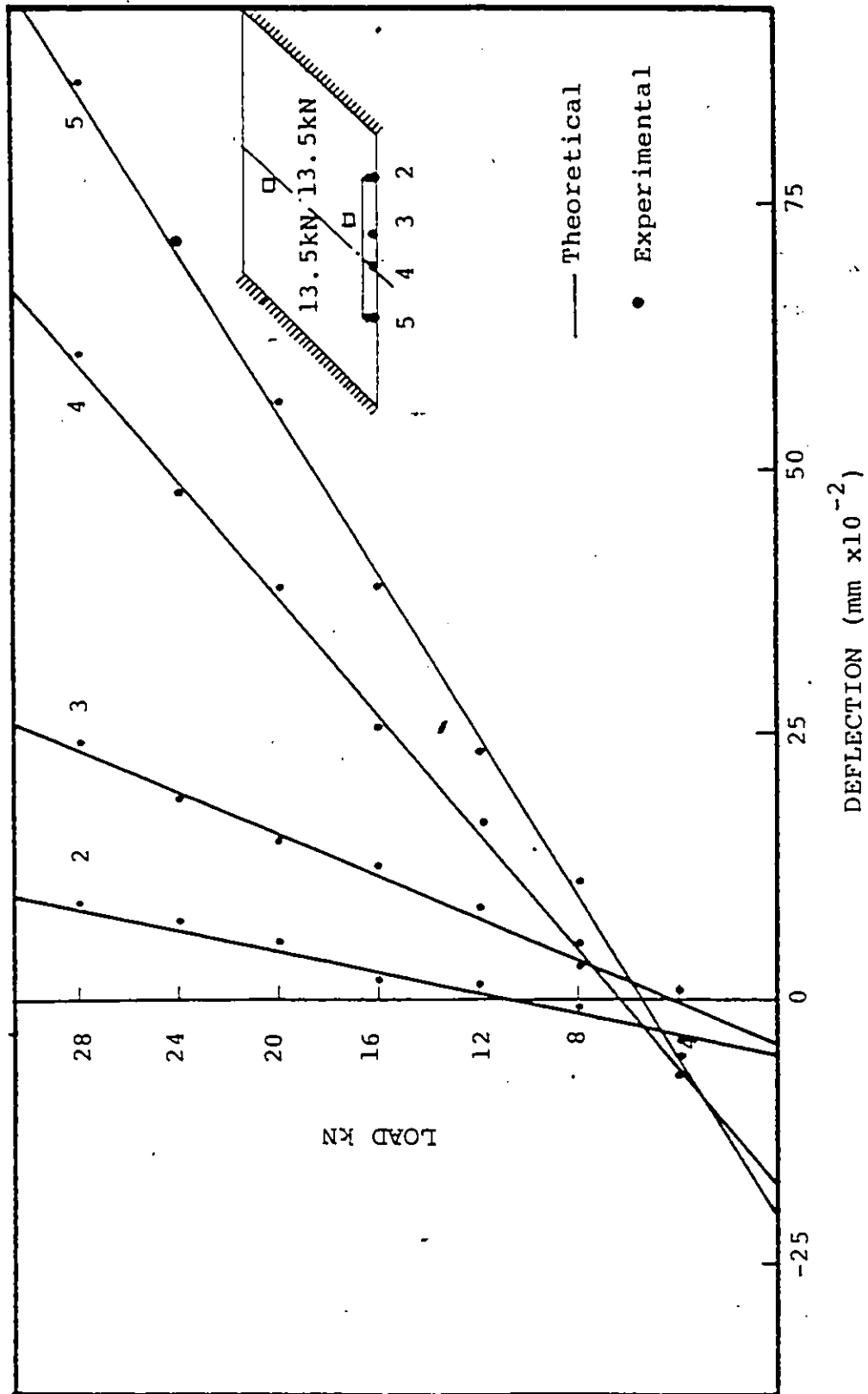


FIGURE 7.47 LOAD DEFLECTION RELATIONSHIP FOR SKEW (PC4) SLAB DUE TO TWO CONCENTRATED LOADS AT THE CENTER OF THE EDGE BEAM

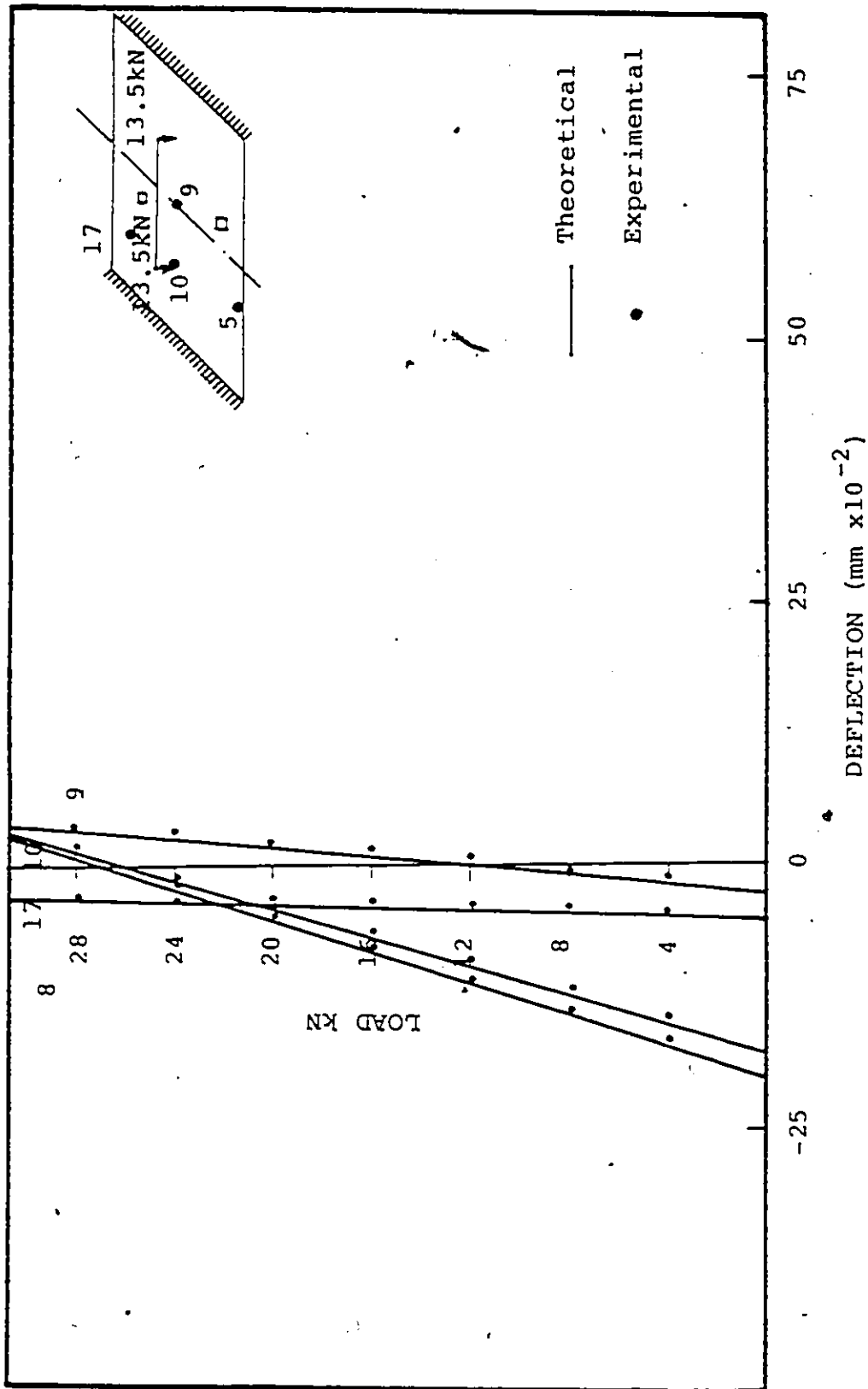


FIGURE 7.48 LOAD-DEFLECTION RELATIONSHIP FOR SKEW SLAB (PC4) DUE TO TWO CONCENTRATED LOADS AT THE CENTER OF EACH SPAN

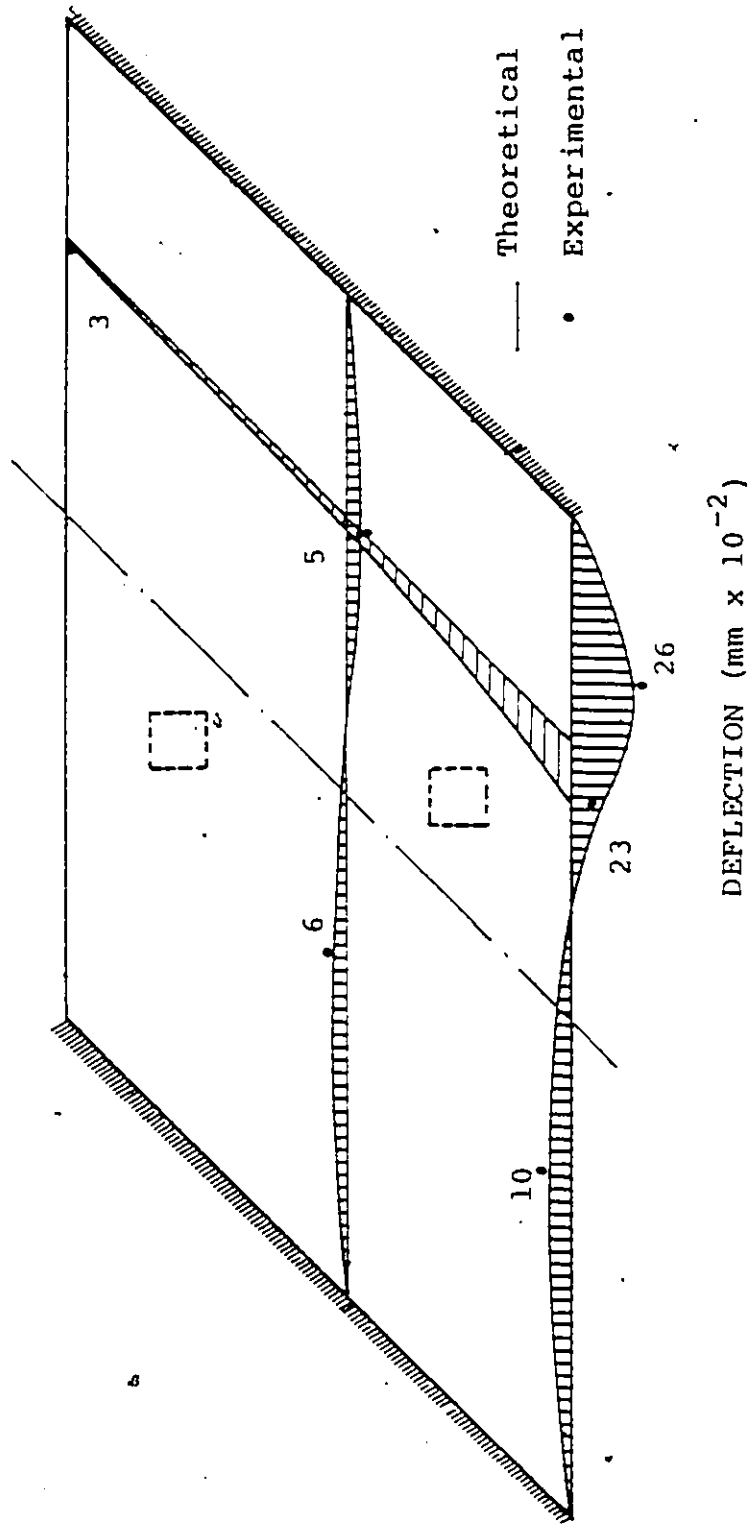


FIGURE 7.49 DEFLECTION DISTRIBUTION FOR SKEW SLAB (PC4) DUE TO A CONCENTRATED LOAD (18 kN) AT THE CENTER OF THE EDGE BEAM

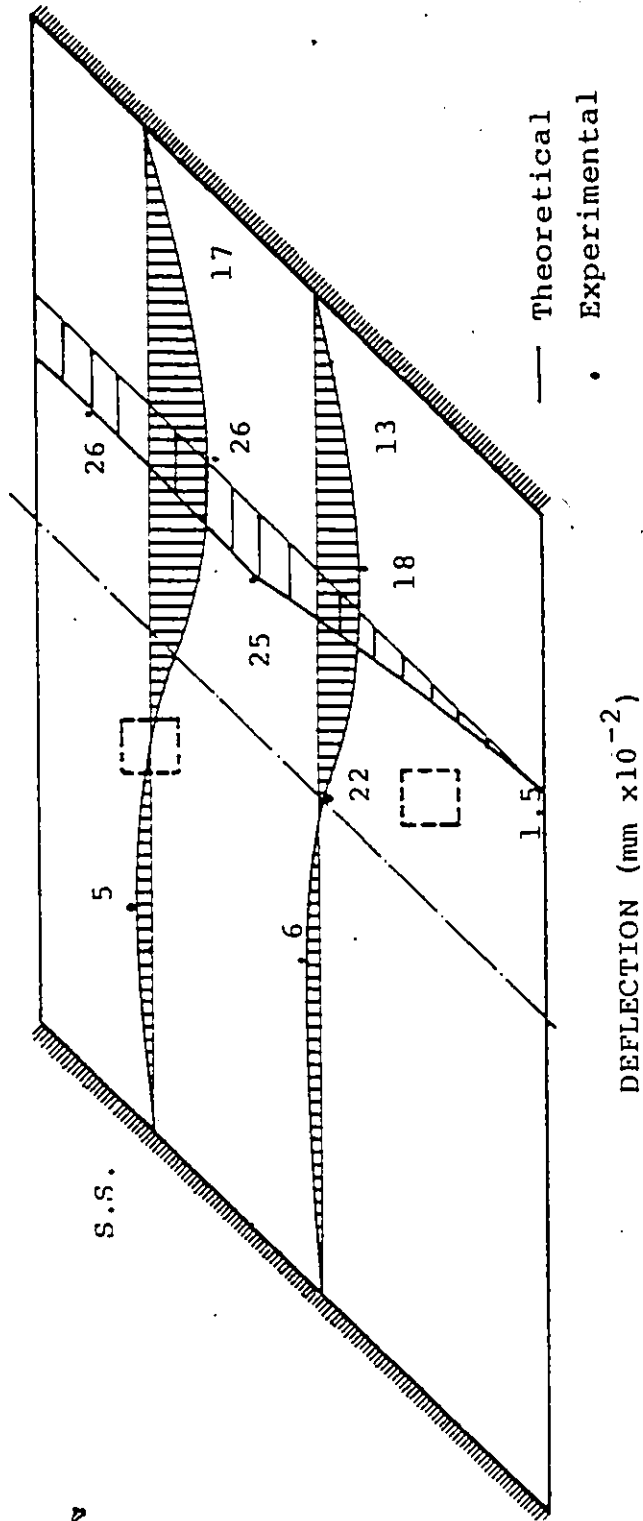


FIGURE 7.50 DEFLECTION DISTRIBUTION FOR SKEW SLAB DUE TO A CONCENTRATED LOAD (18 kN) AT THE CENTER OF THE EDGE BEAM.

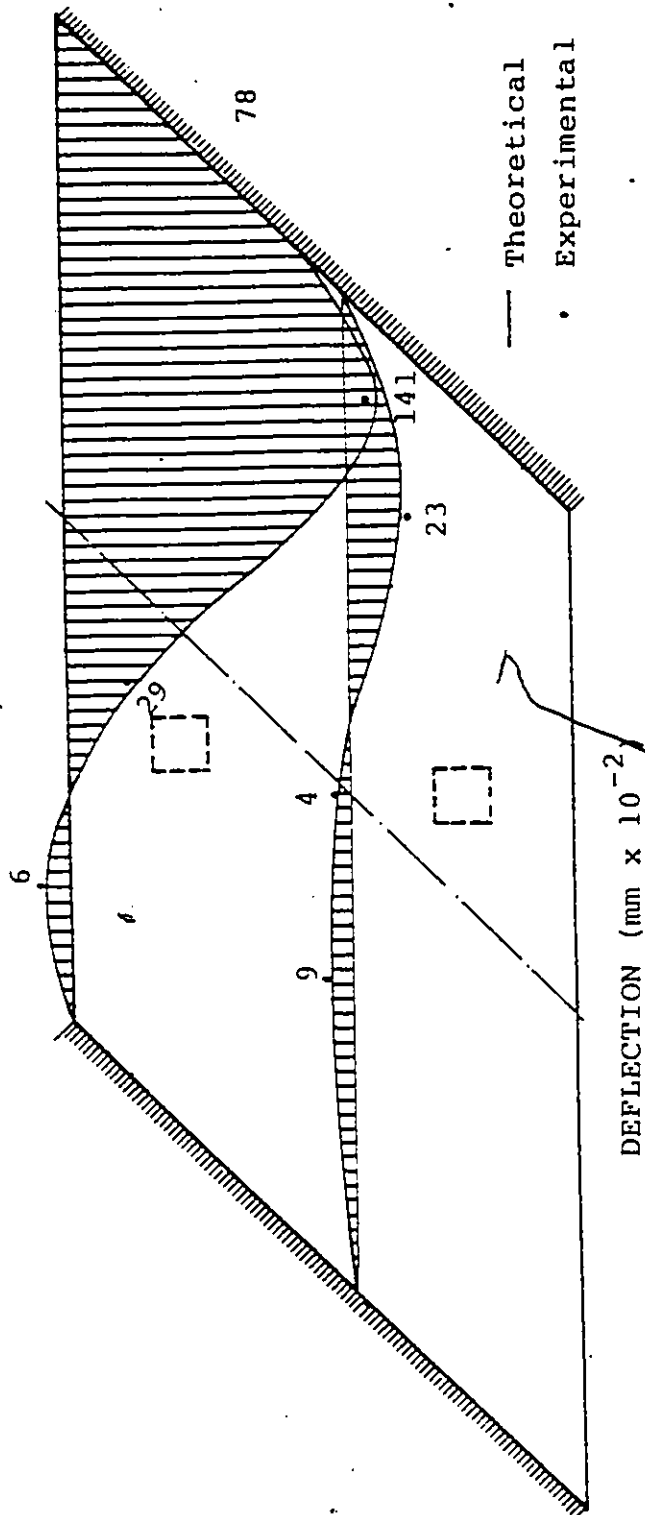


FIGURE 7.51 DEFLECTION-DISTRIBUTION FOR SKEW SLAB DUE TO A CONCENTRATED LOAD (18kN) AT THE CENTER OF THE EDGE BEAM

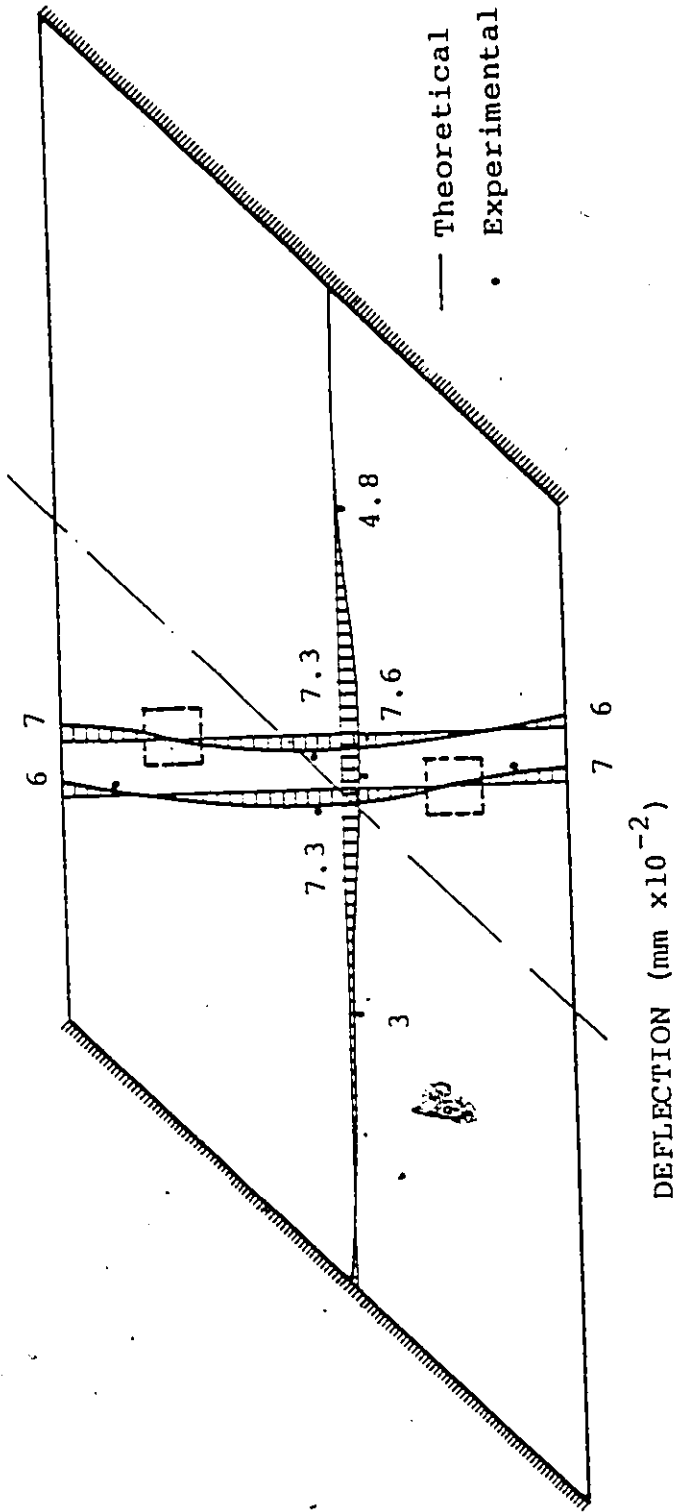


FIGURE 7.52 DEFLECTION DISTRIBUTION FOR SKEW SLAB DUE TO A CONCENTRATED LOAD (18 kN) AT THE CENTER OF THE SLAB

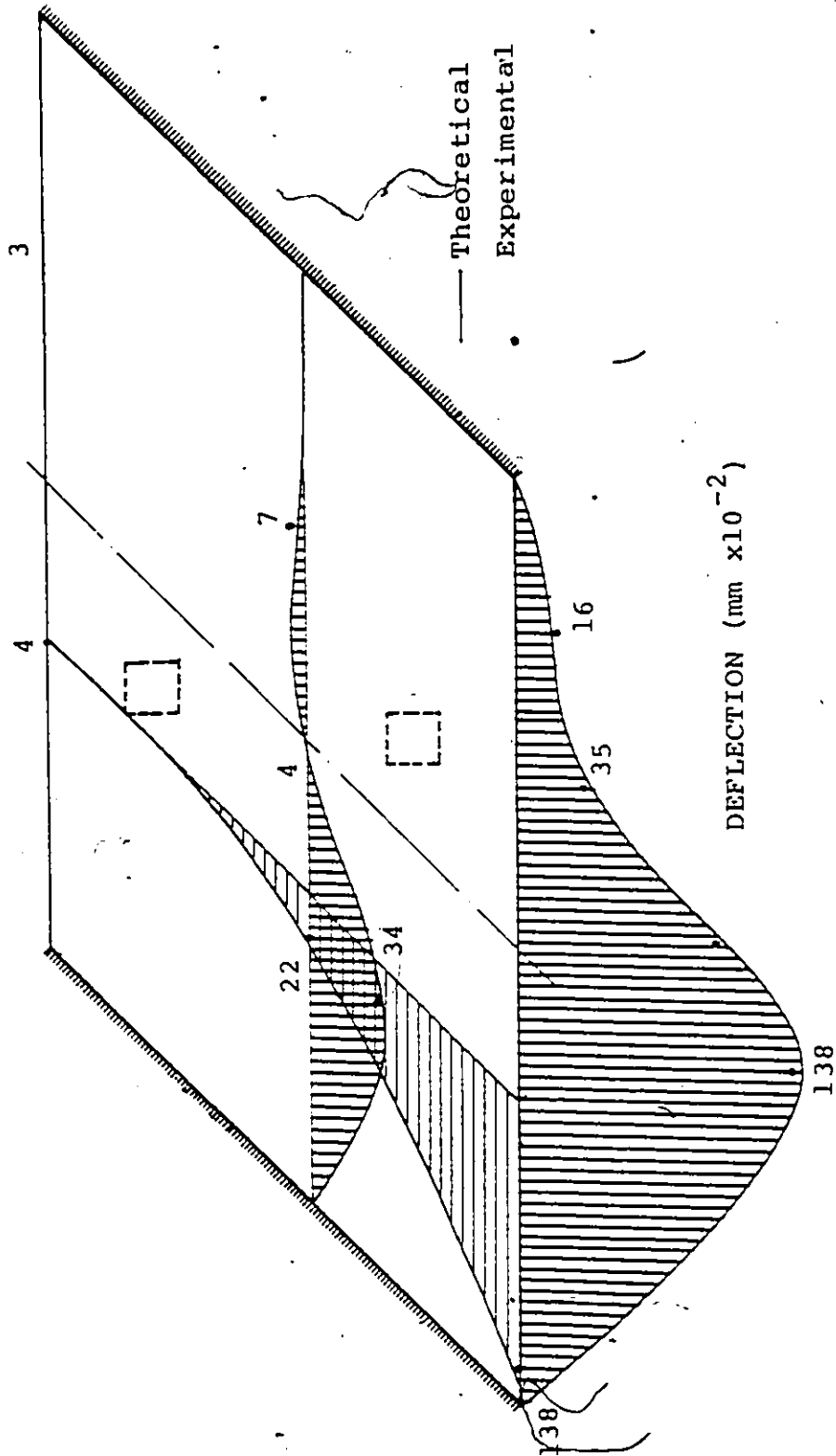


FIGURE 7.53 DEFLECTION DISTRIBUTION FOR SKEW SLAB (PC4) DUE TO TWO CONCENTRATED LOADS (36 kN) EACH AT CENTER OF THE EDGE BEAM

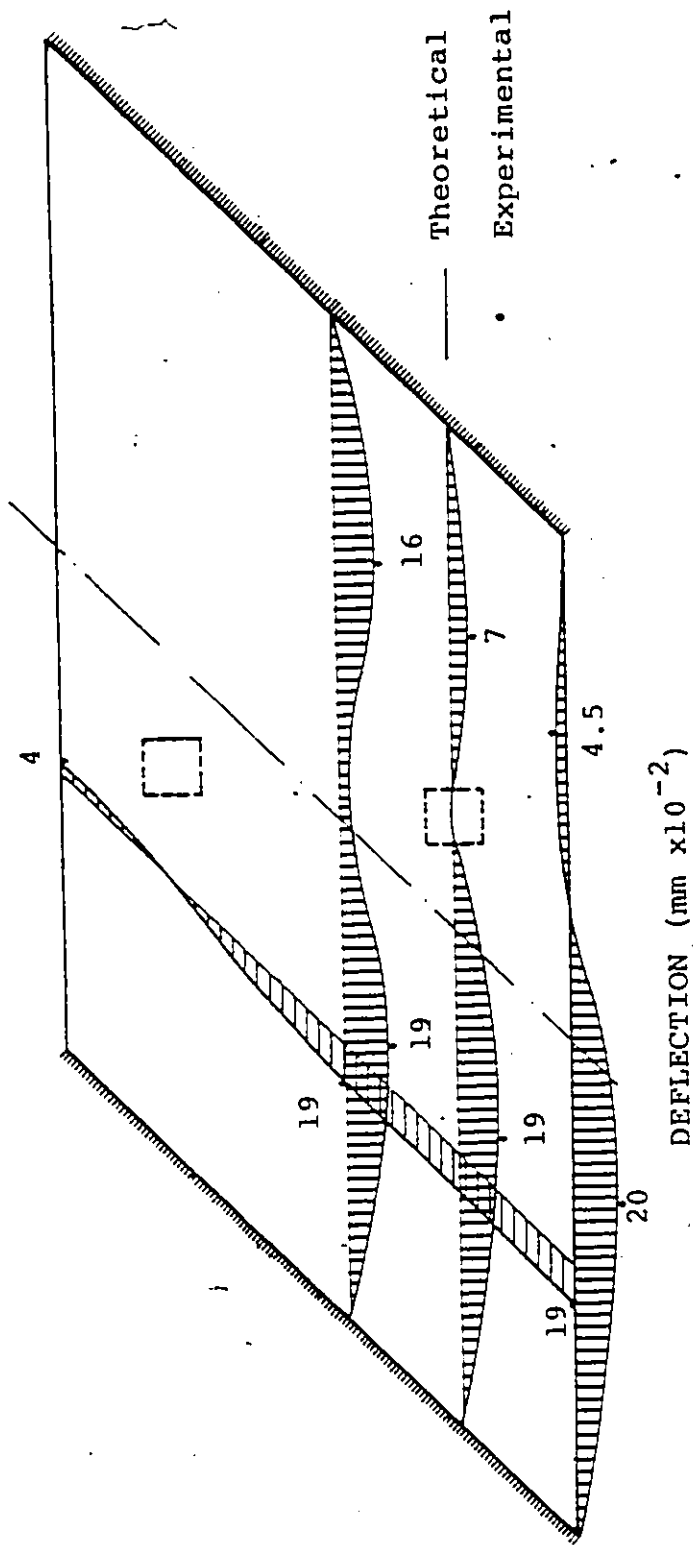


FIGURE 7.54 DEFLECTION DISTRIBUTION FOR SKEW SLAB DUE TO TWO CONCENTRATED LOADS
(36 kN) EACH AT THE CENTER OF EACH SPAN

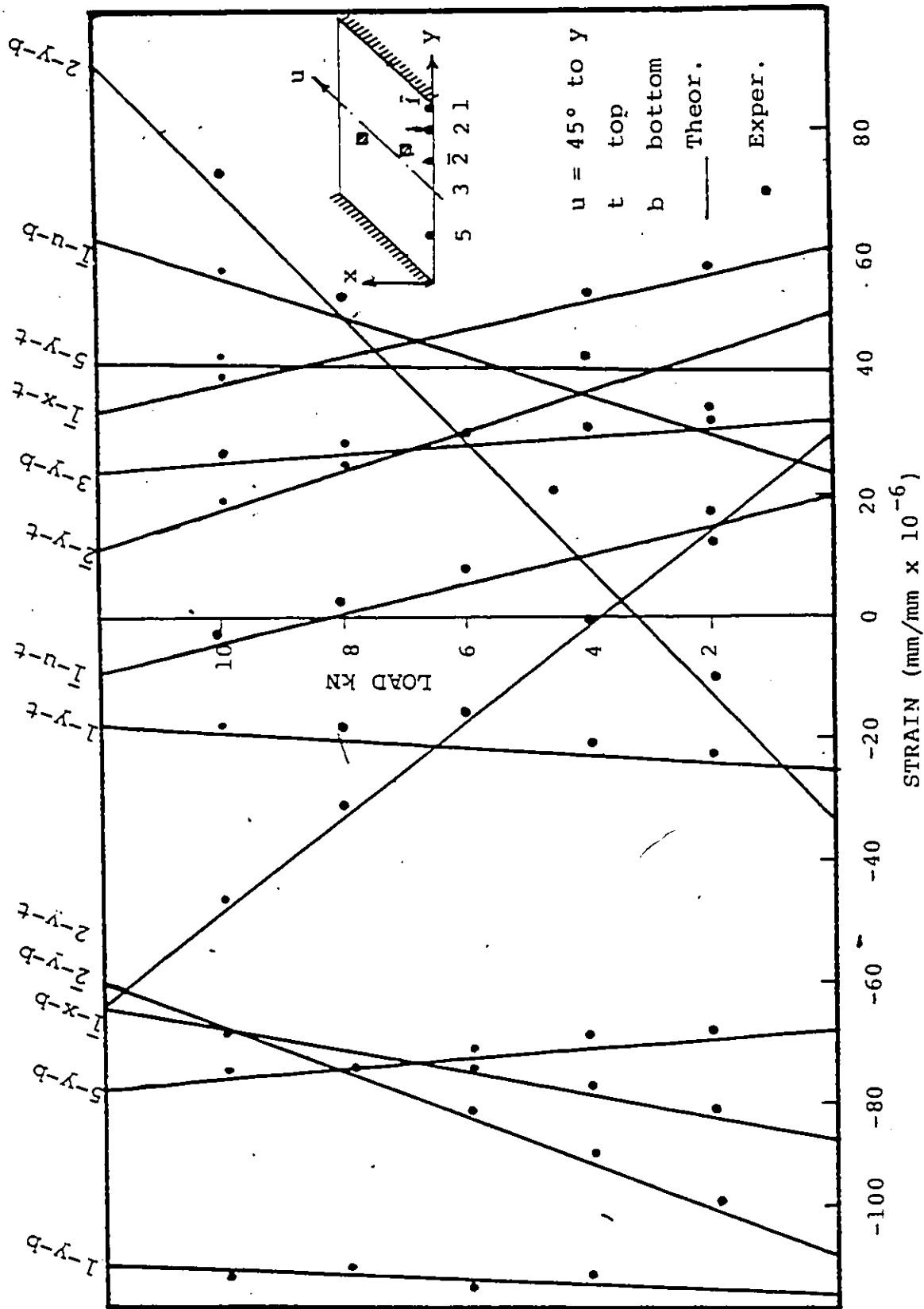


FIGURE 7.55 LOAD-STRAIN RELATIONSHIP FOR SKEW SLAB DUE TO A CONCENTRATED LOAD AT POINT 2

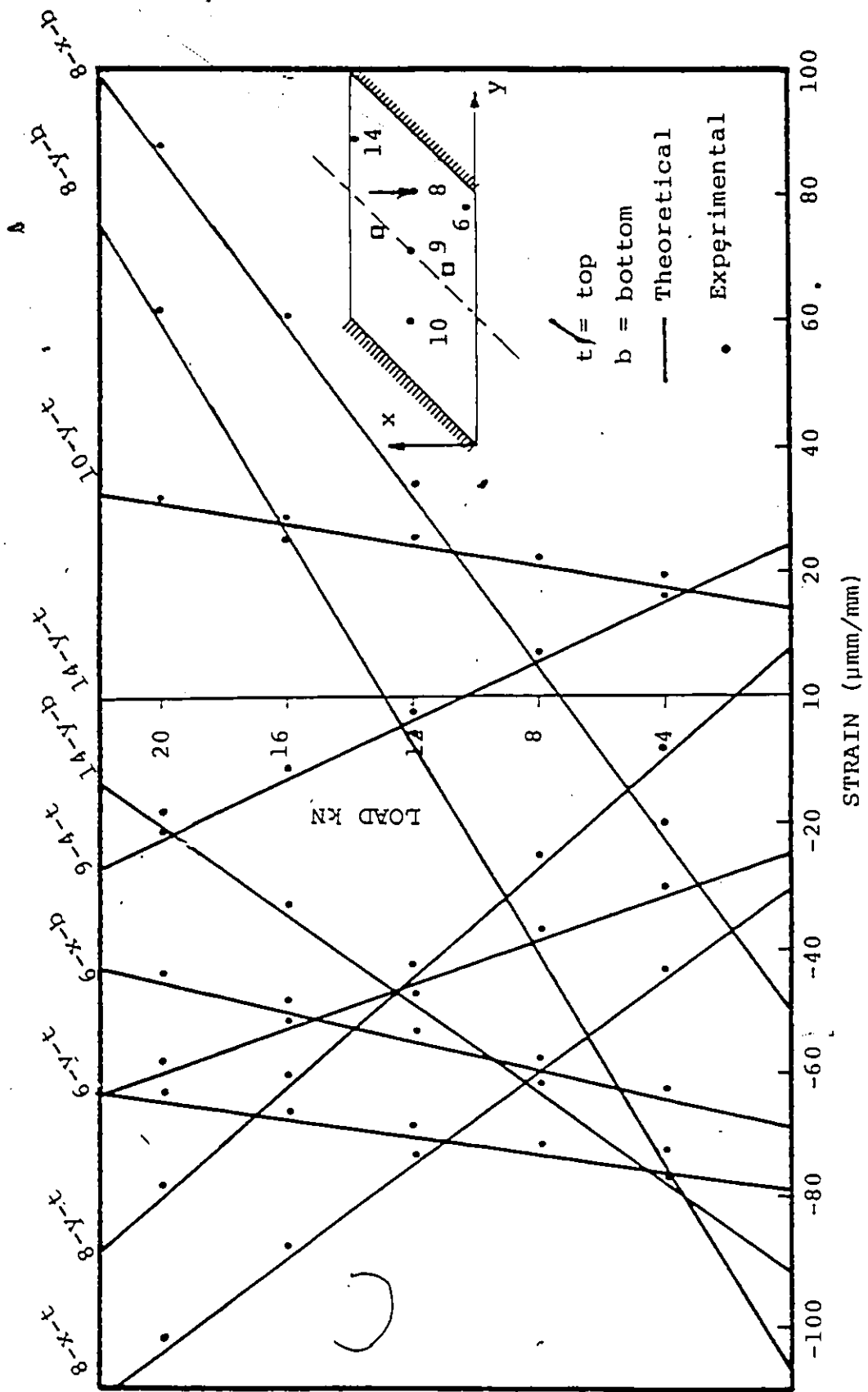


FIGURE 7.56 LOAD-STRAIN RELATIONSHIP FOR SKEW SLAB DUE TO CONCENTRATED LOAD AT CENTRE OF THE SPAN

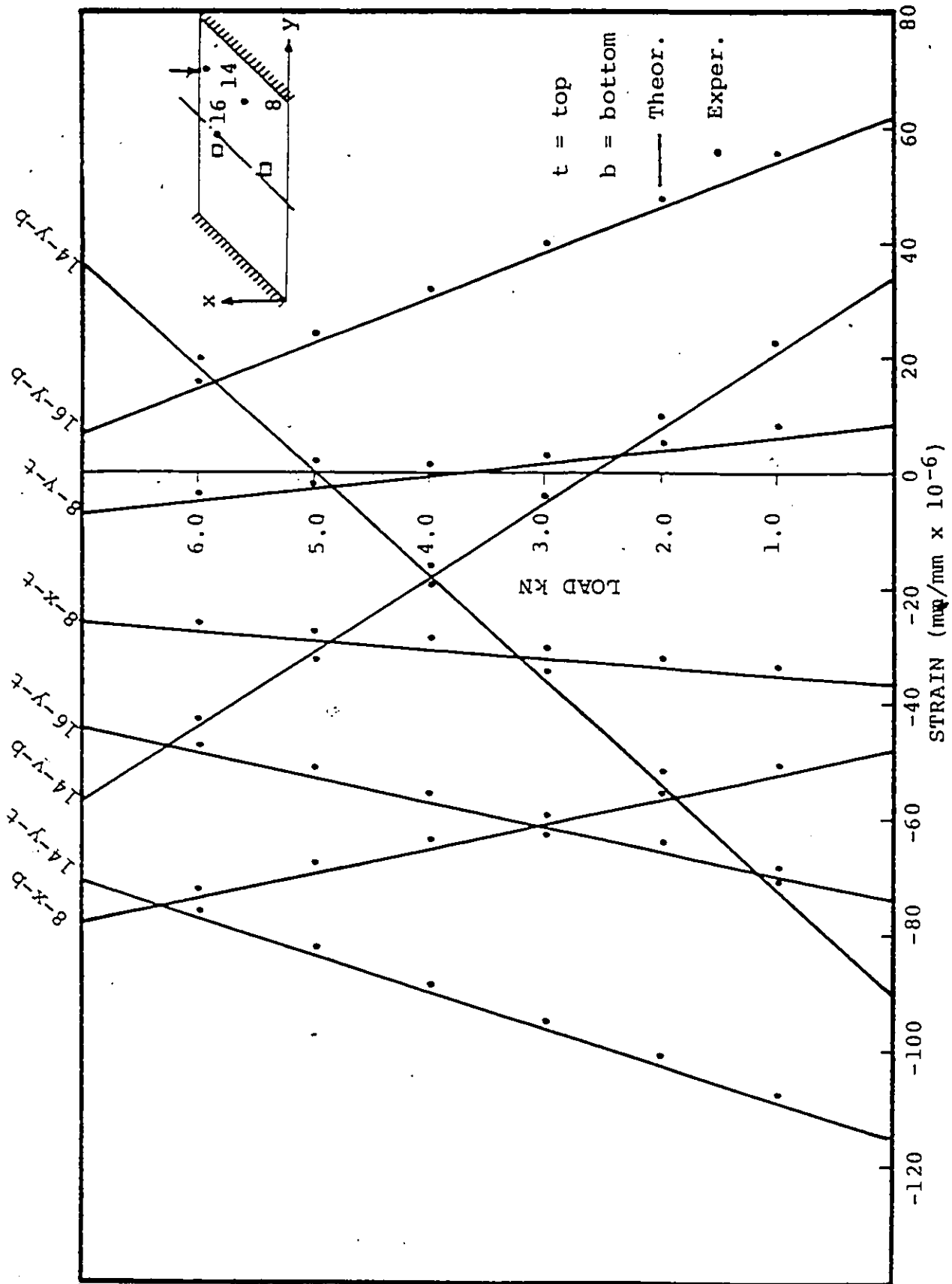


FIGURE 7.57 LOAD-STRAIN RELATIONSHIP FOR SKEW SLAB DUE TO A CONCENTRATED LOAD AT THE CENTER OF THE EDGE BEAM

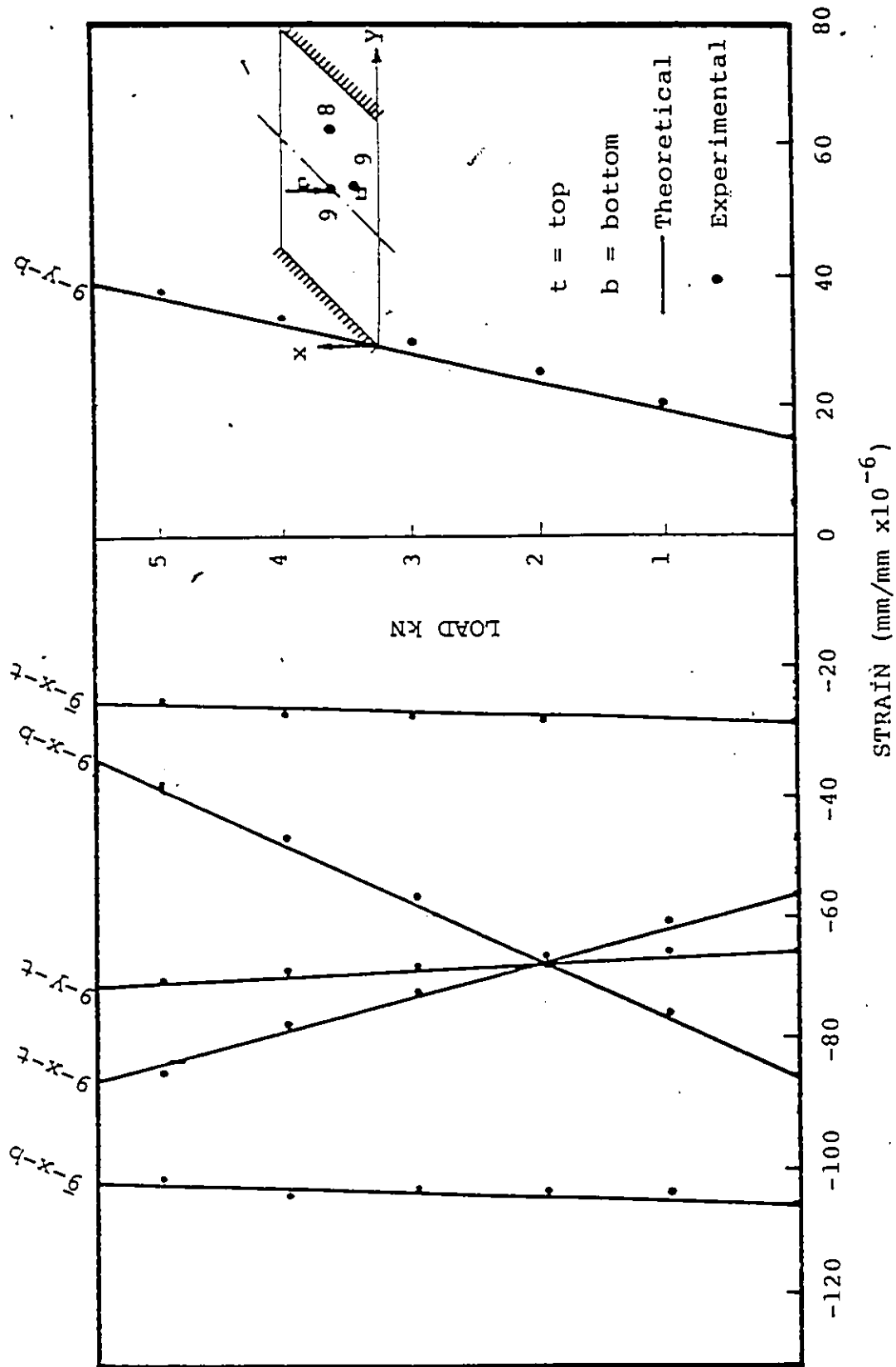


FIGURE 7.58 LOAD STRAIN RELATIONSHIP FOR SKEW SLAB (PC4) DUE TO A CONCENTRATED LOAD AT THE CENTER OF THE SLAB

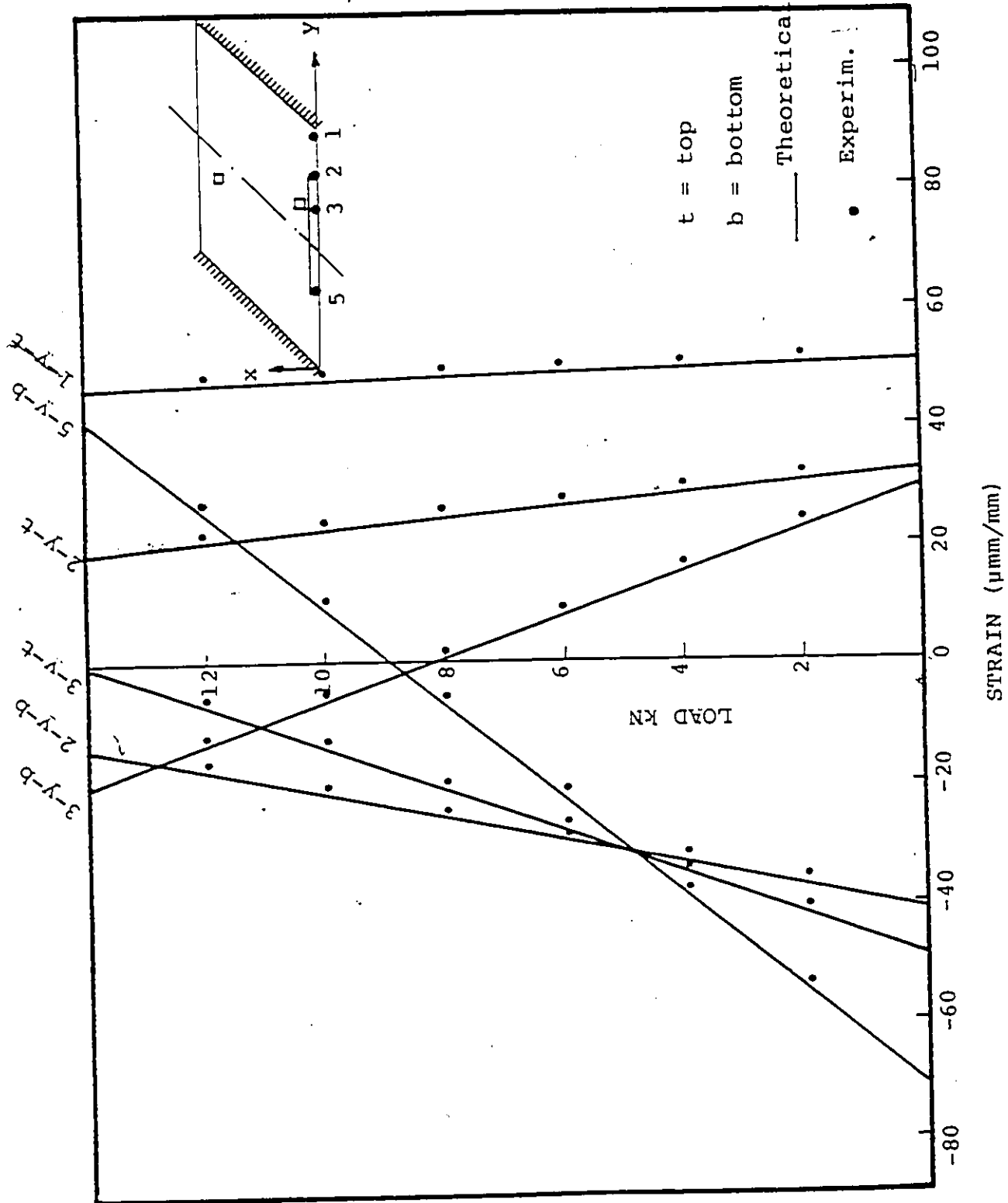


FIGURE 7.59 LOAD STRAIN RELATIONSHIP FOR SKEW SLAB (PC4) DUE TO TWO CONCENTRATED LOADS AT THE CENTER OF THE EDGE BEAM

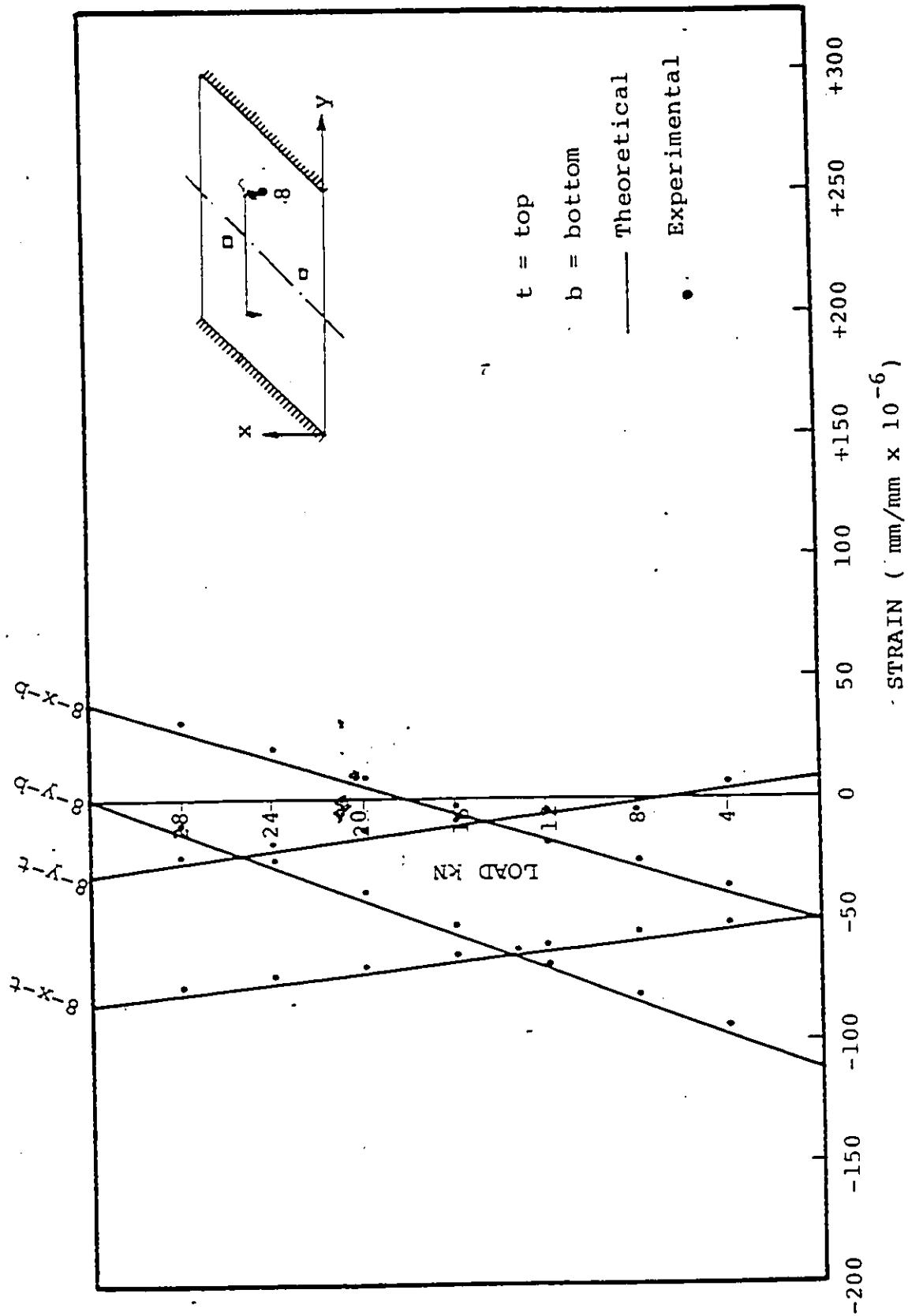


FIGURE 7.60 LOAD-STRAIN RELATIONSHIP FOR SKEW SLAB (PC4) DUE TO TWO CONCENTRATED LOADS EACH AT THE CENTER OF THE SPAN

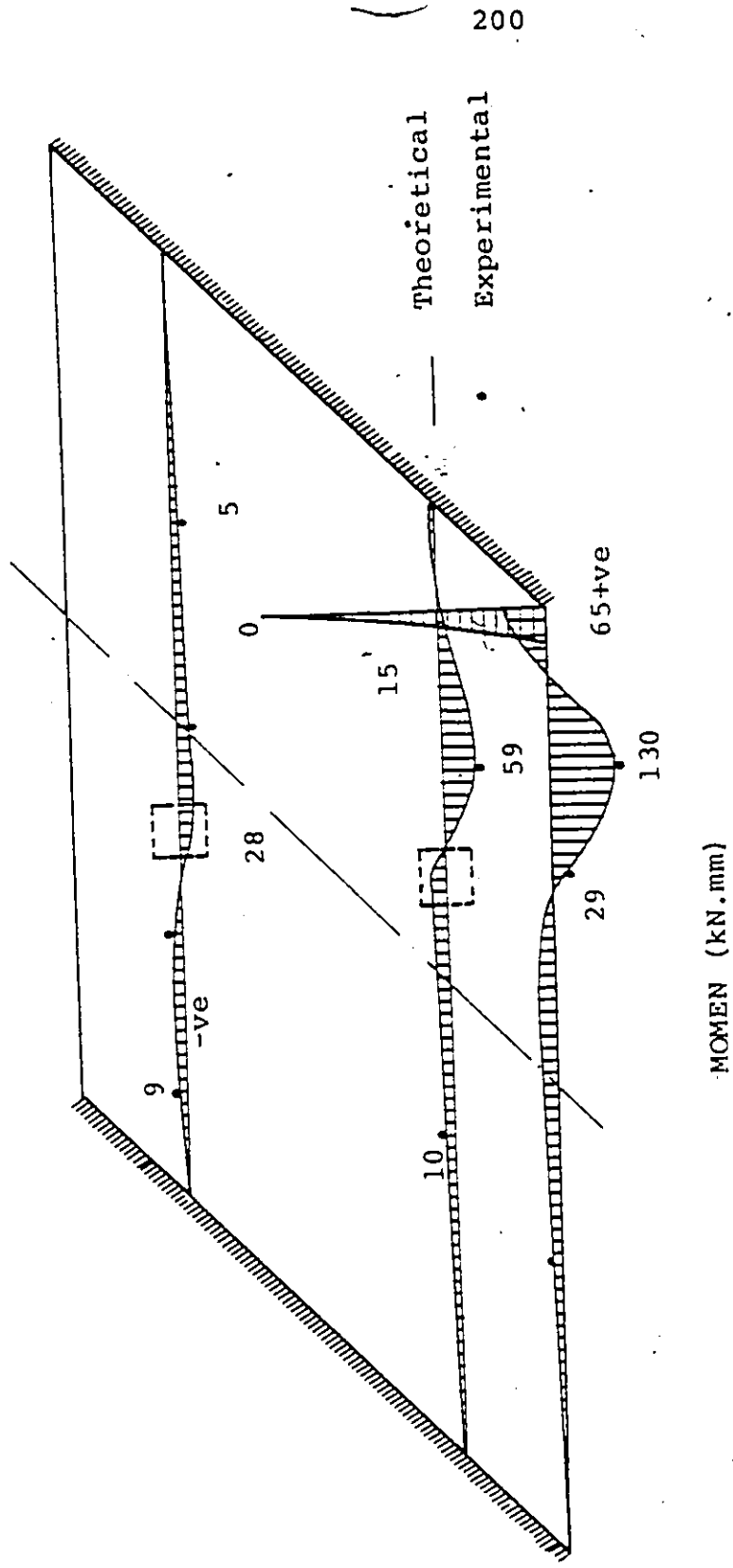


FIGURE 7.61 MOMENT DISTRIBUTION FOR SKEW SLAB DUE TO CONCENTRATED LOAD (18 kN) AT THE CENTER OF THE EDGE BEAM

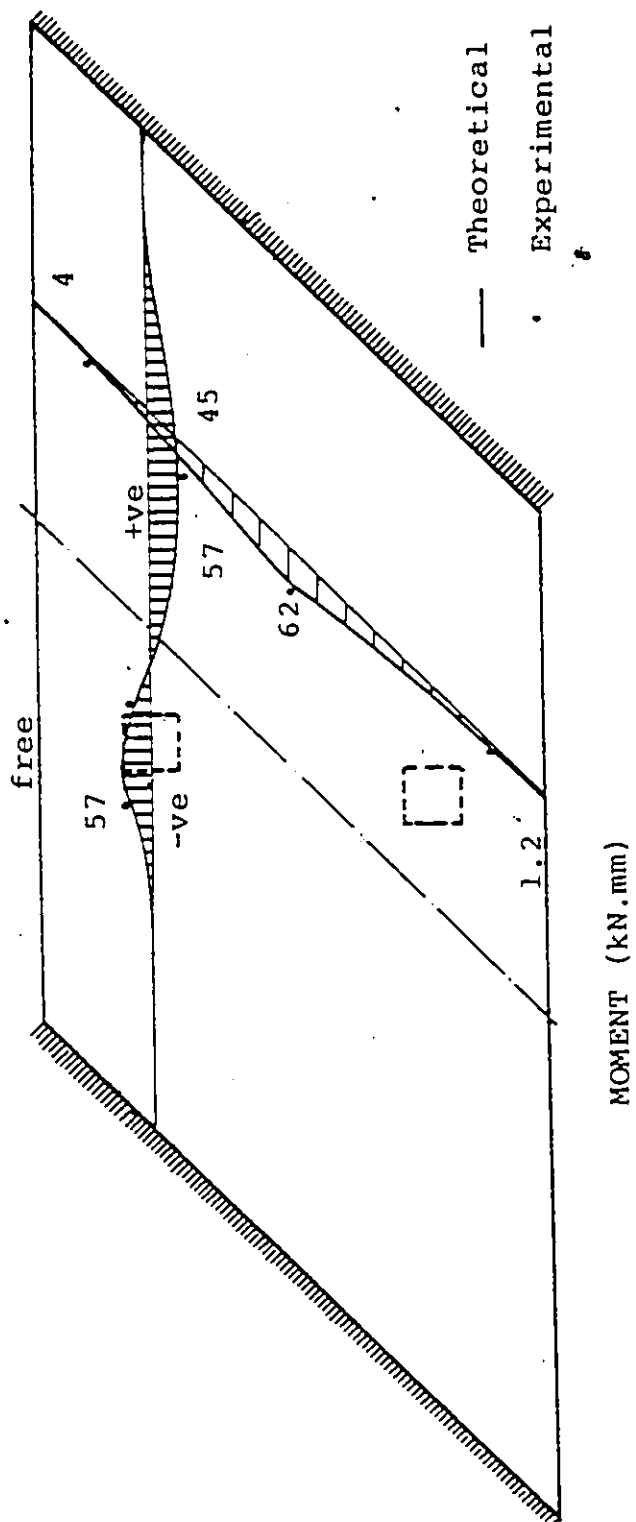


FIGURE 7.62 MOMENT DISTRIBUTION FOR SKEW SLAB (PC4) DUE TO A CONCENTRATED LOA (18 kN) AT THE CENTER OF THE SPAN

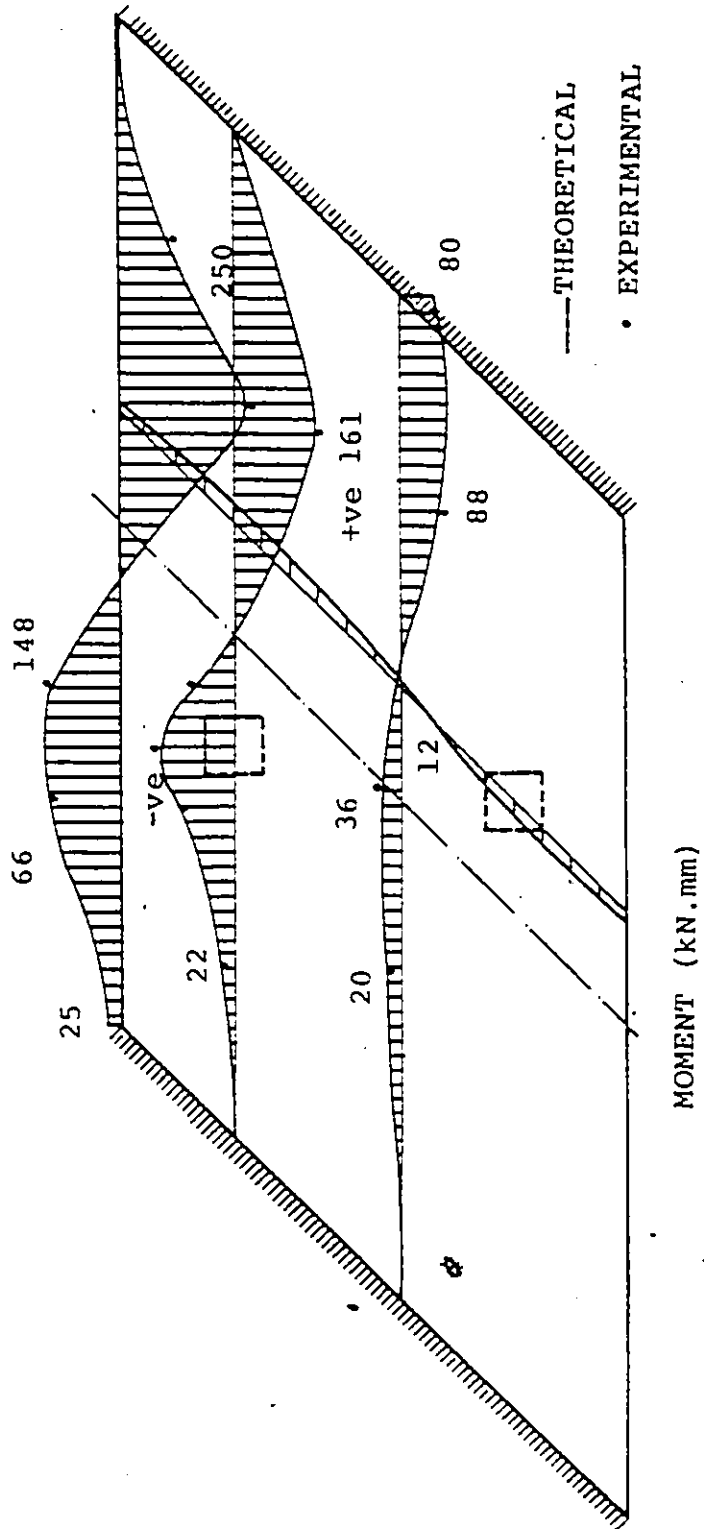


FIGURE 7.63 MOMENT DISTRIBUTION FOR SKEW SLAB (PC4) DUE TO LOAD (18 kN) AT THE CENTER OF THE EDGE BEAM

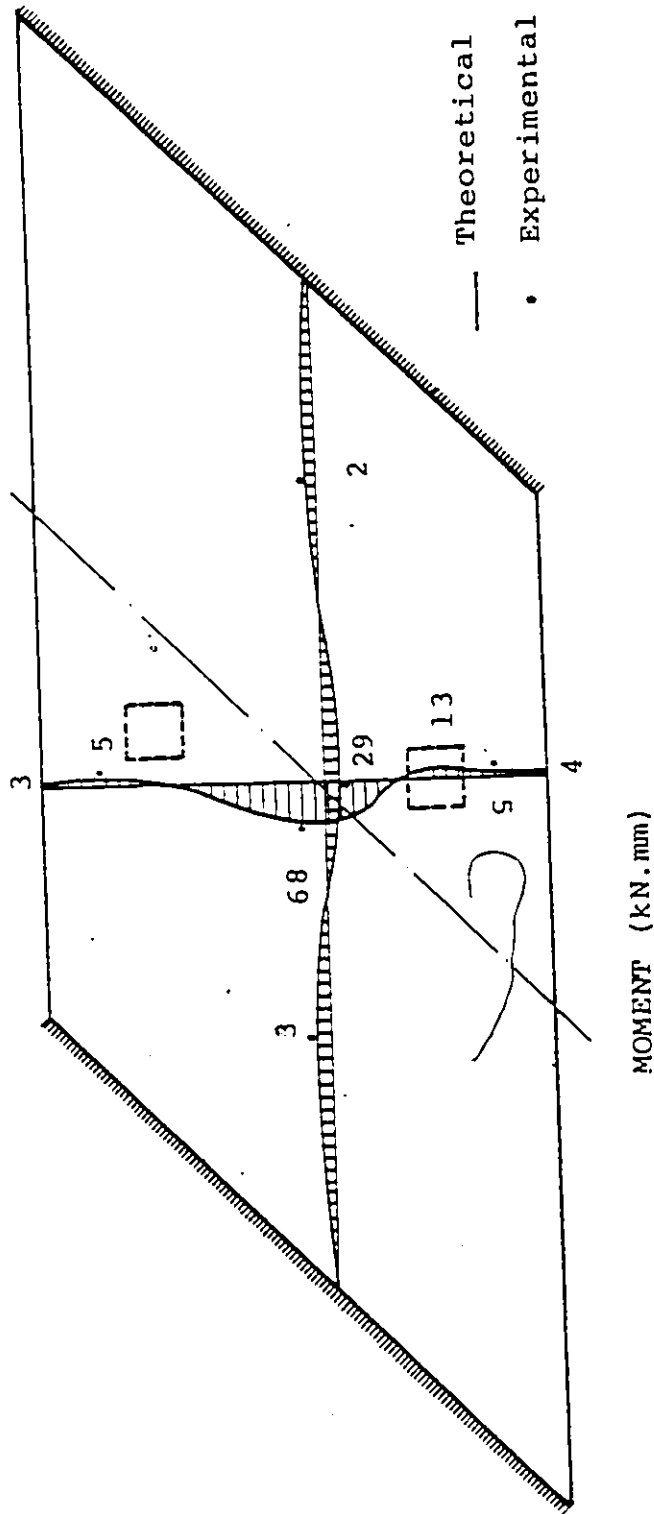


FIGURE 7.64 MOMENT DISTRIBUTION FOR SKEW SLAB (PC4) DUE TO A CONCENTRATED LOAD (18 kN) AT THE CENTER OF THE SLAB

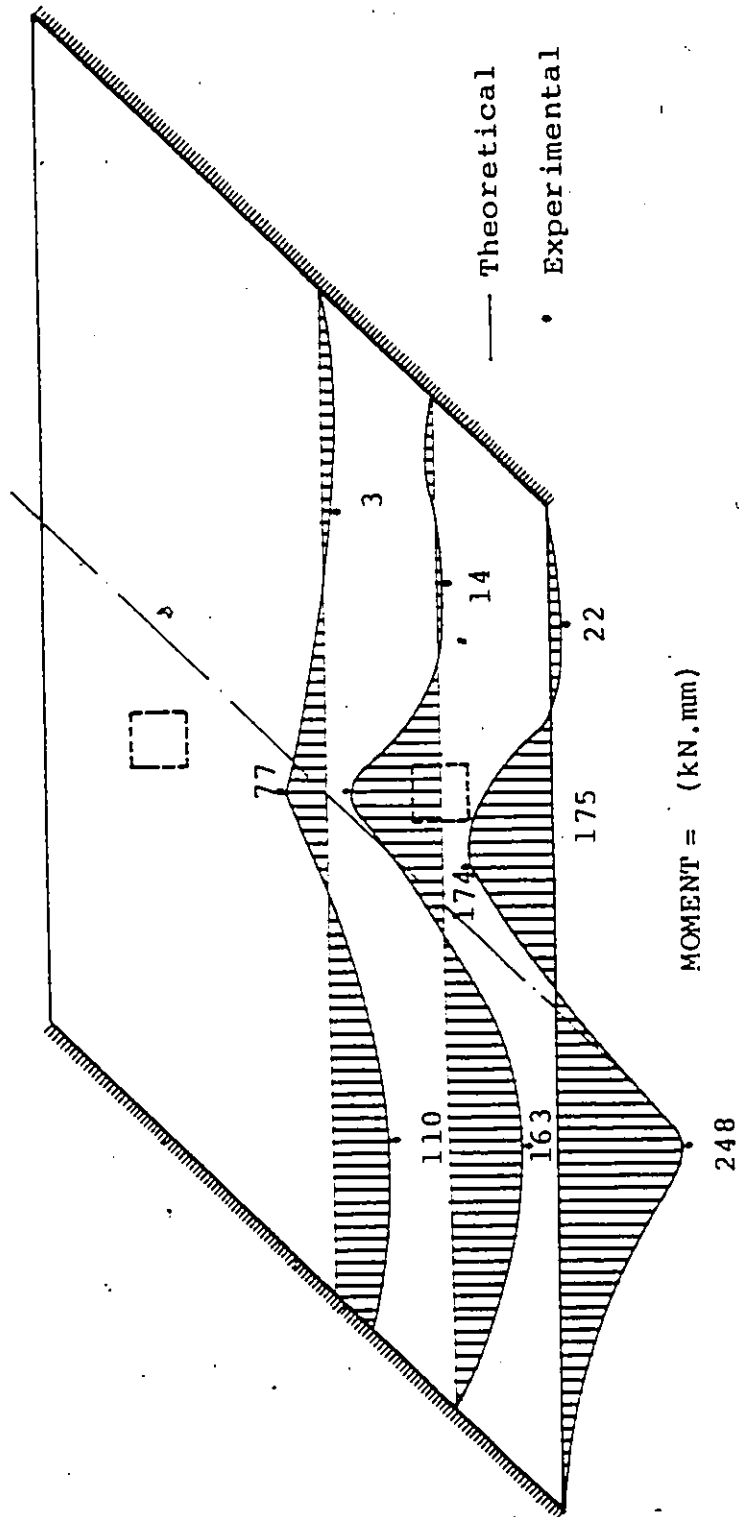


FIGURE 7:65 MOMENT DISTRIBUTION FOR SKEW SLAB DUE TO TWO CONCENTRATED LOADS (36 kN) EACH AT THE CENTER OF THE EDGE BEAM

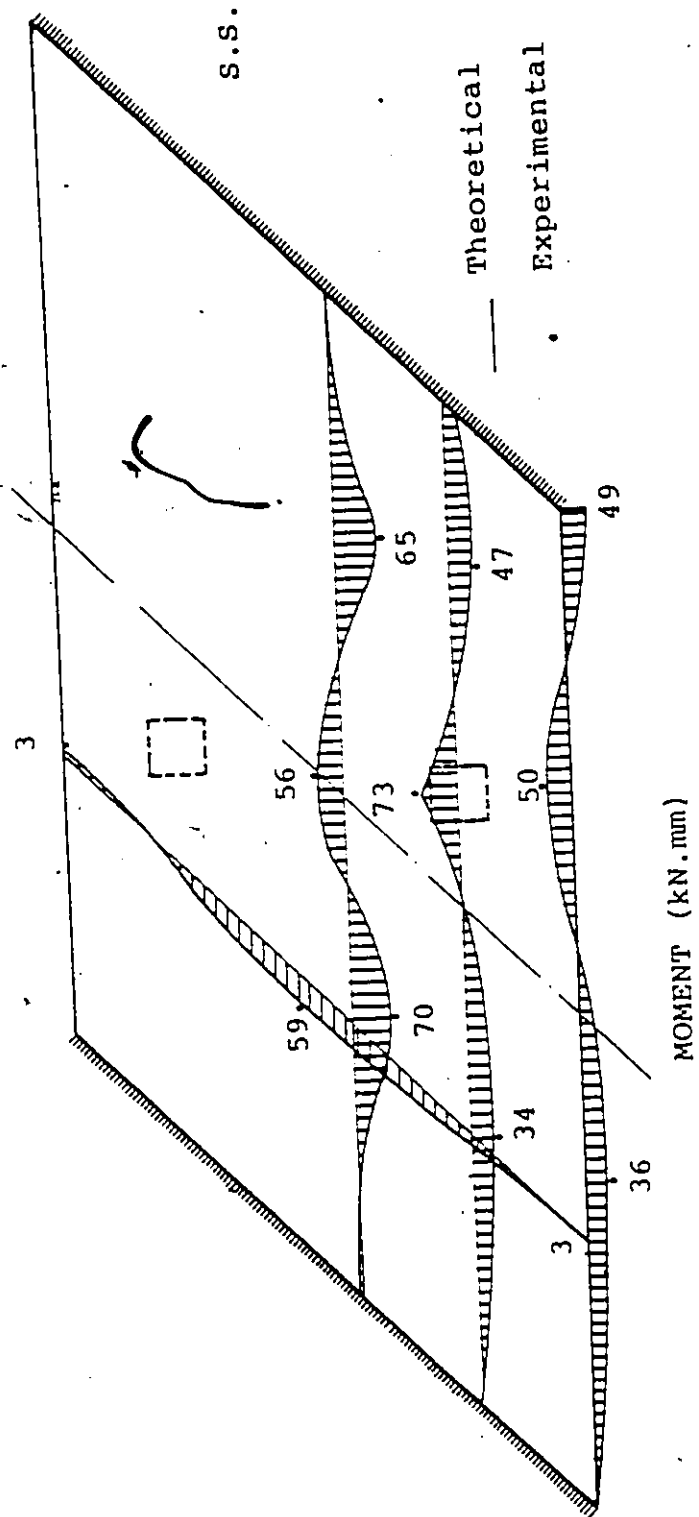


FIGURE 7.66 MOMENT DISTRIBUTION FOR SKEW SLAB (PC4) DUE TO TWO CONCENTRATED LOADS (36 kN) EACH AT THE CENTER OF EACH SPAN

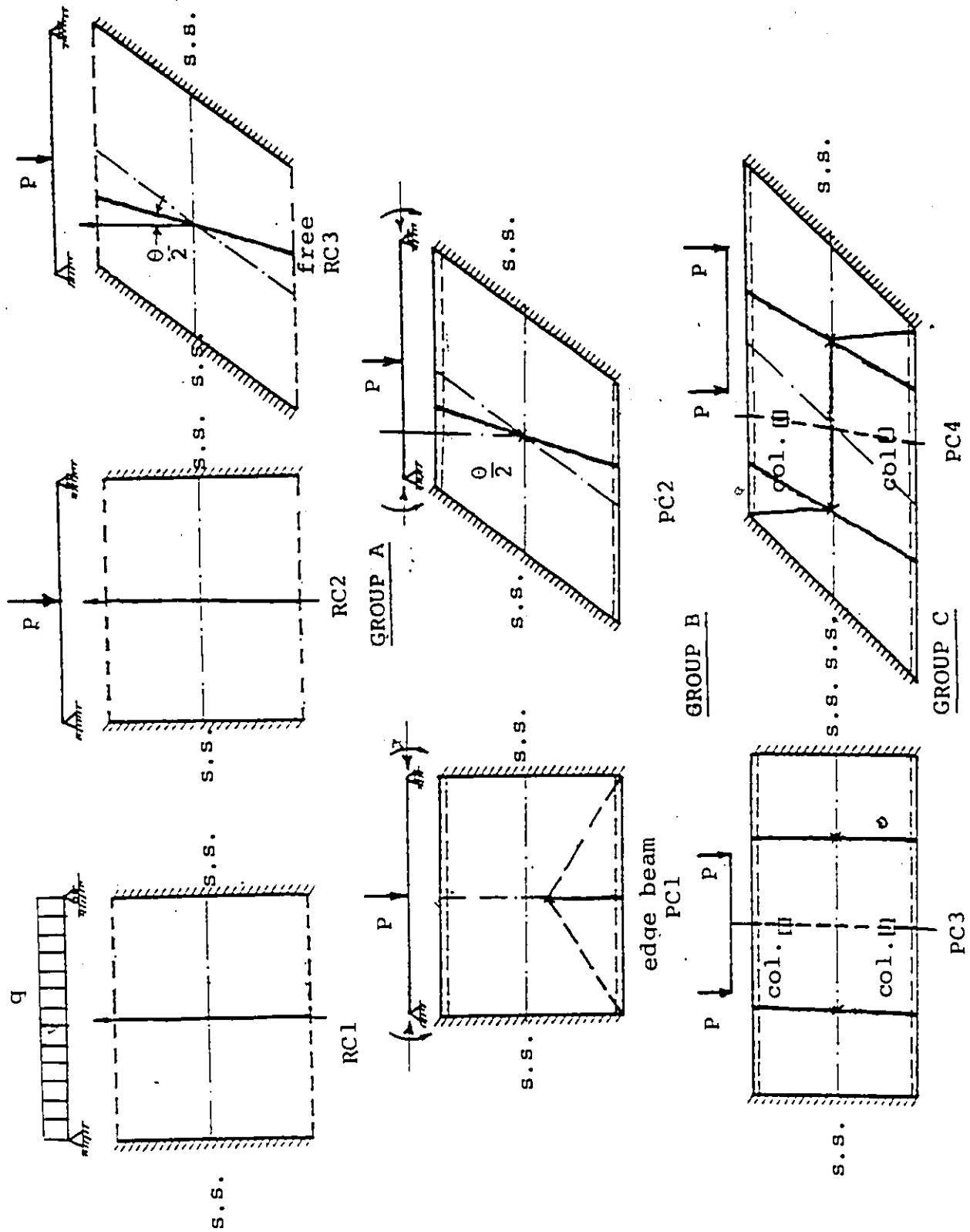


FIGURE 7.67 YIELD LINES IN THE TESTED SLAB MODELS.

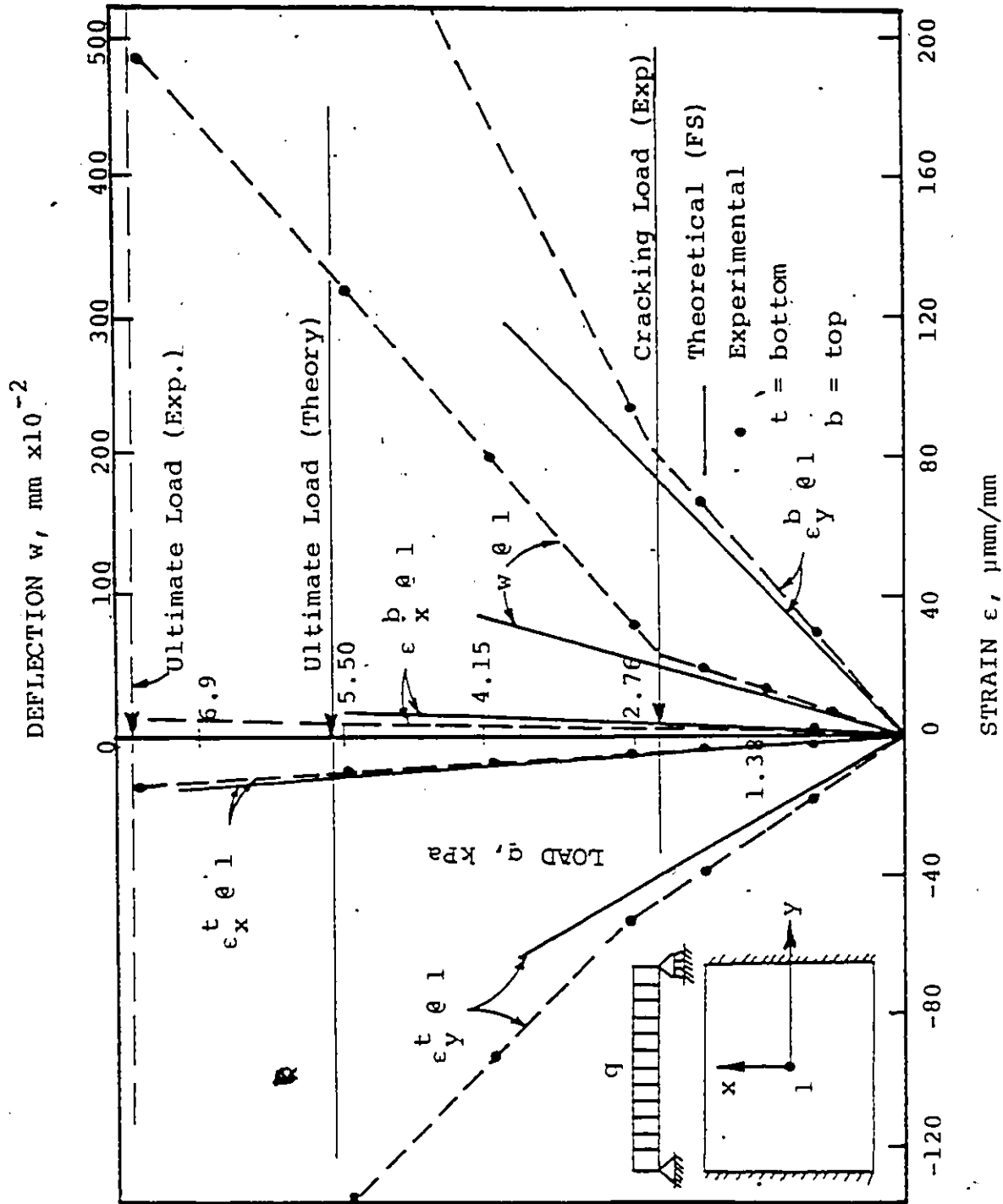


FIGURE 7.68 LOAD VERSUS DEFLECTION AND STRAIN FOR RECTANGULAR SLAB MODEL RC1 UNDER UNIFORMLY DISTRIBUTED LOAD



FIGURE 7.69 SINGLE-LINE CRACK PATTERN OF WAFFLE
SLAB MODEL RC1

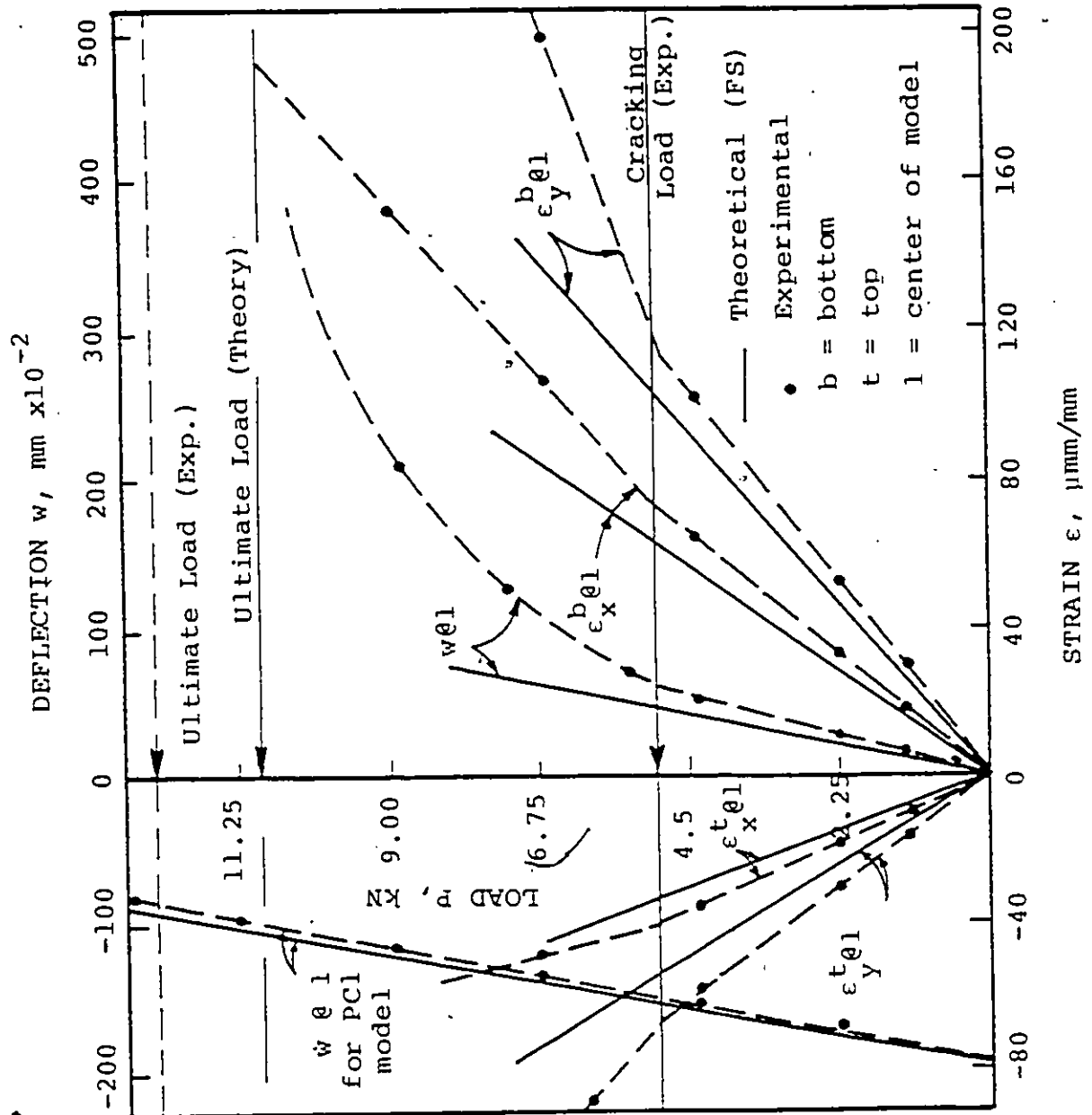


FIGURE 7.70 LOAD VERSUS DEFLECTION AND STRAIN FOR RECTANGULAR REINFORCED (RC2) AND PRESTRESSED MODEL (PC1) UNDER CONCENTRATED LOAD.



FIGURE 7.71 SINGLE-LINE CRACK PATTERN OF WAFFLE
SLAB MODEL RC2

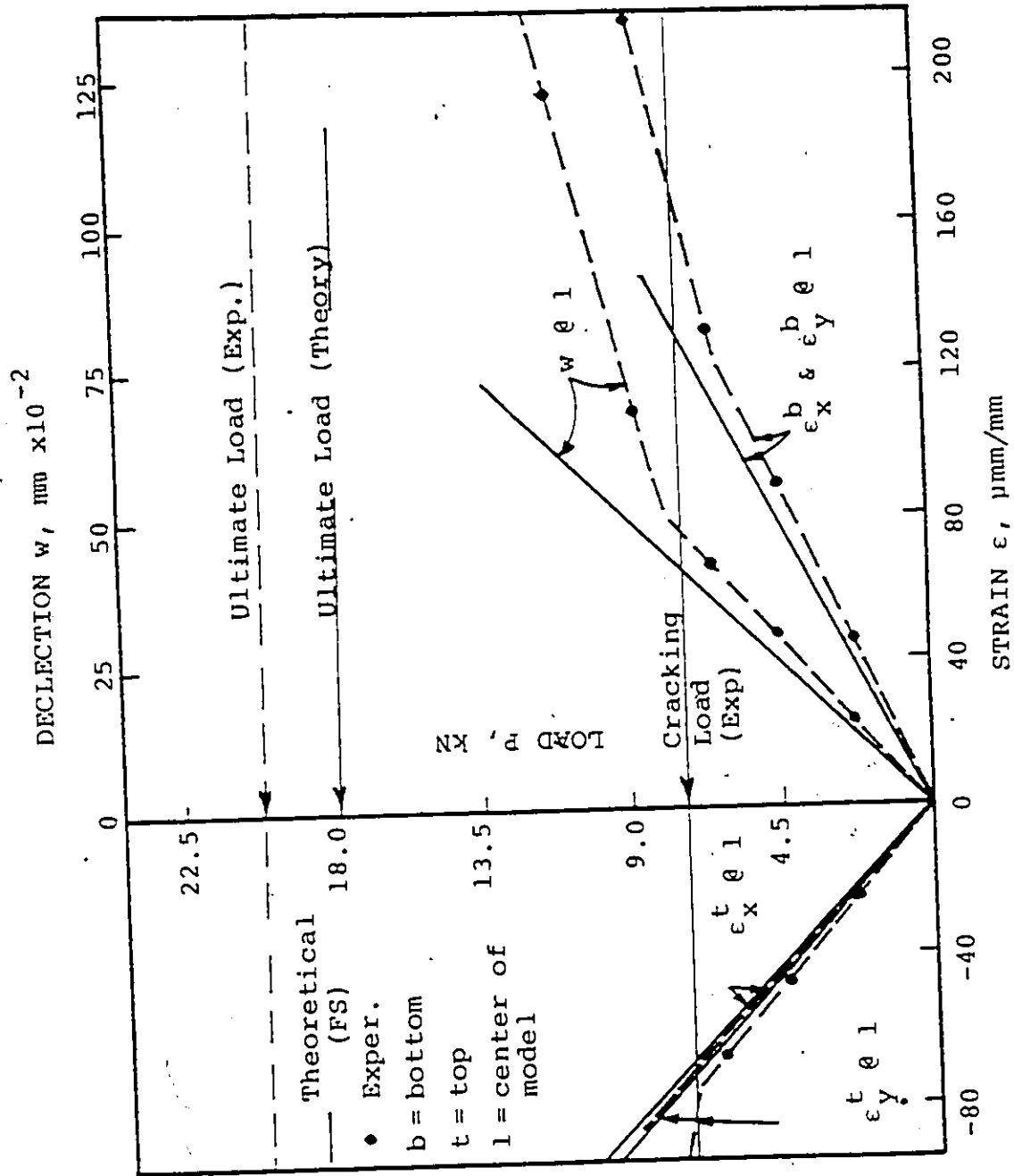


FIGURE 7.72 LOAD VERSUS DEFLECTION AND STRAIN FOR REINFORCED SKEW SLAB (RC3) UNDER A CONCENTRATED LOAD AT CENTER

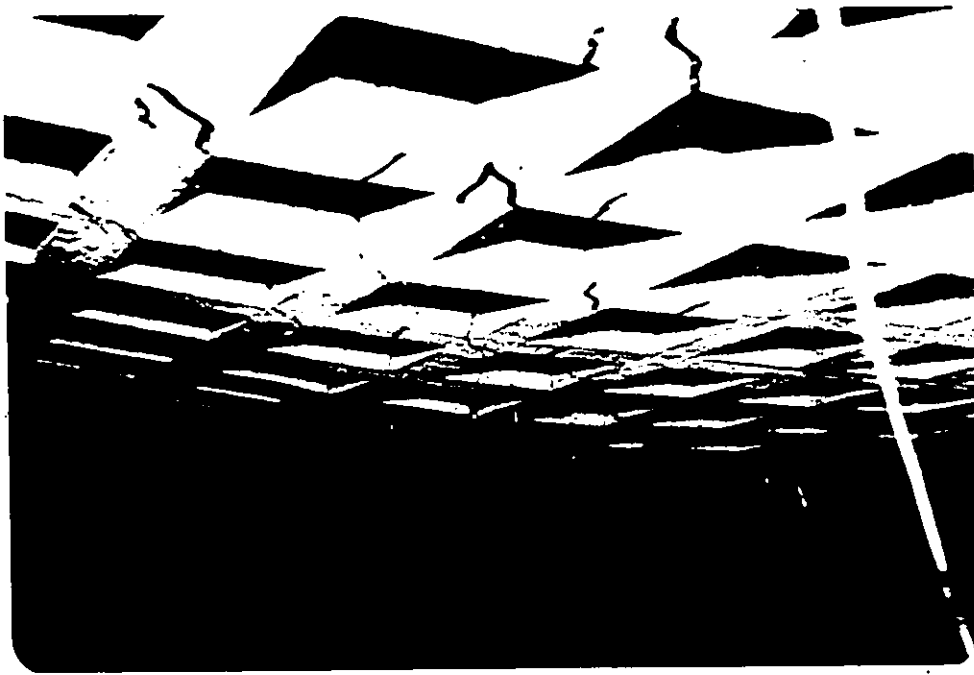


FIGURE 7.73 CRACKS OF SKEW WAFFLE SLAB MODEL RC3

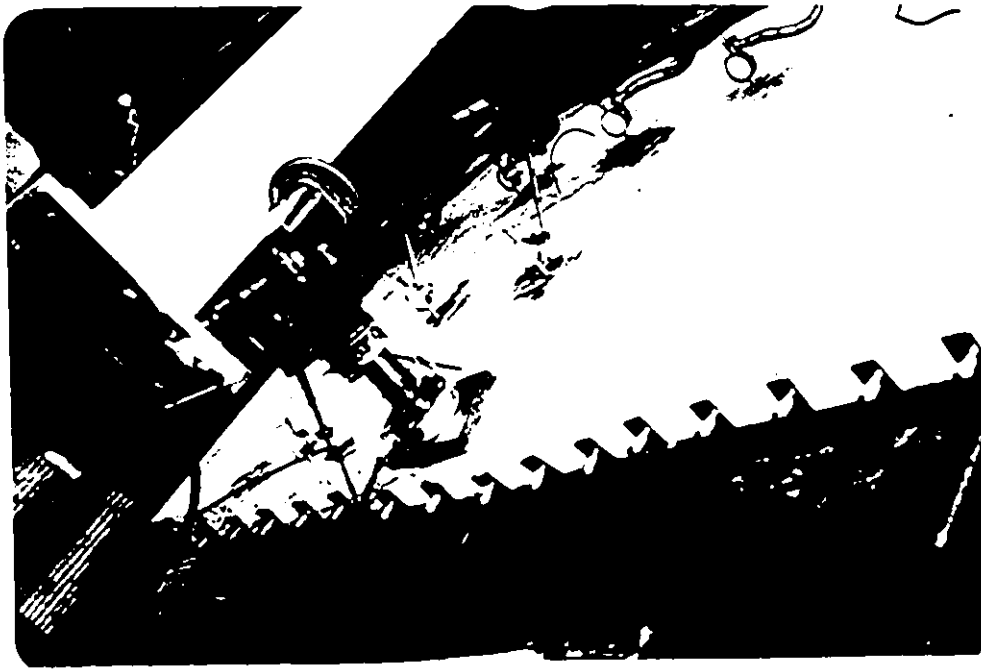


FIGURE 7.75 CRACKS OF WAFFLE SLAB MODEL PCI
 DUE TO EDGE LOAD

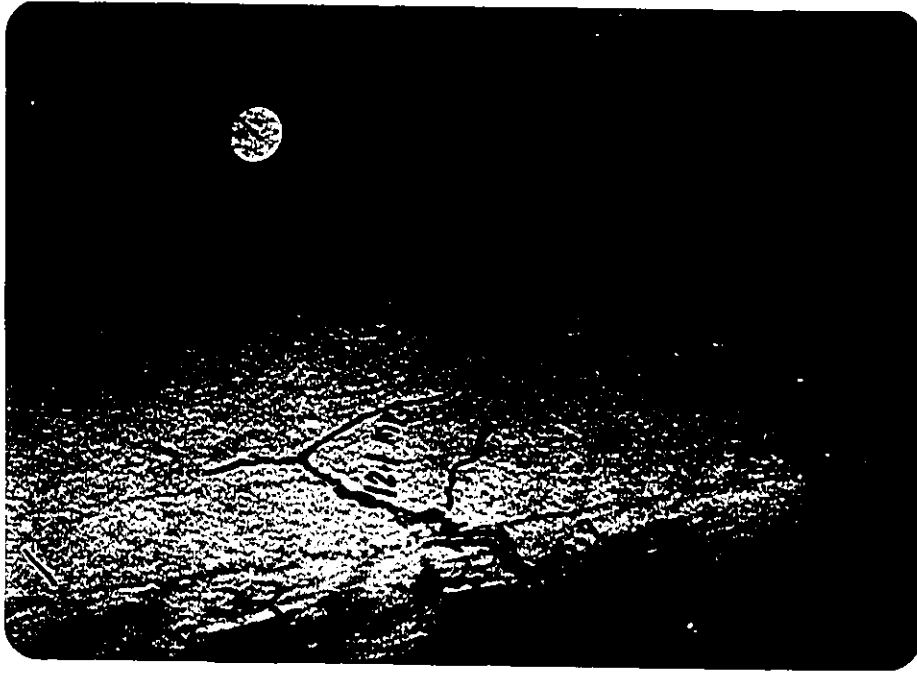


FIGURE 7.77 SINGLE-LINE CRACK PATTERN OF
WAFFLE SLAB MODEL PC2

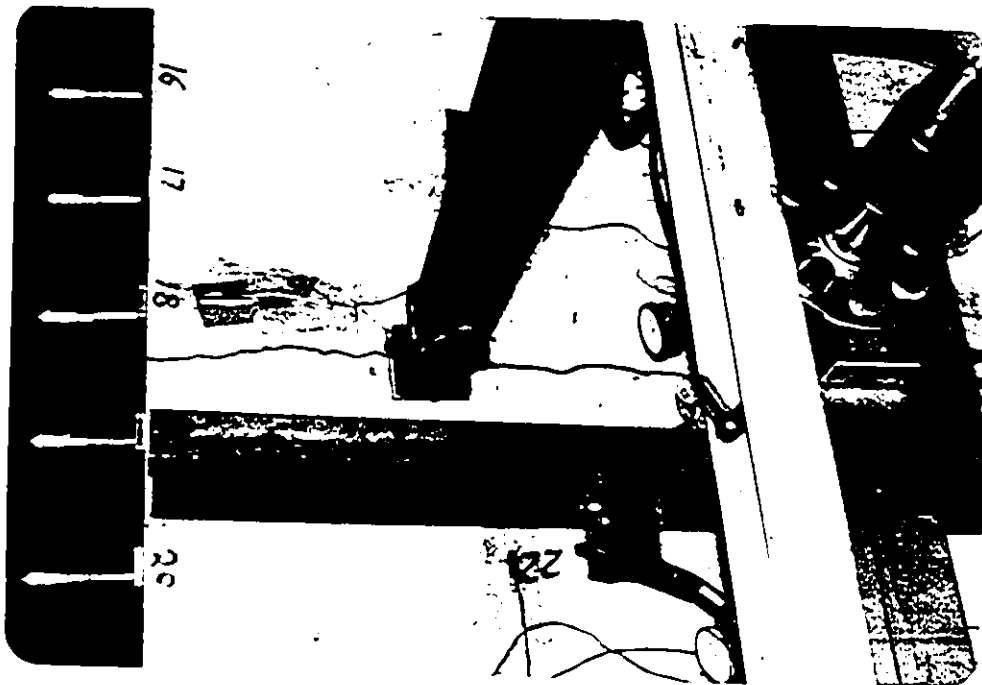


FIGURE 7.78 NEGATIVE SINGLE-LINE CRACK PATTERN
JOINING THE TWO COLUMNS IN WAFFLE
SLAB MODEL PC3

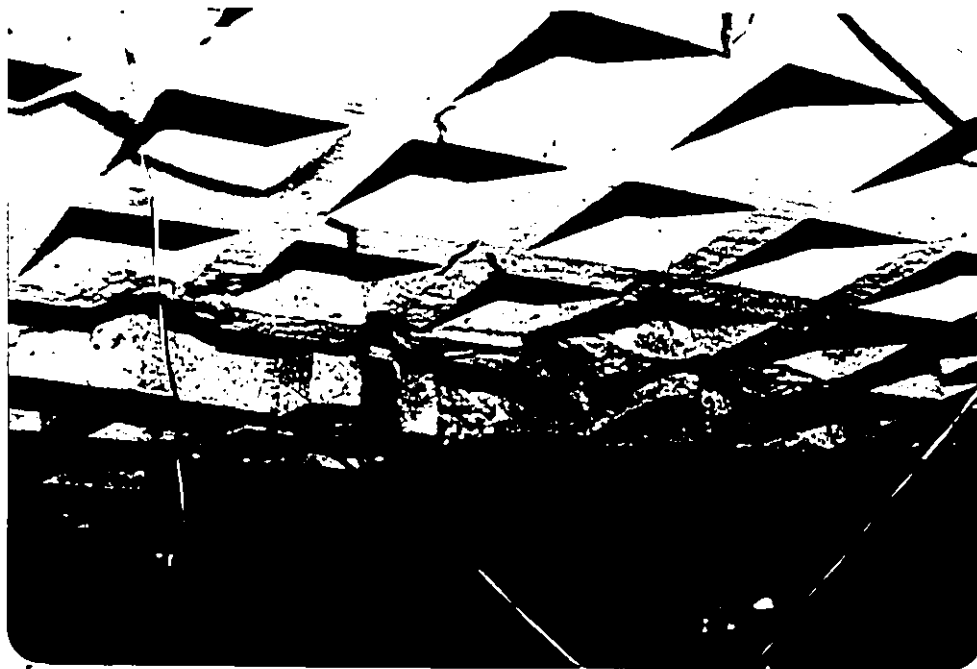


FIGURE 7.79 COMBINED FLEXURAL AND TORSIONAL
CRACKS IN WAFFLE SLAB PC4

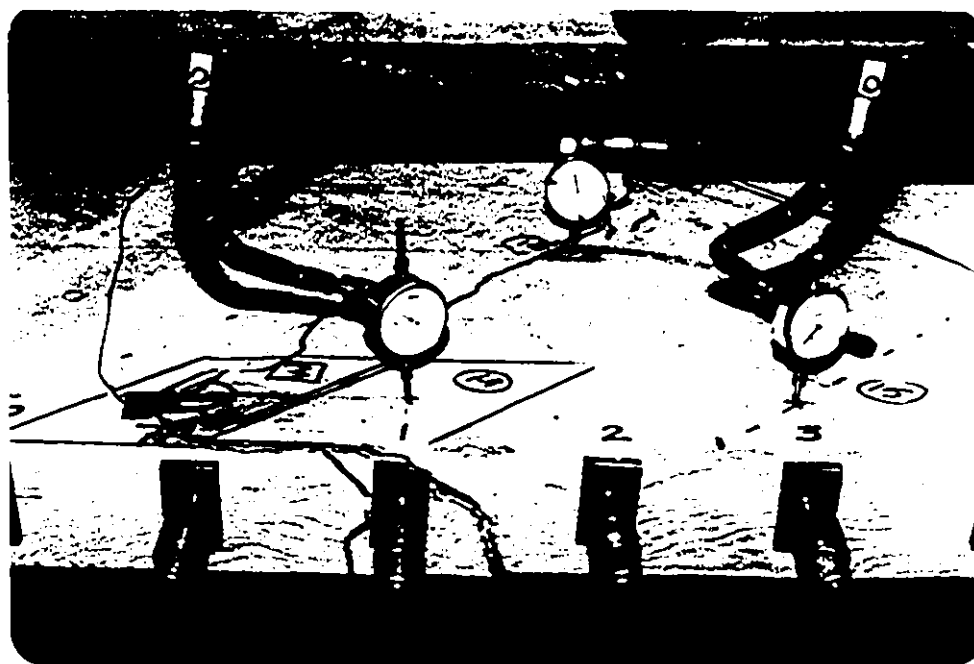
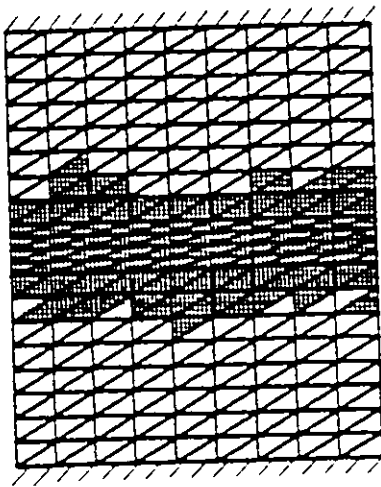
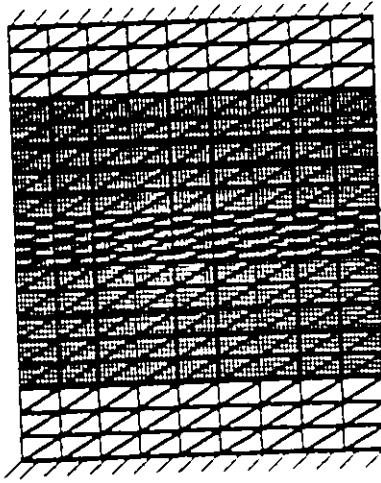


FIGURE 7.80 YIELD LINE IN WAFFLE SLAB PC4

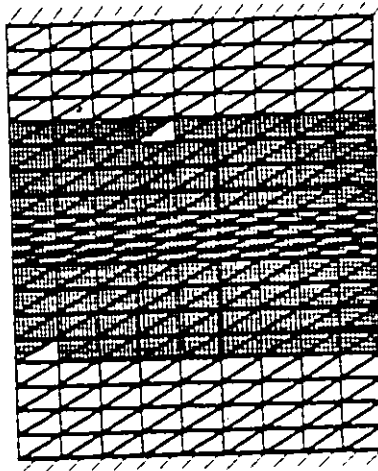


(a) Cracking Load
= 0.38 psi

(b) Load = 0.42 psi



(d) Ultimate Load = 0.82 psi



(c) Load = 0.50 psi

FIGURE 7.81 RECTANGULAR REINFORCED CONCRETE WAFFLE SLAB RC1
SUBJECTED TO UNIFORMLY DISTRIBUTED LOAD

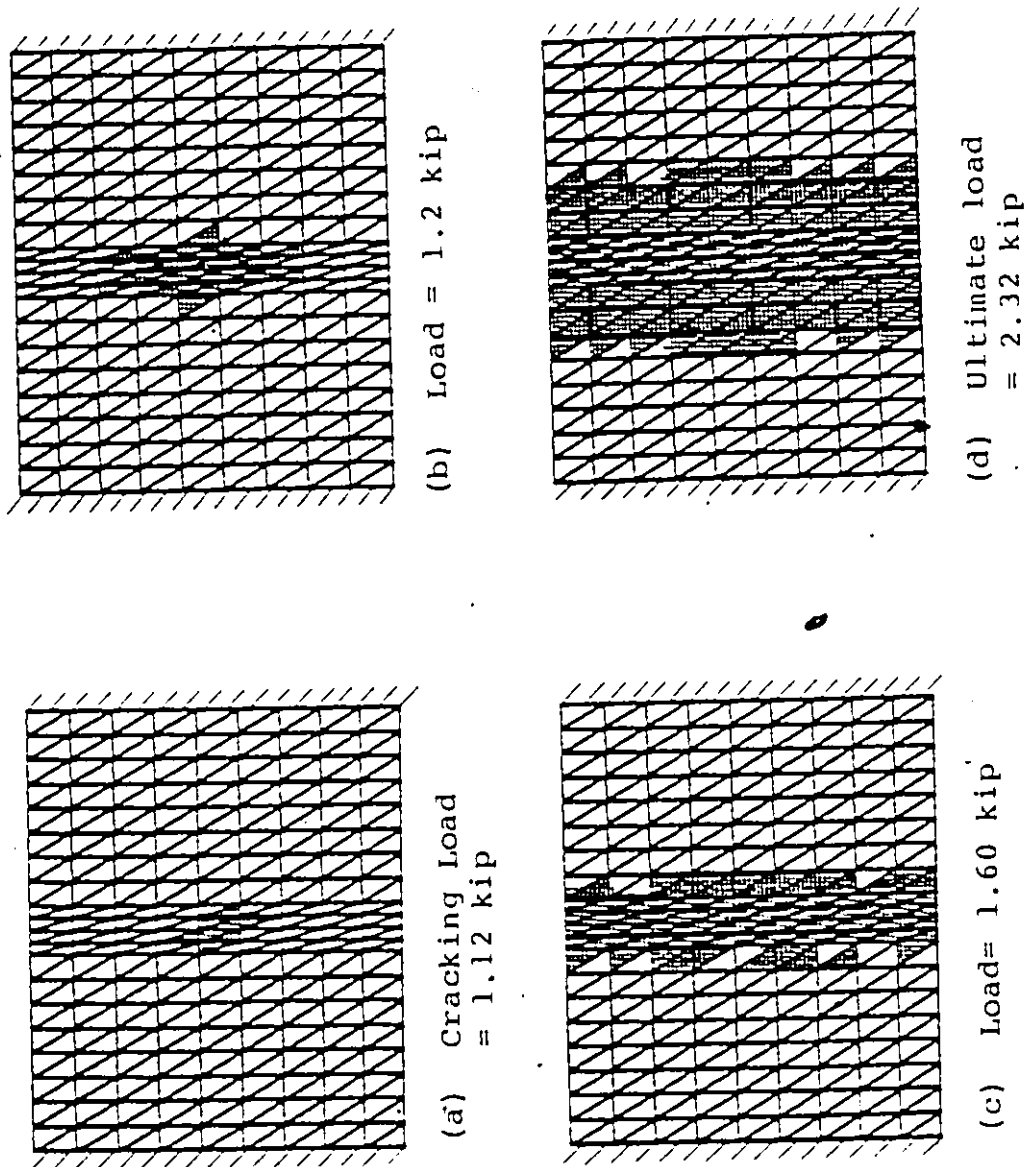


FIGURE 7.82 RECTANGULAR REINFORCED CONCRETE WAFFLE SLAB
(RC2) SUBJECTED TO A SINGLE CONCENTRATED LOAD
AT THE CENTER OF THE SLAB

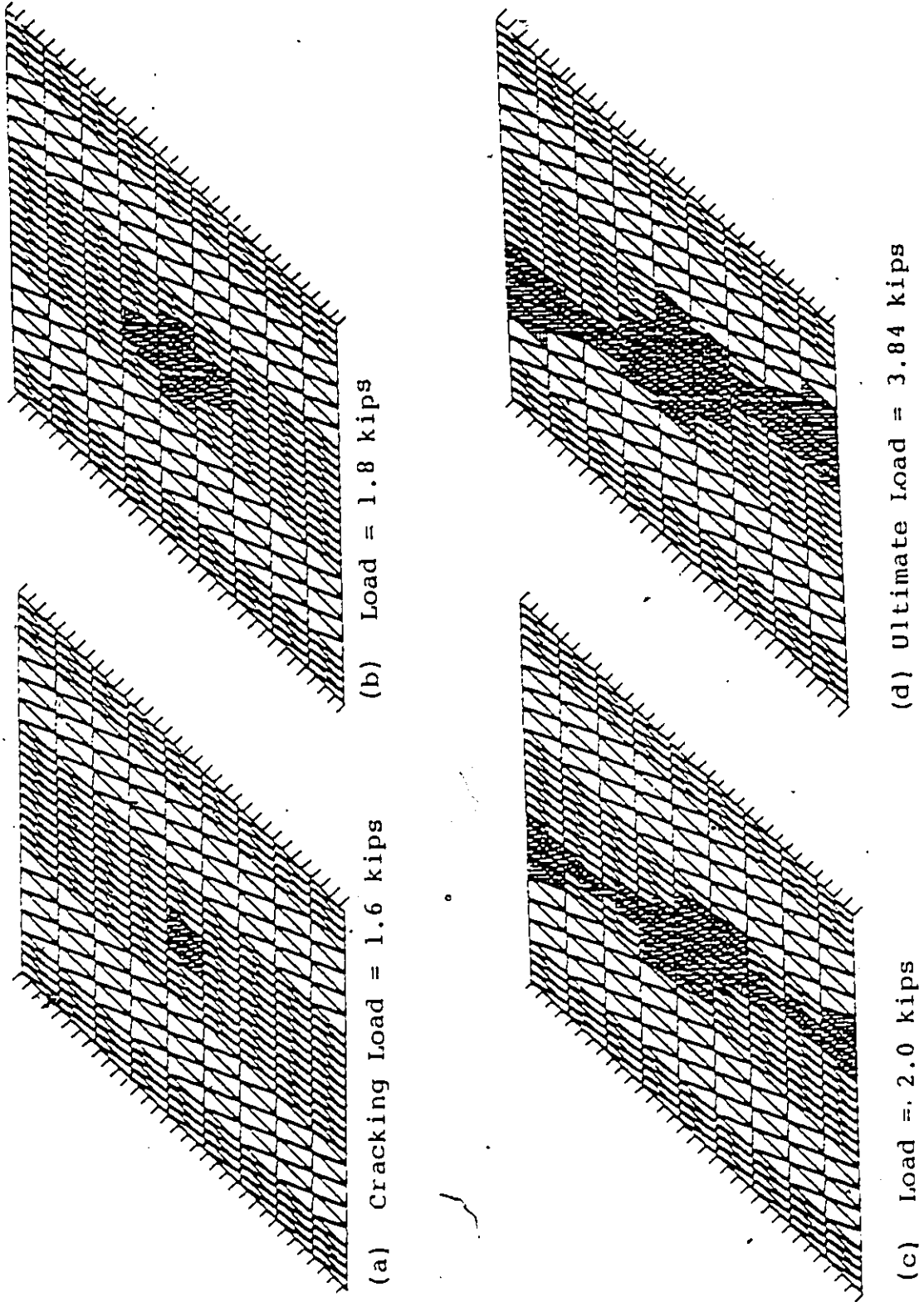


FIGURE 7.83 SKEW REINFORCED CONCRETE WAFFLE SLAB (RC3) SUBJECTED TO A SINGLE CONCENTRATED LOAD AT THE CENTER OF THE SLAB

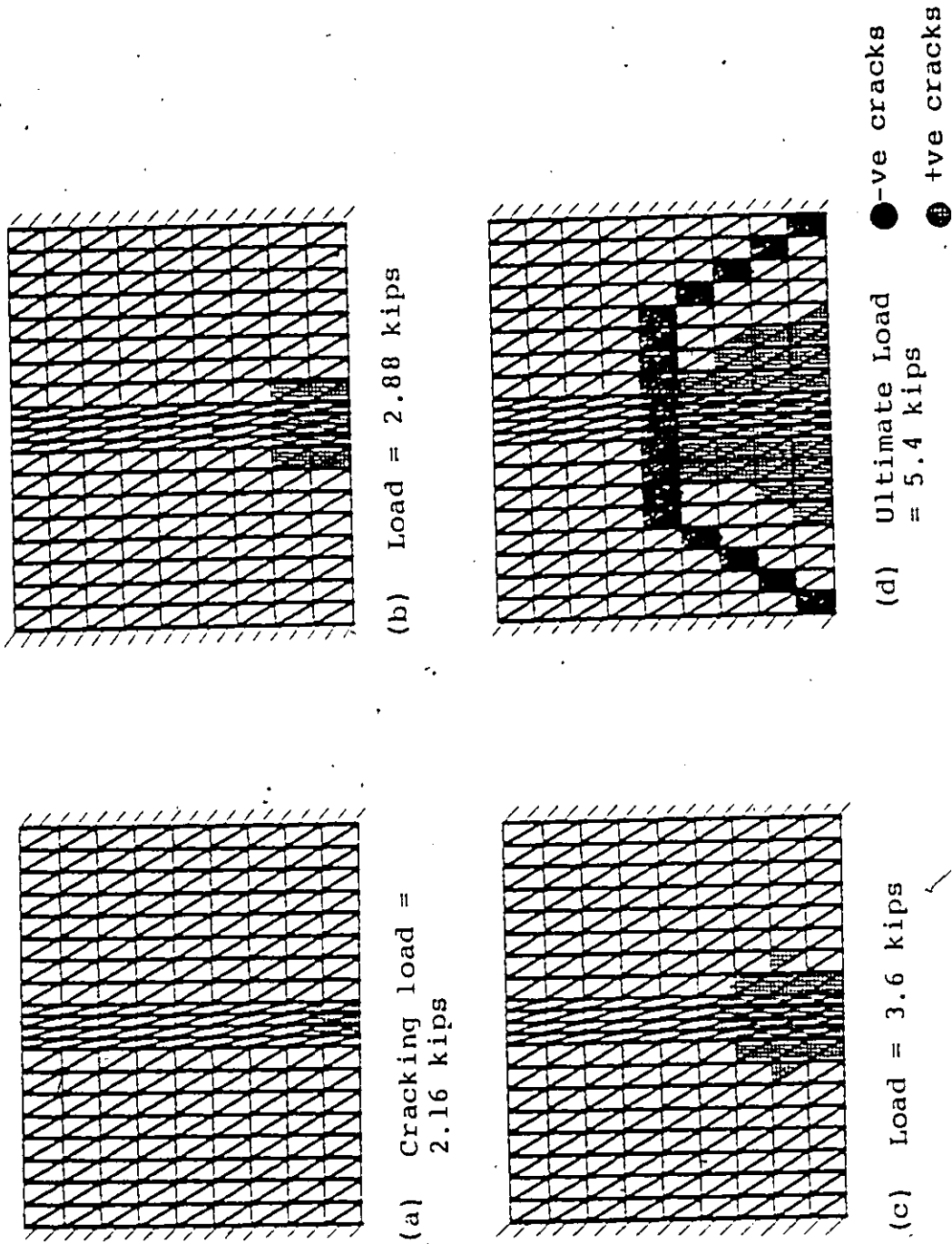
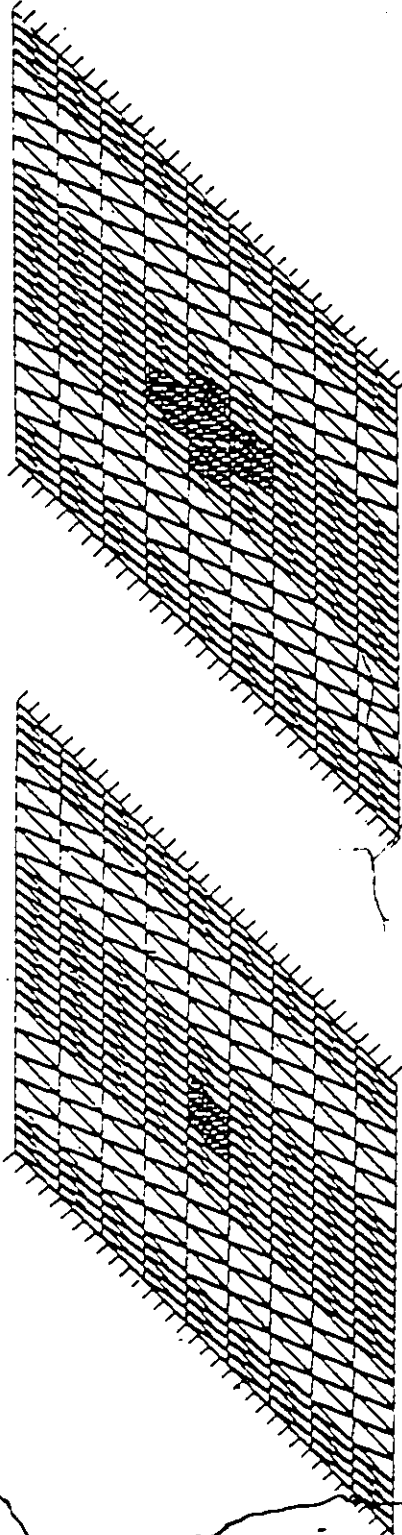
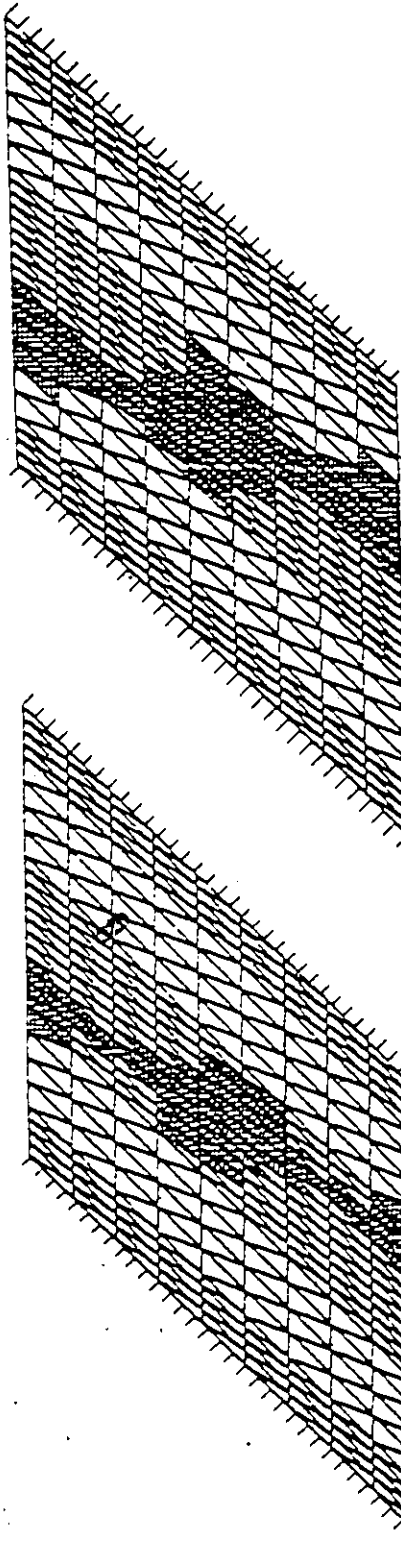


FIGURE 7.84 RECTANGULAR PRESTRESSED CONCRETE WAFFLE SLAB (PC1) SUBJECTED TO A SINGLE CONCENTRATED LOAD AT THE CENTER OF THE EDGE BEAM



(a) Cracking Load = 6.6 kips

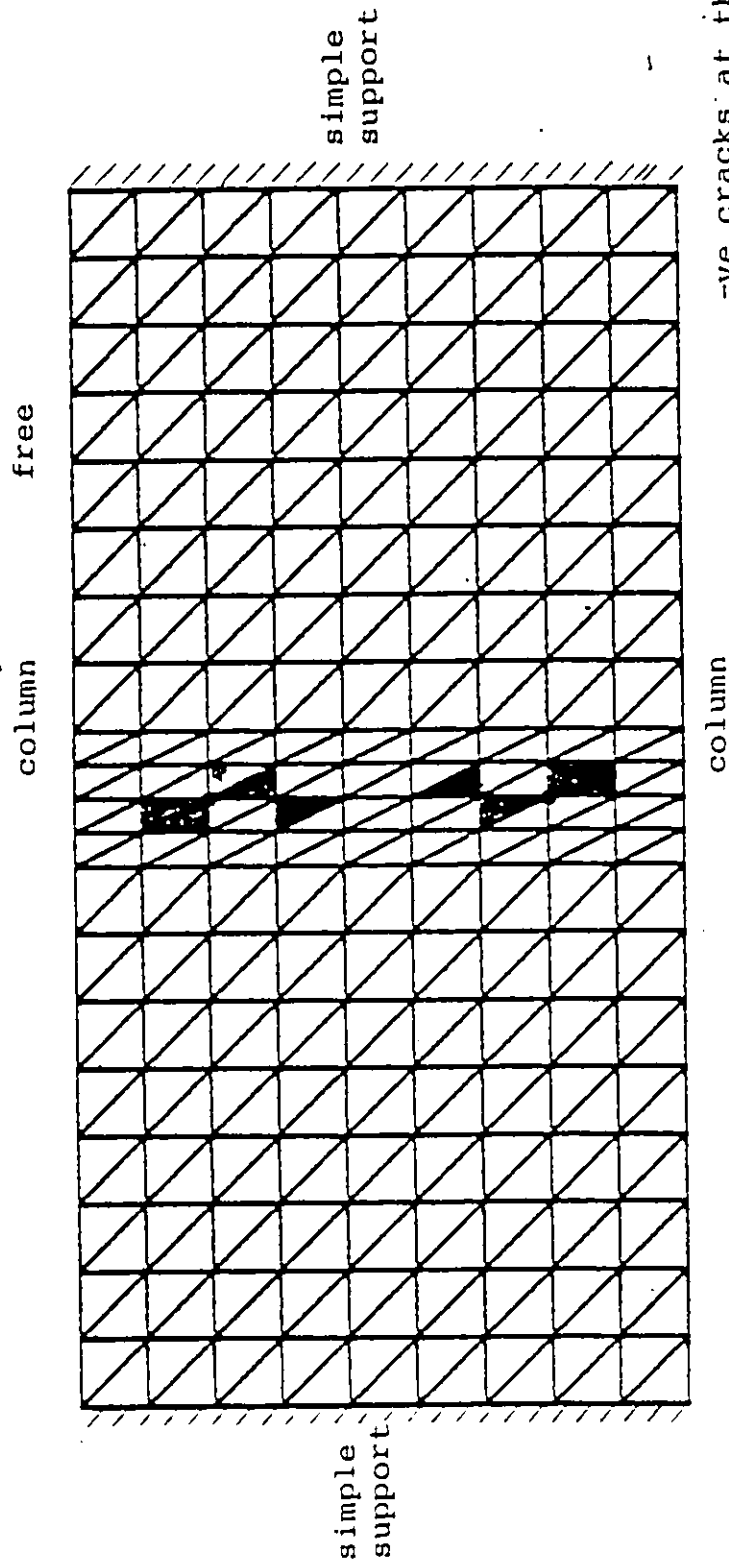
(b) Load = 8 kips



(c) Load = 9 kips

(d) Ultimate load = 11.4 kips

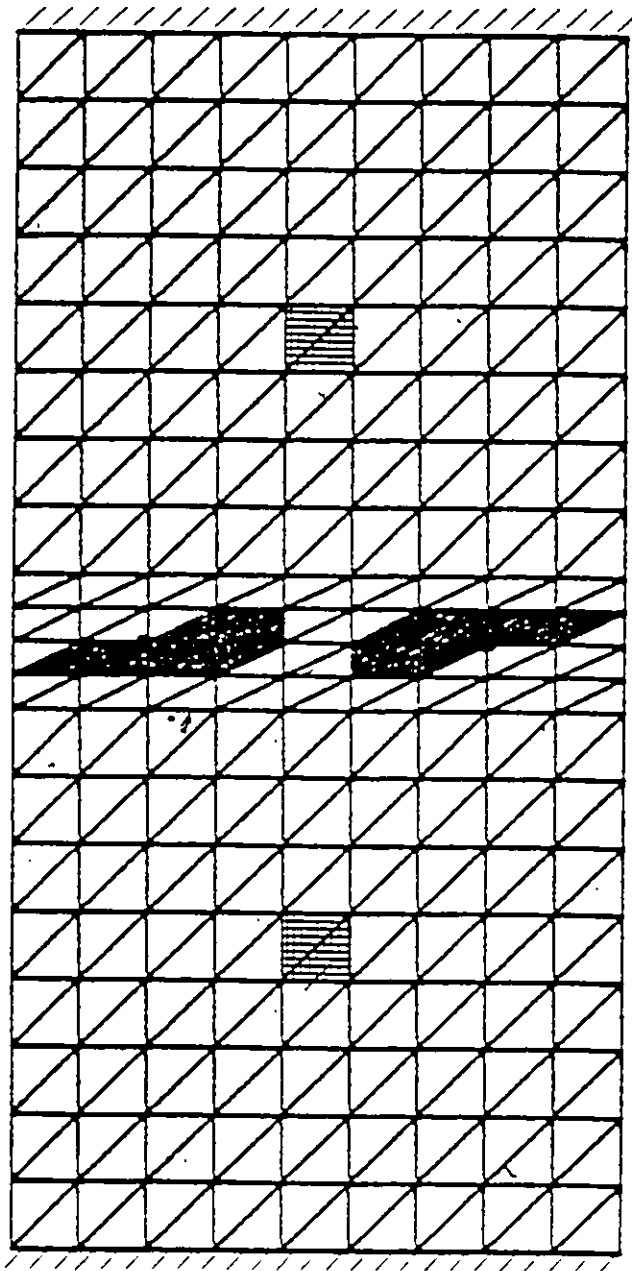
FIGURE 7.85 SKEW PRESTRESSED CONCRETE WAFFLE SLAB (PC2) SLAB SUBJECTED TO A SINGLE CONCENTRATED LOAD AT THE CENTER OF THE SLAB.



● -ve cracks at the top surface of the slab

⦿ the cracks at the bottom surface of the model. (1 kip = 4.448kN)

FIGURE 7.86 RECTANGULAR PRESTRESSED CONTINUOUS WAFFLE SLAB (PC3) SUBJECTED TO TWO CONCENTRATED LOADS OF 14.96 KIPS (CRACKING LOAD) EACH AT THE CENTER OF EACH SPAN PANEL.

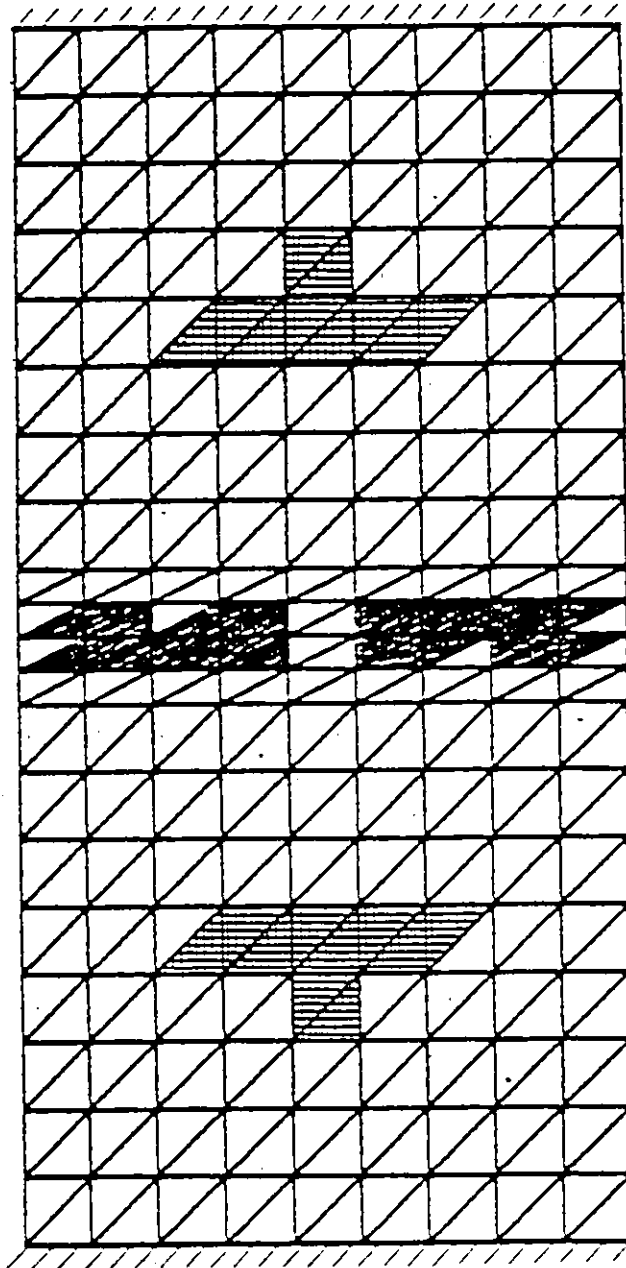


● -ve cracks

⊖ +ve cracks

(1 kip \approx 4.448 kN)

FIGURE 7.87 RECTANGULAR PRESTRESSED CONTINUOUS WAFFLE SLAB (PC3) SUBJECTED TO TWO CONCENTRATED LOADS OF 17.68 KIPS ACTING AT THE CENTRE OF EACH SPAN PANEL



● -ve cracks

● +ve cracks
(1 kip = 4.448 kN)

FIGURE 7.88 CRACKS AT LOAD 19.04 KIPS

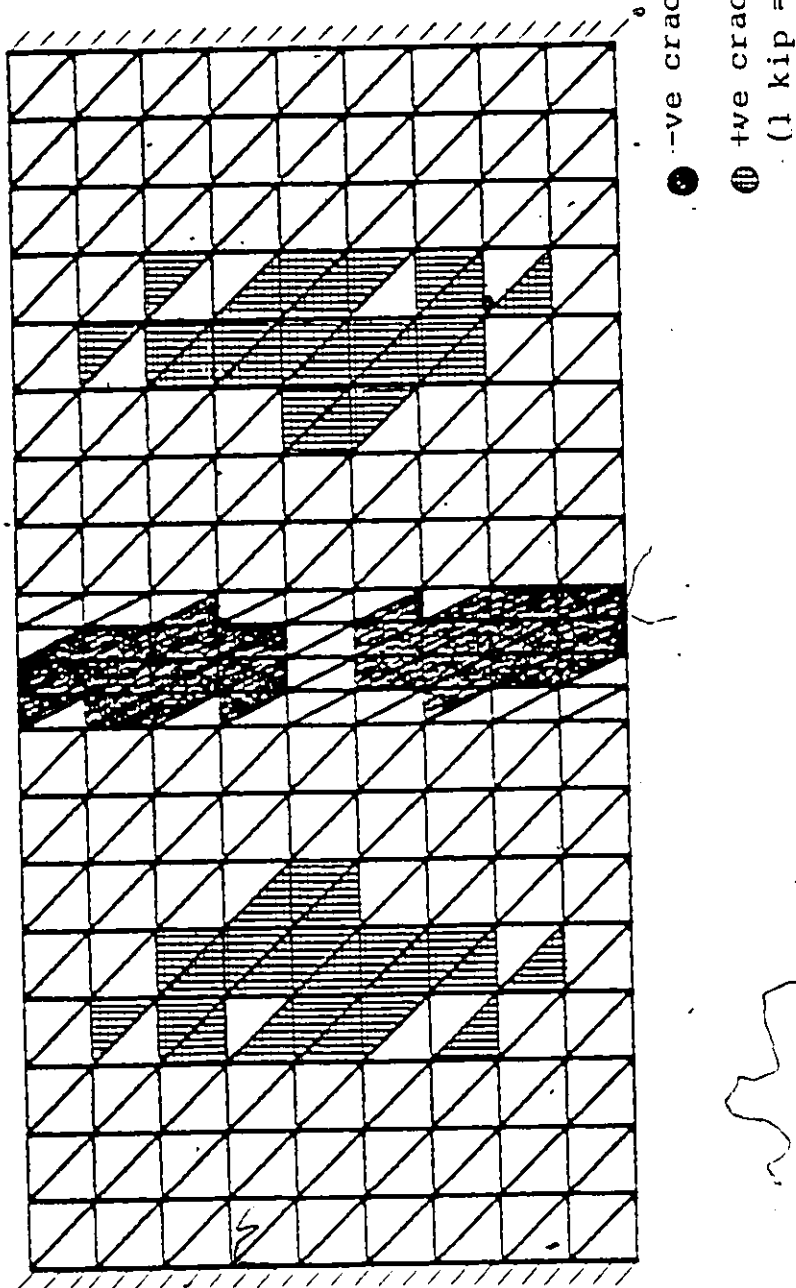


FIGURE 7.89 CRACKS AT LOAD = 20.4 KIPS



FIGURE 7.90 RECTANGULAR PRESTRESSED CONTINUOUS WAFFLE SLAB (PC3) SUBJECT TO TWO CONCENTRATED LOADS OF 24.7 KIPS ULTIMATE LOAD EACH AT THE CENTER OF EACH SPAN PANEL.

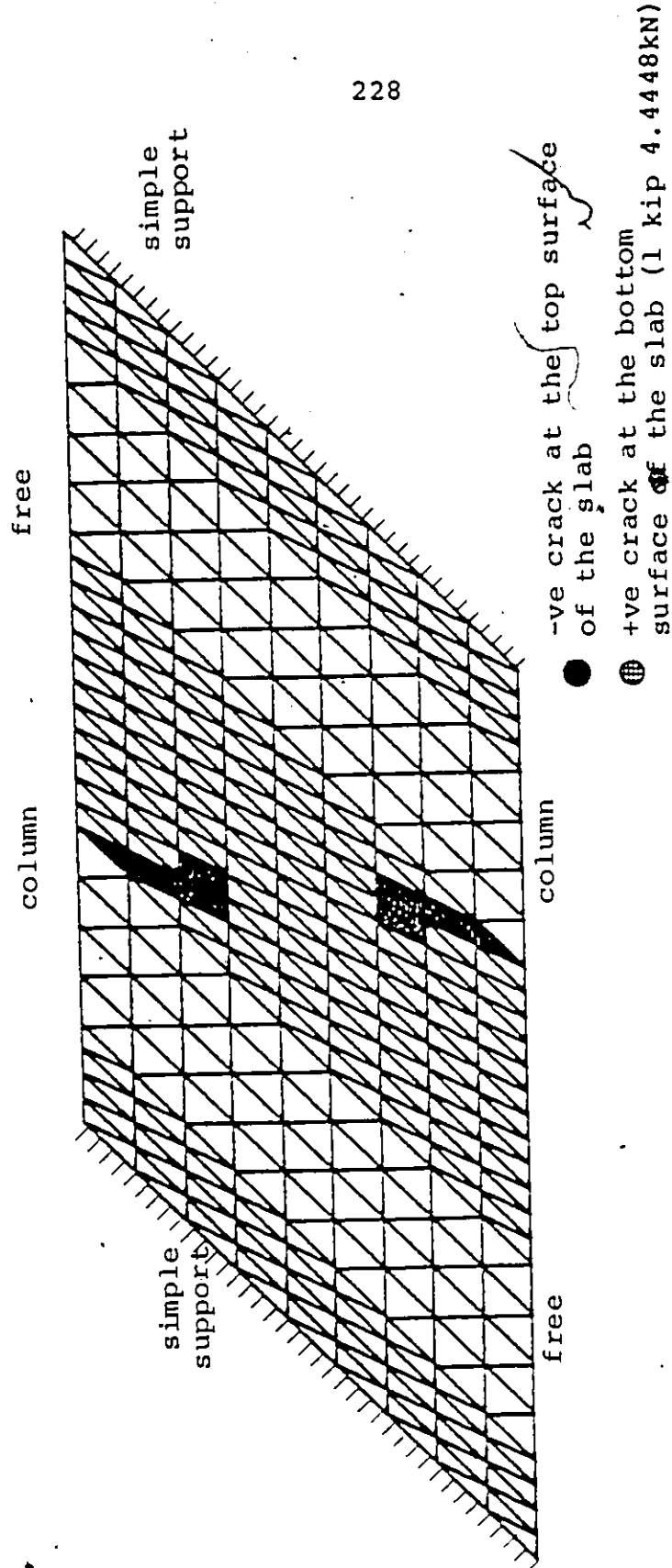


FIGURE 7.91 SKEW PRESTRESSED CONTINUOUS WAFFLE SLAB (PC4) SUBJECTED TO TWO CONCENTRATED LOADS OF 15.84 KIPS (CRACKING LOAD) AT THE CENTER OF EACH SPAN PANEL

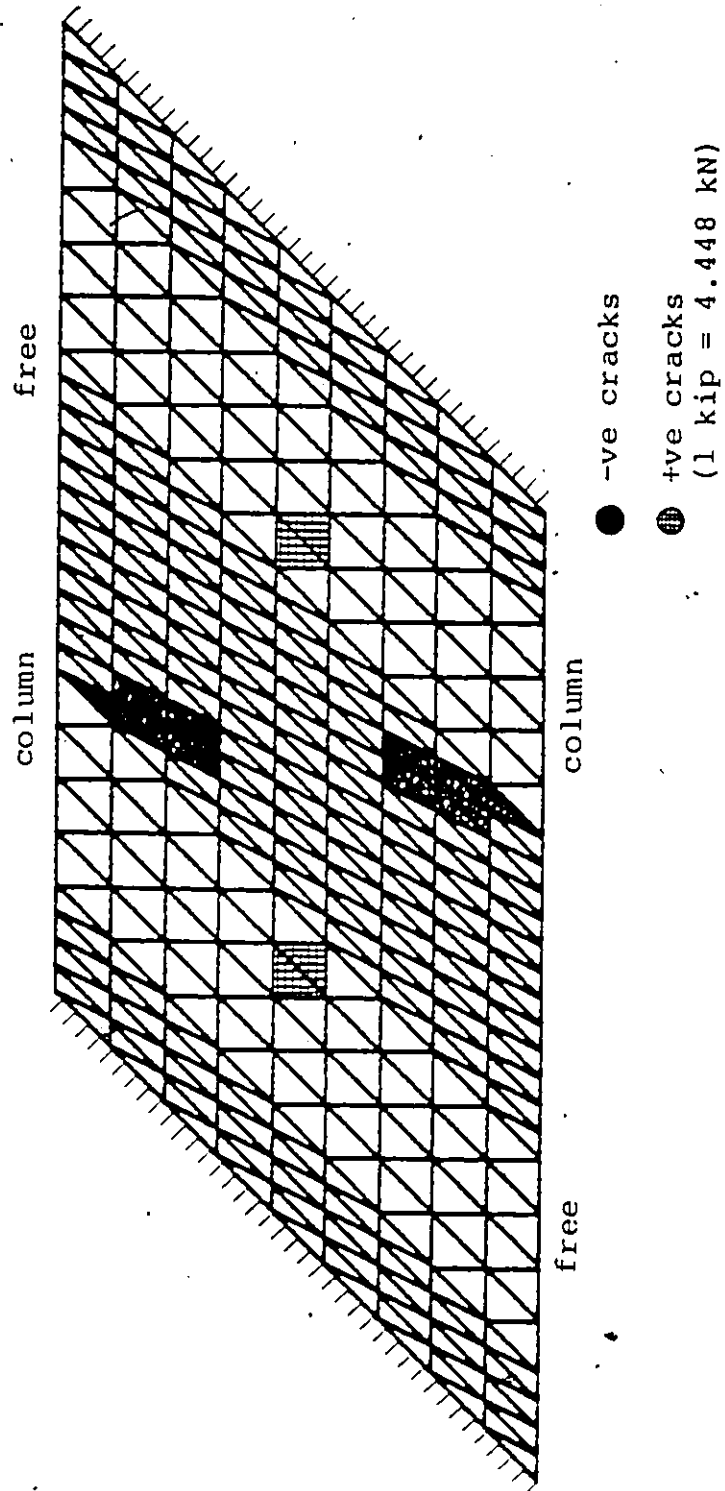


FIGURE 7.92 CRACKS AT LOAD = 18.44 KIPS

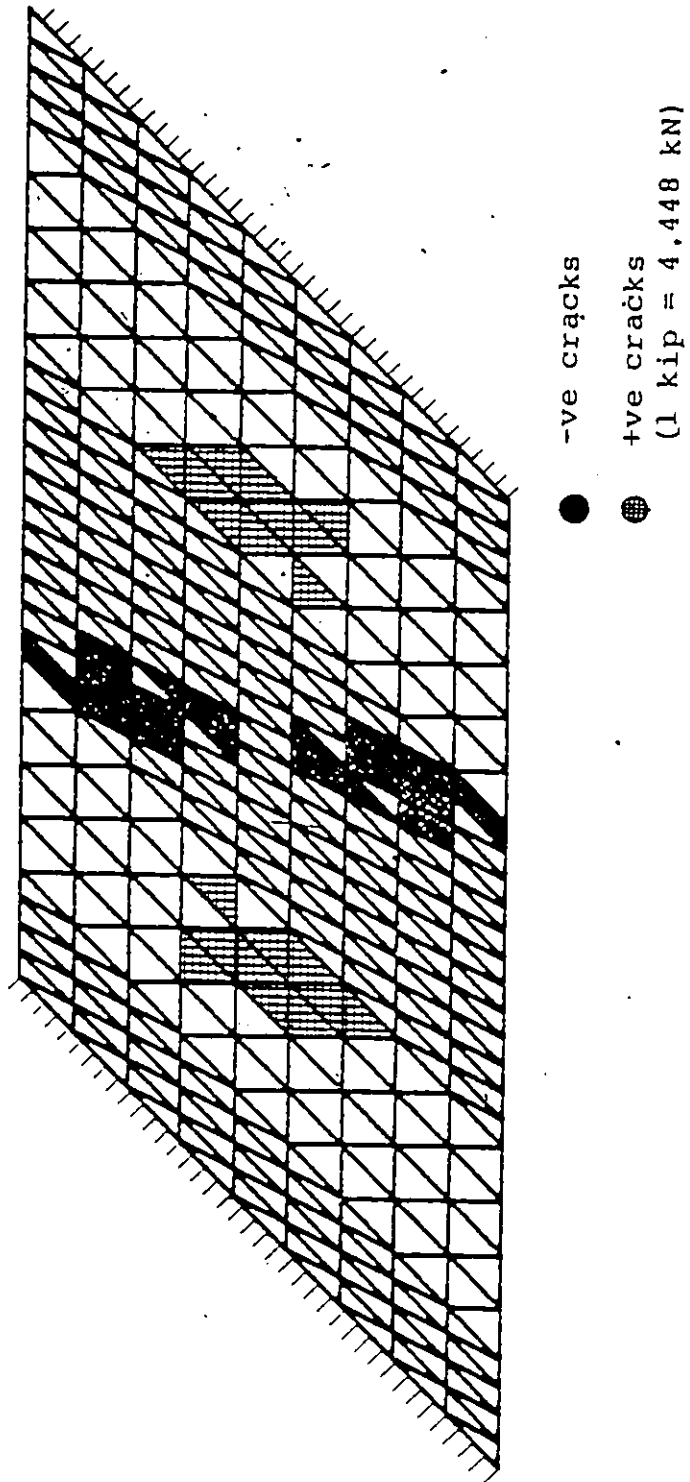


FIGURE 7.93 CRACKS AT LOAD = 22 KIPS

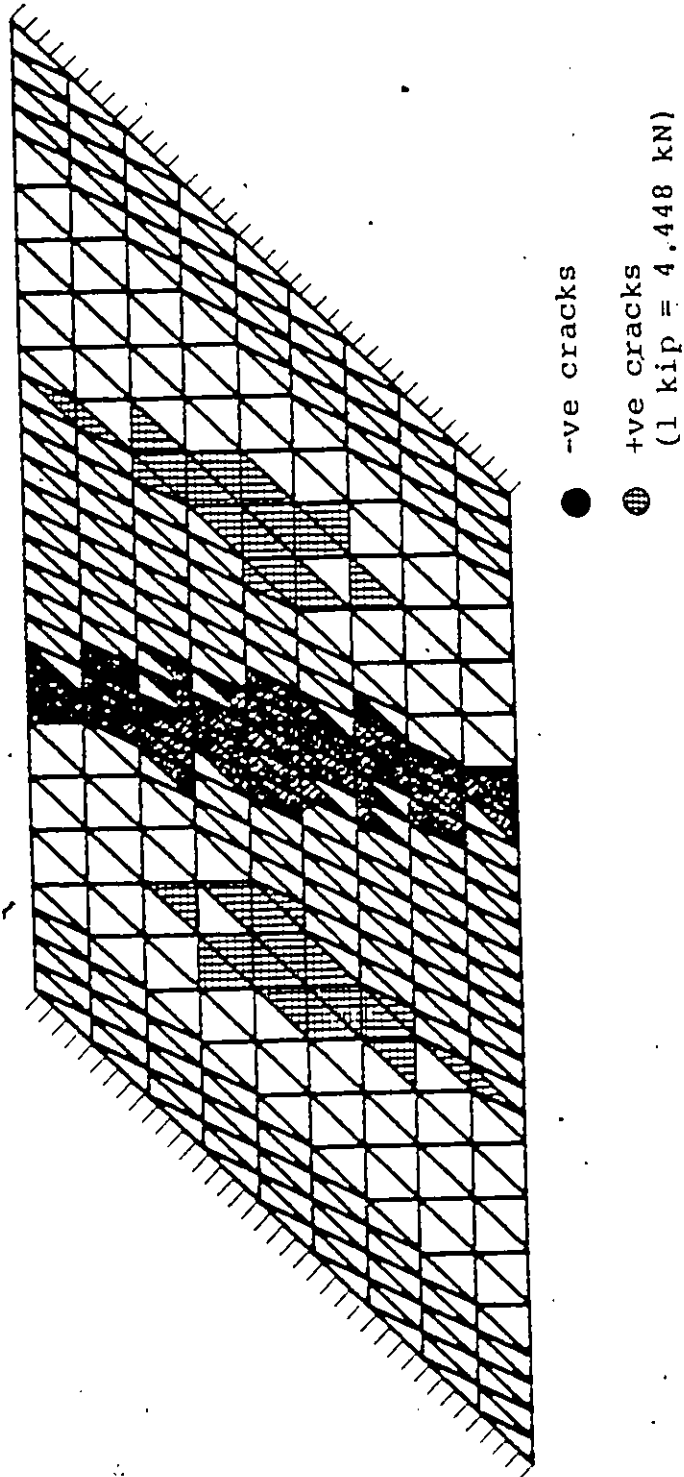
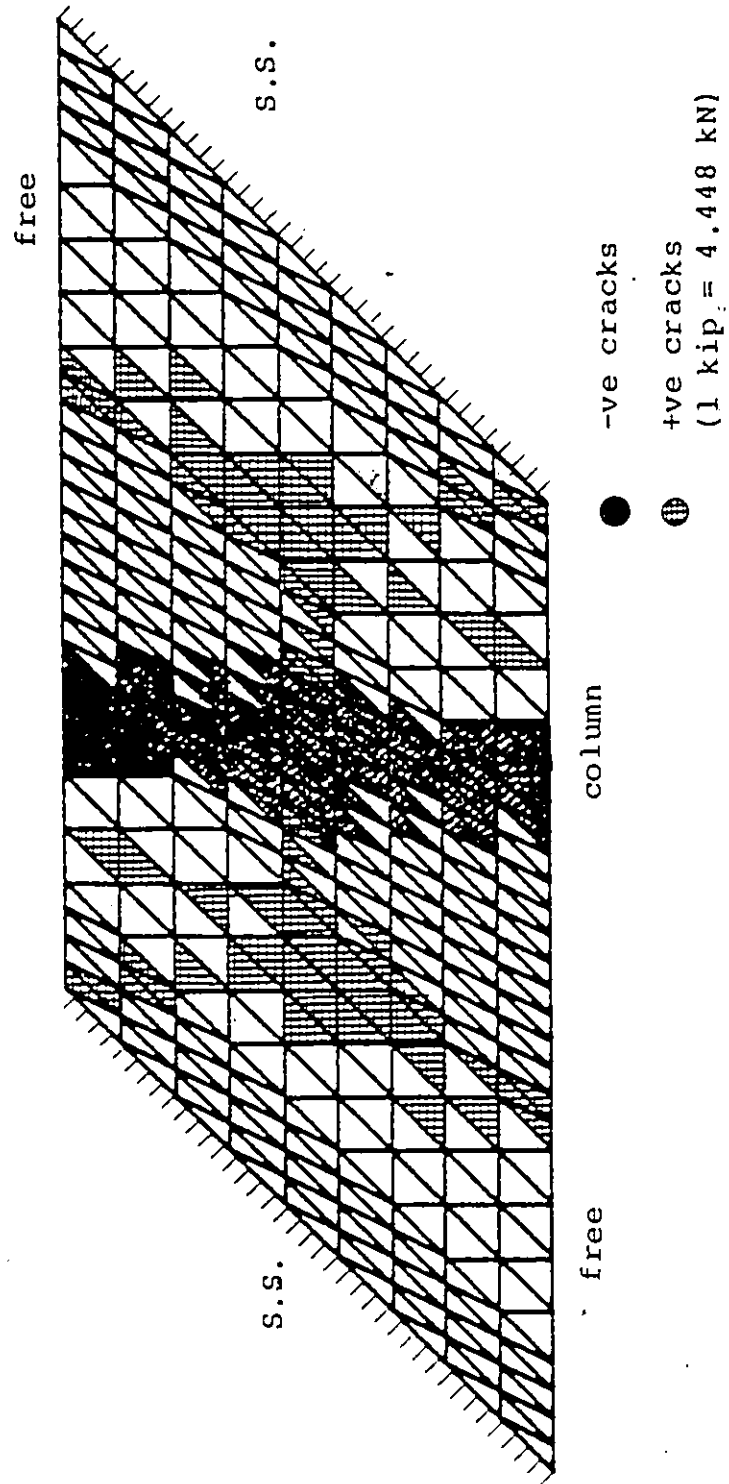


FIGURE 7.94 CRACKS AT LOAD = 24 KIPS



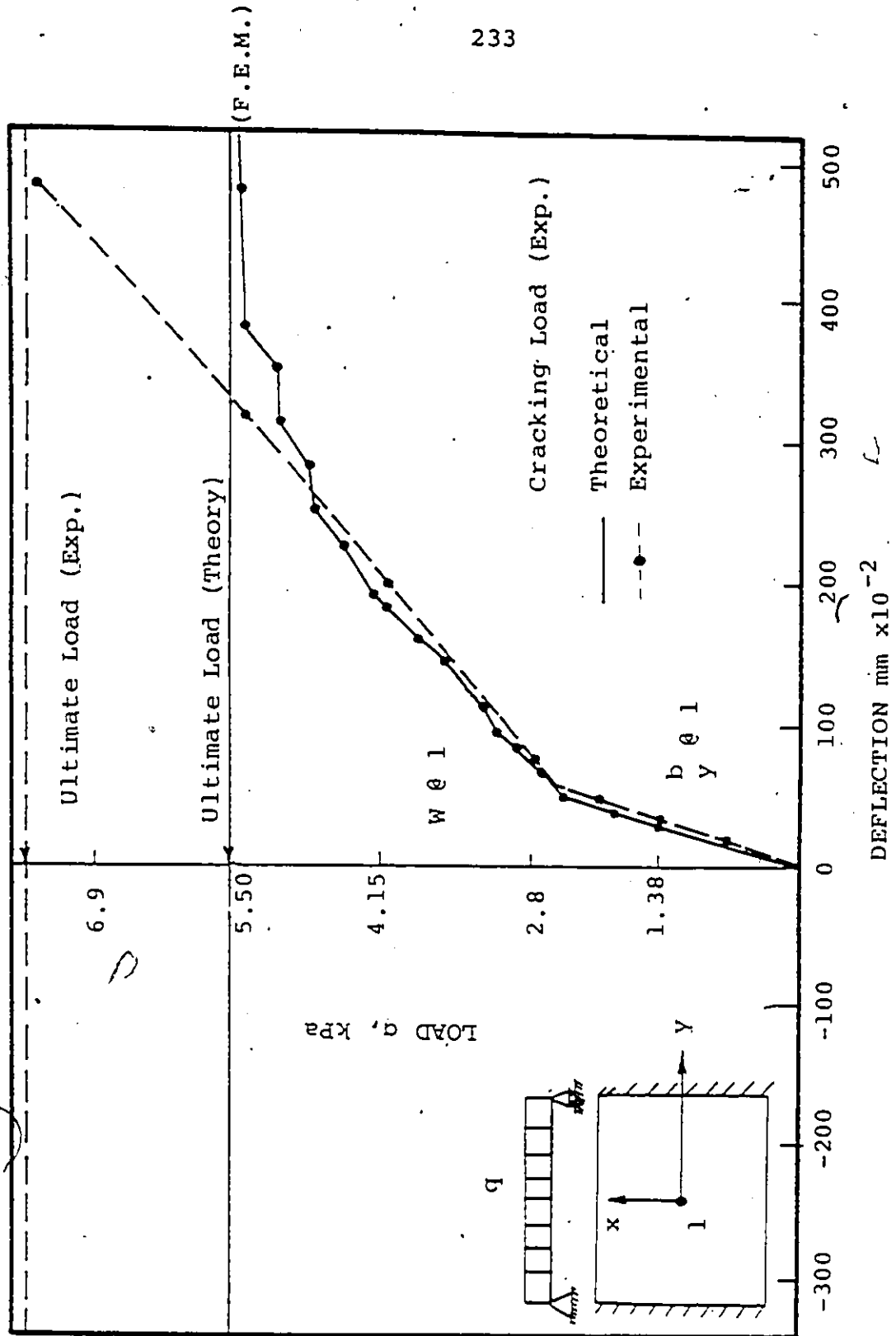


FIGURE 7.96 LOAD VERSUS DEFLECTION FOR RECTANGULAR SLAB (RC1) MODEL UNDER UNIFORMLY DISTRIBUTED LOAD.

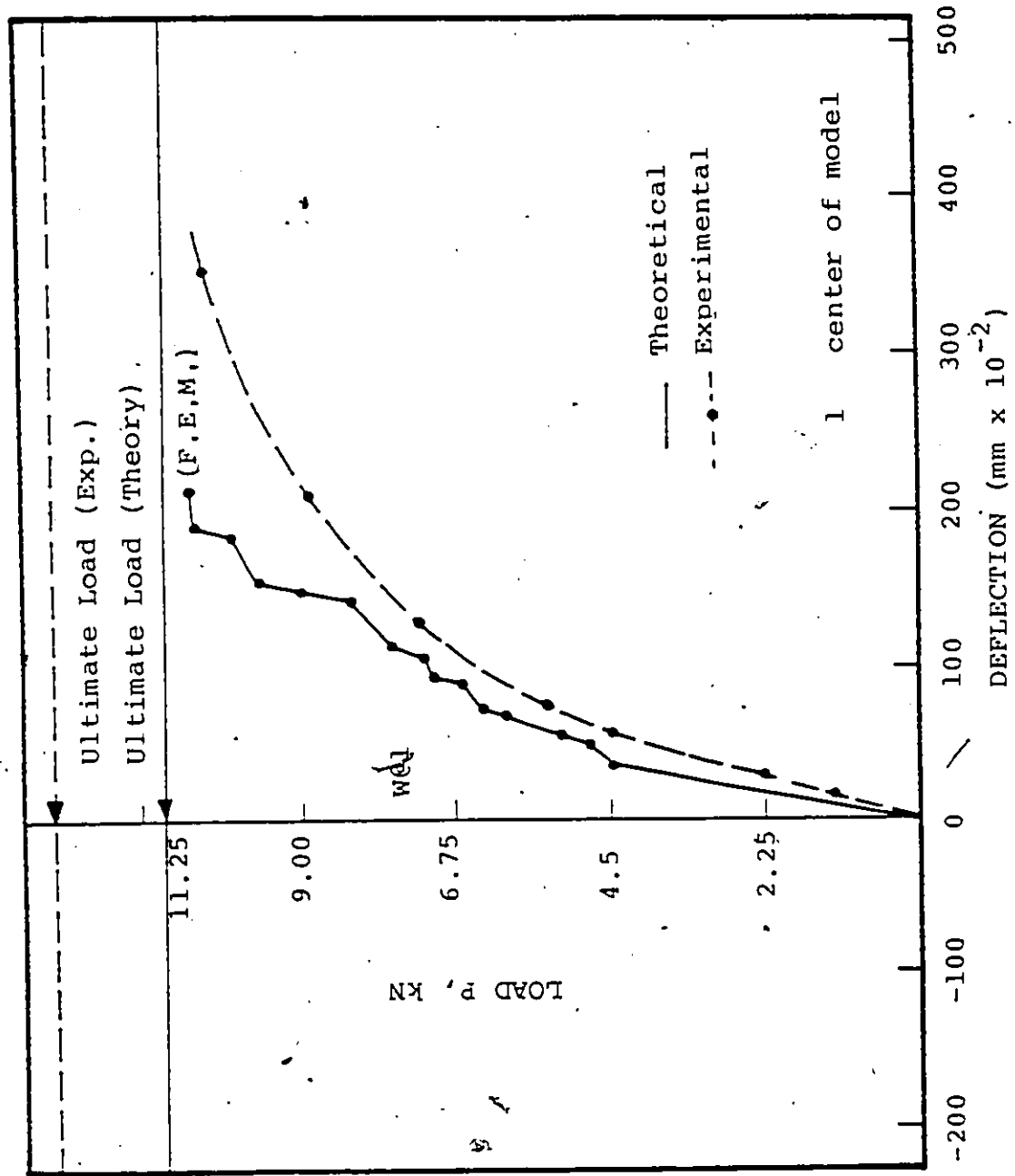


FIGURE 7.97 LOAD VERSUS DEFLECTION FOR RECTANGULAR SLAB MODEL (RC2) UNDER CONCENTRATED LOAD AT THE CENTER

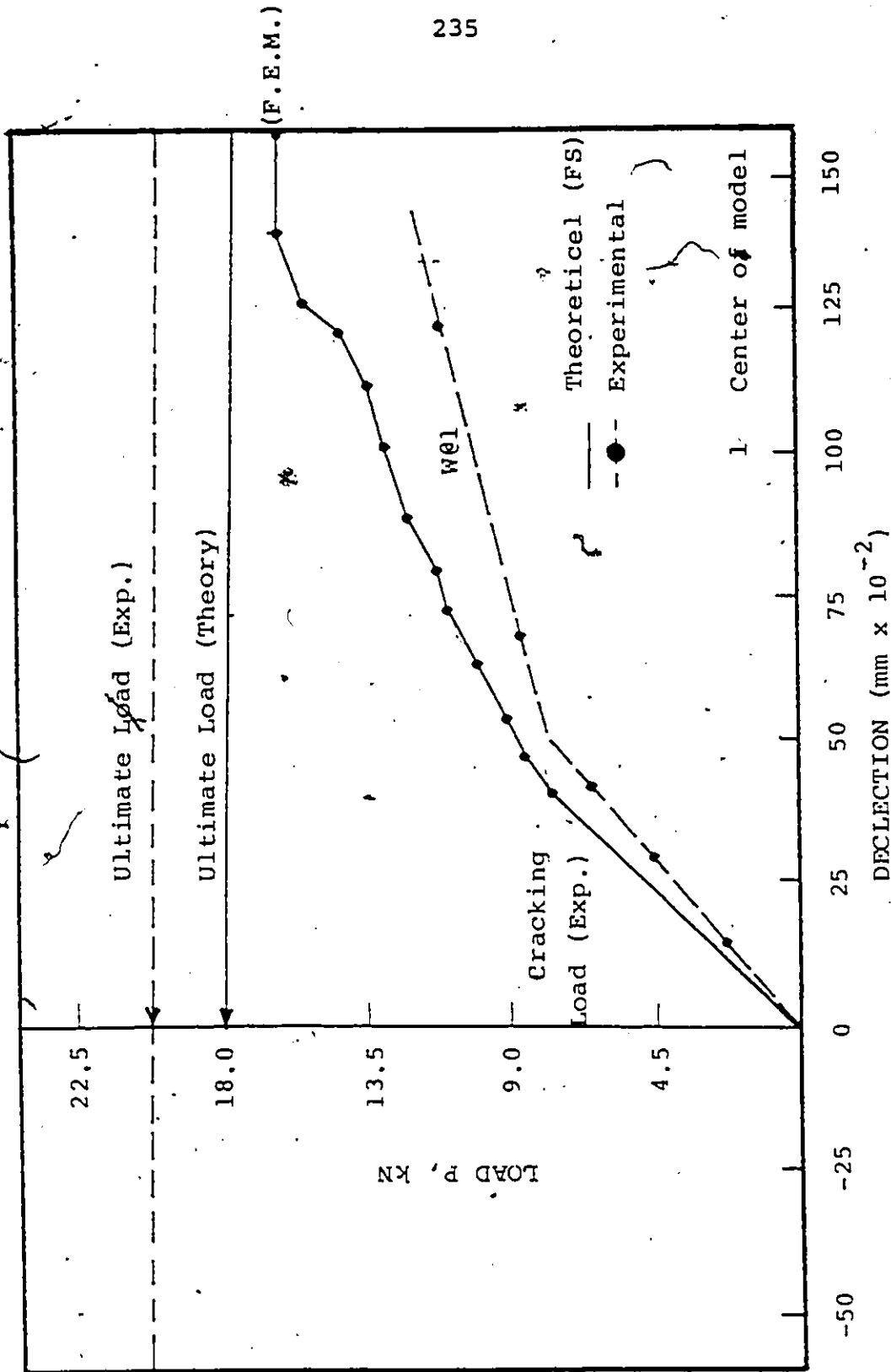


FIGURE 7.98 LOAD VERSUS DEFLECTION FOR REINFORCED SKEW SLAB (RC3) UNDER A CONCENTRATED LOAD AT CENTER.

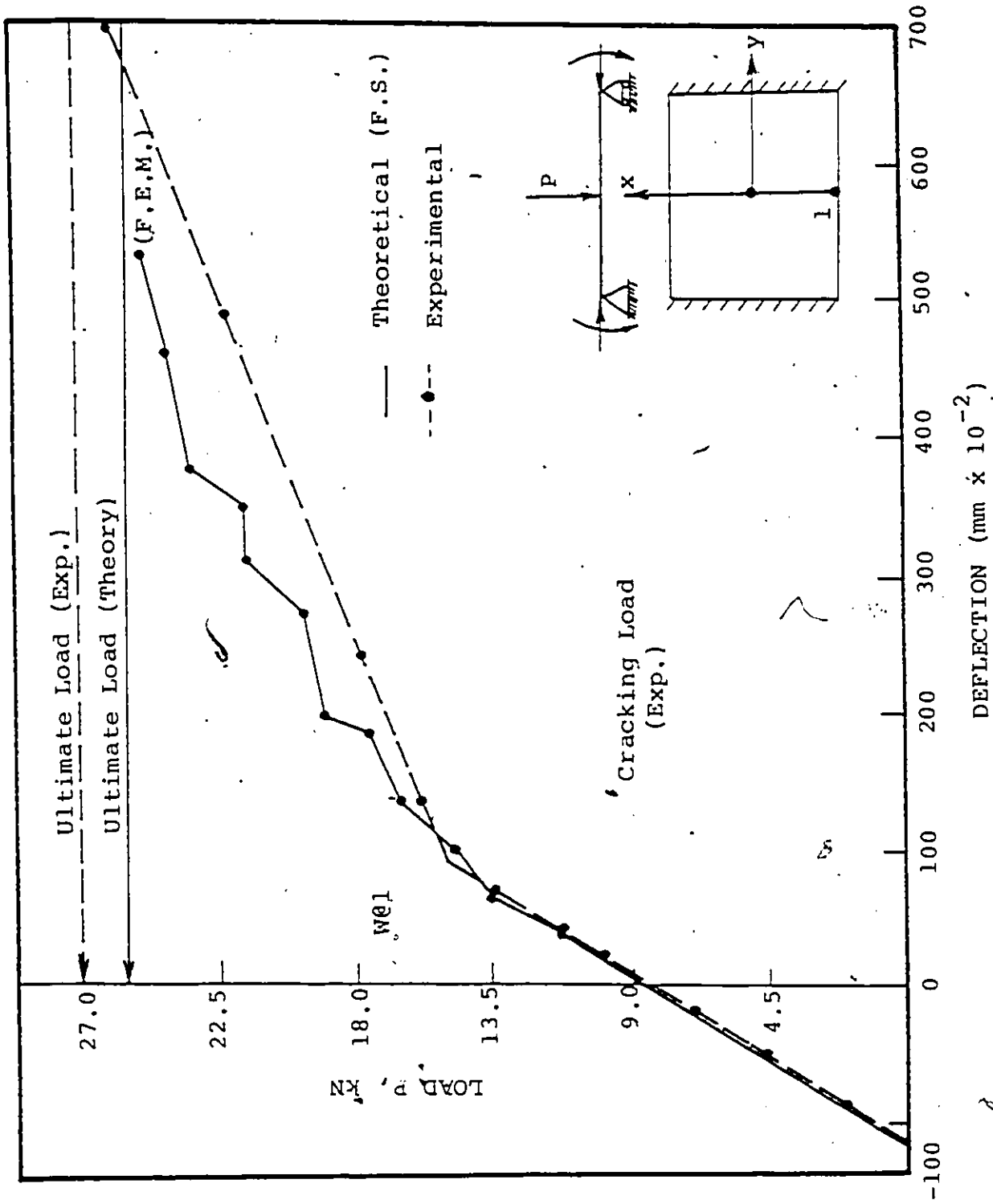


FIGURE 7.99 LOAD VERSUS DEFLECTION FOR PRESTRESSED MODEL (PC1) CONCENTRATED LOAD AT THE CENTER OF EDGE BEAM.

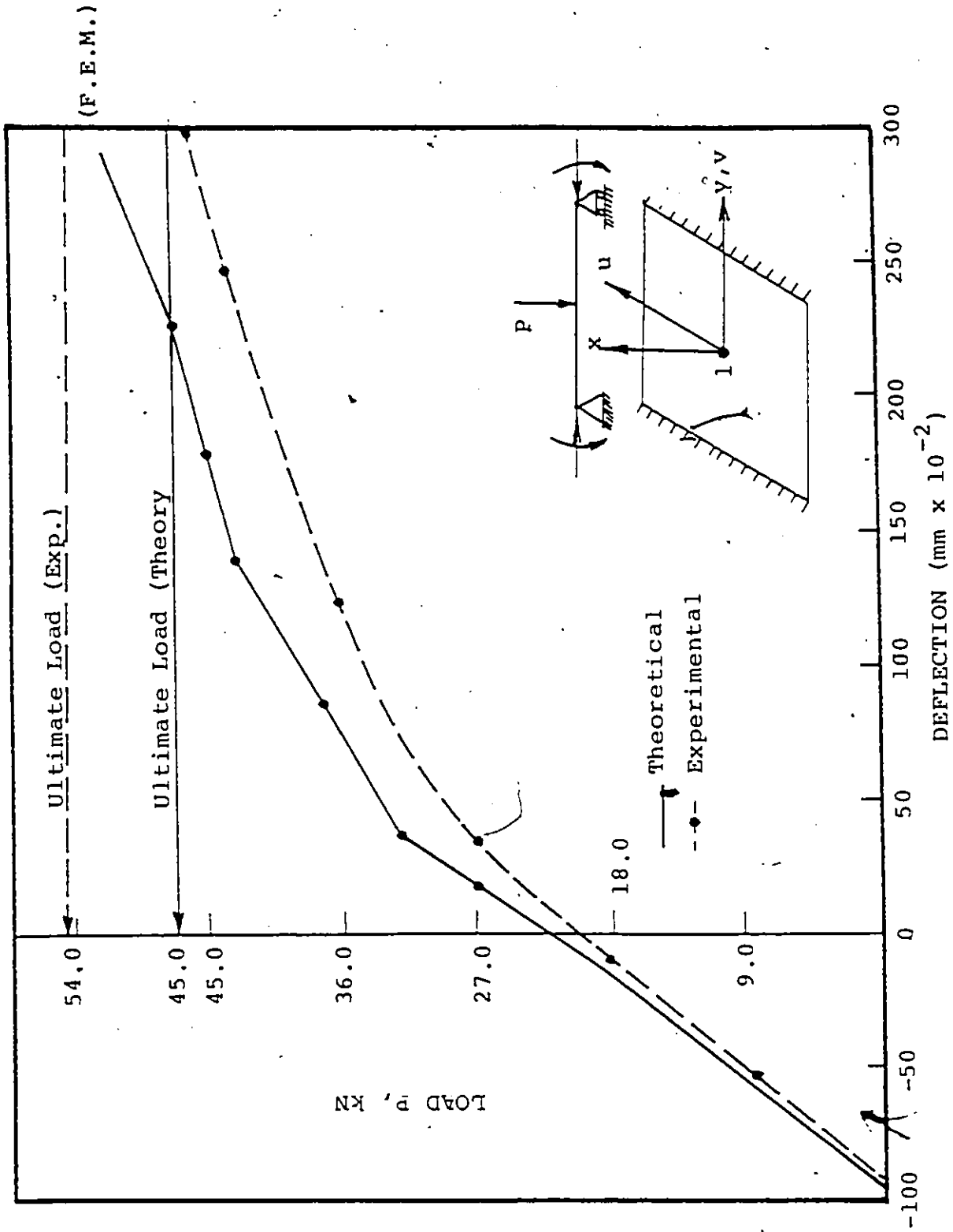


FIGURE 7.100 LOAD VERSUS DEFLECTION FOR PRESTRESSED SKEW MODEL (PC2) UNDER CONCENTRATED LOAD AT THE CENTER OF THE SLAB.

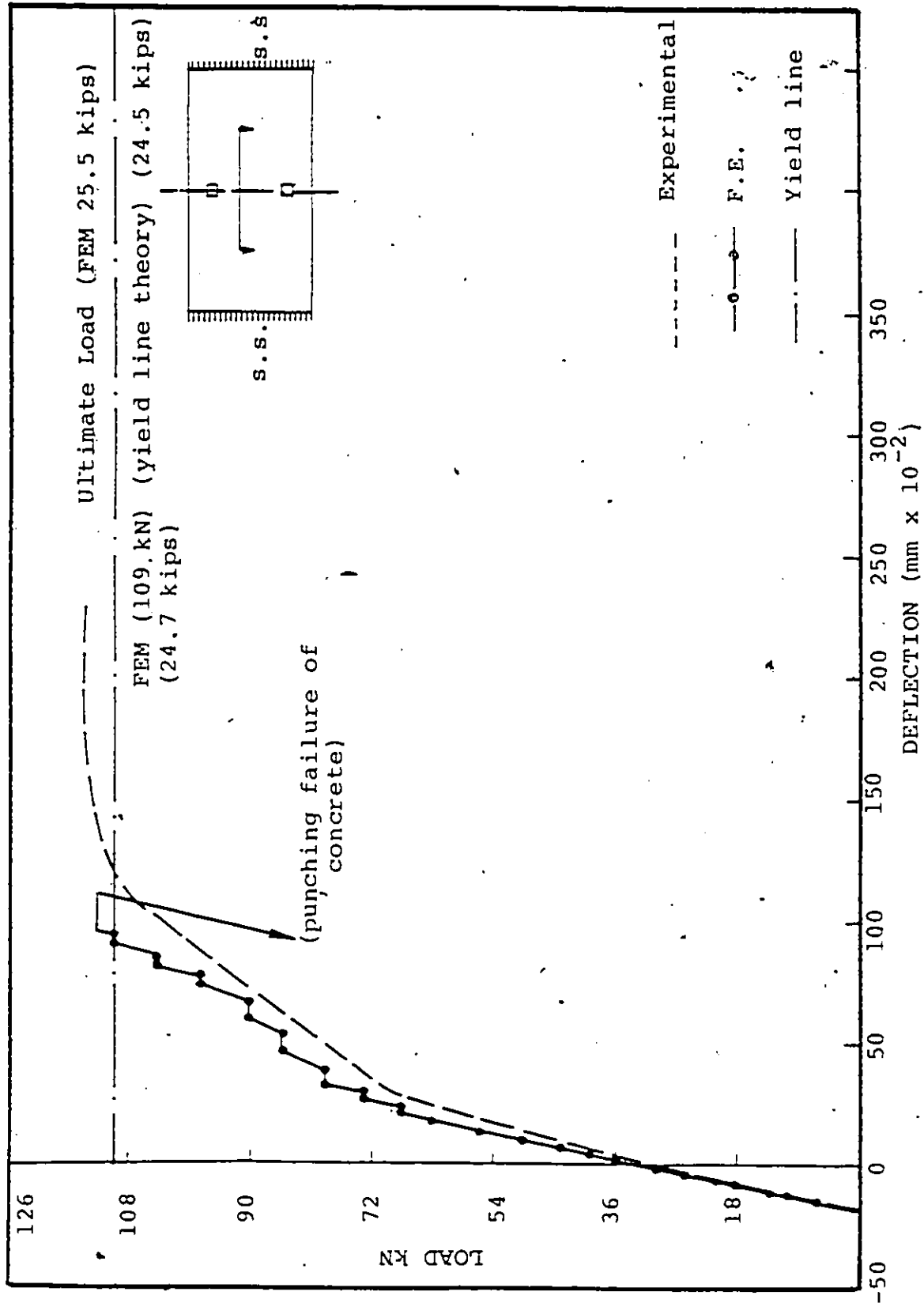


FIGURE 7.101 DEFLECTION RELATIONSHIP FOR RECTANGULAR SLAB DUE TO TWO CONCENTRATED LOADS EACH AT THE CENTER OF EACH SPAN

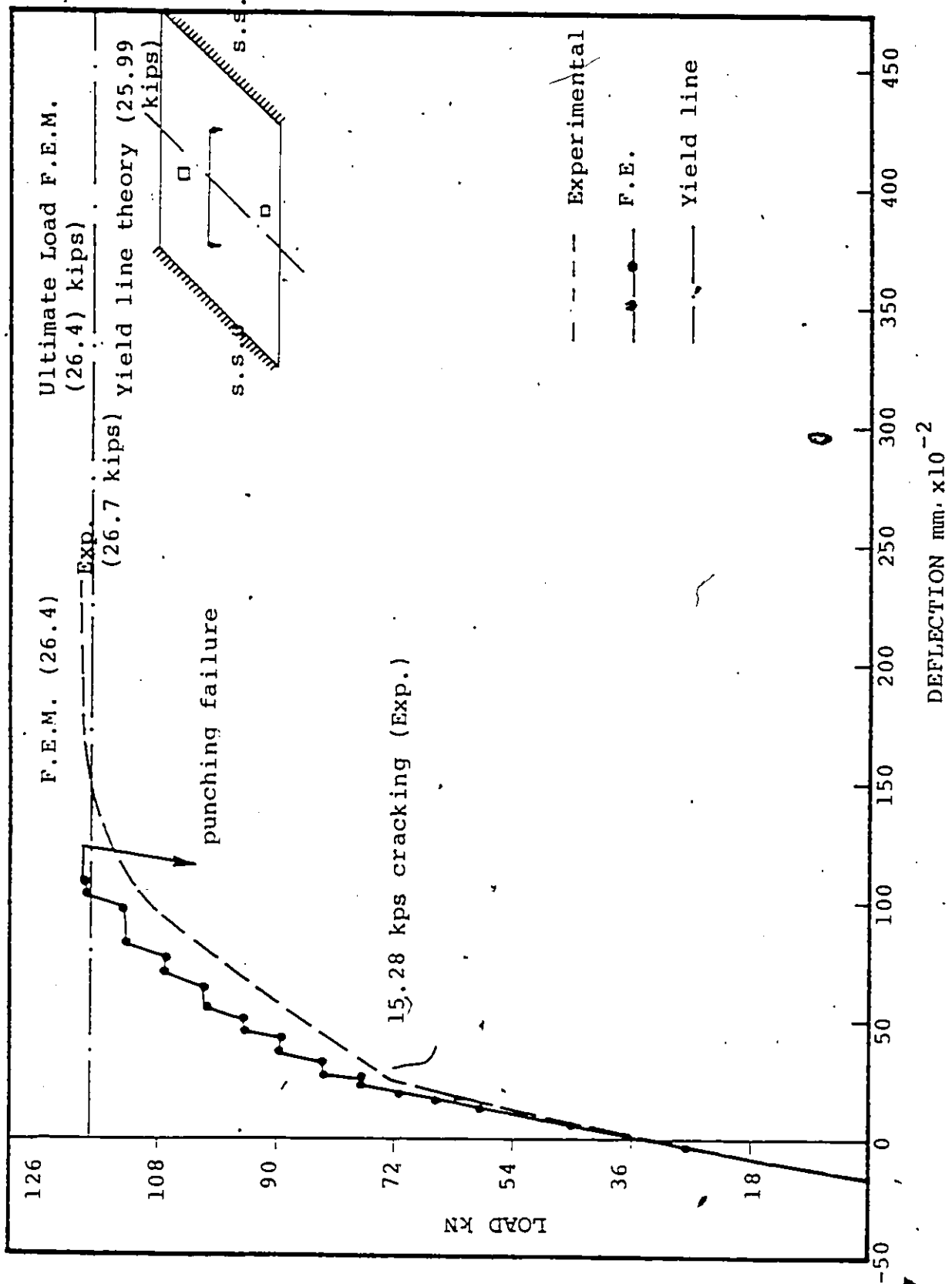


FIGURE 7.102 LOAD-DEFLECTION RELATIONSHIP FOR SKEW SLAB DUE TO TWO CONCENTRATED LOADS EACH AT THE CENTER OF EACH SPAN

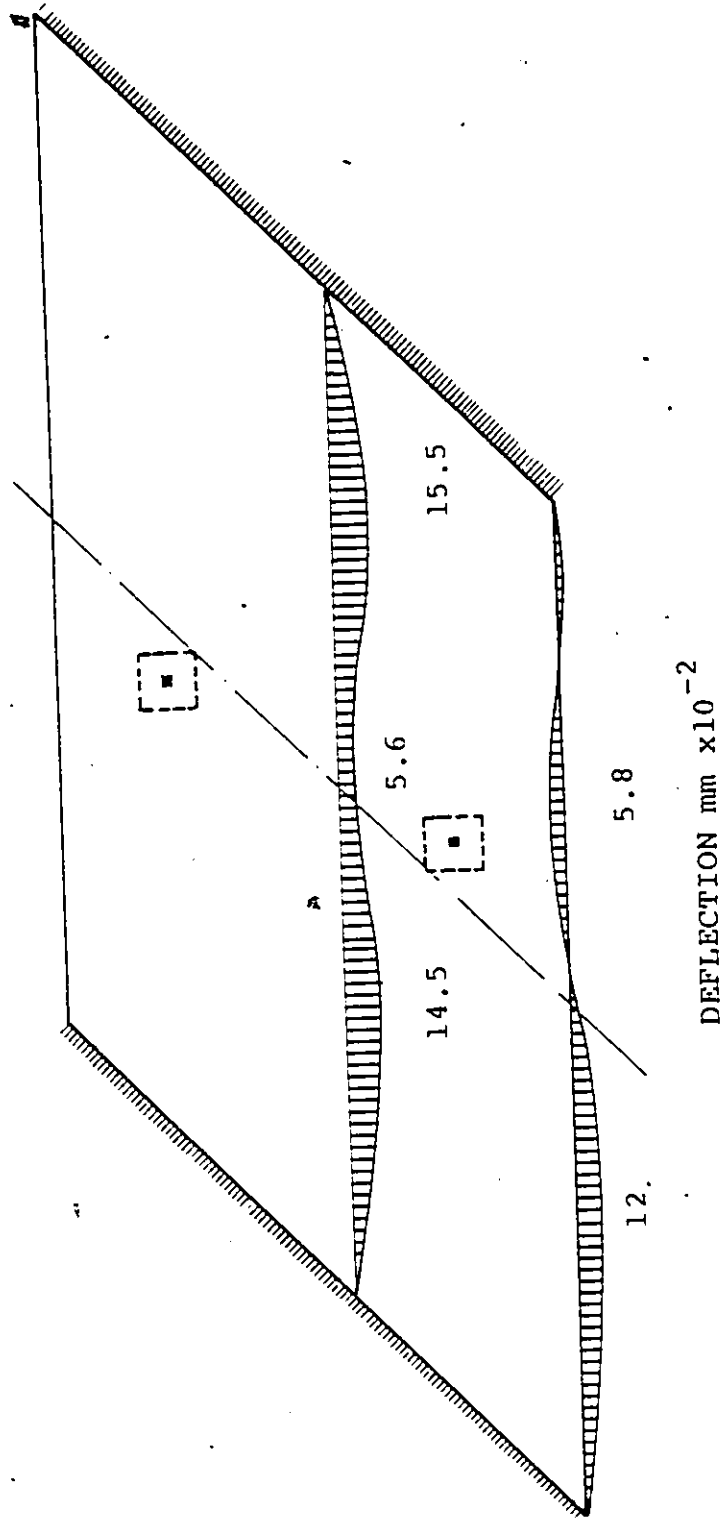


FIGURE 103 DEFLECTION PATTERN DUE TO ROTATING THE TWO COLUMNS ABOUT THE CENTER OF THE BRIDGE MODEL (PC4).

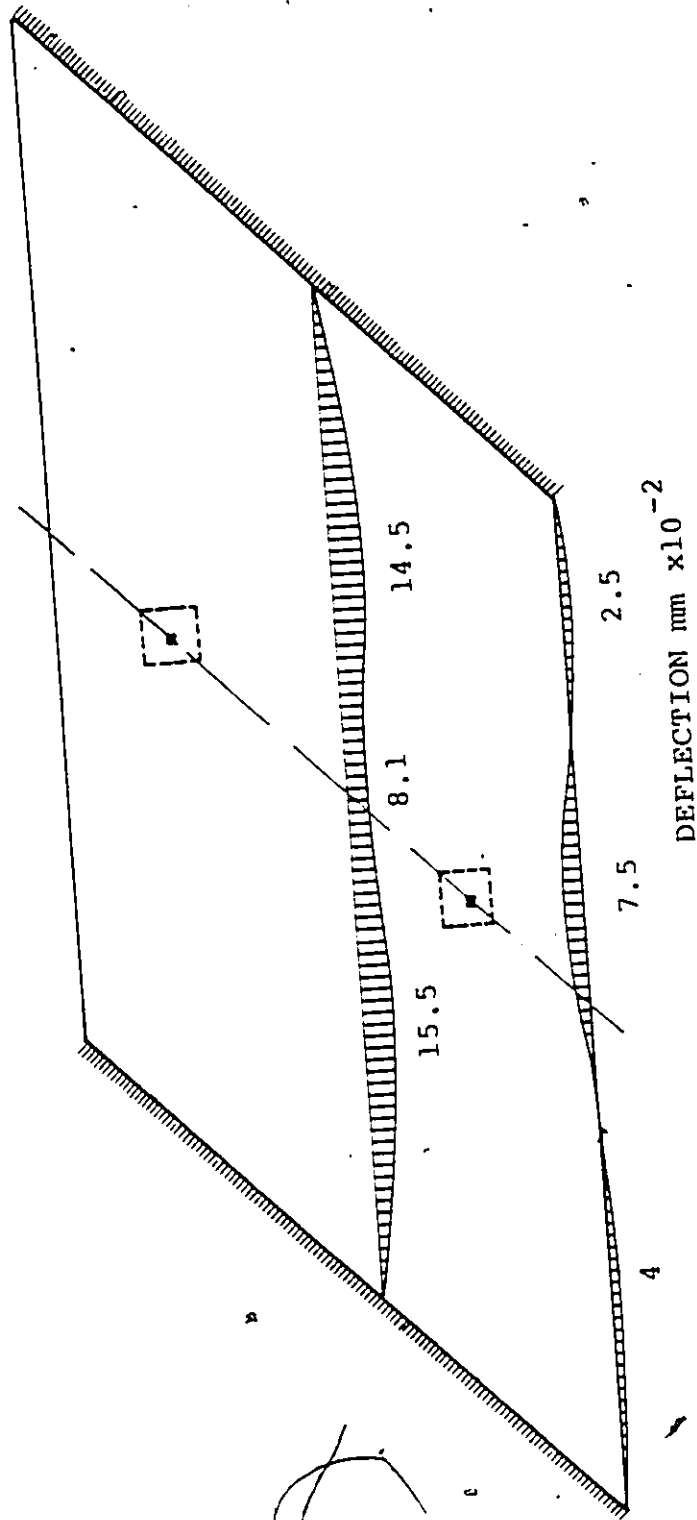


FIGURE 7.104 DEFLECTION PATTERN DUE TO ROTATING THE TWO INTERIOR COLUMNS ABOUT THE CENTER OF THE BRIDGE MODEL PC4.

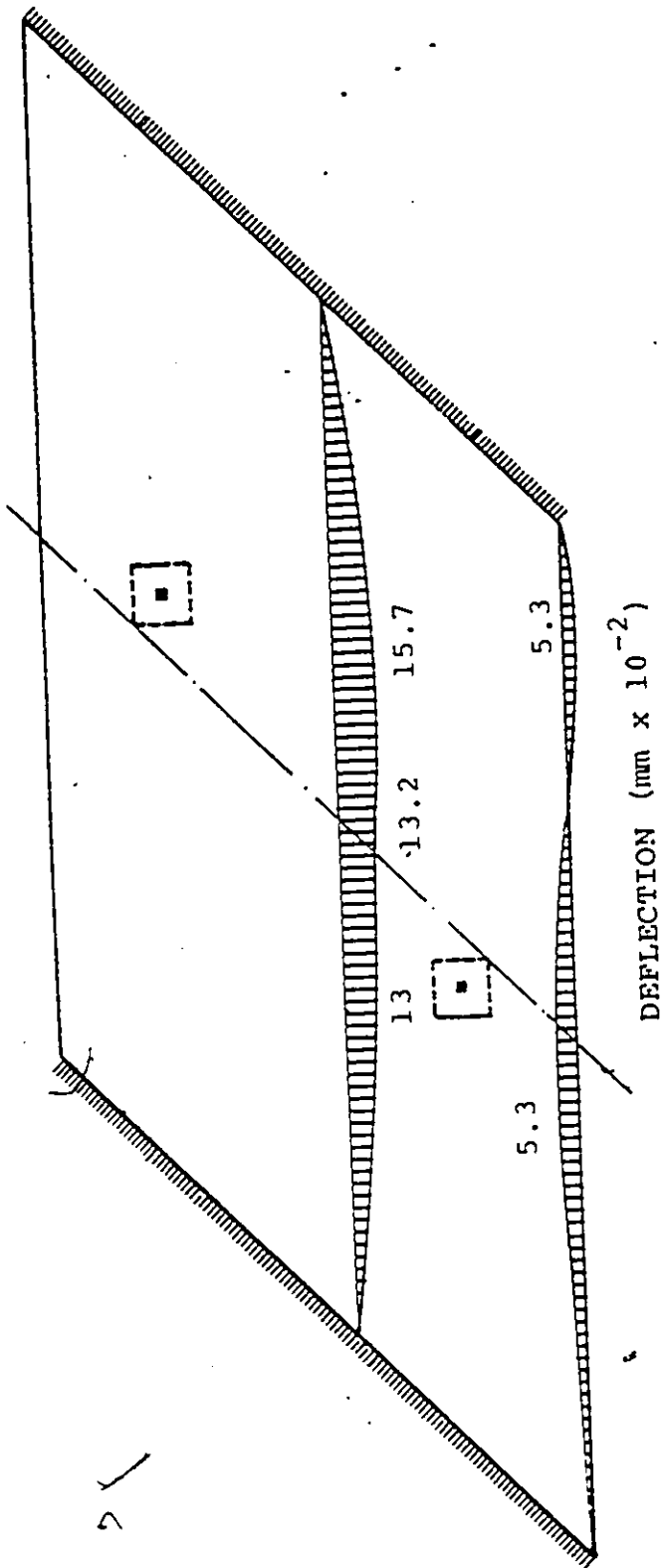


FIGURE 7.105 DEFLECTION PATTERN DUE TO ROTATING THE TWO INTERIOR COLUMNS ABOUT THE CENTER OF THE BRIDGE MODEL (PC4)

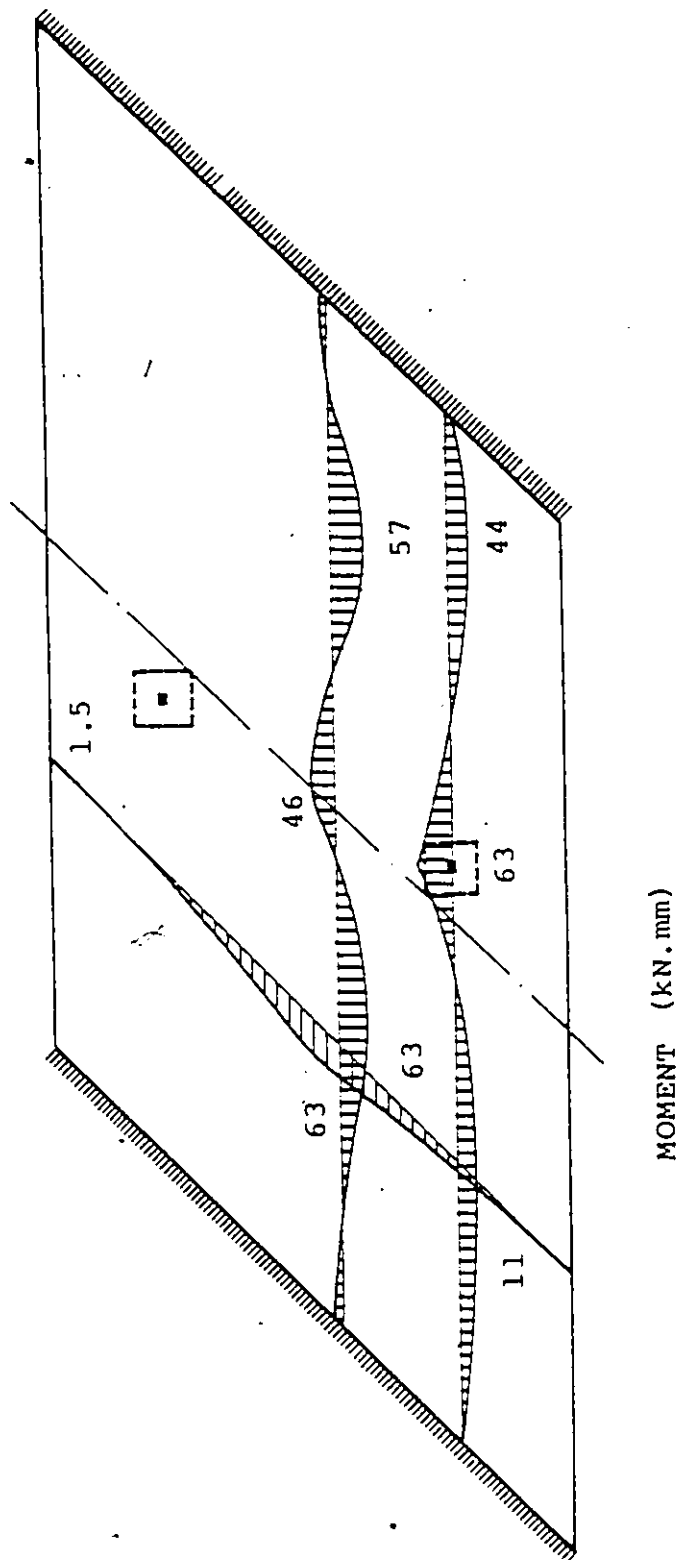


FIGURE 7.106 THE DISTRIBUTION OF MOMENT IN SLAB (PC4) DUE TO ROTATING THE TWO COLUMNS

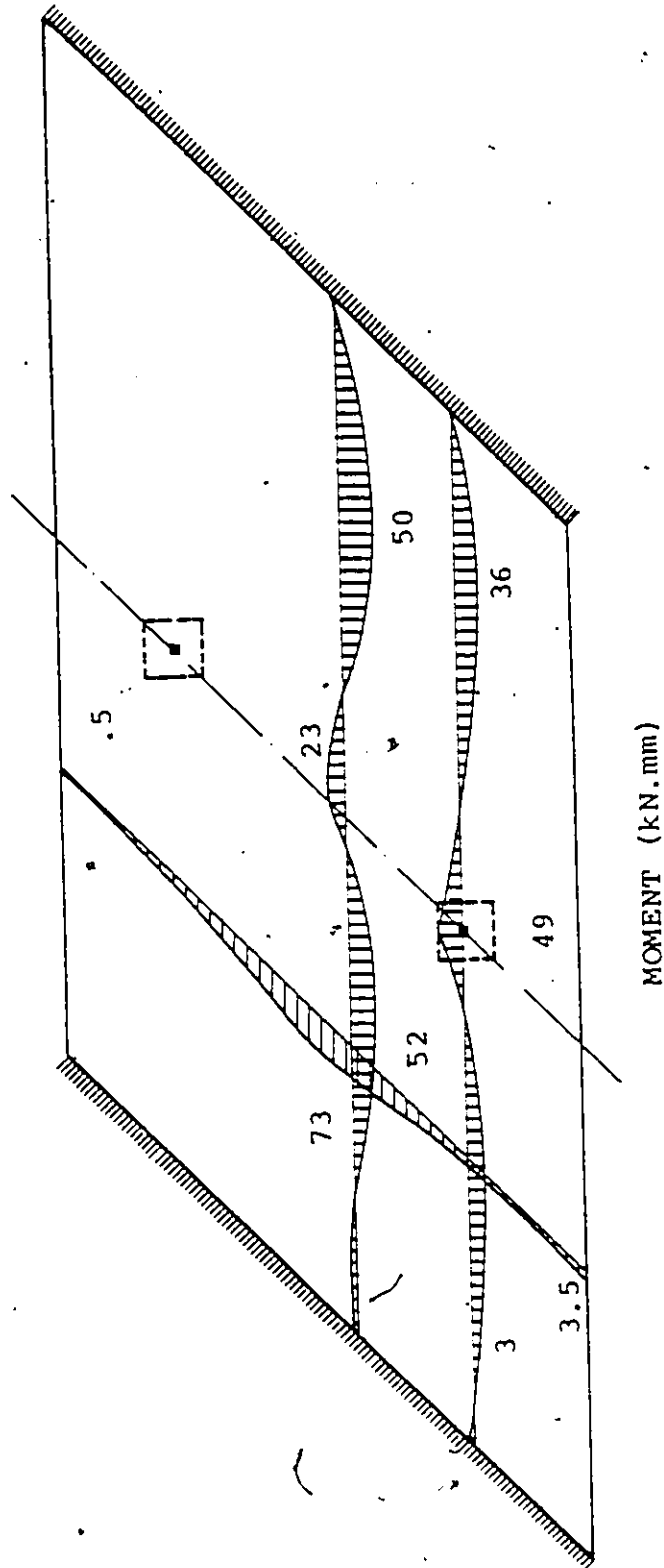


FIGURE 7.107 THE DISTRIBUTION OF MOMENTS IN SLAB (PC4) DUE TO ROTATING THE TWO COLUMNS ABOUT THE CENTER OF THE SLAB

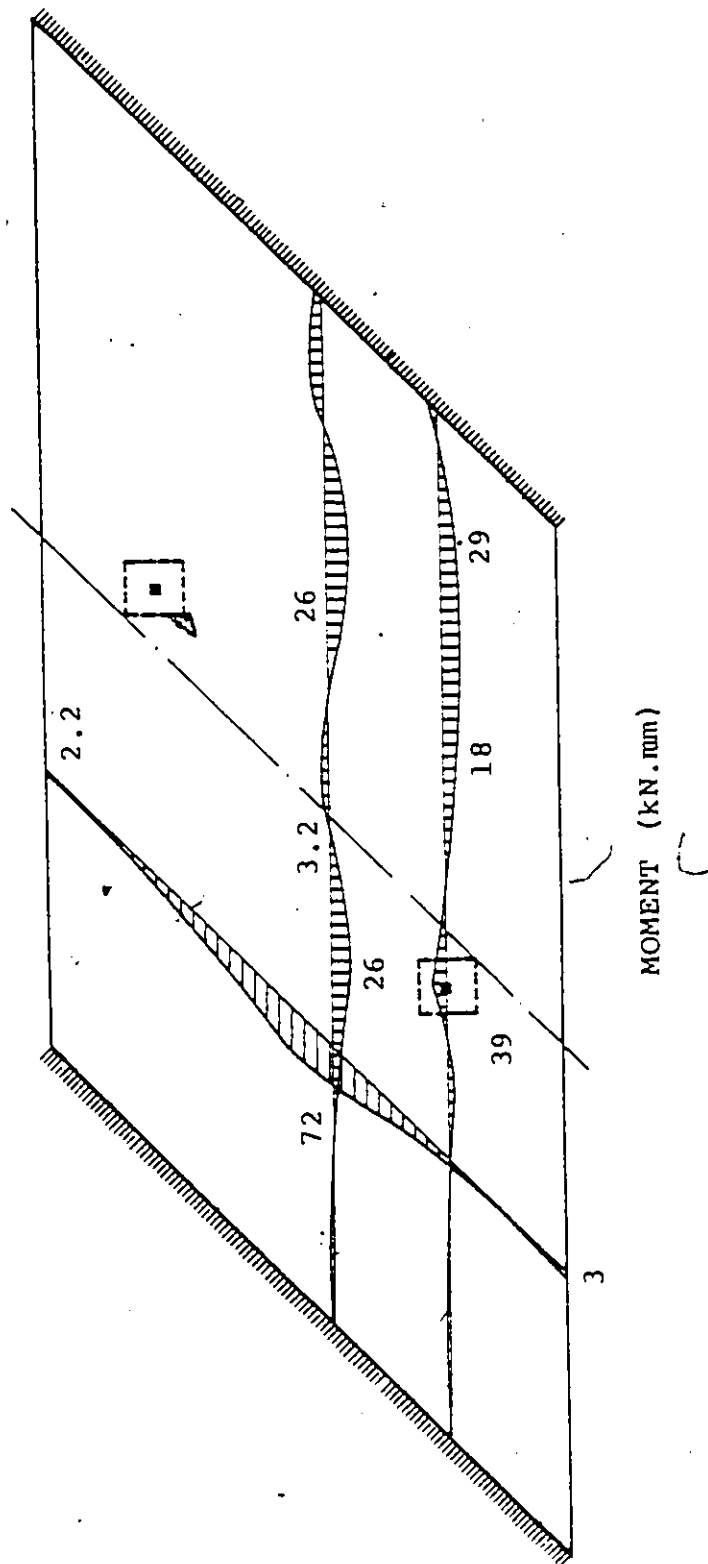


FIGURE 7.108 THE DISTRIBUTION OF THE MOMENT IN SLAB (PC4) DUE TO ROTATING THE TWO COLUMNS ABOUT THE CENTER OF THE SLAB.

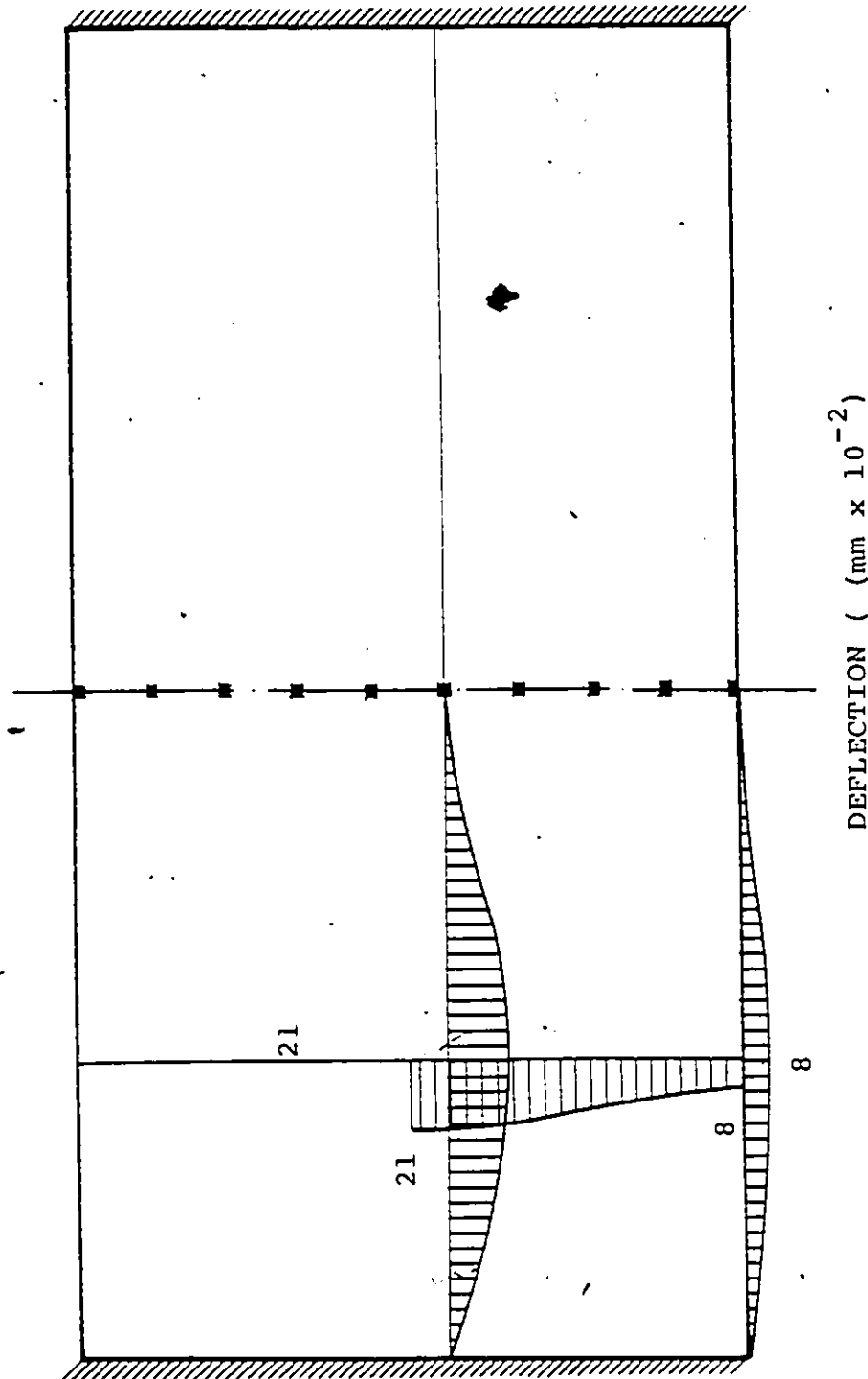


FIGURE 7.109 DEFLECTION PATTERN IN CONTINUOUS WAFFLE SLAB DUE TO TWO CONCENTRATED LOADS

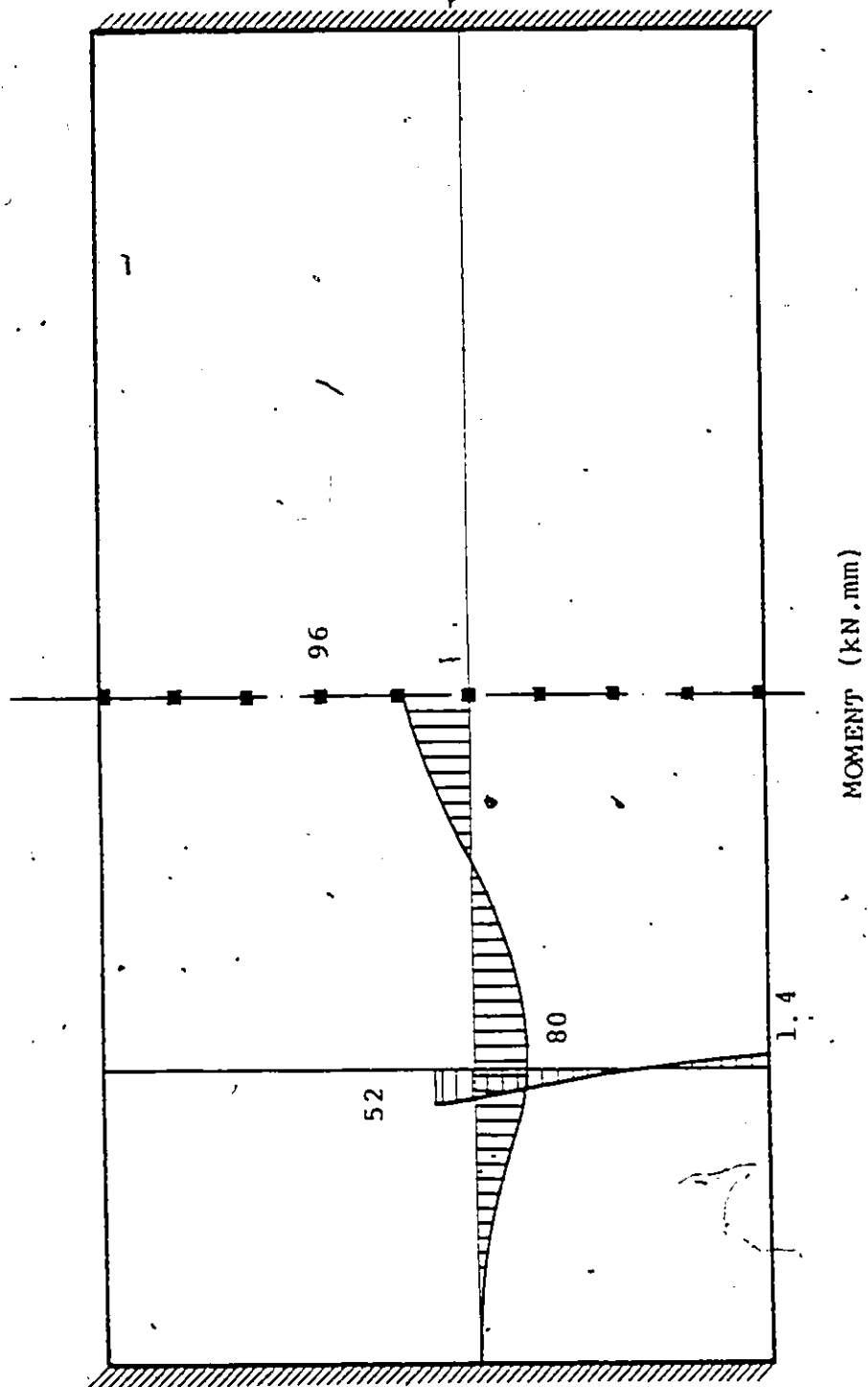


FIGURE 7.110 THE DISTRIBUTION OF THE MOMENT IN RECTANGULAR SLAB WITH CONTINUOUS PIER SUPPORTS DUE TO TWO CONCENTRATED LOADS

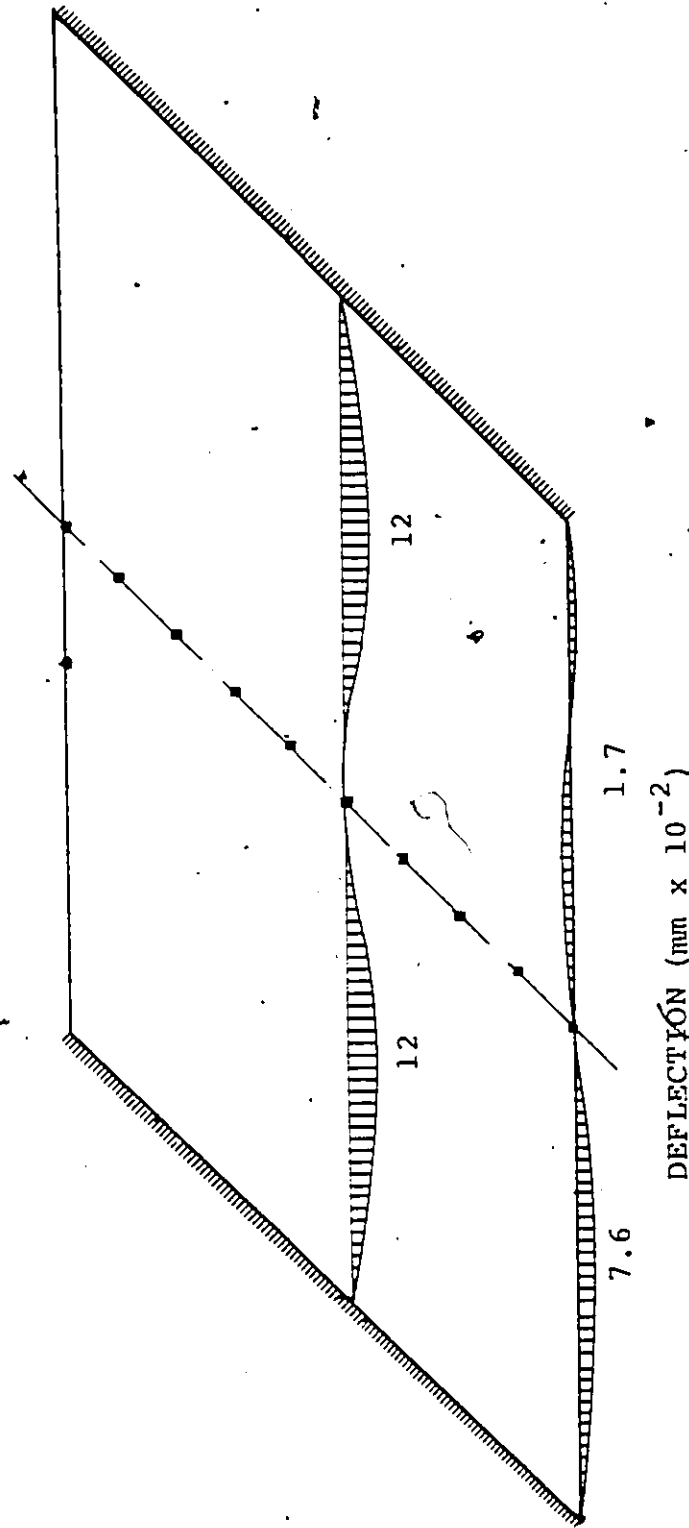


FIGURE 7.111 DEFLECTION PATTERN IN CONTINUOUS SKEW SLAB DUE TO TWO CONCENTRATED LOADS

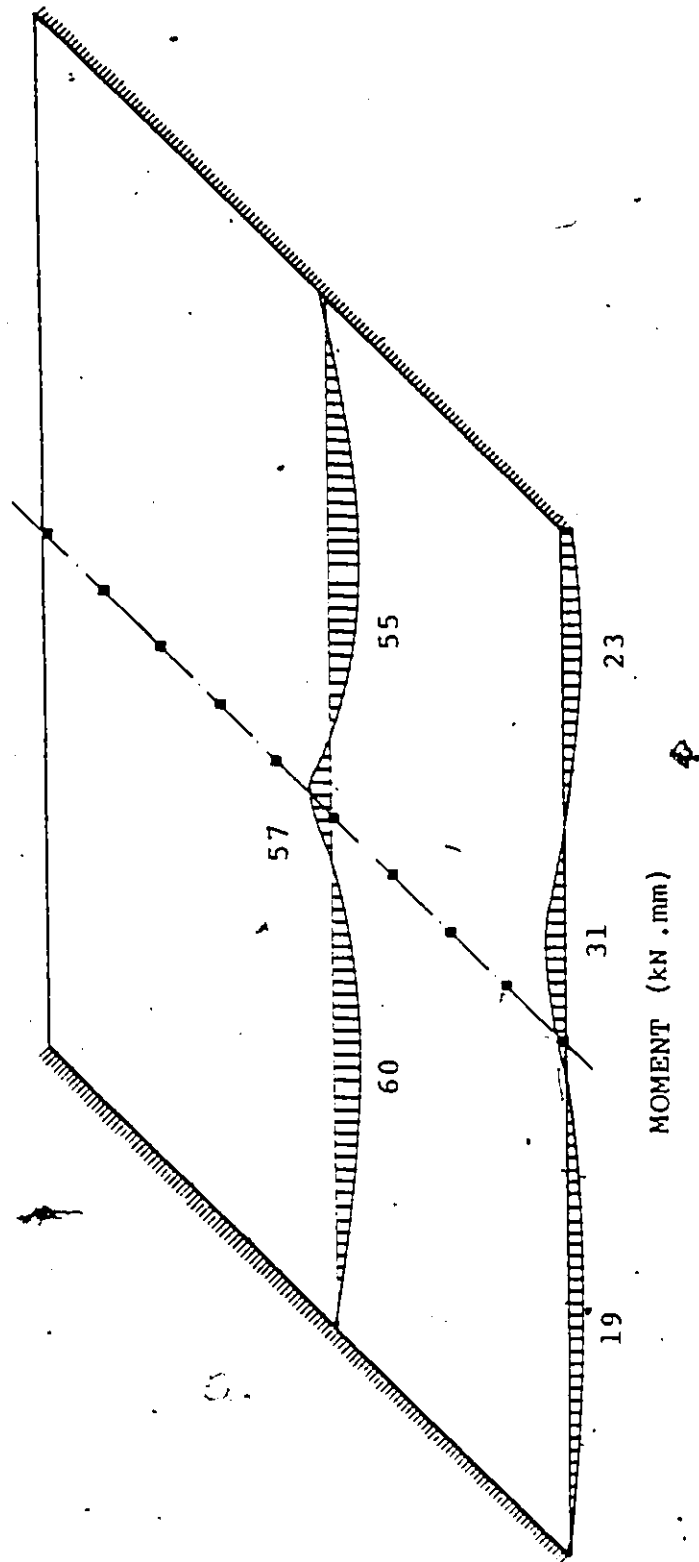


FIGURE 7.112 THE DISTRIBUTION OF THE MOMENT IN SKEW SLAB WITH CONTINUOUS PIER SUPPORTS

TABLES

TABLE 3.1

LIMITATIONS OF STRAND PROGRAMS

1. Number of nodes	500
2. Number of elements (plate and beam combined)	900
3. Half-band width	114
4. Number of rigid boundary nodes (at which all, or any degree of freedom is restrained)	100
5. Number of elastic boundary nodes (at which all, or any degree of freedom is elastically restrained)	100
6. Number of material types	100

TABLE 6.1
DETAILS OF TEST BRIDGE MODELS

Bridge model number (1)	Materials (2)	Skew angle, θ in degrees (3)	Model span, 2b, in inches (4)	Model width, 2a, in inches (5)	f'_c in kip per square inch (6)	E_c , in 10^3 kip per square inch (7)	Poisson's ratio μ (8)	Rigidities, in 10^3 kip-inch ² per inch ²					Rigidities of edge beam, in 10^3 kip-inch ²	
								D_x (9)	D_y (10)	D_1 (11)	D_2 (12)	D_{xy} (13)	EI (14)	GJ (15)
RC1	S.S.	0	84	71.5	5.0	4.0	0.20	10.7 ^b 1.9 ^c	10.9 1.9	0.80 0.05	0.80 0.05	1.7 0.4	0	0
RC2	S.S.	0	84	71.5	6.6	4.7	0.23	12.5 1.9	12.5 1.9	1.00 0.06	1.00 0.06	1.9 0.4	0	0
RC3	S.S.	45	84	101.1	4.7	3.9	0.20	10.3 1.8	10.5 1.8	0.7 0.05	0.7 0.05	1.5 0.4	0	0
PC1	S.S.	0	84	71.5	7.7	5.0	0.25	12.9 1.23	12.9 1.23	1.1 0.04	1.1 0.04	1.9 0.3	60	34
PC2	S.S.	45	84	101.1	8.3	5.2	0.26	13.4 1.2	13.4 1.2	1.2 0.04	1.2 0.04	2.1 0.3	63	35
PC3	C	0	99	49.5	8.7	5.3	0.26	13.7 1.3	13.7 1.3	1.3 0.03	1.3 0.03	2.1 0.3	65	36
PC4	C	45	99	70.	9.5	5.5	0.28	14.3 1.3	14.3 1.3	1.4 0.03	1.4 0.03	2.2 0.3	70	37

^a $D_{xy} = D_{yx}$; ^bRigidities based on uncracked section, Ref. (12,23); ^cRigidities based on cracked section, Ref. (12)

S.S. = simply supported; C = continuous

Notes: 1 in. = 25.4 mm; 1 ksi = 6.89 MPa; 1 k-in²/in = 114 kN-mm²/mm; 1 k-in² = 2.87 MN - mm²

5

TABLE 7.1

COLUMN REACTIONS DUE TO A SINGLE CONCENTRATED
LOAD 4 KIPS ACTING AT THE CENTER OF THE SPAN

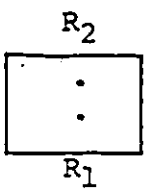
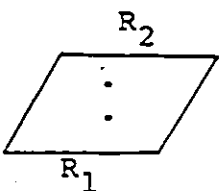
				
Method	Rectangular Slab		Skew Slab (45°)	
	R_1 (kips)	R_2 (kips)	R_1 (kips)	R_2 (kips)
Influence line	1.36	1.36	0.84	1.93
Finite element method	1.35	1.35	0.73	2.10
Experiment	1.34	1.34	0.88	1.80

TABLE 7.2
COLUMN REACTIONS USING FINITE
ELEMENT METHOD

Load Position	Rectangular Slab		Skew Slab	
	R ₁ (kips)	R ₂ (kips)	R ₁ (kips)	R ₂ (kips)
Single concentrated load at the center of the edge beam (4 kips)	3.4	.63	3.27	.46
Single concentrated load at the center of the span (4 kips)	1.35	1.35	0.70	2.10
Single concentrated load at the center of the slab model (4 kips)	1.96	1.96	1.9	1.9
Two concentrated loads, each acting at the center of the span (4 kips)	2.7	2.7	2.8	2.8
Two concentrated loads each acting at the center of the beam (4 kips)	6.7	1.21	7.45	.91

TABLE 7.3
COMPARISON OF THEORETICAL AND EXPERIMENTAL RESULTS
FOR DEFLECTIONS AND ULTIMATE LOADS

Bridge model number (1)	Central deflection at cracking load, in inches			Ultimate load, in kips			Cracking load		Maximum deflection at collapse in inches (10)
	Theory (2)	F.E.M. (3)	Experiment (4)	Yield line theory (5)	F.E.M. (6)	Experiment (7)	Cracking load		
							Exp. (8)	F.E.M. (9)	
RC1	0.020	0.021	0.022	0.81 ^a	0.80	1.10 ^a	0.36	0.38	2.00
RC2	0.019	0.020	0.023	2.45	2.32	2.80	1.10	1.12	2.50
RC3	0.017	0.020	0.019	4.00	3.90	4.50	1.70	1.76	2.25
PC1	0.002	0.002	0.002	5.69 ^b 6.04	5.40	6.00	2.00	2.16	0.60
PC2	0.006	0.009	0.008	10.44 ^b 12.27	11.40	12.10	6.00	6.60	0.18
PC3		0.009	0.011	24.50	24.70	25.0	14.15	14.96	0.25
PC4		0.009	0.010	26.00	26.40	26.7	15.28	15.84	0.20

^a psi for uniformly distributed load

^b Including load punch through plate deck.

NOTE: 1 inc. = 25.4 mm; 1 kip = 4.45 kN

APPENDICES

APPENDIX A

CRACKED AND UNCRACKED RIGIDITIES OF
WAFFLE SLAB STRUCTURES

APPENDIX A

1. Uncracked Rigidities of Waffle Slab

$$f'_{c28} = 9500 \text{ Ib/in}^2$$

$$E \text{ modulus of elasticity} = 57000 \sqrt{f'_c}$$

$$= 57000 \sqrt{9500}$$

$$= 5.55 \times 10^6 \text{ Ib/in}^2$$

$$\mu = \text{Poisson's ratio of concrete}$$

$$= \sqrt{f'_{ci}/350} = \sqrt{9500/350} = 0.28$$

$$\text{Modular ratio of concrete } (n) = \frac{E_s}{E_c} = \frac{30 \times 10^6}{5.55 \times 10^6} = 5.4$$

To find the N.A.

From Figure 3.2

$$e_x = \frac{(1.5)(3)(2.5) + [(5.5)(1)/2(1-.278^2)]}{1.5 \times 3 + [5.5 \times 1/(1-.278)]}$$

$$= \frac{11.25 + 2.98}{4.5 + 5.96} = 1.36 \text{ in.}$$

$$e_y = 1.36 \text{ in.}$$

Moment of inertia of rib

$$I_x = I_y = 1.5 \times 3 (2.5 - 1.36)^2 + \frac{1.53 \times 3^3}{12} = 9.20 \text{ in}^4$$

Flexural Rigidities

$$D_x = D + \{E_h (e_x - h/2)^2 / (1 - \mu^2)\} + E I_x / s_x$$

$$\begin{aligned}
&= \frac{E_h^3}{12(1-\mu^2)} + \{E_h(e_x - h/2)^2 / (1-\mu^2)\} + E I_x / s_x \\
&= \frac{5.55 \times 10^6}{12(1-.278^2)} + \frac{5.555 \times 10^6 \times 1(1.36-.5)^2}{(1-.278^2)} + \frac{5.55 \times 10^6 \times 9.22}{5.5} \\
&= 0.50 \times 10^6 + 4.4526 \times 10^6 + 9.3121 \times 10^6
\end{aligned}$$

$$D_x = D_y = 14.30 \times 10^6 \text{ lb. in}^2/\text{in}$$

$$\begin{aligned}
D_{1x} = \mu D'_x &= (0.278) \left[\frac{7.3 \times 10^6}{12(1-.278^2)} + \frac{7.31 \times 10^6 \times (1.36-.5)^2}{(1-.278^2)} \right] \\
&= 0.278 [0.66 \times 10^6 + 5.8593 \times 10^6] \\
&= 1.40 \times 10^6 \text{ lb. in}^2/\text{in}
\end{aligned}$$

$$I_{xy} = I_{xy1} + I_{xy2} + I_{xy3}$$

$$I_{xy1} = \frac{1}{2} \times .292 \times 5.5 \times 1^3 = 0.80 \text{ in}^4$$

$$I_{xy2} = .229 \times 3 \times 1.5^3 = 2.30 \text{ in}^4$$

$$I_{xy3} = 4 \times .8035(5.4-1)(.0314)^2 / 3.14 = 0.0031 \text{ in}^4$$

$$I_{xyl} = 0.803 \frac{(2.318 + 0.803)}{0.803} = 3.12 \text{ in}^4$$

$$\text{Total } I_{xy} = \frac{(3.121 + 2.318 + .003)}{5.5} = 0.99 \text{ in}^4/\text{in}$$

$$G_{yx} = \frac{E}{2(1+\mu)} = \frac{5.555 \times 1}{2(1+.278)} = 2.17 \times 10^6$$

$$D_{xy} = D_{yx} = 2.1733 \times 10^6 \times .989 = 2.15 \times 10^6 \text{ lb.in}^2/\text{in}$$

Axial Rigidities for Plane Stress Problem

From El. Sebakhy (23)

$$E'_x = E_x \left(\frac{1}{1-u^2} \right) + \frac{A_x}{h}$$

$$= 5.55 \times 10^6 \left[\left(\frac{1}{1-.278^2} \right) + \frac{(1.5)(3)/5.5}{1} \right] = 10.56 \times 10^6 \text{ lb.in}^2/\text{in}$$

$$E_y = 10.56 \times 10^6 \text{ lb.in}^2/\text{in}$$

$$E_1 = E_2 = 0.278 \frac{(5.55 \times 10^6)}{(1-.278^2)} = 1.67 \text{ lb.in}^2/\text{in}$$

$$G = \frac{5.55 \times 10^6}{2(1+.278)} = 2.17 \times 10^6 \text{ lb.in}^2/\text{in}$$

∴ for the STRAND program

$$D_{11} = E'_x h = 10.56 \times 10^6 \text{ lb.in}^2/\text{in}$$

$$D_{12} = E_1 h = 1.67 \times 10^6 \text{ lb.in}^2/\text{in}$$

$$D_{22} = E_y h = 10.56 \times 10^6 \text{ lb.in}^2/\text{in}$$

$$D_{33} = Gh = 2.17 \times 10^6 \text{ lb.in}^2/\text{in}$$

2. Rigidities of Cracked SectionA. Cracked Section in Bottom Surface of Concrete

To find the N.A. in Fig. 3.2

$$Kd_x = K$$

$$nA_s [h + d_x - d'] - Kd_x]$$

$$-S_x (Kd_x)^2 / 2(1-u^2) = 0$$

$$5.4 \frac{(\pi x .2^2)}{4} [(4-1.0) - Kd_x] - 5.5(Kd_x^2)/2(1-.278^2)$$

$$.5089 - .16964 Kd_x - 2.98 Kd_x^2 = 0$$

$$Kd_x^2 + .056921 Kd_x - .1707 = 0$$

$$Kd_x = \frac{(-.0569218 \pm \sqrt{.0032408 + 4x.1707})}{2} = +.038 \text{ in}$$

$$I_{cx} = \alpha_x (Kd_x)^3/3$$

$$= 5.5(.3856)^3/3 = 0.105 \text{ in}^4$$

$$I_{cy} = 0.105 \text{ in}^4$$

$$I_{sx} = 5.4 \frac{(\pi x .2^2)}{4} [3-.3856]^2 = 1.16 \text{ in}^4$$

$$D_x = 5.55 \times 10^6 [1.159545 + \frac{0.10551}{(1-.278^2)}] / 5.5$$

$$= 1.285 \times 10^6 \text{ lb.in}^2/\text{in}$$

$$D_y = 1.285 \times 10^6 \text{ lb.in}^2/\text{in}$$

$$D_1 = .278 \times 0.114951 \times 10^6 = 0.0319 \times 10^6 \text{ lb.in}^2/\text{in}$$

$$D_2 = 0.0319 \times 10^6 \text{ lb.in}^2/\text{in}$$

Torsional Rigidities

$$= (D_{xy} + D_{yx} + D_1 + D_2) / 2 D_x D_y^{1/2}$$

$$= (2.1494 + 2.1494 + 1.377 + 1.377) \times 10^6 / 2 \times \sqrt{14.2647 \times 14.2647 \times 10^{12}}$$

$$= 0.247$$

$$\begin{aligned}
 D_{xy} &= (D_x D_y)^{1/2} \\
 &= 0.2472 \sqrt{(1.285 \times 1.285 \times 10^{12})} \\
 &= 0.317 \times 10^6 \text{ lb.in}^2/\text{in}
 \end{aligned}$$

B. Cracked Section in Top Surface of the Concrete

To find the N.A. in Fig. 3:2

$$(5.4)(.031415)(3.25 - Kd_x) - \frac{1.5(Kd_x^2)}{2(1 - .278^2)} = 0$$

$$0.55134 - 0.16964 Kd_x - .8128 Kd_x^2 = 0$$

$$Kd_x^2 + 0.2087 Kd_x - .678 = 0$$

$$\begin{aligned}
 Kd_x &= \frac{-0.2087 \pm \sqrt{.0435 + 4 \times .678}}{2} \\
 &= \frac{-0.2087 \pm 1.6599}{2} = 0.7256 \text{ in}
 \end{aligned}$$

$$I_{cx} = \frac{1.5 \times .7256^3}{3} = 0.191$$

$$I_{sx} = (5.4)(0.031415)(3.25 - .7256)^2 = 1.08 \text{ lb.in}^2/\text{in}$$

$$D_x = 5.55 \times 10^6 [1.08 + 1.91]/5.5 = 1.282 \times 10^6 \text{ lb.in}^2/\text{in}$$

$$D_y = 1.282 \times 10^6 \text{ lb.in}^2/\text{in}$$

$$D_1 = 0$$

$$D_2 = 0$$

$$\alpha = .247 \text{ (from previous calculation)}$$

$$D_{xy} = .247(1.282 \times 10^6 \times 1.282 \times 10^6) = 0.317 \times 10^6 \text{ lb.in}^2/\text{in}$$

APPENDIX B

THEORETICAL COLLAPSE LOAD BY
YIELD-LINE THEORY

APPENDIX B

CALCULATIONS OF THEORETICAL
COLLAPSE LOADS

All computations are performed with reference to Fig. 4.1. Given data: $A_s = A'_s = 0.0368 \text{ in}^2$ (24 mm^2); $f_y = 40 \text{ ksi}$ (276 MPa); $b = 42 \text{ in.}$ (1062 mm); $\ell = 71.5 \text{ in.}$ (1816 mm); $s_x = s_y = 5.5 \text{ in.}$ (140 mm); unfactored $q_D = 0.2 \text{ psi}$ (1.4 kPa).

(1) Bridge Model (RC1) Subjected to Uniformly Distributed

Load: [$f'_c = 5 \text{ ksi}$ (34.5 MPa)

(From $C = T$, or $(\beta f'_c) (ks_y) = A_s f_y$, with $\beta = 0.80$ (10),
 $k = 0.067 \text{ in.}$ (1.7 mm).

Therefore

$$m_1 = A_s f_y (\text{lever arm}) / s_y = (0.0368) (40,000) (4.0 - 0.625 - 0.033) / 5.5$$

$$= 894 \text{ lb-in./in.} \text{ (4.0 kN.m/m). From Eq. 4.10,}$$

$$q_u = (2) (894) / (42)^2 = 1.01 \text{ psi (7.0 kPa)}$$

$$\text{with } q_D = 0.20 \text{ psi (1.4 kPa) the net } q_u = 1.01 - 0.2 = 0.81 \text{ psi (5.6 kPa).}$$

(2) Bridge Model (RC2) Subjected to Concentrated Load at

Center: [$f'_c = 6.6 \text{ ksi}$ (45.5 MPa)]

Here $k = 0.056 \text{ in.}$ (1.2 mm). As before, $m_1 = A_s f_y$
(lever arm) / $s_y = 896 \text{ lb-in./in.}$ (4.0 kN.m/m). From

Eq. 4.16 with $q_D = 0.2$ psi (1.4 kPa), $P_u = 2.45$ kips (11.0 kN).

(3) Bridge Model (RC3) Subjected to Concentrated Load at

Center: [$f'_c = 4.7$ psi (32.4 MPa)]

From $C = T$, or $(0.83)(4700)(k)(5.5) = (0.0368)(40,000)$,
 $k = 0.07$ in. (1.8 mm).

Therefore

$$m_1 = (0.0368)(40,000)(4.0 - 0.625 - 0.035)/5.5 =$$

$$894 \text{ lb-in./in. (4.0 kN.m/m)}$$

and,

$$vm_1 = (0.0368)(40,000)(4.0 - 0.875 - 0.035)/5.5 = 827$$

$$\text{lb-in./in. (3.6 kN.m/m)}$$

Substituting in Eq. 4.15, with $\theta = 45^\circ$, yields $P_u =$
 4.00 kips (17.9 kN).

(4) Bridge Model (PC1) Subjected to Concentrated Load at

Center of Edge Beam: [$f'_c = 7.7$ ksi (53 MPa)]

f_{su} in the y-direction = 4 kips (17.80 kN); f_{su} in the
 x-direction = 2.85 kips (12.6 kN) [NOTE: Values of f_{su}
 are obtained from the measured strains; if unknown, use
 $f_{su} = 1.15 f_e$.] From $C = T$ in the y-direction: $4000 =$
 $(0.66)(7.7)(k)(5.5)$, $k = 0.14$ in. (3.6 mm); thus $m_1 =$
 $(4000)(3.0 - 0.07)/5.5 = 2.13 \text{ kip-in./in. (9.5 kN.m/m)}$.

The negative moment of resistance of section at rupture

of the concrete, assuming a modulus of rupture of 400 psi (2.76 MPa), is $m_2 = 0.71$ kip. in./in. (3.15 kN.m/m); from symmetry of section, $nm_2 = 0.71$ kip in./in. (3.15 kN.m/m). The moment of resistance of the edge beam $M_B = 1.5$ kip. in (6.6 kN.m). Substituting in Eq. 4.22, the collapse load becomes $P_u = 5.69$ kips (35.3 kN). Considering the punching shear capacity of the plate deck, the average punching distance is assumed as $0.5k$, due to the position of the load on the bridge model, with an effective perimeter p of 10 in. (254 mm); thus, $P_{us} = (0.07)(10)(500) = 0.35$ kips (1.45 kN). Therefore the total theoretical collapse load increases to $P_u = 5.69 + 0.35 = 6.04$ kips (26.8 kN).

(5) Bridge Model (PC2) Subjected to Concentrated Load at

Centre: [$f'_c = 8.3$ ksi (57 MPa)]

f_{su} in the y-direction = 4 kips (17.8 kN); f_{su} in the x-direction = 3.5 kips (15.6 kN). From $C = T$ in the y-direction: $4000 = (0.65)(8.3)(k)(5.5)$, hence $k = 0.14$ in. (3.6 mm); thus $m_1 = (4000)(3.0 - 0.07)/5.5 = 2.13$ kip. in./in. (9.5 kN.m/m); similarly, $vm_1 = 1.706$ kip-in./in (7.5 kN.m/m). The moment resistance of the edge beam $M_B = 1.5$ kip. in (6.6 kN.m). Therefore, substituting in Eq. 4.13, with $\theta = 45^\circ$, $P_u = 10.44$ kips (46.3 kN). The load required to punch through the plate deck a distance of 0.14 inch (3.6 mm) is $P_{us} =$

(perimeter of loading plate) $(0.14)(500) = 1.83$ kips
 (8.2 kN). Therefore total collapse load $P_u = 10.44 +$
 $1.83 = 12.27$ kips (54.6 kN).

- (6) Bridge Model (PC3) Subjected to Two Concentrated Loads,
each applied at Center of Each Span Panel: $f'_c = 8.70$
 ksi (60 MPa)

Area of prestressing steel = 0.0314 in^2 (20 mm^2).

Maximum yield stress of the steel = 178 ksi (1230 MPa)

Initial average longitudinal prestressing force =
 3.3 kips (14.7 kN).

Longitudinal prestressing force at punching failure =
 $3.3 \times 1.15 = 3.8$ kips (16.9 kN).

Initial average transverse prestressing force = 3.0
 kips (13.4 kN).

Transverse prestressing force at punching failure =
 $3 \times 1.15 = 3.5$ kips (15.6 kN)

To find the depth of stress block at ultimate load

∴ for +ve moment, and from $C = T$, from Eq. 4.1,

$$3.80 = (0.65)(8.70) k \quad (5.5)$$

$$\therefore k = 0.122 \text{ in (3 mm)}$$

$$m_1 = 3.8 (3.0 - 0.061) / 5.5 \cong 2.03 \text{ kip.in/in (9.0 kN.m/m)}$$

For -ve moment, and from $C = T$

$$3.80 = (0.65)(8.70) k \quad (1.5)$$

$$\therefore k = 0.447 \text{ in (11.4 mm)}$$

$\therefore m_2 = 3.8(3.19 - 0.22)/5.5 = 2.05 \text{ kip.in/in (9.1 kN.m/m)}$ substituting in Eq. 4.27, with $M_B = M'_B = m_D = 0$
 $P_u = 12.22 \text{ kips (54.4 kN)}$
 $\therefore \text{the total load} = 2P_u = 24.44 \text{ kips (108.8 kN)}$

- (7) Bridge Model (PC4) Subjected to Two Concentrated Loads,
each at the center of one span: $f'_c = 9.50 \text{ ksi (65 MPa)}$
 Initial average longitudinal prestressing force = 2.70
 kips (12 kN); longitudinal prestressing force at punching
 failure = $2.70 \times 1.15 = 3.10 \text{ kips (13.8 kN)}$; initial
 average longitudinal prestressing force = 2.90 kips (12.9
 kN); lateral prestressing force at punching failure =
 $2.90 \times 1.15 = 3.3 \text{ kips (14.8 kN)}$. The depth of the
 stress block k , from Eq. 4.1,
 $3.1 = (0.65)(9.5) k (5.5)$
 $\therefore k = 0.091 \text{ in longitudinal direction}$
 $\therefore \text{from Eq. 4.2}$
 $m_1 = 1.67 \text{ kips. in/in (7.43 kN.m/m)}$
 $k = 0.36 \text{ in (9 mm)}$
 $m_2 = 1.86 \text{ kip. in/in (8.2 kN.m/m)}$

Transverse Direction

For tension at bottom surface $m_1 = 0.859 \text{ kip. in/in}$
 (3.8 kN.m/m). For tension at top surface $m_2 = 1.44$
 kip. in/in (6.4 kN.m/m). From Fig. 4.5 and after

determining point 0

$$x_1 = 22.0 \text{ in } (.56 \text{ m}); \quad x_2 = 27.5 \text{ in } (.7 \text{ m})$$

$$x_3 = 13.2 \text{ in } (.34 \text{ m}); \quad x_4 = 16.5 \text{ in } (.42 \text{ m})$$

$$x_5 = 30.8 \text{ in } (.78 \text{ m}); \quad x_6 = 38.5 \text{ in } (.97 \text{ m})$$

Substituting the assumed deflections in Eq. 4.30,

$$\begin{aligned} P.2\delta &= 2 [(m_1 (24.75) (\delta/27.5 + \delta/38.5)/2 \\ &\quad + m_1 (24.75) (.75\delta/22 + 1.25\delta/30.8)/2 \\ &\quad + m_1 (24.75) (0.5\delta/16.1 + 0)/2 \\ &\quad + m_1 (24.75) (.75\delta/22 + .75\delta/22)/2 \\ &\quad + m_1 (24.75) (0 + .5\delta/16.1) + m_1 (24.75) (0 + \delta/27.5) \\ &\quad + m_2 (24.75) (1.25\delta/30.8 + .75\delta/22)/2 \\ &\quad + m_2 (24.75) (.75\delta/22 + .75\delta/13.2)/2 \\ &\quad + \mu m_1 (22) (0 + .5\delta/24.75)/2 \\ &\quad + \mu m_1 (22) (.5\delta/24.75 + .5\delta/24.75)/2 \\ &\quad + \mu m_1 (12.17) (2) (.5\delta/24.75) + \mu m_1 (2.75) (2) (\delta/24.75) \\ &\quad + \mu m_2 (5.75) (.5\delta/24.75) (2)] \\ P.2\delta &= 2 [(.77142 + .924 + .384 + .843 + .768 + .90) m_1 \delta \\ &\quad + (.924 + 1.125) m_2 \delta + (.222 + .444 + .491 + .222) \mu m_1 \\ &\quad + .232 \mu m_2] \\ 2P &= (9.184 m_1 + 4.098 m_2 + 2.761 \mu m_1 + .464 \mu m_2) \\ \therefore 2P &= 15.337 + 7.622 + 2.371 + .668 \end{aligned}$$

The Total Load = 26 kips (115.7 kN)

APPENDIX C.

THE INPUT DATA FOR THE STRAND PROGRAM

NOTATIONS OF STRAND PROGRAM

NFOR	Input file on (disk) or tape
NPROB	Number of problems to be solved in one run
NL	Results from SAAD to be kept
NSIZ	Max. half-band width
NAVE	Average nodal stresses from SAADS
NCEN	Central element stresses required from SAADS
KEEP	Element stiffnesses to be store for future run
NDF	Number of degrees of freedom at a node
AL	Length of the bridge along x axis
BL	Bridge width along y axis
ALPHA	Angle of skew (anti-clockwise from x axis
NDIV	Number of the divisions across the bridge width
NEQI	Are the above divisions equal
NSPAN	Number of regions over the length
MDIV	Number of divisions over the length of the bridge
K	Region number
NDVS	Number of divisions in the region
NEQ2	Are the above divisions equal
SL	Length of the region along x axis
NBEAM	Number of rows of the beam element
NPMAT	Number of the type of plate material

MPA		Number of the plate element material	
NBMAT		Number of the types of beam material	
IPR		Is the deck to be prestressed	
GASH(I)	DX DY D1 DXY	Plate rigidities	
IG		Material type number	
GASH(I)	D11 D22 D12 D33 t1	Elastic constants	
I1 J1	ith) jth)	Starting point of plate material	
I2 J2	ith) jth)	Ending point of the plate material	
MAIN		Material type number	
MB		Number of rigidly restrained boundary nodes	
NST		Number of elastically restrained boundary nodes	
I1 J1	ith jth	Grid cord. of restrained node	
NFIX(N)	W θx θy		Plate Banding
US(N,I), I=1,3	W θx θy	Specified displacement	
I1 J1 X Y ST(I)		Specified X Specified Y	Plane Stress

Elastically

I1 ith
J1 jth

Grid Co-ord. of the restrained nook

(ST(N,I),I=b3)

Stiffness for W
Stiffness for θ_x
Stiffness for θ_y

Bending

Plane Stress

NLD

number of load cases

Load case

I1

Load case number

subtracting

NOPRINT

are results to be printed

TLOAD

Load case title

LPA

Number of U.D.L.

NKEL

Number of knife edge

NHB

Number of abnormal vehicle

Bending

NPL

Number of nodes loaded with
point load

NBEAM

Number of beam load

Plane stress

I1 1th)

J1 jth)

Grid Co-ord of the load case node

R(I)

Load in the w direction
Load in the θ_x direction
Load in the θ_y direction


DATA PREPARATION FOR INPUT2

Card Type	Column on Card	Description
1		FORM OF OUTPUT CARD
		One Card
	5	0 - Input file for SAADS is to be generated in formatted BCD form on punch cards
		1 - Input file for SAADS is to be generated as binary file on magnetic tape or disc units
2		PROBLEM CARD
		One card
	1-5	Number of the problems to be solved in one run
3		TITLE CARD
		One card
	1-72 ⁺	Title of problem
4		UNIT CARD
		One card
	1-72+	Description of units used in the problem
5		MESH TYPE CARD
		one card
	5	0 - Mesh of a parallelogram type
		1 - Mesh of a circular type

Card Type	Column on Card	Description
		2 - Mesh of a transitional spiral type
		3 - Mesh of a pseudo-regular type
6		CONTROL CARD
		One Card
	5	Are the results from SAADS to be kept on a magnetic file?
		0 - No
		1 - Yes
	6-10	Maximum half-band width implied by coupling the elastic boundary conditions. If there is no coupling fill in as zero
	15	Are average nodal stresses required from SAADS?
		0 - No
		1 - Yes
	20	Are centroidal element stresses required from SAADS?
		1 - No
		0 - Yes
	25	Are element stiffnesses to be stored on a magnetic tape for future runs?
		0 - No
		1 - Yes
	30	Number of the degrees of freedom at a node (for plane stress = 2; for plate bending = 3)

Continue at Card Type 7 if the mesh is of a regular type (parallelogram, circular or transition spiral)

Continue at Card Type 10 if the mesh is of a pseudo-regular type

Card Type	Column on Card	Description
7		GEOMETRY CONTROL CARDS
		Two cards
7A		Card one
	1-10*	(a) Parallelogram type: Length of the bridge [✓] side measured along the X axis
		(b) Circular type: Angle in degrees subtended by the bridge [✓]
		(c) Transition spiral type: Length along the inside edge of the bridge [✓]
	11-20*	(a) Parallelogram type: Bridge [✓] width measured parallel to the Y axis
		(b) Circular on transition spiral type: Bridge [✓] width measured along a radius
	21-30*	(a) Parallelogram type: Contained angle of skew in degrees between the bridge [✓] sides measured anti-clockwise from the X axis at the origin
		(0° < θ < 180°)
		(b) Circular type: Radius of the inside edge of the bridge [✓]
		(c) Transition spiral type: Minimum radius of the inside of the bridge [✓]
7B		Card two
	1-5	Number of the divisions across the bridge [✓] width
	10	Are the above divisions equal? 
		0 - No
		1 - Yes

☛ For plane stress analysis replace 'bridge' by 'plate'

Card Type	Column on Card	Description
	11-15	Number of the regions over the length of the bridge [✓]
	16-20	Number of the divisions over the length of the bridge [✓]
8		WIDTH DIVISION CARDS
		One card per each division. These cards are omitted if the divisions are of equal width
	1-10	Number of the division
	11-29*	(a) Parallelogram type: Division width measured parallel to the Y axis (b) Circular or transition spiral: Division width measured along a radius
9		LENGTH DIVISION CARDS
		This set is repeated for each region. If the region contains equal division widths only subset 9A is required. If the region contains unequal divisions subsets 9A and 9B must be specified
9A		One card
	1-5	Number of the region. The numbering must be from one and be sequential
	6-10	Number of the divisions in the region
	15	Are the above divisions equal? 0 - No 1 - Yes
	16-25*	(a) Parallelogram type: Length of the region measured along the X axis

[✓] For plane stress analysis replace 'bridge' by 'plate'

Card Type	Column on Card	Description
9A	Continued 16-25*	(b) Circular type: Angle in degrees subtended by the region (c) Transition spiral: Length of the region measured along the inside edge of the bridge*
9B		One card for each division in the region. This subset is omitted if the divisions are equal
	1-10	Number of the division. The numbering must be from one and be sequential for each region
	11-20*	(a) Parallelogram type: Length of the division measured along the X axis (b) Circular type: Angle subtended by the division (c) Transition spiral: Length of the division measured along the inside edge of the bridge*
	Continue on Card Type 12	
10		GEOMETRY CONTROL CARD (PSEUDO - REGULAR MESH) One card
	1-5	Number of the divisions across the width of the bridge*
	6-10	Number of the divisions over the length of the bridge*
	15	0 - Mesh of triangles as in Fig. 2.3(b) Diagonal from i_{m+1}, j_n to i_m, j_{n+1} 1 - Mesh of triangles as in Fig. 2.3(b) 2 - Mesh of best conditioned triangles Shortest diagonal

* For plane stress analysis replace 'bridge' by 'plate'

Card Type	Column on Card	Description
11		WIDTH DIVISION CARDS
		Sub-sets A and B are repeated for each j grid line (the i grid lines are not necessarily straight)
11A		One card
	1-10*	X co-ordinate of starting nodal point of the grid line
	11-20*	Y co-ordinate of starting nodal point of the grid line
	21-30*	X co-ordinate of end nodal point of the grid line
	31-40*	Y co-ordinate of end nodal point of the grid line
11B		One card for each 8 division widths along j grid line
	1-10*	Width of 1st division measured along the j grid line
	11-20*	Width of 2nd division measured along the j grid line, etc.
12		BEAM CONTROL CARD
		One card
		Number of rows of the beam elements
13		BEAM CARDS
13		One card for each row of the beam elements. If the number of the rows of the beam elements is zero these cards are omitted
	1-5	i th) Grid co-ord. of the starting
	6-10	j th) of the row

Card Type	Column on Card	Description
13	Continued	
	11-15	ith) } Grid co-ord of the end nodal point jth) of the row
	16-20	
	21-30	Material number of the row of beam elements
	31-40	Beam load number of the row of beam elements. A number is not assigned if the beam is not loaded (Plate bending only)
14		MATERIAL CONTROL CARD
		One card
	1-5	Number of the types of plate materials
	6-10	Number of the plate element material patches. These patches must have a plate element material property number assigned to them
	11-15	Number of the types of beam materials
15		MATERIAL PROPERTY CARDS
		One or two cards for each different material property. Plate element properties must precede beam element properties and must be numbered in sequence
15A		TRIANGULAR PLATE ELEMENTS
		<u>Bending (Normal Loading) Analysis</u>
		If only this analysis is to be performed (ie plate is not to be pre-stressed) type (i) or (ii) data is required with one card for each material type

Card Type	Column on Card	Description
15A	Continued	
		<u>Prestress Analysis</u>
		For the analysis of decks which are to be prestressed some additional data might be necessary. If the plate is solid and isotropic only data type (i) is required. If, however, the plate is voided and/or orthotropic a card (ii) followed by a card (iii) is required for each type of material
		<u>Plane Stress Analysis</u>
		For plane stress analysis one card of type (i) or (iii) is required for each type of material
15A (i)		(i) Solid, isotropic slab
	1-10	Material type number
	11-20*	Young's modulus
	21-30*	Poisson's ratio
	31-40*	Plate thickness
15A (ii)		(ii) Voided and/or orthotropic slab (Plate Bending)
	1-10	Material type number
	11-20*	DX)
)
	21-30*	DY)
) Plate rigidities
	31-40*	D1)
)
	41-50*	DXY)
15A (iii)		(iii) Voided and/or orthotropic slab (Plane Stress)

Card Type	Column On Card	Description
15A (iii)	Continued	
	1-10	Material type number
	11-20*	D11}
	21-30*	D22} Elastic constants
	31-40*	D12}
	51-60*	t^1 The equivalent plate thickness
15B		
15B		BEAM ELEMENTS
15B (i)		<u>Bending and Prestress Analysis</u>
		One card for each material type
	1-10	Material type number
	11-20*	Young's modulus
	21-30*	Second moment of area about the NA of the beam
	31-40*	Carry-over factor for the bending moments. This is 0.5 for constant section beams, but varies for haunched beams
	41-50*	Torsion factor J^1 ($=JG/E$)
	51-60*	Area of cross-section. This is only included if the structure is to be designed as prestressed
15B (ii)		<u>Plane Stress Analysis</u>
		One card for each type of material
	1-10	Material type number
	11-20*	Young's modulus
	21-30*	Area of Cross section

Card Type	Column on Card	Description
16		PLATE MATERIAL PATCH CARDS
		One card for each plate material patch
	1-5	ith)
	6-10	jth) Grid co-ord of the nodal point starting the patch
	10-15	ith)
	16-20	jth) Grid co-ord of the nodal point ending the patch
	21-30	Material type number of the plate elements within the patch
17		BOUNDARY CONTROL CARD
		One card
	1-5	Number of rigidly restrained boundary nodes with or without fixed displacements
	6-10	Number of elastically restrained boundary nodes
18		RIGIDLY RESTRAINED BOUNDARY CARDS
		One card for each rigidly restrained boundary node, in ascending nodal order. This set is omitted if all the boundary conditions are elastic
18 (i)		<u>Plate Bending Analysis</u>
	1-15	ith))
	6-10	jth)) Grid co-ord of the restrained node
	13	Is the w degree of freedom restrained?
		0 - No
		1 - Yes

Card Type	Column on Card	Description
18 (i)	Continued	
	14	Is the θ_x degree of freedom restrained? 0 - No 1 - Yes
	15	Is the θ_y degree of freedom restrained? 0 - No 1 - Yes
	16-25*	Specified w displacement of the node
	26-35*	Specified θ_x displacement of the node
	36-45*	Specified θ_y displacement of the node
18 (ii)		<u>Plane Stress Analysis</u>
	1-15	ith) Grid line of the restrained node
	6-10	jth)
	14	Is the X degree of freedom restrained? 0 - No 1 - Yes
	15	Is the Y degree of freedom restrained? 0 - No 1 - Yes
	16-25*	Specified X displacement of the node
	26-30:	Specified Y displacement of the node
	Note:	The displacements can only be specified for the rigidly restrained degrees of freedom

Card Type	Column on Card	Description
19		ELASTICALLY RESTRAINED BOUNDARY CARDS
		One card for each elastically restrained boundary node. The nodes must be in ascending nodal order. This set is omitted if all the boundary conditions are rigid.
19 (i)		<u>Plate Bending Analysis</u>
	1-5	ith) Grid co-ord of the strained node
	6-10	jth)
	11-30*	Stiffness for the w degree of freedom
	31-50*	Stiffness for the θ_x degree of freedom
	51-70*	Stiffness for the θ_y degree of freedom
19 (ii)		<u>Plane Stress Analysis</u>
	1-5	ith)
	6-10	jth) Grid line of the restrained node
	11-30*	Stiffness in the X direction
	31-50*	Stiffness in the Y direction
20		LOAD CASE CONTROL CARD
		One card
	1-5	Number of load cases
21		LOAD CASE CARD
		One card
	1-5	Load case number. The load case numbers must begin at one and be sequential

Card Type	Column on Card	Description
21	Continued	
	10	Are results to be printed? 0 - Yes 1 - No
	11-78+	Load case title
22		LOAD TYPE CARD One card
22 (i)		<u>Plate Bending Analysis</u> 1-5 Number of uniformly distributed loads 6-10 Number of knife edge loads 11-15 Number of abnormal vehicles 16-20 Number of nodes loaded with point loads 21-25 Number of beam load property numbers used in load case
22 (ii)		<u>Plane Stress Analysis</u> 1-5 Number of uniformly distributed area loads in the load case 6-10 Number of point loads in the load case
23		UNIFORMLY DISTRIBUTED LOAD CARDS
23 (i)		<u>Plate Bending Analysis</u> One card for each UDL 1-5 ith) 6-10 jth) Grid co-ord of the node starting the loaded area

Card Type	Column on Card	Description
23 (i)	Continued	
	11-15	ith)) Grid co-ord of the node ending
	16-20	jth) the loaded area
	21-30*	Load per unit area
23 (ii)		<u>Plane Stress Analysis</u>
		One card for each area load
	1-5	ith)) Grid line of the node starting
	6-10	jth) the loaded area
	11-15	ith)) Grid line of the node ending
	16-20	jth) the loaded area
	21-30*	Load per unit area in the X direction
	31-40*	Load per unit area in the Y direction
24		KNIFE EDGE LOAD CARDS (Plate Bending Analysis Only)
		One card for each knife edge load
	1-5	ith)) Grid co-ord of the node starting
	6-10	jth) the load
	11-15	ith)) Grid co-ord of the node ending
	16-20	jth) the load
	21-30*	Load per unit length along the line acting in the z direction
	31-40*	Load per unit length along the line acting in the θ_x direction
	41-50*	Load per unit length along the line acting in the θ_y direction
	<u>Note:</u> The loads can only lie along the i or j grid lines	

Card Type	Column on Card	Description
25		ABNORMAL VEHICLE LOAD CASES (Plate Bending Analysis Only)
		Subsets A and B are repeated for each abnormal vehicle
25A		One card
	1-5	Number of bogies (ie pairs of axles) of the vehicle applied to the structure
25B		One card for each bogie
	1-5	ith) Grid co-ord of the node starting
	6-10	jth) the area in which the bogie sits
	11-15	ith) Grid co-ord of the node ending
	16-20	jth) the area in which the bogie sits
	21-30*	X co-ordinate of the centroid of the bogie
	31-40*	Y co-ordinate of the centroid of the bogie
	41-50*	Angle of orientation of the bogie axles to the Y axis (positive clockwise)
	51-60*	Axle length ie distance between the outer wheels on each axle
	51-70*	Load acting from each wheel of the bogie
	Note: Each axle has 4 wheels and each bogie consists of a pair of axles and each abnormal vehicle may have 1 or 2 bogies	
26		POINT LOAD CARDS
		One card for each node loaded

Card Type	Column on Card	Description
26	Continued	
26		<u>Plate Bending Analysis</u>
(i)	1-5	ith)
	6-10) Grid co-ord of the loaded node jth)
	11-20*	Load in the w direction
	21-30*	Load in the θ_x direction
	31-40*	Load in the θ_y direction
26		<u>Plane Stress Analysis</u>
(ii)	1-5	ith)
	6-10) Grid line of the node which is jth) loaded.
	11-20*	Load in the X direction
	21-30*	Load in the Y direction
27		BEAM LOAD CARDS (Plate Bending Analysis Only)
		One card for each beam load property number used in the load case
	1-5	Beam load property number
	5-15*	Load per unit run of the beam
Notes:	(i)	<u>Plate Bending Analysis</u>
	1.	Repeat Cards Types 21 to 27 for each load case
	2.	Repeat Cards Types 3 to 27 for each problem in the run
	(ii)	<u>Plane Stress Analysis</u>
	1.	Cards Types 22 to 23 and 26 are repeated for each load case
	2.	Card Types 3 to 23 and 26 are repeated for each problem in the run

Card Type	Column on Card	Description
1	1-10	(F10.2) flexure cracked rigidity in x direction
	11-20	(F10.2) flexure cracked rigidity in y direction
	21-30	(F10.2) coupling cracked rigidity
	31-40	(F10.2) torsional cracked rigidity
	41-50	(F10.2) maximum positive moment causing cracks
	51-60	(F10.2) flexure cracked rigidity in x direction
	61-70	(F10.2) flexure cracked rigidity in y direction
	71-80	(F10.2) coupling cracked rigidity
2	1-10	Torsional cracked rigidity (top surface)
	11-20	Maximum -ve moment causing cracks in top surface of concrete
3	1-10	Ultimate positive moment causing yielding of steel or crushing of concrete
	11-20	Ultimate negative moment causing yielding of steel or crushing of concrete
4	10	Either leave blank or insert 1 if the first problem to be run is of the same type as the first problem of a previous SAADS run on the same structure in which the element stiffnesses were kept.
	15	Either leave blank or insert 1 if the second problem to be run is of the same type as the second problem of the previous SAADS run on the same structure in which the element stiffnesses were kept.

Card Type	Column on Card	Description
4	Continued	Note: When a prestress analysis takes place (using data prepared by PPUT) two separate problems are analyzed consecutively. The first problem is the plate bending problem and the second problem is the plane stress problem for the same structure. If the element stiffnesses are saved from a prestress analysis they will therefore be saved in the same order, i.e., plate bending as problem 1; plane stress as problem 2.

DATA PREPARATION FOR PPUT

Step 1 CONTROL DATA

Card Type	Columns on Card	Description
1		<u>INPUT UNIT DEFINITION CARD</u>
		One Card.
	5	0 - Input file for SAADS is in formatted form on punched cards (generated by IPUT2 or prepared by hand)
		1 - Input file for SAADS generated by IPUT2 is in binary form magnetic tape or disc units.
	10	1 - Enter if SAADS input file is in card form. If not, leave blank.
2		<u>PRESTRESSING STAGE CONTROL CARD</u>
		One Card
	1-5	Number of prestressing stages to be analyzed in the problem.

Step 2 DATA FOR SAADS ON CARDS

This step is omitted if the data for SAADS is not on cards.

The data on cards which has been either generated by IPUT2 or prepared by hand according to the SAADS input instructions is included here.

Step 3 PLANE STRESS BOUNDARY DATA

Card Type	Columns on Card	Description
3		<u>IN-PLANE BOUNDARY CONDITIONS CONTROL CARD</u>
		One Card
	1-5	Number of rigidly restrained boundary nodes with or without fixed displacements.

Card Type	Columns on Card	Description
3	Continued	
	6-10	Number of elastic boundary conditions.
4		<u>IN-PLANE RIGIDLY RESTRAINED BOUNDARY CARDS</u>
		One card for each rigidly restrained boundary node is ascending nodal order. This set is omitted if all the boundary conditions are elastic.
	1-5	Boundary node number.
	9	Is the X degree of freedom restrained? 0 - No 1 - Yes.
	10	Is the Y degree of freedom restrained? 0 - No 1 - Yes.
	11-30*	Specified X displacement of the node.
	31-50*	Specified Y displacement of the node. The displacements can only be specified for the rigidly restrained degrees of freedom.
5		<u>IN-PLANE ELASTICALLY RESTRAINED BOUNDARY CARDS</u>
		One card for each elastic boundary stiffness in ascending nodal order of N_r ($N_r < N_c$). If all the boundary conditions are rigid then this set of cards is omitted.
	1-5	Node number N_r .
	10	Is the stiffness at N_r in the X or Y direction?

Card Type	Columns on Card	Description
5	Continued	
	10	1 - means X 2 - means Y.
	11-15	Node number N_c .
	20	Is the stiffness at N_c in the X or Y direction? 1 - means X 2 - means Y.
	21-30*	Stiffness

Step 4 PRESTRESS CABLE DATA

This set of data (Card Types 6-10) is repeated for each prestressing stage.

Card Type	Columns on Card	Description
6		<u>PRESTRESSING STAGE CARD</u> One card.
	1-5	Number of prestressing stage. The prestressing stage numbers must begin at one and be sequential for each problem.
	10	0 - SAADS results will be printed 1 - SAADS results will not be printed.
	11-77 ⁺	Title of prestressing stage.
7		<u>CABLE CONTROL CARD</u> One Card.

Card Type	Columns on Card	Description
7	Continued	
	1-5	Number of cables in prestressing stage.
	10	0 Nodal loadings will be printed. 1 Nodal loadings will not be printed.
Cards Types 8-10 are repeated for each cable in the prestressing stage.		
8		<u>CABLE PARAMETER CARD</u>
		One Card.
	1-5	Cable Number.
	6-10	Number of points along cable at which the cable position is defined. Usually this is the same number as the mesh lines which are crossed by the cable.
	20	Is the plan shape of the cable straight or curved? 0 - means straight. 1 - means curved.
	30	Is the elevation shape of the cable straight? 0 - means straight. 1 - means parabolic. 2 - means arbitrary.
	31-40*	Maximum effective prestressing force in the cable.
9		<u>CABLE POINT DATA</u>
		One card for each point on the cable whose position is to be defined.

Card Type	Columns on Card	Description
9	Continued	
		<u>Plan shape of cable</u>
		a. Straight. The end co-ordinates and one intermediate co-ordinate at each point are entered.
		b. Curved. The co-ordinates at all the points must be given.
		<u>Elevation shape of cable</u>
		a. Straight. Only cable eccentricities at the end points need be specified. The other eccentricities may be left blank.
		b. Parabolic. Only eccentricities at the end points of the parabolas need be stated. The other eccentricities may be left blank.
		c. Arbitrary. The eccentricities at all the points on the cable must be specified.
		The eccentricities are measured in a positive sense downwards from the neutral axis of the structure.
1-10		Number assigned to the cable point. These numbers must begin at one for each cable and be sequential.
11-20*		X co-ordinate of point if it is required.
21-30*		Y co-ordinate of point if it is required.
31-35		Adjacent finite element node to the right of the point.

Card Type	Columns on Card	Description
9	Continued	
	36-40	Adjacent finite element node to the left of the point. The right and left sense is defined by looking along the cable from end point one. If the cable passes through a node point, the left node number may be left blank.
	41-50*	Eccentricity of cable point.
	51-60*	Percentage loss of the maximum effective prestressing force at the point
10		<u>PARABOLIC ELEVATION CABLE DATA</u> Subsets A and B are only required if the cables have been specified as parabolic in elevation. Otherwise the subsets are omitted.
10A		One Card.
	1-5	Number of parabolas along the cable.
10B		One card per parabola.
	1-5	Number assigned to the parabola. The numbers must begin at one and be consequential for each cable.
	6-10	Starting cable point number of the parabola.
	11-15	Ending cable point number of the parabola.
	16-25*	Maximum dip of the parabola.

DATA PREPARATION FOR SPUT

Card Type	Columns on Card	Description
1		<u>CONTROL CARD</u>
		One card.
	5	Are nodal averaged or element centroidal results from SAADS to be processed? (see note below)
		1 - Nodal Averaged
		0 - Element Centroidal
	10	Are the stress field and principal stress field of extreme fibre stresses to be printed?
		0 - Both
		1 - Principal Stresses only.)
	15	Are results from SAADS for both normal loading and prestress loading to be processed?
		0 - Both
		1 - Prestress results only
	20	Are results required at every node (or element) or only at ranges of nodes (or elements) or at particular nodes (or elements)?
		0 - Results at every node (or element)
		1 - Results at ranges of nodes (or elements)
		2 - Results at particular nodes (or elements)
	25	Is an output tape of SPUT results required?

Card Type	Columns on Card	Description
1	Continued	<p>1 - Yes</p> <p>0 - No</p> <p>30 Are combined reactions to be printed?</p> <p>0 - Yes</p> <p>1 - No</p> <p>Note: (i) Centroidal element values must be processed if beam elements are present. If plate elements only are used then either centroidal or or nodal averaged results may be processed by SPUT</p>
2		<p><u>RESULTS CONTROL CARDS</u></p> <p>If there is a 0 in column 20 of card type 1 go to card type 3 otherwise one card of type 2a + One or Two cards type 2b required.</p>
2a	1-5	<p>Number of ranges of nodes (or elements) or number of particular nodes (or elements) at which results to be printed.</p> <p>Max. number of ranges = 15; max. no. of particular nodes (or elements) = 30</p> <p><u>RANGES OF NODES (or ELEMENTS)</u></p>
2b	1-5	Start node (or element) of first range
	6-10	End node (or element) of first range
	11-15	Start node (or element) of second range
	16-20	End node (or element) of second range
	etc.	etc.
		Note: This pattern is repeated up to

Card Type	Columns on Card	Description
2b	Continued	<p>8 times on one card. For more than 8 ranges a second card is required. The node or element numbers must appear in ascending order.</p> <p><u>PARTICULAR NODES (or ELEMENTS)</u></p> <p>2b 1-5 First node (or element) number</p> <p> 6-10 Second node (or element) number</p> <p> 11-15 Third node (or element) number</p> <p> etc. etc.</p> <p>Note: Up to 16 nodes (or elements may be included on one card. For more than 16 nodes a second card is required. The node or element numbers must appear in ascending order.</p>
3		<p><u>STRESS CONTROL CARD</u></p> <p>One card</p> <p> 1-5 Number of different allowable stresses in slab for one load case combination.</p>
4		<p><u>MATERIAL CONTROL CARD</u></p> <p>One card</p> <p> 1-5 Number of types of plate and beam materials.</p>
5		<p><u>NODAL OR CENTROIDAL MATERIAL PROPERTY CARDS</u></p> <p>One card for each nodal or centroidal property type. If nodal averaged values are to be processed the material properties must be those at the nodal points. If centroidal results are to be processed the properties must be those of the element centroids.</p>

Card Type	Columns on Card	Description
5A		<u>PLATE PROPERTIES</u>
		One card of type (i) or (ii) for each type of property.
5A(i)		(i) Solid or isotropic plate
	1-10	Property type number
	11-20*	Plate thickness, t .
5A(ii)		(ii) Voided and/or orthotropic plate.
	1-10	Property type number
	11-20*	Equivalent plate thickness, t' .
	21-30*	Section modulus per unit length of plate for bending about the y axis - Z_x
	31-40*	Solid Area per unit length of plate for direct stress in the x direction - A_x
	41-50*	Section modulus per unit length of plate for bending about the x axis - Z_y
	51-60*	Solid Area per unit length of plate for direct stress in y direction - A_y
	61-70*	Torsion modulus per unit length of the plate, Z_{xy}
	71-80*	Shear area per unit length of plate A_{xy}
5B		<u>BEAM PROPERTIES</u>
	1-10	Property type number
	11-20*	Beam section modulus
	21-30*	Beam X-sectional area

Card Type	Columns on Card	Description
6		<u>MATERIAL ALLOCATION CARDS</u>
		One card for each nodal point or element where the material type or allowable stress begins, in ascending nodal or element order. This set must start with first node and end with the last node or element specified.
	1-5	Nodal point or element number
	6-10	Property type number
	11-15	Stress type number
		Note: If nodal average results are to be processed, nodal point numbers must be specified. If centroidal values are to be processed then the element numbers must be given
7		<u>COMBINATION CARD</u>
		One Card
	1-5	Number of combinations of factored load cases to be examined
8		<u>COMBINATION CASE CARD</u>
		One card
	1-5	Load combination number. The load combination numbers must begin at one and be sequential.
	6-10	Number of load cases in the combination
9		<u>ALLOWABLE STRESS CARDS</u>
		One card for each different allowable stress type.
	1-10	Allowable stress type number
	11-20*	Maximum allowable principal tensile stress

Card Type	Columns on Card	Description
9	Continued	
	21-30*	Maximum allowable principal compressive stress
10		<u>LOAD CASE CARD</u>
		One card for each load case in the combination
	1-5	Normal load case number or prestress stage number
	10	Is the load case due to normal loading or prestressing?
		0 - means prestressing
		1 - Means normal loading
	11-20*	Multiplying factor for the load case
Note: Card types 8, 9 and 10 are repeated for each combination.		

APPENDIX D

CALIBRATION OF LOAD CELLS AND
TENSION TEST ON WIRES

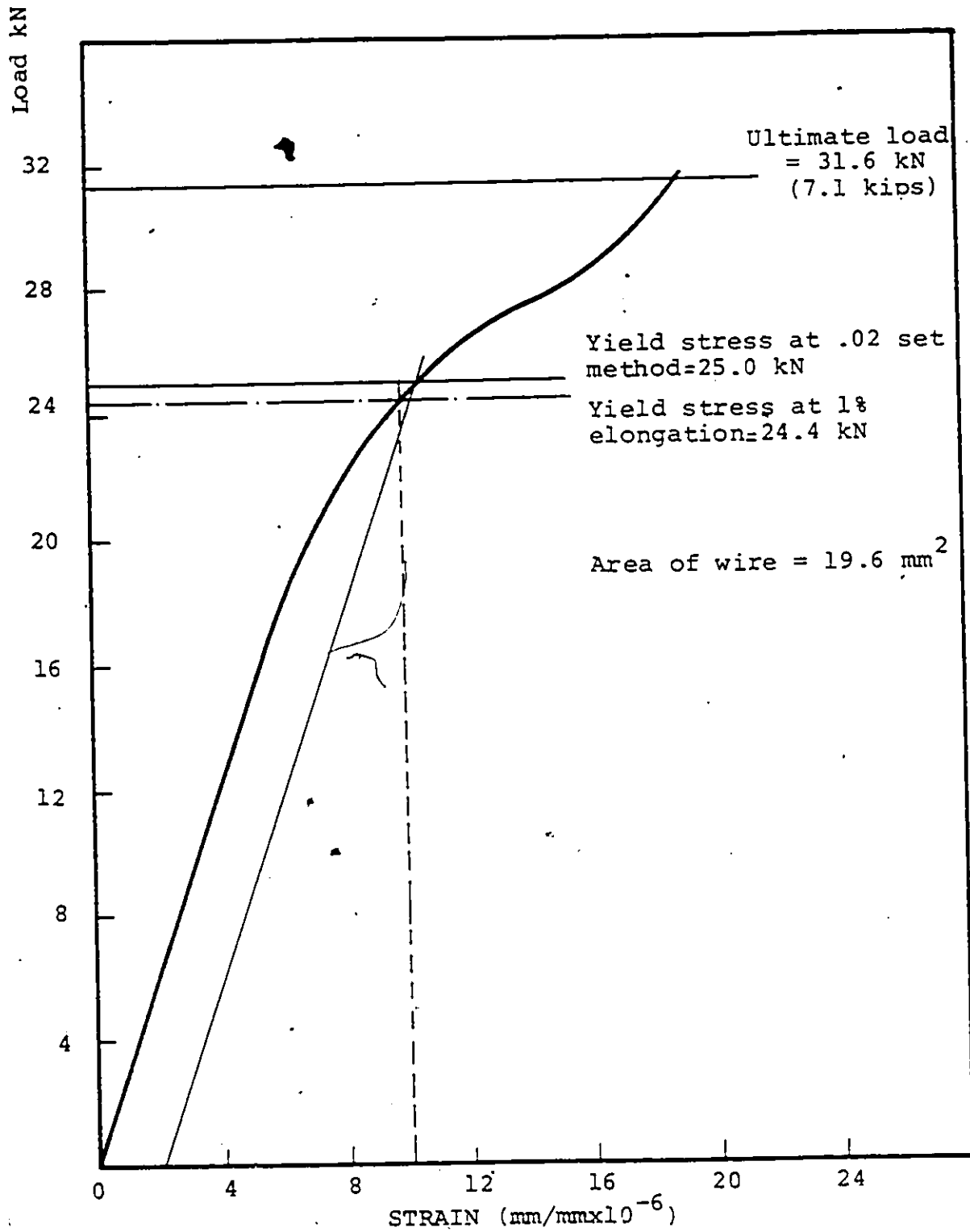


FIGURE D1 TENSION TEST OF THE PRESTRESSING WIRE

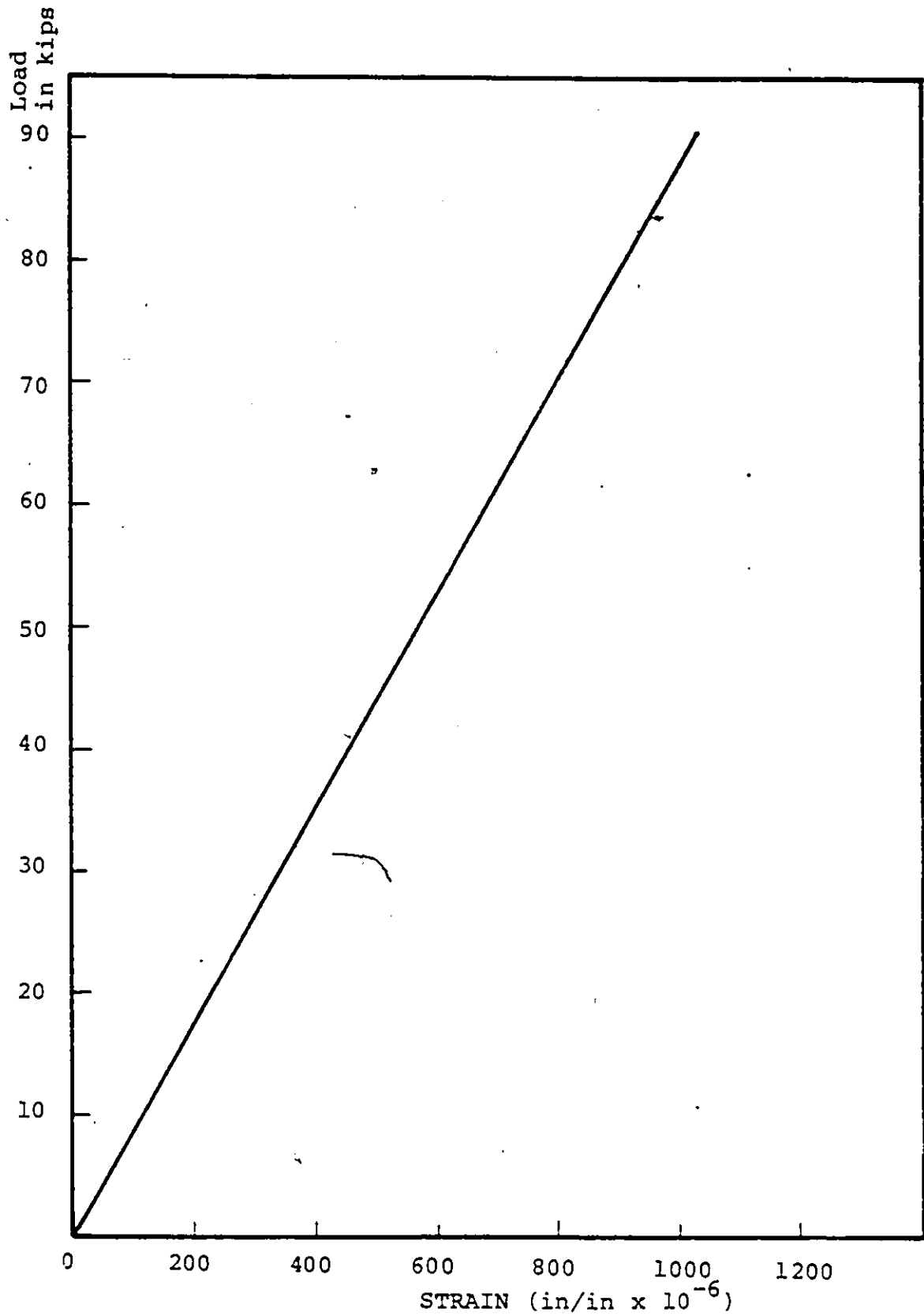


FIGURE D2 CALIBRATION OF LOAD CELL 20 kips
(FOR LOADING) {(CYLINDRICAL)}

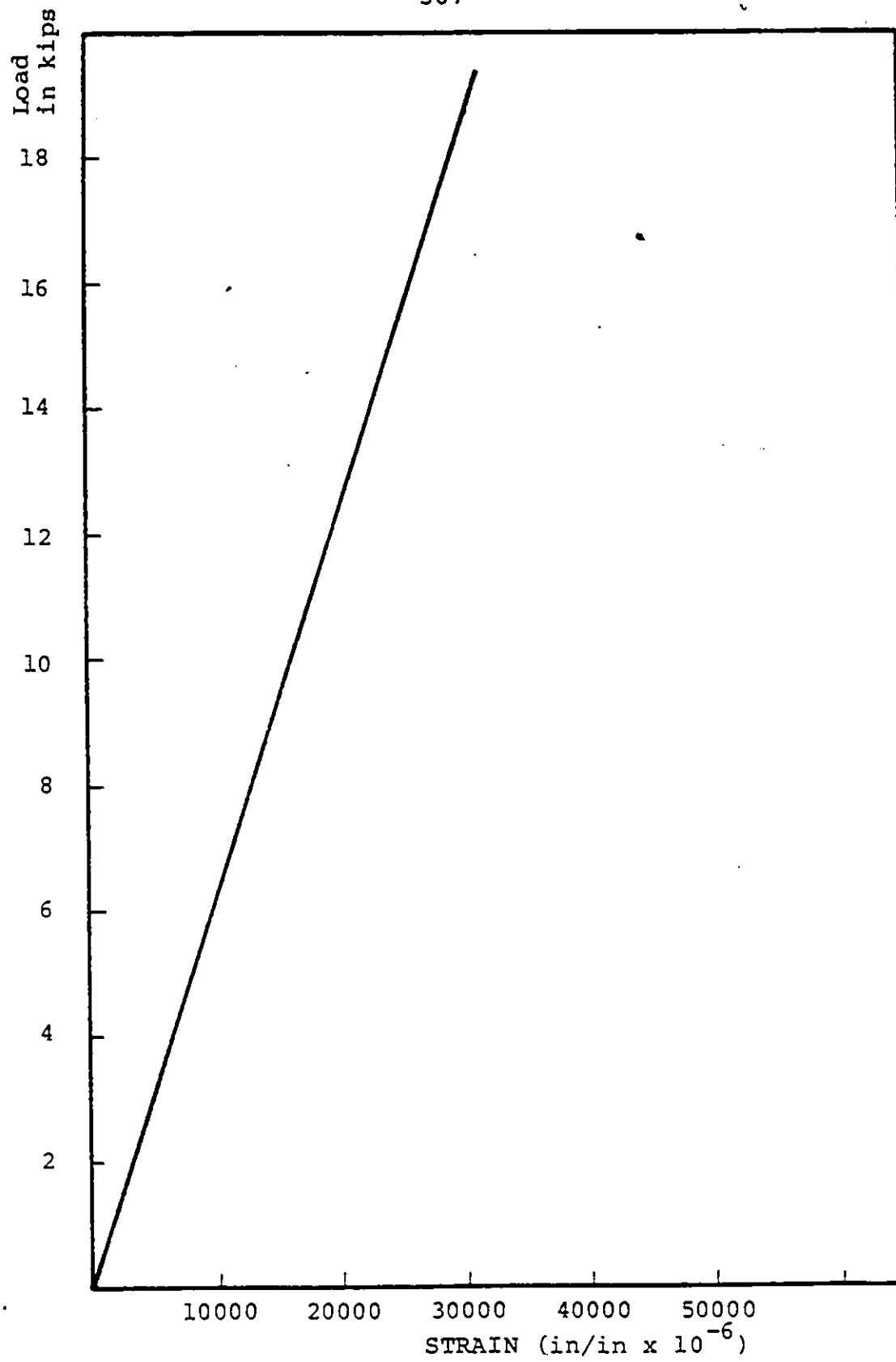


FIGURE D3 CALIBRATION OF LOAD CELL 25 KIPS

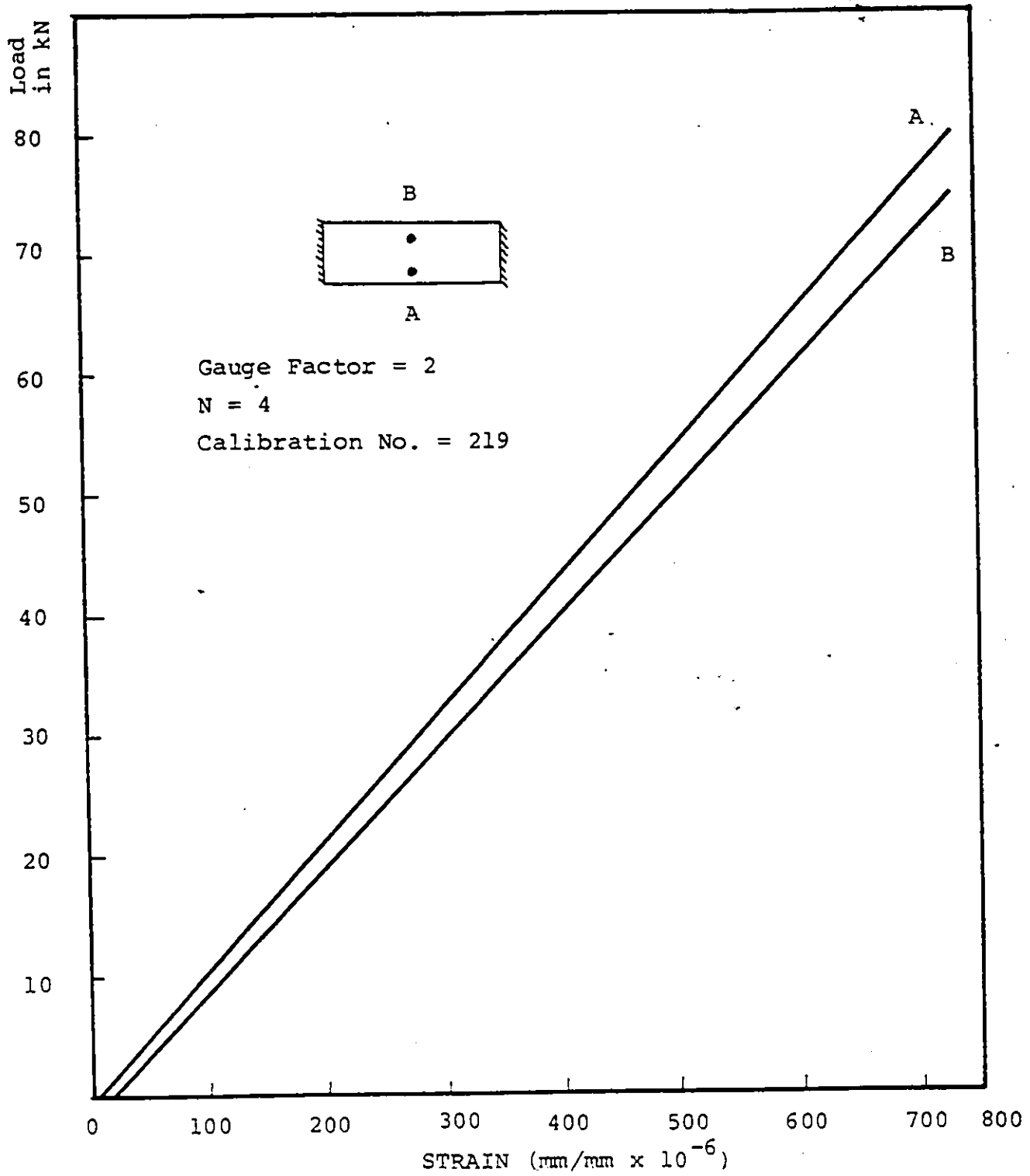


FIGURE D4 THE TWO LOAD CELL MEASURING THE COLUMN REACTIONS

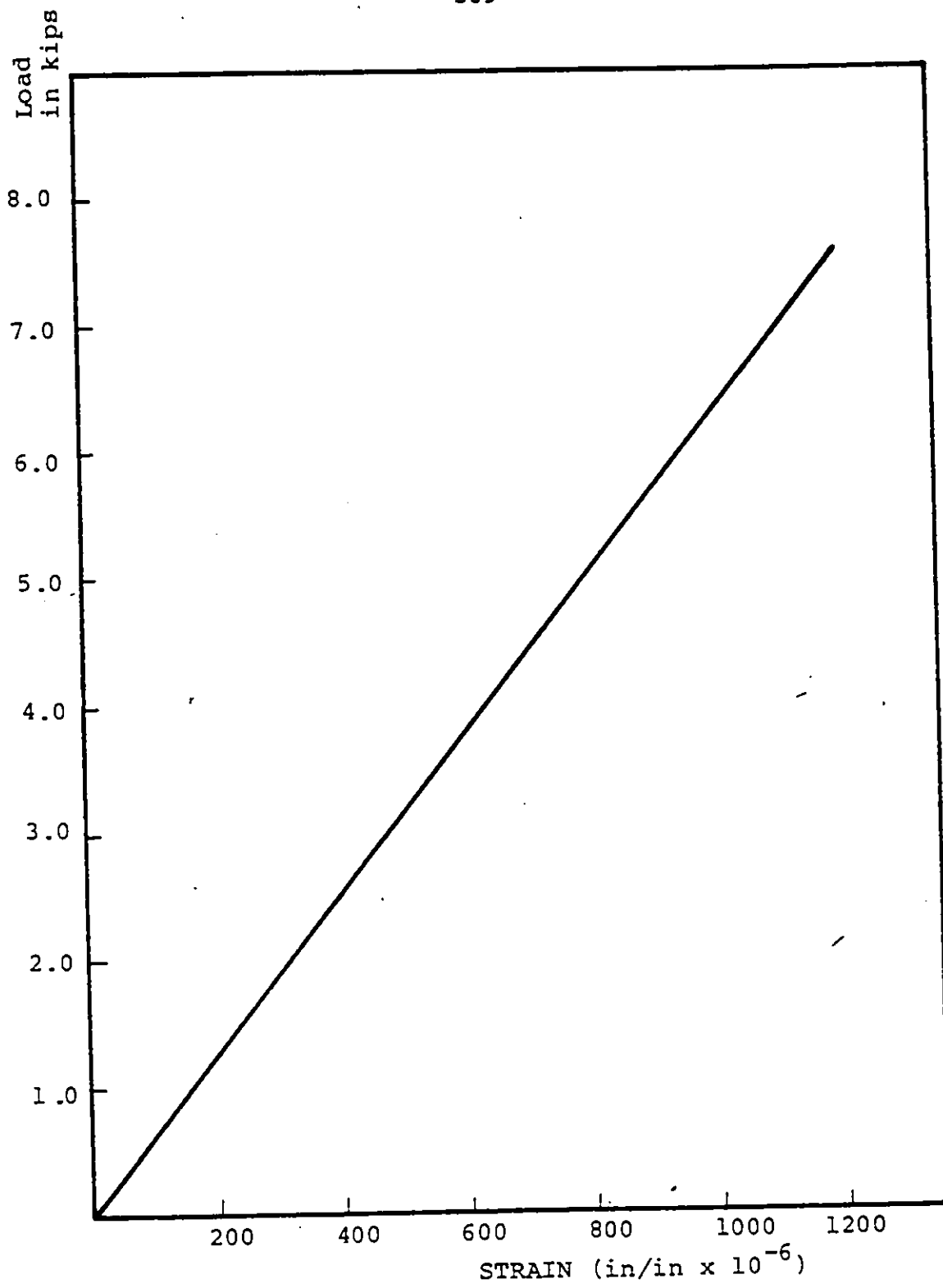


FIGURE D5 CYLINDRICAL LOAD-CELLS FOR PRESTRESSING

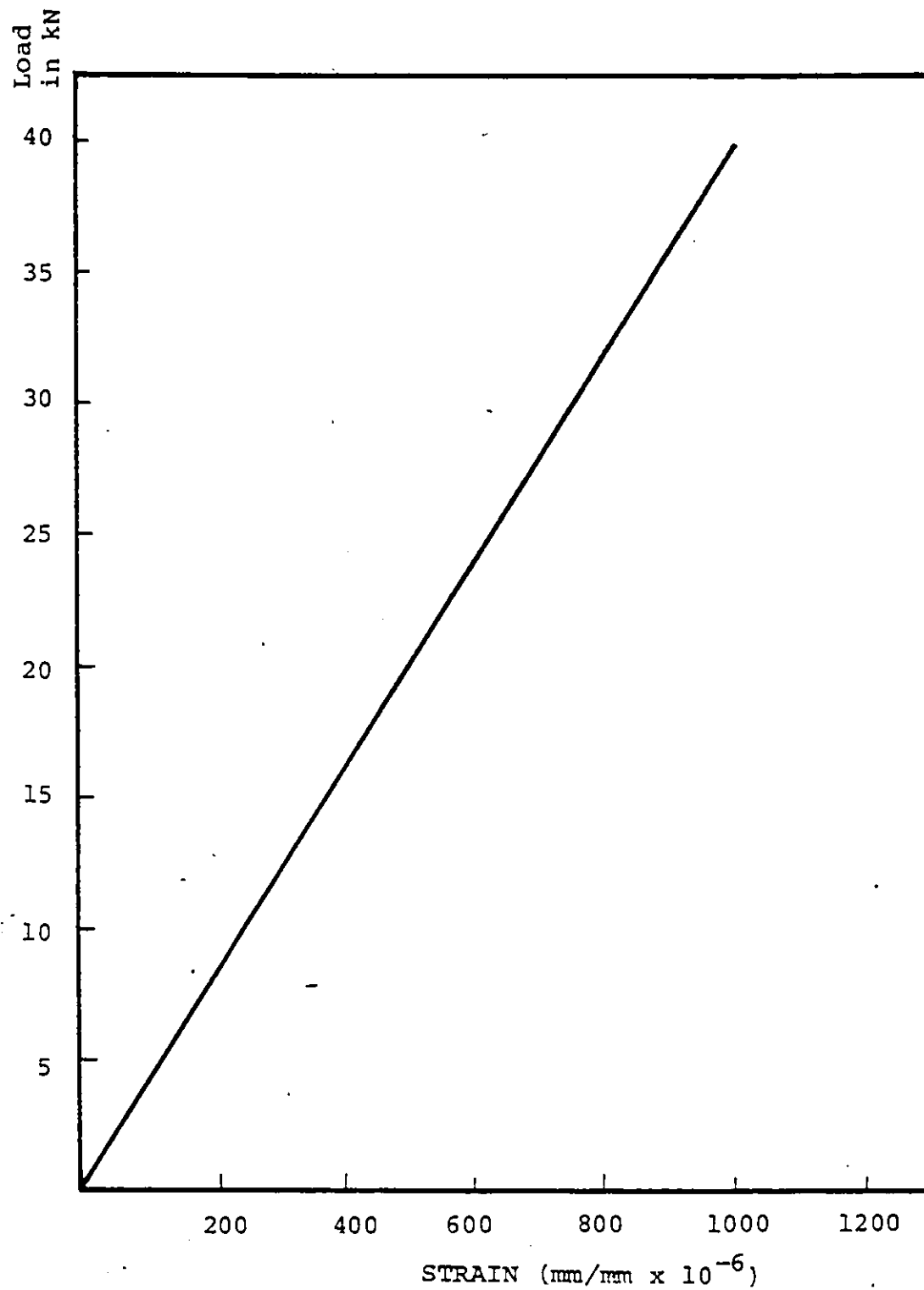


FIGURE D6 CYLINDRICAL-LOAD CELLS FOR PRESTRESSING
(ELECTRONIC STRAIN INDICATOR)

REFERENCES

REFERENCES

1. "Forming a Giant Waffle Slab," Engineering News Record, May, 1967.
2. Kennedy, J. B., and Ghobrial, M., "Waffle Slab Construction for Concrete Bridge Decks - Phase I," Report 11-26, Industrial Research Institute of the University of Windsor, Windsor, Ontario, Canada, 1980.
3. McDonald, J. L., "Design of a Two Way Post-Tensioned Waffle Slab," Civil Engineering Magazine, ASCE, May, 1973.
4. Rawles, R. H., "Dallas Bridge Has Post-Tensioned Concrete Decks," Civil Engineering Magazine, ASCE, April 1973.
5. T. Y. Lin and Felix Kulka, "Construction of Rio Colorado Bridge," Journal of the Prestressed Concrete Institute, Vol. 18, No. 6, Nov.-Dec. 1973.
6. Timoshenko, S., and Woinowsky-Krieger, S., Theory of Plates and Shells, McGraw-Hill Book Co., New York, (1959).
7. Szilard, R., "A Simplified Method for Torsional Analysis of Gridworks," ACI sp-35, American Concrete Institute, Detroit (1973).
8. Szilard, R., Theory and Analysis of Plates: Classical and Numerical Methods, Prentice-Hall Inc., Englewood Cliffs, New Jersey, (1974).
9. Lekhnitskii, S. G., Anisotropic Plates, Gordon and Breach, Science Publishers, Inc., New York, (1968).
10. Huffington, N. J., Jr., "Theoretical Determination of Rigidity properties of Orthogonally Stiffened Plates," Journal of Applied Mechanics, Transaction S, ASME, Vol. 87, Paper No. 55-A-12, Mar., 1956, pp. 15-20.
11. Jackson, N., "The Torsional Rigidities of Concrete Bridge Decks," Concrete, V. 2, n. 11, Nov., 1968, pp. 465-474.
12. Kennedy, J. B., and Bali, S. K., "Rigidities of Concrete Waffle-type Slab Structures," Canadian Journal of Civil Engineering, Vol. 6, No. 1, March 1979, pp. 65-74.

13. Perry, P. G., and Heins, C. P., "Rapid Design of Orthotropic Bridge Floor Beams," Journal of the Structural Division, Proc., ASCE, Vol. 98, No. ST11, 1972, pp. 2491-2506.
14. Cardenas, A. E., and Sozen, M. A., "Flexural yield Capacity of Slabs," ACI Journal, Feb., 1973.
15. Cardenas, A. E., Lenschow, R. J., and Sozen, M. A., "Stiffness of Reinforced Concrete Plate," Journal of the Structural Division, Proc., ASCE, Vol. 98, No. ST11, Nov., 1972, pp. 2587-2603.
16. Bares, R. and Massonet, C., "Analysis of Beam Grids and Orthotropic Plates by the Guyon-Massonet-Bares Method," Frederick Unger Publishing Co., New York, 1968.
17. Rowe, R. E., Concrete Bridge Design, C. R. Books Limited, 1962.
18. Kennedy, J. B., and Martins, I. C., "Stresses Near Corners of Skewed Stiffened Plates," The Structural Engineer, Vol. 41, 1963.
19. Kennedy, J. B., and Huggins, M. W., "Series Solution of Skewed Stiffened Plates, Journal of the Engineering Mechanics Division, ASCE, Vol. 90, No. EM1, Feb., 1964.
20. Kennedy, J. B., and Ng, S. F., "Analysis of Skewed Plate Structures with Clamped Edges," Trans. of the Engrg. Inst. of Canada, Paper EIC-6S-BR STR9, Dec., 1965.
21. Kennedy, J. B., and Gupta, D. S. R., "Bending of Skew Orthotropic Plate Structures," Journal of the Structural Division, Proc., ASCE, Vol. 102, No. ST8, August, 1976, pp. 1559-1574.
22. Kennedy, J. B., and El-Sebakhy, I. S., "Prestressed Waffle Slab Bridges - Elastic Behavior," Journal of the Structural Division, ASCE, Vol. 106, No. ST12, Proc. Paper 15929, Dec., 1980, pp. 2443-2462.
23. El-Sebakhy, I. S., "Behavior of Reinforced and Prestressed Waffle Slabs," M.A.Sc. Thesis, University of Windsor, Ontario, Canada, 1979.
24. Scordelis, A. C., Lin, T. Y., and Itaya, R., "Behavior of a Continuous Slab Prestressed in Two Directions," Journal of the American Concrete Institute, Dec., 1959, pp. 441-459.

25. Scordelis, A. C., Samarzich, W., and Pirtz, D., "Load Distribution on a Prestressed Concrete Slab Bridge," Prestressed Concrete Institute Journal, June, 1960, pp. 18-33.
26. Hondros, G., and Smith, G. C., "Model and Theoretical Analysis of a Post-Tensioned Diagrid Flat Plate," PCI Journal, Vol. 14, No. 2, Apr., 1969, pp. 63-87.
27. Muspratt, M. A., "Behaviour of a Prestressed Concrete Waffle Slab with Unbonded Tendons," Journal of the American Concrete Institute, Vol. 66, No. 12, Dec., 1969, pp. 1001-1004.
28. Lin, T. Y., Kulka, F., and Yang, Y. C., "Post-Tensioned Waffle and Multispan Cantilever System with Y-Piers Composing the Hegenberger Overpass," Concrete Bridge Design, SP 23-27, American Concrete Institute, Vol. 66, No. 12, Dec., 1969, pp. 1001-1004.
29. Lin, T. Y., Design of Prestressed Concrete Structures, Second Edition, John Wiley and Sons, Inc., 1963.
30. Desai, C. S., and Abel, J. F., Introduction to the Finite Element Method, Van Nostrand Reinhold Company, New York, 1972.
31. Zienkiewicz, O. C., The Finite Element Method, Third Edition, McGraw-Hill Book Company (U.K.) Limited, London, 1977.
32. Department of the Environment, Suite of Bridge Design and Analysis Programs, Program HECB/B/13 STRAND (Version 1) User Manual: Part 1 and 2, London, April, 1974.
33. Zienkiewicz, O. C. and Cheung, Y. K., The Finite Element Method in Structural and Continuum Mechanics, McGraw-Hill, London, 1967.
34. Ingerslev, A., "The Strength of Rectangular Slabs," Struc. Eng., Vol. 1, No. 1, January, 1923, pp. 3-14.
35. Johansen, K. W., Yield-Line Theory, Cement and Concrete Association, London, 1962.
36. Hognestad, E., "Yield-line theory for the ultimate flexural strength of reinforced concrete slabs," Journal of the American Concrete Institute, Vol. 24, No. 7, March, 1953.

37. Wood, R. H., Plastic and Elastic Design of Slabs and Plates, London, Thames and Hudson, 1961, pp. 344.
38. Jones, L. L., Ultimate Load Analysis of Reinforced and Prestressed Concrete Structures, Chatto and Windus, London, 1962.
39. Jones, L. L., and Wood, R. H., Yield-line Analysis of Slabs, Thames & Hudson and Chatto and Windus, London, 1967.
40. American Concrete Institute Code, "Building Code Requirements for Reinforced Concrets," (ACI 318-77), Detroit, Michigan, 1977.
41. Frederick P. Wiesinger, "Design of Flat Plates with Irregular Column Layout," Jour. ACI, 70, No. 2, Feb. 1973, p. 117.
42. Frederick P. Wiesinger, "Yield Line Method - Strip Method - Segment Equilibrium Method," ASCE preprint 2505, ASCE Natl. Structural Convention, April, 1975.
43. Reynolds, G. C., "The Strength of Right Prestressed Concrete Slab Bridges with Edge Beams," Magazine of Concrete Research, Cement and Concrete Association, Vol. 9, No. 27, London, Nov. 1957, pp. 141-144.
44. Reis, Jr., E., Mozer, J. D., Bianchini, A. C., Kesler, C. E., "Causes and Control of Cracking in Concrete Reinforced with High-strength Steel Bars - A Review of Research," Engineering Experiment Station Bulletin 479, University of Illinois, College of Engineering, 1965.
45. Clark, L. A., "Crack Control in Slab Bridges," Technical Report, Cement and Concrete Association. London, October, 1972.
46. Clark, L. A., "Flexural Crack Similitude in Slabs Spanning One-way," Technical Report, Cement and Concrete Association, London, October, 1974.
47. British Standards Institution, Draft British Standard Code of Practice for the Structural Use of Concrete. London, September, 1969.
48. Kemp, K. O., "A lower bound solution to the collapse of an orthotropically reinforced slab on simple supports," Magazine of Concrete Research, Vol. 14, No. 41, July, 1962.

49. Holmes, M., Upper and Lower Bound Solutions to the Collapse of a Continuous Slab Under Uniform Load," Magazine of Concrete Research, Vol. 16, No. 47, June 1964.
50. Parkhill, D. L., "The Flexural Behaviour of slabs at ultimate load," Magazine of Concrete Research, Vol. 18, No. 56, Sept., 1966.
51. Wood, R. H., "The Reinforcement of Slab in Accordance with the Predetermined Field of Moments," Concrete, Vol. 2, No. 2, Feb., 1968, pp. 69-76.
52. Clark, L. A., "Tests on slab elements and skew slab bridges designed in accordance with the factored elastic moment field," Technical Report, Cement and Concrete Association, Sept., 1972.
53. Clark, L. A., "The provision of reinforcement in simply supported skew bridge slabs in accordance with elastic moment fields," Technical Report, Cement and Concrete Association, London, Nov., 1970.
54. Clark, L. A., "The service load response of short-span skew slab bridges designed by yield-line theory," Technical Report, Cement and Concrete Association, London, May, 1972.
55. Granholm, G. A., and Rowe, R. E., "The Ultimate Load of Simply Supported Skew Slab Bridges," Cement and Concrete Association, Research Report, No. 12, June, 1961.
56. Kemp, K. O., "The elevation of nodal and edge forces in yield-line theory," MCR Special Publication, Cement and Concrete Association, London, May, 1965.
57. Morley, C. T., "Equilibrium methods for least upper bounds of rigid-plastic plates," MCR Special Publication, Cement and Concrete Association, London, May, 1965.
58. Nielsen, M. P., "A new nodal-force theory," MCR Special Publication, Cement and Concrete Association, London, May, 1965.
59. Wood, R. H., "New techniques in nodal-force theory for slabs," MCR Special Publication, Cement and Concrete Association, London, May, 1965.

60. Jones, L. L., "The Use of Nodal Forces in Yield-Line Analysis," MCR Special Publication, Cement and Concrete Association, London, May, 1965.
61. Kwiecinski, M. W., "Yield criterion for initially isotropic reinforced slab," Magazine of Concrete Research, Vol. 17, No. 51, June 1965.
62. Kwiecinski, M.W., "Some tests on the yield criterion for a reinforced concrete slab," Magazine of Concrete Research, Vol. 17, No. 52, September 1965.
63. Taylor, R., "Effect of the arrangement of Reinforcement on the behaviour of reinforced concrete slabs," Magazine of Concrete Research, Vol. 18, No. 55, June 1966.
64. Gamble, W.L., Sozen, M. A., and Siess, C. P., "Measured and Theoretical Bending Moments in Reinforced Concrete Floor Slabs," University of Illinois, Civil Engineering Studies, Structural Research Series, No. 246, June 1962.
65. Jain, S. C., "Ultimate Strength and Behavior in Reinforced Concrete Slabs," Ph.D. Dissertation, University of Windsor, Windsor, Ontario, 1971.
66. Kennedy, J. B., and Tamberg, K. G., "Problems of Skew in Concrete Bridge Design," Department of Highways, Report No. RR144, Ontario, March, 1969.
67. Hughes, B. P., Limit State Theory for Reinforced Concrete Design, Van Nostrand Reinhold Company, New York, 1976.
68. Ferguson, P. M., Reinforced Concrete Fundamentals, John Wiley & Sons, New York, 1979.
69. Marcal, P., and Mallett, R., "Elastic-Plastic Analysis of Flat Plates by the Finite Element Method," American Society of Mechanical Engineers, Winter Annual Meeting and Energy Systems Exposition, New York, N. Y., Dec., 1968.
70. Armen, H., Pifko, A. and Levine, H., "A Finite Element Method for the Plastic Bending Analysis of Structures," Proceedings 2nd Conference on Matrix Methods in Structural Mechanics, Wright-Patterson Air Force Base, Ohio, 1968.

71. Whang, B., "Elasto-Plastic Orthotropic Plates and Shells," Proceedings of the Symposium on Application of Finite Element Methods in Civil Engineering, Vanderbilt University, Nashville, Tennessee, Nov. 1969.
72. Bhaumik, A. K. and Hanley, J. T., "Elasto-Plastic Plate Analysis by Finite Differences," Proceedings of the American Society of Civil Engineers, Vol. 93, No. ST5, October, 1967, pp. 279-294.
73. McNeice, G. M., and Kemp, K. O., "Comparison of Finite Element and Unique Limit Analysis Solutions for Certain Reinforced Slabs," Proceedings of the Institution of Civil Engineers, Vol. 43, August, 1969, pp. 629-640.
74. Jofriet, J. C. and McNeice, G. M., "Finite Element Analysis of Reinforced Concrete Slabs," Proceedings of the American Society of Civil Engineers, Structural Division, Vol. 97, No. ST3, March, 1971, pp. 785-806.
75. Bell, J. C., and Elms, D. G., "Non-Linear Analysis of Reinforced Concrete Slabs," Magazine of Concrete Research, Vol. 24, No. 79, London, June 1972, pp. 63-70.
76. Przemieniecki, J. S., Theory of Matrix Structural Analysis," McGraw-Hill Book, Inc., New York, 1968.
77. Gupta, D.S.R., and Kennedy, J. B., "Continuous Skew Orthotropic Plate Structures," Journal of the Structural Division, ASCE, Vol. 104, No. ST2, Proc. Paper, 13566, Feb., 1978, pp. 313-328.

VITA AUCTORIS

Ibrahim Sayed Ahmed El-Sebakhy

The author was born on January 1, 1949 in Tanta, Egypt. In 1967, he completed his secondary school education at Ahmedia School, Tanta, Egypt. He attended the Military Technical College for one year in Cairo, Egypt. Then he joined the Faculty of Engineering, Alexandria University, where he was granted undergraduate scholarships for four consecutive years. In 1973, upon graduating from Alexandria University with a degree of Bachelor of Science in Civil Engineering (Honours), he was appointed as a Teaching and Research Assistant at the Civil Engineering Department, Alexandria University. At the same time, he was engaged by Civil Engineering Consultants in Alexandria as a part-time design engineer.

In 1976, he joined the Civil Engineering Department at the University of Windsor, Windsor, Ontario, Canada, as a Teaching and Research Assistant. In 1979, the author obtained a Master of Applied Science Degree in Civil Engineering from the University of Windsor. The author prepared this dissertation in partial fulfillment of the requirements for the Degree of Doctor of Philosophy.